AD-A165 538 SURVEY OF ATMOSPHERIC RADIATION COMPONENTS FOR THE
AAMMA AND COSMIC RAY A. (U) SEVERN COMMUNICATIONS CORP
SEVERNA PARK MD 31 MAY 85 N00014-84-C-2089

1/2

UNCLASSIFIED F/G 3/1 NL

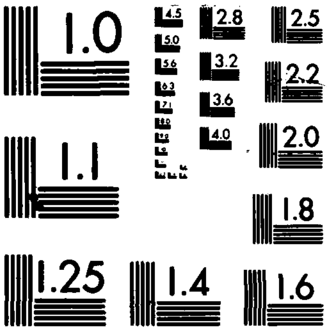
1.0
4.5
5.0
5.6
6.3
7.1
8.0
2.8
3.2
3.6
4.0
2.5
2.2
2.0
1.1
1.8
1.25
1.4
1.6

MICROCOPY RESOLUTION TEST CHART

DARDS-1963-A

2

AD-A165 538

DTIC
ELECTE
MAR 1 9 1986
S D
D

FINAL REPORT

Survey of Atmospheric Radiation Components
for the
Gamma and Cosmic Ray Astrophysics Branch
# of the
Space Science Division
# of the
Naval Research Laboratory

Prepared by

Severn Communications Corporation
Box 544, Severna Park, Maryland 21146

Contract Number N00014-84-C-2089

31 May 1985

DTIC FILE COPY

This document has been approved for public release and sale; its distribution is unlimited.

86 3 17 147

Table of Contents

Introduction 3
Statement of Work 4
Survey of Atmospheric Radiation Components 5
Improvement of Propagation Codes and Cross Sections 6
Cosmic Ray Heavy Ions Below 50,000 Feet 7
Neutron-Induced Single Event Upsets in the Atmosphere 7
List of Papers, Reports, and Summaries 8
List of Conferences Attended 9
Electron Capture Decay of Cosmic Rays A-1
Cosmic Ray Heavy Ions at and Above 40,000 Feet A-16
Neutron Generated Single-Event Upsets in the Atmosphere A-18
Nuclear Cross Sections, Cosmic Ray Propagation and Source Composition A-20
Radiation Transport of Cosmic Ray Nuclei in Lunar Material and Radiation Doses A-41
Non-Geometric Behavior of Nucleus-Nucleus Total Inelastic Cross Sections A-50
Environmental Models for Single Event Upset Estimation A-58
Uncertainties in Cosmic Ray Source Composition A-71
Late Stage in Acceleration of Cosmic Rays A-72
Ultraheavy Cosmic Rays and Electron Capture A-73
Propagation of Heavy Cosmic Ray Nuclei A-74
On the Abundances of Ultraheavy Cosmic Rays A-86
LET-Distributions and Doses of HZE Radiation Components at Near-Earth Orbits A-90
Radiation Doses and LET Distributions of Cosmic Rays A-95

Introduction

The following is the final report of research performed for the Gamma and Cosmic Ray Astrophysics Branch, Space Science Division, Naval Research Laboratory under contract number N00014-84-C-2089. The work was performed by Severn Communications Corporation, Severna Park, Maryland from 28 Feb 1984 through 28 Mar 1985. The principal investigator in this effort was Dr. John R. Letaw.

The research results of this contract are contained in reports and publications appearing during the period of performance of this contract, and in the months following. Papers referenced in this report are contained in Appendices at the end.

Statement of Work

Background:

The Gamma and Cosmic Ray Astrophysics Branch of the Space Science Division plans to extend the current work on the atmospheric radiation environment and to contract the Severn Communications Corporation for the continuing employment of Dr. John R. Letaw as the on-site contractor scientist.

Scope:

The contractor shall provide 12 man-months of on-site technical service to the Space Science Division in the area of radiation effects in the atmosphere from cosmic ray components. The contractor will have the use of the NRL library and computer facilties including the VAX at Space Science Division.

Tasks:

1. Conduct a literature search to determine the current knowledge of the effect of atmospheric radiation components on semiconductor materials at various air depths. Emphasis shall be placed on the production of secondary particles and their interactions with matter.

2. Improve propagation and cross section codes for more reliable estimation of the radiation components from cosmic ray nuclei.

3. Calculate the cosmic ray fluxes and LET spectra as a function of zenith and azimuthal angles for various geomagnetic latitudes at depths below 50,000 feet.

4. Estimate the neutron fluxes and related LET spectra due to their interactions with matter.

Survey of Atmospheric Radiation Components

Our analysis of atmospheric radiation components showed several sources of radiation which can be of imnportance in causing single event upsets. These are:

1) Heavy Ions
2) Neutrons
3) Cosmic Ray Protons
4) Secondary Protons
5) Pions
6) Muons

Our survey of these radiation components is presented in the paper "Neutron Generated Single Event Upsets in the Atmosphere." We find that devices are affected by the radiation components in the order specified.

Heavy ions are the most important cause of SEUs at high altitudes (above 50,000 feet). The heavy ions are rapidly attenuated in the atmosphere by nuclear fragmentation collisions with nitrogen and oxygen nuclei. The resulting fragmentation products include many neutrons and secondary protons. Neutrons are the main cause of SEUs (from atmospheric radiation components) between sea level and 50,000 feet. Pions make only a small contribution to the upset rate.

In very sensitive devices, capable of being affected by minimum ionizing particles, the outlook is slightly different. In this case, at high altitudes protons are the dominant source of upsets. Below about 20,000 feet muons dominate the upset rate.

Accesion For
NTIS CRA&I ☑
DTIC TAB ☐
Unannounced ☐
Justification
By ltr. on file
Distribution /
Availability Codes
Dist | Avail and / or Special
A-1

QUALITY INSPECTED 3

Improvement of Propagation Codes and Cross Sections

Over the duration of this contract several major improvements in propagation codes were completed. These were:

1) Increasing the modularity of code resources allowing for more versatility in application.

2) Development of routines for studying propagation of cosmic rays through virtually an material.

3) Development of a treatment of fragmentation cross sections of heavy nuclei.

4) Estimation of error correlations in cosmic ray propagation.

5) Evaluation of inhomogenity in target media and its affects on electron capture isotopes.

The first two accomplishments were validated in several applications. Calculations of fragmentation of Kr and Ho beams in water and CR-39 were performed and delivered to Dr. James H. Adams for comparison with his measurements. Calculations of cosmic ray propagation in the lunar regolith were reported in "Radiation Transport of Cosmic Rays in Lunar Material and Cosmic Ray Doses."

An improvement to Karol's soft spheres model of nuclear reaction cross sections (P.J. Karol, Phys. Rev. C, 11, 1203 (1975)) has been developed for use in estimating total inelastic cross sections in nucleus-nucleus cross sections. This work has been discussed in "Non-Geometric Behavior of Nucleus-Nucleus Total Inelastic Cross Sections". Using these cross sections and the NRL semiempirical formulas (YIELDX and SCALAR) allows estimates of fragmentation parameters for cosmic rays in any material to be computed and normalized to be consistent with overall fragmentation probability.

Error correlations were discussed in preliminary form in "Uncertainties in Cosmic Ray Composition." A talk on this subject was presented at the 1984 American Astronomical Society Meeting. Further details are to be presented in the Proceedings of the 19th International Cosmic Ray Conference (Summer, 1985).

Electron capture decay has been reviewed in "Electron Capture Decay of Cosmic Rays" to be published in Fall, 1985 in Astrophysics and Space Science. Within this paper we demonstrated that electron capture decay is an important factor in the intergalactic propagation of ultraheavy cosmic rays. Elemental abundances of several rare earth elements can vary by factors of two or three if electron capture decay occurs. In addition, there are several isotopes occuring in cosmic rays whose abundances are dependent on density inhomogeneities in the interstellar medium.

Cosmic Ray Heavy Ions Below 50,000 Feet

Our results on this task are discussed in detail in "Cosmic Ray Heavy Ions at and above 40,000 Feet." In this work, results for cosmic ray heavy ions in the atmosphere which were reported in the Final Report on NRL contract number N00014-83-C-2042 have been extended down to 40,000 feet altitude. At this level it was found that neutrons are the dominant cause of single event upsets in most microcircuits.

Neutron Generated Single Event Upsets in the Atmosphere

Our results on this task are discussed in detail in "Neutron-Generated Upsets in Shielded Computer Components." In this paper we demonstrate the importance of heavy ion secondaries emanating from high energy neutron collisions in silicon. These secondaries have been neglected in previous treatments of neutron generated upsets. Energy deposition rates for high energy neutrons were computed.

A simple model of neutrons in the atmosphere was defined based on measurements and Monte Carlo nuclear transport codes. This model was a function of altitude, geomagnetic cutoff, and phase in the solar cycle. Combined with energy deposition curves, some estimates of single event upset rates were made.

List of Papers, Reports and Summaries

The following papers were written during the contract period:

"Electron Capture Decay of Cosmic Rays," (to appear in Astrophysics and Space Science, November, 1985)

"Cosmic-Ray Heavy Ions at and Above 40,000 Feet," IEEE Transactions on Nuclear Science, **NS-31**, 1066 (1984)

"Neutron-Generated Upsets in Shielded Computer Components," IEEE Transactions on Nuclear Science, **NS-31**, 1183 (1984)

"Nuclear Cross Sections, Cosmic Ray Propagation and Source Composition," (to appear in NATO Advanced Studies Series, ed. M.M.-Shapiro, Reidel Publishing Company, Dordrecht, Holland, 1985)

"Radiation Transport of Cosmic Ray Nuclei in Lunar Material and Radiation Doses," Proceedings of the Symposium on Lunar Bases and Space Activities (1984, in press)

"Non-Geometric Behavior of Nucleus-Nucleus Total Inelastic Cross Sections," (unpublished).

"Environmental Models for Single Event Upset Estimation," Proceedings of the Spacecraft Anomalies Conference, 274 (1984)

"Late Stage in Acceleration of Cosmic Rays," Bulletin of the American Physical Society, **29**, 735 (1984)

"Ultraheavy Cosmic Rays and Electron Capture Decay," Bulletin of the American Physical Society, **29**, 735 (1984)

"Uncertainties in Cosmic Ray Source Composition," Bulletin of the American Astronomical Society, **16**, 448 (1984)

The following papers were completed and appeared in published form:

"Propagation of Heavy Cosmic Ray Nuclei," Astrophysical Journal Supplements, **56**, 369 (1984)

"On the Abundances of Ultraheavy Cosmic Rays," Astrophysical Journal, **279**, 144 (1984)

"Radiation Doses and LET Distributions of Cosmic Rays," Radiation Research, **98**, 209 (1984)

"LET-Distributions and Doses of HZE Radiation Components at Near-Earth Orbits," Advances in Space Research, **4**, 143 (1984)

List of Conferences Attended

Spring Meeting of the American Physical Society, Crystal City, Virginia, 24-27 April 1984.
Presented a paper entitled "Ultraheavy Cosmic Rays and Electron Cpature Decay"

164th Meeting of the American Astronomical Society, Baltimore, Maryland, 10-13 June 1984.
Presented a paper entitled "Uncertainties in Cosmic Ray Source Composition"

Spacecraft Anomalies Conference, Colorado Springs, Colorado, 30-31 October 1984.
Presented a paper entitled "Environmental Models for Single Event Upset Estimation"

Neutral Particle Beams Lethality/Emissions Computer Codes Workshop, Air Force Weapons Laboratory, Albuquerque, New Mexico, 1 November 1984.
Presented a paper entitled "NRL Energy Deposition Codes"

Third Annual DOD/DOE/NASA Symposium on Single Event Effects, Los Angeles, California, 5-6 March 1985.
Presented a paper entitled "Single Event Upsets in Fractional Orbits"

Electron Capture Decay of Cosmic Rays

John R. Letaw
Severn Communications Corporation
Severna Park, Maryland 21146

and

J.H. Adams, Jr., Rein Silberberg, and C.H. Tsao
E.O. Hulburt Center for Space Research
Naval Research Laboratory
Washington, D.C. 20375

Rein Silberberg
Naval Research Lab
Code 4154
Washington, DC 20375
202 767-2965

Abstract

Cosmic ray nuclei are close to fully ionized during their passage through he galaxy. Electron capture decay is rare among these nuclides because most do not have bound electrons. Under certain conditions, specifically low energies and/or high charges, electron capture becomes an essential factor in determining cosmic ray composition. In this paper we discuss the general nature of electron capture decay in cosmic rays and describe specific measurements which can reveal the existence of electron capture decay, and energy and density-dependent processes in the interstellar medium.

1. Introduction

Among the cosmic ray nuclides which are stable, or nearly stable, in their passage through the galaxy, roughly 1/3 are unstable to electron capture decay (Letaw, Silberberg, and Tsao, 1984). In spite of their numerical prominence, there is little compositional evidence for the decay of the electron capture nuclides in cosmic rays. The best measured cosmic ray nuclides ($Z < 30$) have a mean free path for electron attachment much greater than their mean pathlength in the galaxy. Electron capture decay can therefore have little effect on isotopic or elemental abundances in this charge range. Measurements of higher charges have so far been restricted to elements or groups of elements. Electron capture decays in this charge range, though possible, are undetected in present observations either because the relative number of electron capture nuclides is small or because cancellation occurs among neighboring elements.

The study of electron capture decay of cosmic ray nuclei began with Yiou and Raisbeck (1970) who treated the nuclide ^{7}Be. They demonstrated that the effects of electron capture decay on the abundance of this nuclide appear below 20 MeV/nucleon (MeV/N) outside the heliosphere. Detection at this low energy is impossible within the heliosphere because of solar modulation. Similar conclusions apply to other light, secondary nuclei such as ^{37}Ar, ^{41}Ca, ^{49}V, ^{51}Cr, and ^{55}Fe in standard propagation models. For these nuclides, at cosmic ray energies, so little attachment occurs that they are nearly stable.

Recently it has been noted (Silberberg et al., 1983) that if cosmic rays undergo acceleration during or after secondary production, many anomalies in cosmic ray composition are resolved. Such an acceleration, which is determined to be about a factor of 4 in kinetic energy, would allow observation of electron capture decay among some secondary nuclei at about 600 MeV/N. Measurements of ^{37}Ar, ^{49}V, and ^{51}Cr (Webber, 1981) are consistent with this model and roughly one standard deviation below predictions of the standard model. The nuclides ^{41}Ca and ^{55}Fe are obscured by nearby, abundant isotopes.

Long-lived electron capture nuclei, such as ^{53}Mn, behave as cosmic ray "clocks" if they have attached electrons (Reames, 1970) and their lifetime is comparable to the cosmic ray confinement time of about 10^{7} years. Except at unobservably low energies electron attachment to ^{53}Mn is too rare to affect composition. If the mean density of interstellar gas were several orders of magnitude larger or there were substantial inhomogeneities in regions of cosmic ray propagation, then nuclei with shorter lifetimes would make appropriate "clocks" or "hydrometers" (Raisbeck et al., 1975).

The possibility of electron capture decay among primary cosmic rays prior to their principal acceleration has been explored by Soutoul, Casse, and Juliusson (1978) for the case of Fe, Co, and Ni. Prior to acceleration these nuclides have energies less by a factor of 1000 than their propagation energy. At such low energies the nuclides ^{57}Co, ^{56}Ni, and ^{59}Ni easily attach electrons. Their decay causes variations in the Co/Ni ratio for pre-acceleration times of up to 10^{5} years. Results, in principle, can reveal the time between nucleosynthesis and cosmic ray acceleration. Measurements are consistent with full decay prior to acceleration, but inconclusive about the delay between nucleosynthesis and acceleration. A measurement of the abundance of ^{44}Ti might eliminate the possibility of a short delay (Shapiro and Silberberg, 1975).

One notable deficiency in the literature of electron capture decay in cosmic rays is a discussion of ultraheavies having charges $Z > 30$. These nuclides are potentially of great interest because the rate of electron attachment increases rapidly with charge. They therefore decay at median cosmic ray energies of 1 or 2 GeV/N. Electron capture nuclides in this charge range are common enough that even elemental abundances can be affected by their decay. Thus we expect large variations in some elemental abundances with energy.

In this paper we present a general discussion of the nature of electron capture decay of cosmic rays. The treatment of the decay process begins with rate equations governing the attachment and stripping of electrons from nuclei, and the decay of these nuclei. The solution of these rate equations yields four general conclusions:

1) Multiple electron attachment may be ignored for all cosmic rays except actinides.

2) Cosmic rays approach statistical charge state equilibrium at a rate greater than the electron stripping rate.

3) Cosmic rays approach statistical charge state equilibrium at a rate greater than their effective electron capture rate.

4) Cosmic rays maintain statistical charge state equilibrium relative to other physical processes affecting composition.

With the above general conclusions a simplified treatment of electron capture decay in cosmic ray propagation is possible. This reveals two general classes of electron capture nuclides: attachment-limited and capture-limited. Attachment-limited nuclides decay rapidly once they attach an electron. Since attachment depends only on the total quantity of matter passed through, these nuclides reveal nothing about the interstellar matter density. The strong energy dependence of the attachment mean free path,

however, implies strong energy dependence of abundance, making these nuclides useful for identifying energy dependent processes in cosmic ray propagation. Capture-limited nuclides have long electron capture lifetimes and hence, once an electron is attached, behave as other unstable nuclides. These nuclides are typical cosmic ray clocks and may be used to measure the density of interstellar matter. ^{59}Ni and ^{81}Kr are potentially important capture-limited electron capture nuclides.

In Section 3, we present results of cosmic ray propagations incorporating the electron capture decay process. Our results demonstrate that it is essential to include electron capture decay in cosmic ray propagation calculations as some elemental abundances are affected by several hundred percent. We also demonstrate the strong energy dependence of isotopic and elemental abundances of ultraheavy cosmic rays due to electron capture decay modes. We conclude that electron capture nuclides effectively identify acceleration processes occuring at all energies in cosmic ray propagation. They are an important tool for studying solar modulation and distributed acceleration (Silberberg et al., 1983) both of which involve significant energy shifts.

In Section 4 we discuss the effect of inhomogeneities in the ISM on electron capture nuclides in cosmic rays. In a two component ISM these nuclides can be capture-limited in the denser regions and attachment-limited in the rarefied regions. In the dense regions (or clouds) decay is inhibited because stripping is rapid, whereas in the rarefied regions little decay occurs because attachment is rare. In a homogeneous ISM the decay rate is maximized because the fraction of nuclides with an electron attached compounded with the time for decay is maximized. Thus, the existence or absence of these nuclides in cosmic rays indicate the nature of inhomogeneities in the propagation region.

2. Decay Model and General Results

We model the electron capture decay of cosmic rays using the following rate equations:

$$dN/dt = -aN + sN^* - dN \qquad (1)$$

$$dN^*/dt = aN - sN^* - (d + e)N^* \qquad (2)$$

Here, N and N^* represent the abundances of a nuclide fully ionized and with a single electron attached, respectively. The attachment and stripping rates are a and s, respectively. d is the decay rate for all non-electron capture modes and e is the effective decay rate for electron capture. e is roughly one-half the laboratory decay rate because cosmic rays usually have only one K-shell electron to be captured (Wilson, 1978).

The attachment and stripping mean free paths, λ_a and λ_s, are computed using the results of Wilson (1978) and Crawford (1979). They are shown in Figures 1 and 2 as a function of charge and energy. λ_a and λ_s are independent of the density of the interstellar medium; hence so long as the electron capture process is dominated by attachment and stripping, electron capture nuclides cannot be used as cosmic ray "clocks" or "hydrometers". Attachment and stripping rates are used in Equations (1) and (2) for convenience. For purposes of this paper it is only necessary to recognize that they are inversely proportional to their corresponding mean free paths.

Implicit in the rate equations is the assumption that multiple electron attachment never occurs in cosmic rays and that nuclear fragmentation cannot affect the decay process. These assumptions are justified in what follows.

An exact solution to the rate equations can be obtained. Solving only for the ratio (N^*/N) one finds that it approaches an equilibrium value:

$$(N^*/N)_{eq} = \left(\sqrt{(s+e-a)^2 + 4as} - (s+e-a)\right)\Big/2s \qquad (3)$$

at the rate

$$R^* = \sqrt{(s-a+e)^2 + 4as} \qquad (4)$$

The equilibrium described here is statistical, that is, although at any time the number of nuclei which have attached electrons is constant, stripping and attachment rapidly alter the state of a given nucleus. Analysis of this solution leads to general conclusions about the decay process in cosmic ray propagation.

Proposition 1: Multiple electron attachment may be ignored in models of cosmic ray electron capture decay, except for actinides.

The equilibrium charge ratio (3) takes the simple form

$$(N^*/N)_{eq} = a/s = \lambda_s/\lambda_a \qquad (5)$$

when there is no decay (e=0). Contours of this function (Figure 3) show that it is much less than one for all nuclides except actinides, and ultraheavies with $70 < Z < 83$ and energies well below the spectral peak. Including decay substantially decreases the equilibrium charge ratio of the ultraheavies. The fraction of nuclei with multiple electrons is roughly the square of the fraction with a single electron, implying that multiple attachment may be ignored except when the equilibrium charge ratio is close to one. Recent measurements on Cu (Gould et al., 1984) confirm theoretical estimates of the equilibrium charge.

Proposition 2: Equilibrium charge ratio is approached at least at the stripping rate s.

This result follows directly from (4).

Proposition 3: Equilibrium charge ratio is approached at least at the effective decay rate e, if $s > a$.

This result follows directly from (4). The restriction $s > a$ is satisfied for most cosmic rays, exceptions occuring where the equilibrium charge ratio in Figure 3 is greater than one.

Proposition 4: Cosmic rays are effectively always in statistical charge state equilibrium.

For cosmic rays the escape mean free path is roughly 7 g/cm^2 and the fragmentation mean free path is never less than 0.75 g/cm^2. Electron stripping occurs with a mean free path less than (usually much less than) 0.2 g/cm^2. Charge state equilibrium is therefore attained much faster than other processes in cosmic ray propagation. This conclusion holds for actinides even though the equilibrium may involve more than two charge states.

When an electron capture nuclide is in charge state equilibrium Equations (1) and (2) may be summed to yield a single equation for the time evolution of the abundance

$$\frac{d(N^*+N)}{dt} = -\left[d + \frac{e(N^*/N)_{eq}}{1+(N^*/N)_{eq}}\right](N^*+N) \qquad (6)$$

To this equation may be added additional effects such as fragmentation and ionization loss. The rapid process of electron attachment and stripping is reduced to the much slower effective decay process in Equation (6). Explicit treatment of charge states is avoided.

Two limiting cases of Eq. 6 may be described. We begin with the generic situation where $s + e \gg a$ and there is no decay mode other than electron capture ($d=0$):

$$\frac{d(N^*+N)}{dt} = -\frac{ae}{s+e}(N^*+N) \qquad (7)$$

If $e \gg a$, that is, if the rate of nuclear electron capture is much greater

than the rate of electron attachment, then the decay is attachment-limited. In this case as soon as an electron becomes available the nuclide is considered to decay. The effective decay rate is a, therefore the effective decay mean free path is the attachment mean free path as shown in Figure 1. The vast majority of cosmic ray electron capture nuclides are attachment-limited because attachment is slow in the tenuous interstellar medium while capture lifetimes are generally some small fraction of a year.

If $a \gg e$, that is, if the nuclear electron capture process proceeds much more slowly than the attachment and stripping of electrons, then the decay is capture-limited. In this case the nuclides behave as any other cosmic ray "clock" with an effective decay rate of $(a/s)e$. The suppression factor (a/s) is shown in Figure 3. ^{59}Ni and ^{81}Kr, with their somewhat shorter halflives, may eventually add to our information on cosmic ray confinement time.

3. Abundances of Electron Capture Nuclides in Cosmic Rays

The techniques described in the previous section have been incorporated into our standard cosmic ray propagation model (Letaw, Silberberg, and Tsao, 1984) and used to compute the cosmic ray elemental abundances at 600, 1000, 2500, and 5000 MeV/N. This demonstrates the overall importance of electron capture in cosmic ray propagation and the energy dependences introduced by this effect. In addition, elements which are particularly sensitive to electron capture decay may be identified.

Table 1 contains the abundances of cosmic rays with charges $Z = 26$ to $Z = 83$. In addition results of a calculation at 600 MeV/N where electron capture decays were not allowed are shown. Omitting electron capture decay at 5000 MeV/N has little effect on abundances. Immediately apparent from the Table is the necessity of incorporating electron capture decay into propagation calculations. This is a departure from lore acquired for elements lighter than Fe. The reason for the change can be found in Figure 1.

Since most cosmic ray electron capture decays are attachment-limited, the mean free path for decay may be taken from Figure 1. At 500 MeV/N or above (propagation energy) decay of nuclides lighter than Fe is inhibited because mean free paths exceed the 5 to 10 g/cm^2 mean cosmic ray pathlength. For higher charges electron capture rapidly becomes important, e.g., the mean free path for Pb at 1 GeV/N is about 0.1 g/cm^2. Also seen in Figure 1 is the strong energy dependence of the attachment mean free path. For elements around $Z = 40$ to 50 this variation allows full decay at 500 MeV/N while almost prohibiting decay at the highest energies. Decay of attachment-limited actinides is likely to proceed uninhibited at observed energies below 5 GeV/N. This energy dependence necessitates the detailed treatment given in Section 2.

Figures 4 and 5 show graphically the abundances of Eu and Dy, respectively, as calculated both including and omitting electron capture decay. Both figures show the strong energy dependence introduced by electron capture decay. In general the abundances of rare earth nuclides are increased relative to nuclides in the Pt/Pb peak by electron capture decay.

The hypothesis of distributed acceleration (Silberberg et al., 1983) states that, after their principal acceleration and much of their fragmentation interaction with the interstellar medium, cosmic rays receive additional acceleration amounting to about a factor of 4 increase in kinetic energy. With this hypothesis several anomalies in cosmic ray composition are explained. Electron capture nuclides present a clear test of this hypothesis. Whereas the standard model predicts observed abundances at 2500 MeV/N as in Table 1, distributed acceleration predicts abundances at 2500 MeV/N to be similar to those of the standard model at 600 MeV/N. With Eu this represents a difference of a factor of 2 in observed abundance.

4. Propagation in an Inhomogeneous Interstellar Medium

The standard model of cosmic ray propagation (see, for example, Letaw, Silberberg, and Tsao, 1984) assumes the propagation medium is homogeneous and that elapsed time is proportional to the amount of matter traversed. Fragmentation, and therefore the abundances of most cosmic rays, is insensitive to this assumption. Measurements of at least two unstable nuclei (for example, ^{10}Be and ^{26}Al) are needed to test the assumption of homogeneity. Present data (Wiedenbeck, 1983) are incapable of resolving even the most extreme inhomogeneity in the galaxy.

Realistic models of the ISM (e.g., McKee and Ostriker, 1977) suggest that most of the galaxy is filled with hot, tenuous gas having a density of roughly 0.003 atoms/cm^3. Roughly 20% of space is filled with warm clouds (density about 0.25 atoms/cm^3) having cold cores of much higher density (about 40 atoms/cm^3). In these models cosmic rays must encounter large inhomogeneities to accumulate sufficient grammage to produce observed secondaries. Within the clouds the electron capture decay rate will be much greater than in the hot, tenous regions if the transition from attachment-limited to capture-limited decay has occured. The transition is sensitive to both density and cosmic ray energy. While the decay rate is higher in dense regions, the mean pathlength needed for decay is actually lower. Less decay occurs in an inhomogeneous medium than in a homogeneous medium. In this section we describe the influence of inhomogeneity on cosmic-ray electron-capture nuclides.

The effective mean free path and mean time for decay extracted from the generally valid Eq. 7 are

$$\lambda_{eff} = \lambda_a [1+kn_H\tau/\lambda_s] \quad (8)$$

$$\tau_{eff} = \lambda_{eff}/kn_H \quad (9)$$

where kn_H is the conversion from time to pathlength (we use $kn_H = 2.9 \times 10-^{6}8$ (g/cm^2)/year when n_H is the ISM density in atoms/cm^3) and τ is the mean time for decay with one electron attached:

A-1

$$\tau = 2\gamma\tau_{1/2}/\ln 2 \quad (10)$$

Graphs of λ_{eff} and τ_{eff} are shown in Figures 6 and 7 for ^{44}Ti at 100 MeV/N. Note that for low densities the decay is attachment-limited and the effective decay mean free path is independent of density. For high densities (capture-limited decay) the effective mean decay time is independent of density. The transition density in this example is 12.4 g/cm^2. In general

$$n_{Ht} = \lambda_s/k\tau \quad (11)$$

n_{Ht}, and λ_{eff} and τ_{eff} at low and high densities, are tabulated for ^{44}Ti at several energies in Table 2. At intermediate densities λ_{eff} and τ_{eff} are the sum of the high and low density parts. In particular, at transition density, λ_{eff} is twice the low density value and τ_{eff} is twice the high density value.

From Table 2 we observe that very little ^{44}Ti decays in cosmic rays at E > 500 MeV/N. The minimum pathlength required for decay is λ_{eff} at low density, 19.4 g/cm^2, which is much greater than the cosmic ray escape

pathlength. In order to observe inhomogeneity, ^{44}Ti must undergo the transition from low density (slow decay) to high density (rapid decay) in the ISM. The transition density is roughly independent of energy and about 12 atoms/cm^3. ^{44}Ti is a "hydrometer" showing fundamentally different behavior if densities greater than this are encountered.

As an example consider a two component medium consisting of hot,tenuous gas at 0.003 atoms/cm^3 and clouds with 40 atoms/cm^3. In our model the total grammage traversed in the tenuous gas in 10^7 years is less than 0.1 g/cm^2. From Table 2, ^{44}Ti in low density regions cannot decay over this pathlength for energies of 50 MeV/N or more. Essentially all decay must take place in clouds. At 100 MeV/N the mean pathlength required for decay is 1.9 g/cm^2 (about 4×10^4 years in this model), therefore substantial decay occurs in the clouds where most of the grammage is encountered. In contrast with the two-component model, the mean pathlength required for decay in a homogeneous galaxy is 0.6 g/cm^2 at 100 MeV/N. Significantly more decay is possible in a homogeneous galaxy than in an inhomogeneous galaxy.

The surviving fractions of three nuclides sensitive to density inhomogeneities - ^{44}Ti, ^{93}Mo, and ^{157}Tb - are shown as a function of energy in Figures 8, 9, and 10. Results were based on the assumed density of 0.003 atoms/cm^3 in the hot, tenuous phase of the galaxy using an energy-dependent mean path-length. The curves are labeled according to the assumed (uniform) cloud density in the galaxy. As expected, the lighter elements are most sensitive to this electron capture effect at low energies, while variations in heavier elements may occur above 1 GeV/N. This is associated with the increased binding energy of higher charged ions. The region of sensitivity to cloud densities depends both on the charge and lifetime of the nuclide. ^{93}Mo is very sensitive to expected density enhancements in the ISM. One therefore hopes that the next generation of cosmic-ray-isotope experiments might extend to Z=42. ^{91}Nb is also sensitive to density enhancements; however, its halflife is unknown so detailed predictions cannot yet be made.

5. Summary

We began this paper with a brief review of previous work on the problem of electron capture decay in cosmic rays. There is presently little evidence of electron capture because of limitations on experimental isotopic and charge resolution, and because low energy cosmic rays are not observed in the heliosphere. Electron capture nuclides are potentially important for identifying energy and density-dependent processes in cosmic ray propagation.

In Section 2 we presented a formulation of the electron stripping and attachment problem in terms of one effective equation. This equation uses the concept of charge state equilibrium which integrates the effect of very rapid stripping and attachment reactions. Two important classes of electron capture decay are identified: attachment-limited, where decay rate is determined by the electron pickup rate, and capture-limited, where decay rate is determined by the nuclear K-capture rate.

The remaining sections demonstrate astrophysical conditions where electron capture nuclides are useful in elucidating physical processes in the ISM. In Section 4 we show that some elemental abundances, especially rare earths, are very sensitive to the energy of propagation. They may be used to identify such processes as distributed acceleration where significant acceleration of cosmic rays occurs after most secondary formation. In Section 5 we show that some nuclides (^{44}Ti, ^{91}Ni, ^{93}Mo, and ^{157}Tb) have decay rates determined by cloud densities in the ISM.

References

Crawford, H.J.: 1979, Ph.D. Thesis, Univ. of California (Berkeley).

Gould, H.A.: 1984, Phys. Rev. Lett. 52, 180.

Letaw, J.R., Silberberg, R., and Tsao, C.H.: 1984, "Propagation of Heavy Cosmic Ray Nuclei" (to appear in Ap. J. Suppl.)

McKee, C.F. and Ostriker, J.P.: 1977, Ap. J. 218, 148.

Raisbeck, G.M., Comstock, G., Perron, C., and Yiou, F.: 1975, Proc. 15th Int. Cosmic Ray Conf. (Munich) 2, 560.

Reames, D.V.: 1970, Ap. J. 162, 837.

Shapiro, M.M. and Silberberg, R.: 1975, Proc. 15th Int. Cosmic Ray Conf. (Munich) 2, 538.

Silberberg, R., Tsao, C.H., Letaw, J.R., and Shapiro, M.M.: 1983, Phys. Rev. Lett. 51, 1217.

Soutoul, A., Casse, M., and Juliusson, E.: 1978, Ap. J. 219, 753.

Webber, W.R.: 1981, Proc. 17th Int. Cosmic Ray Conf. (Paris) 2, 80.

Wiedenbeck, M.E.: 1983, Proc. 18th Int. Cosmic Ray Conf. (Bangalore) OG2-53 (late papers).

Wilson, L.W.: 1978, Ph.D. Thesis, Univ. of California (Berkeley).

Yiou, F. and Raisbeck, G.M.: 1970, Ap. Lett. 7, 129.

Table I

Cosmic Ray Elemental Abundances

	No EC	Electron Capture Decay Included			
	600 MeV/N	600 MeV/N	1000 MeV/N	2500 MeV/N	5000 MeV/N
Fe	1.0×10^{6}	1.0×10^{6}	1.0×10^{6}	1.0×10^{6}	1.0×10^{6}
Co	5.8×10^{3}	5.6×10^{3}	5.6×10^{3}	5.3×10^{3}	5.1×10^{3}
Ni	5.3×10^{4}	5.4×10^{4}	5.4×10^{4}	5.5×10^{4}	5.5×10^{4}
Cu	6.7×10^{2}	6.8×10^{2}	6.7×10^{2}	6.6×10^{2}	6.5×10^{2}
Zn	8.3×10^{2}	8.4×10^{2}	8.4×10^{2}	8.4×10^{2}	8.3×10^{2}
Ga	7.4×10^{1}	7.5×10^{1}	7.4×10^{1}	7.3×10^{1}	6.9×10^{1}
Ge	1.5×10^{2}	1.5×10^{2}	1.5×10^{2}	1.5×10^{2}	1.4×10^{2}
As	1.1×10^{1}	1.1×10^{1}	1.1×10^{1}	1.1×10^{1}	9.9×10^{0}
Se	5.6×10^{1}	5.6×10^{1}	5.7×10^{1}	5.8×10^{1}	5.4×10^{1}
Br	9.9×10^{0}	1.0×10^{1}	1.0×10^{1}	1.0×10^{1}	9.2×10^{0}
Kr	2.7×10^{1}	2.8×10^{1}	2.8×10^{1}	2.8×10^{1}	2.6×10^{1}
Rb	1.3×10^{1}	1.3×10^{1}	1.3×10^{1}	1.3×10^{1}	1.3×10^{1}
Sr	3.9×10^{1}	3.9×10^{1}	4.0×10^{1}	4.1×10^{1}	4.0×10^{1}
Y	6.8×10^{0}	6.8×10^{0}	7.1×10^{0}	7.1×10^{0}	7.0×10^{0}
Zr	1.5×10^{1}	1.5×10^{1}	1.6×10^{1}	1.6×10^{1}	1.6×10^{1}
Nb	2.2×10^{0}	2.3×10^{0}	2.7×10^{0}	2.6×10^{0}	2.4×10^{0}
Mo	5.2×10^{0}	5.5×10^{0}	6.2×10^{0}	6.0×10^{0}	5.6×10^{0}
Tc	1.4×10^{0}	1.3×10^{0}	1.7×10^{0}	1.7×10^{0}	1.5×10^{0}
Ru	5.3×10^{0}	5.7×10^{0}	6.5×10^{0}	5.8×10^{0}	5.3×10^{0}
Rh	1.5×10^{0}	1.5×10^{0}	1.8×10^{0}	1.6×10^{0}	1.4×10^{0}
Pd	5.1×10^{0}	4.8×10^{0}	5.7×10^{0}	4.9×10^{0}	4.4×10^{0}
Ag	1.4×10^{0}	1.8×10^{0}	1.9×10^{0}	1.4×10^{0}	1.3×10^{0}
Cd	3.9×10^{0}	4.3×10^{0}	4.7×10^{0}	3.9×10^{0}	3.5×10^{0}
In	1.6×10^{0}	1.4×10^{0}	1.6×10^{0}	1.5×10^{0}	1.3×10^{0}
Sn	8.6×10^{0}	9.1×10^{0}	9.6×10^{0}	8.2×10^{0}	7.7×10^{0}
Sb	1.2×10^{0}	1.2×10^{0}	1.2×10^{0}	1.0×10^{0}	9.4×10^{-1}
Te	5.3×10^{0}	5.7×10^{0}	5.8×10^{0}	5.0×10^{0}	4.8×10^{0}
I	1.7×10^{0}	1.3×10^{0}	1.5×10^{0}	1.4×10^{0}	1.3×10^{0}

Table I continued

Cosmic Ray Elemental Abundances

	No EC	Electron Capture Decay Included			
	600 MeV/N	600 MeV/N	1000 MeV/N	2500 MeV/N	5000 MeV/N
Xe	4.0×10^{0}	4.0×10^{0}	4.2×10^{0}	3.5×10^{0}	3.2×10^{0}
Cs	5.7×10^{-1}	8.5×10^{-1}	8.1×10^{-1}	6.6×10^{-1}	6.1×10^{-1}
Ba	6.7×10^{0}	6.5×10^{0}	6.7×10^{0}	6.4×10^{0}	6.3×10^{0}
La	6.9×10^{-1}	8.0×10^{-1}	8.2×10^{-1}	7.1×10^{-1}	6.8×10^{-1}
Ce	1.9×10^{0}	1.8×10^{0}	2.0×10^{0}	1.8×10^{0}	1.8×10^{0}
Pr	4.0×10^{-1}	4.1×10^{-1}	4.4×10^{-1}	3.5×10^{-1}	3.3×10^{-1}
Nd	1.4×10^{0}	1.6×10^{0}	1.6×10^{0}	1.3×10^{0}	1.3×10^{0}
Pm	3.0×10^{-1}	1.7×10^{-1}	2.7×10^{-1}	2.4×10^{-1}	2.2×10^{-1}
Sm	1.5×10^{0}	1.4×10^{0}	1.5×10^{0}	1.1×10^{0}	1.0×10^{0}
Eu	1.6×10^{-1}	3.9×10^{-1}	3.5×10^{-1}	2.0×10^{-1}	1.7×10^{-1}
Gd	9.2×10^{-1}	1.1×10^{0}	1.0×10^{0}	8.0×10^{-1}	7.5×10^{-1}
Tb	2.5×10^{-1}	2.7×10^{-1}	2.7×10^{-1}	1.9×10^{-1}	1.8×10^{-1}
Dy	1.1×10^{0}	1.4×10^{0}	1.4×10^{0}	9.2×10^{-1}	8.2×10^{-1}
Ho	5.4×10^{-1}	3.3×10^{-1}	3.6×10^{-1}	3.0×10^{-1}	2.9×10^{-1}
Er	7.4×10^{-1}	9.2×10^{-1}	8.4×10^{-1}	5.6×10^{-1}	5.1×10^{-1}
Tm	1.9×10^{-1}	2.0×10^{-1}	1.8×10^{-1}	1.2×10^{-1}	1.1×10^{-1}
Yb	9.5×10^{-1}	1.0×10^{0}	8.8×10^{-1}	5.9×10^{-1}	5.4×10^{-1}
Lu	5.9×10^{-2}	2.1×10^{-1}	1.8×10^{-1}	1.0×10^{-1}	7.2×10^{-2}
Hf	8.8×10^{-1}	9.1×10^{-1}	7.6×10^{-1}	5.1×10^{-1}	4.6×10^{-1}
Ta	3.0×10^{-2}	1.6×10^{-1}	1.1×10^{-1}	5.3×10^{-2}	3.6×10^{-2}
W	6.2×10^{-1}	6.6×10^{-1}	5.4×10^{-1}	3.6×10^{-1}	3.1×10^{-1}
Re	3.3×10^{-1}	2.1×10^{-1}	1.8×10^{-1}	1.5×10^{-1}	1.5×10^{-1}
Os	1.1×10^{0}	9.8×10^{-1}	8.2×10^{-1}	6.6×10^{-1}	6.1×10^{-1}
Ir	5.0×10^{-1}	4.9×10^{-1}	4.2×10^{-1}	3.7×10^{-1}	3.7×10^{-1}
Pt	7.7×10^{-1}	1.0×10^{0}	8.6×10^{-1}	7.6×10^{-1}	7.5×10^{-1}
Au	2.0×10^{-1}	2.0×10^{-1}	1.7×10^{-1}	1.4×10^{-1}	1.3×10^{-1}
Hg	7.7×10^{-1}	6.0×10^{-1}	4.4×10^{-1}	4.0×10^{-1}	3.7×10^{-1}
Tl	2.9×10^{-1}	2.3×10^{-1}	1.9×10^{-1}	2.1×10^{-1}	2.2×10^{-1}
Pb	2.3×10^{0}	2.2×10^{0}	2.1×10^{0}	2.2×10^{0}	2.3×10^{0}
Bi	1.1×10^{-1}	9.4×10^{-2}	9.7×10^{-2}	1.0×10^{-1}	1.1×10^{-1}

Table II

Electron Capture Decay Parameters for ^{44}Ti (half-life = 47 years)

Energy (MeV/N)	Transition Density (g/cm^3)	Lifetime (years) Low Density (x n_H)	Lifetime (years) High Density	Pathlength (g/cm^2) Low Density	Pathlength (g/cm^2) High Density (/ n_H)
20	8.35	5.5×10^4	6.5×10^4	3.2×10^{-2}	3.9×10^{-3}
50	10.6	1.7×10^5	1.6×10^4	1.5×10^{-1}	1.4×10^{-2}
100	12.4	4.7×10^5	3.8×10^4	5.9×10^{-1}	4.7×10^{-2}
200	13.7	1.6×10^6	1.1×10^5	2.6	1.9×10^{-1}
500	13.0	8.8×10^6	6.8×10^5	1.9×10^1	1.5
1000	10.2	3.2×10^7	3.1×10^6	8.1×10^1	8.0
2000	6.59	9.5×10^7	1.5×10^7	2.6×10^2	4.0×10^1
5000	2.95	3.0×10^8	1.0×10^8	8.5×10^2	2.9×10^2

Figure Captions

Figure 1 : The mean free path for attachment of electrons to hydrogen-like ions in the interstellar medium (6.8% He). Curves are shown for 50, 100, 200, 500, 1000, 2000, 5000, and 10000 MeV/N. The mean free path increases monotonically for a given charge over this range of energies.

Figure 2 : The mean free path for stripping of electrons from hydrogen-like ions in the interstellar medium (6.8% He). Curves are shown for 50, 100, 200, 500, and 1000 MeV/N. The mean free path increases monotonically for a given charge over this range of energies. Between 1000 and 10000 MeV/N the mean free path is roughly independent of energy.

Figure 3 : The equilibrium charge ratio (N^*/N) of ions in the interstellar medium. When this ratio is greater than 1.0 there is appreciable multiple electron attachment.

Figure 4 : The arriving abundance of Eu (Z = 63) computed both including and omitting electron capture decay modes.

Figure 5 : The arriving abundance of Dy (Z = 66) computed both including and omitting electron capture decay modes.

Figure 6 : The effective mean free path for decay of ^{44}Ti as a function of density at 100 MeV/N.

Figure 7 : The effective mean free lifetime for decay of ^{44}Ti as a function of density at 100 MeV/N.

Figure 8 : Surviving fraction of ^{44}Ti (halflife = 47 years) as a function of energy for several cloud models as well as a homogeneous ISM.

Figure 9 : Surviving fraction of ^{93}Mo (halflife = 3000 years) as a function of energy for several cloud models as well as a homogeneous ISM.

Figure 10 : Surviving fraction of ^{157}Tb (halflife = 150 years) as a function of energy for several cloud models as well as a homogeneous ISM.

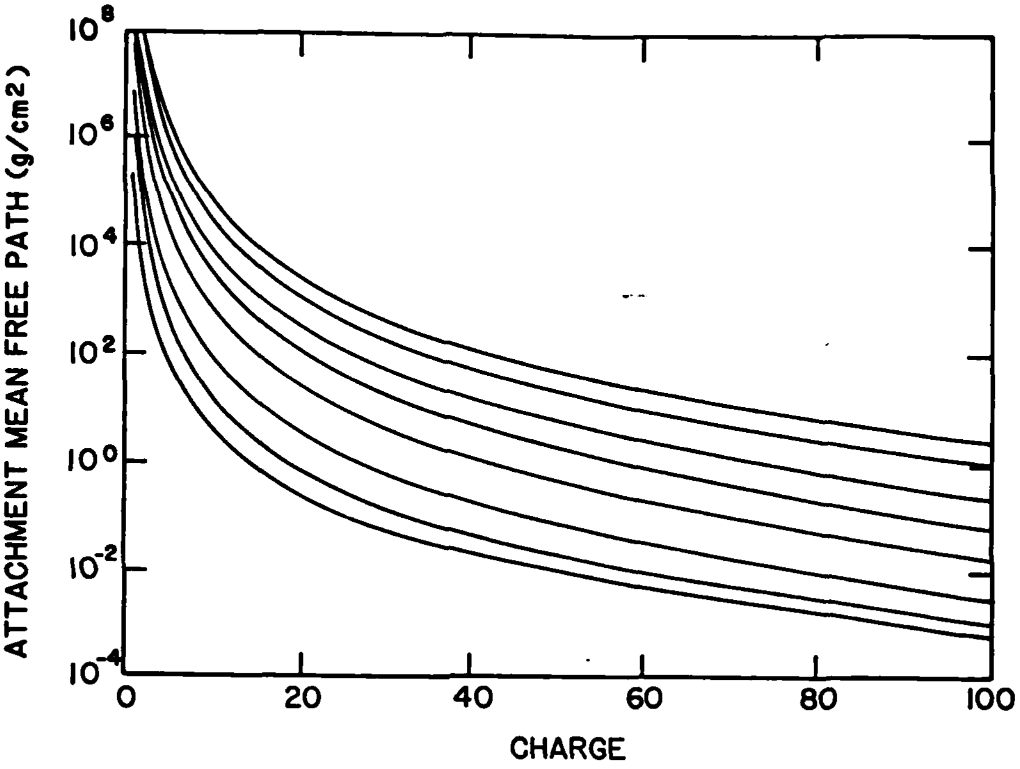

10^8
10^6
10^4
10^2
10^0
10^{-2}
10^{-4}
ATTACHMENT MEAN FREE PATH (g/cm2)
0
20
40
60
80
100
CHARGE

Fig. 1

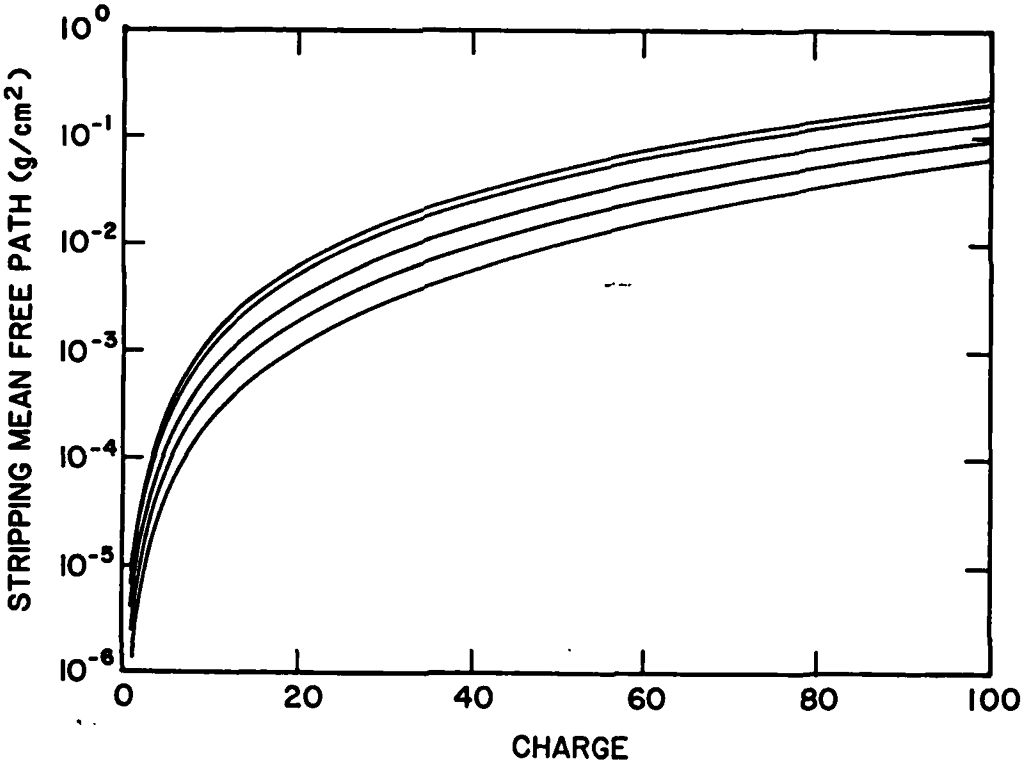

10^0
10^{-1}
10^{-2}
10^{-3}
10^{-4}
10^{-5}
10^{-6}
STRIPPING MEAN FREE PATH (g/cm^2)
0
20
40
60
80
100
CHARGE

Fig. 2

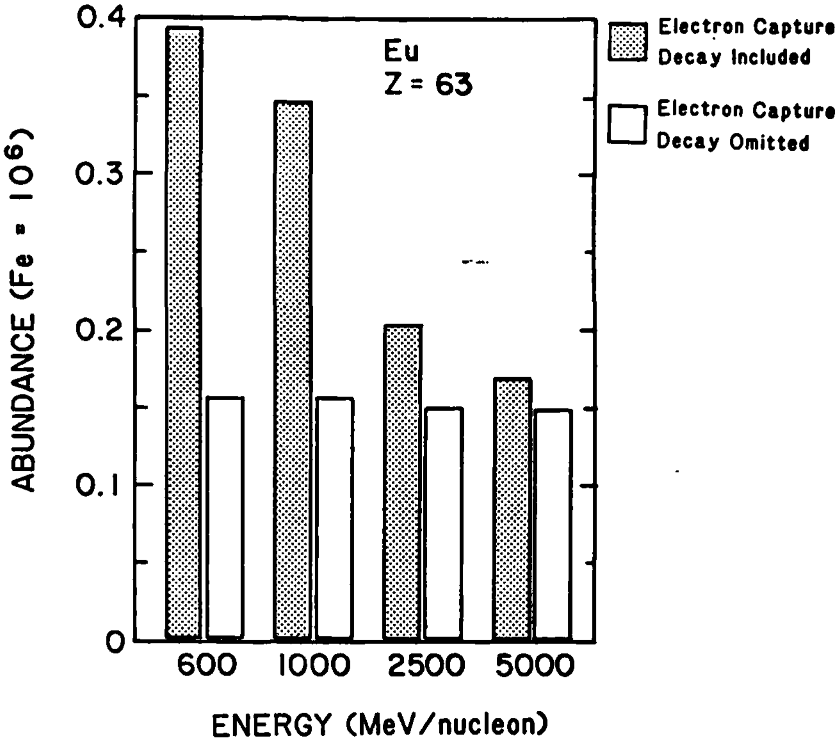
0.4
0.3
0.2
0.1
0
ABUNDANCE (Fe = 10^6)
Eu
Z = 63
▨ Electron Capture Decay Included
☐ Electron Capture Decay Omitted
600
1000
2500
5000
ENERGY (MeV/nucleon)

Fig. 4

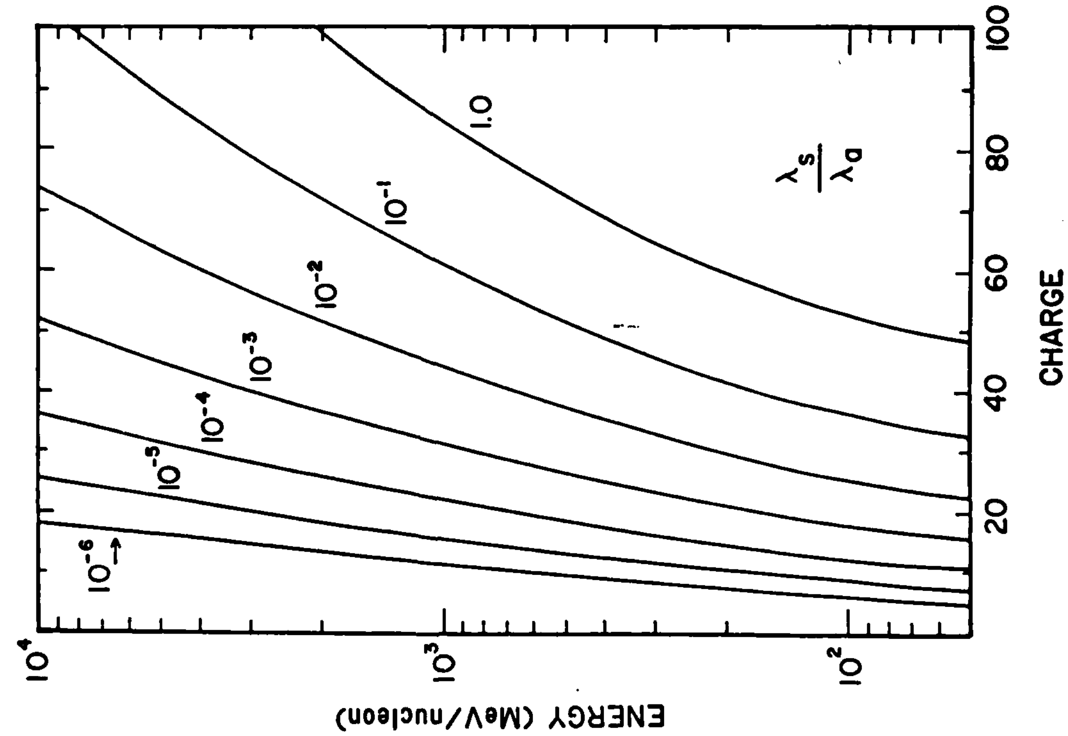
$\frac{\lambda_s}{\lambda_a}$
1.0
10^{-1}
10^{-2}
10^{-3}
10^{-4}
10^{-5}
10^{-6} →
CHARGE
100
80
60
40
20
10^4
10^3
10^2
ENERGY (MeV/nucleon)

Fig. 3

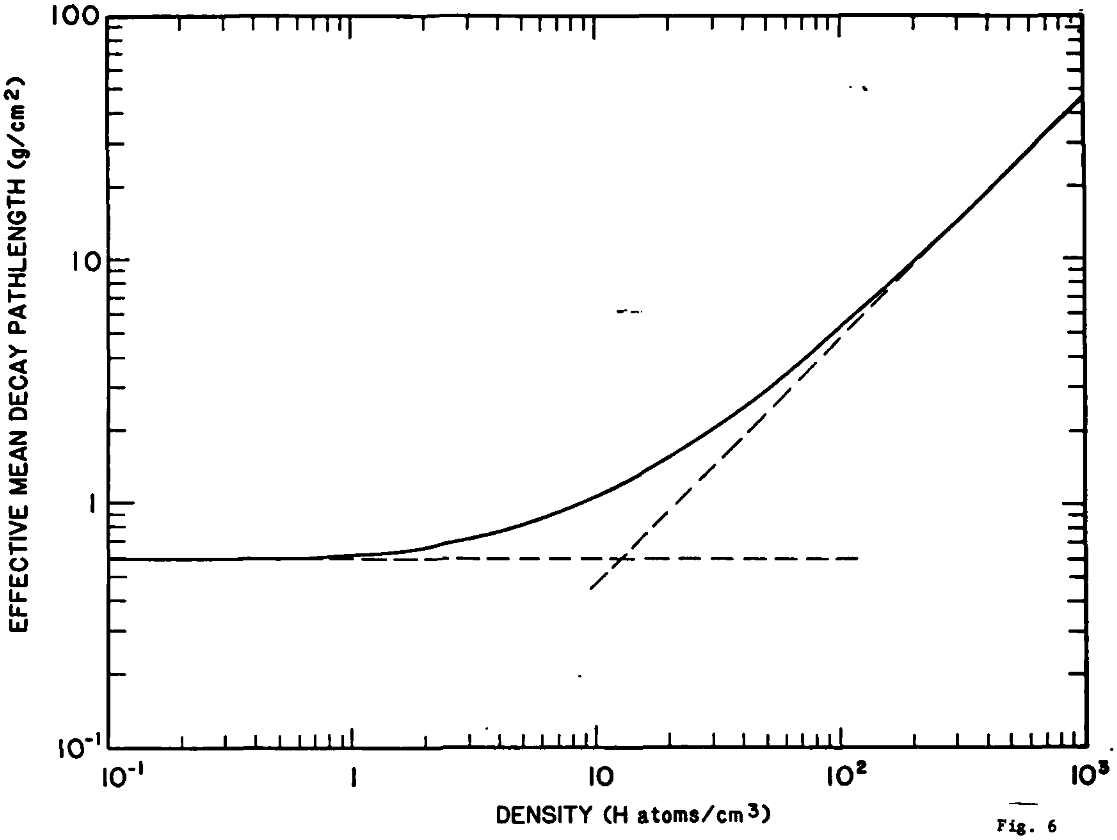
100
10
1
10⁻¹
10⁻¹
1
10
10²
10³
EFFECTIVE MEAN DECAY PATHLENGTH (g/cm²)
DENSITY (H atoms/cm³)

Fig. 6

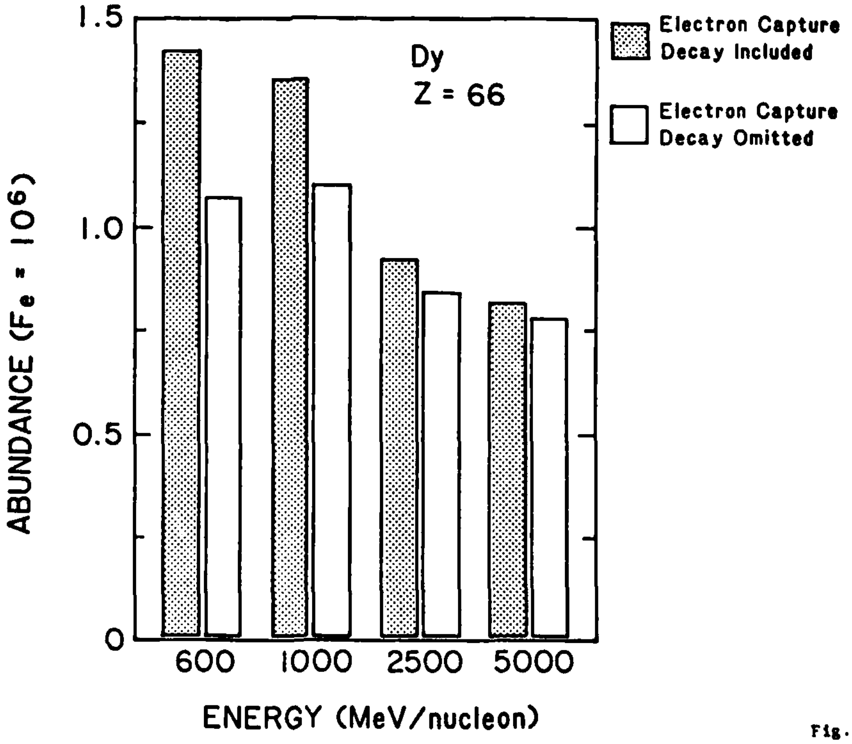
1.5
1.0
0.5
0
ABUNDANCE (Fe = 10⁶)
Dy
Z = 66
▨ Electron Capture Decay Included
☐ Electron Capture Decay Omitted
600
1000
2500
5000
ENERGY (MeV/nucleon)

Fig. 5

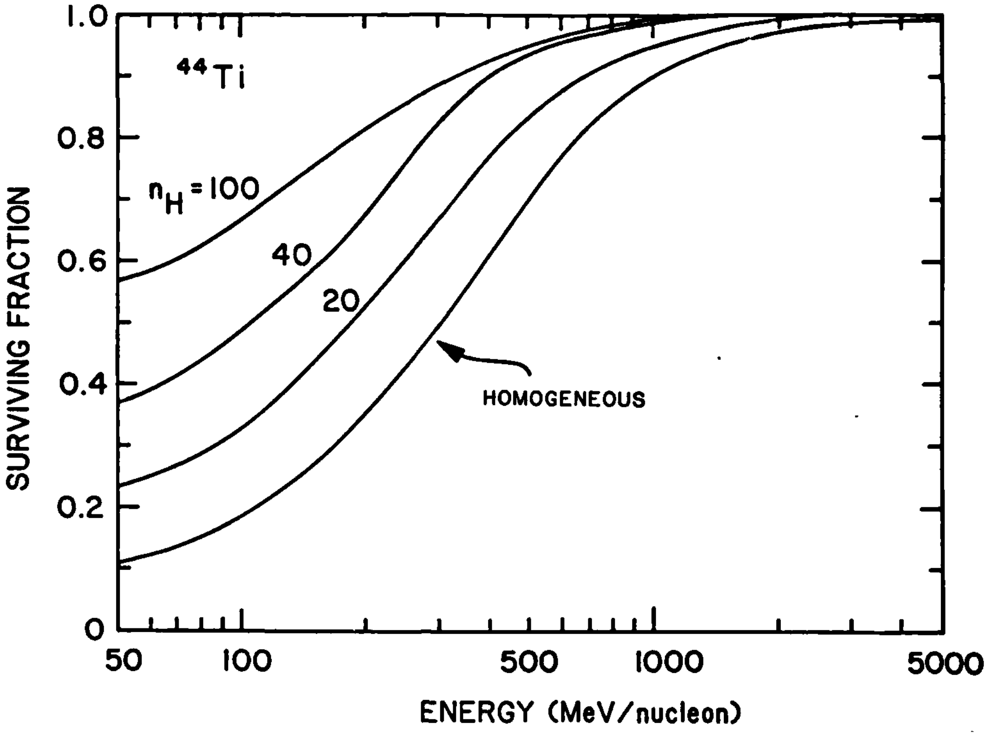

^{44}Ti
n_H=100
40
20
HOMOGENEOUS
SURVIVING FRACTION
1.0
0.8
0.6
0.4
0.2
0
50
100
500
1000
5000
ENERGY (MeV/nucleon)

Fig. 8

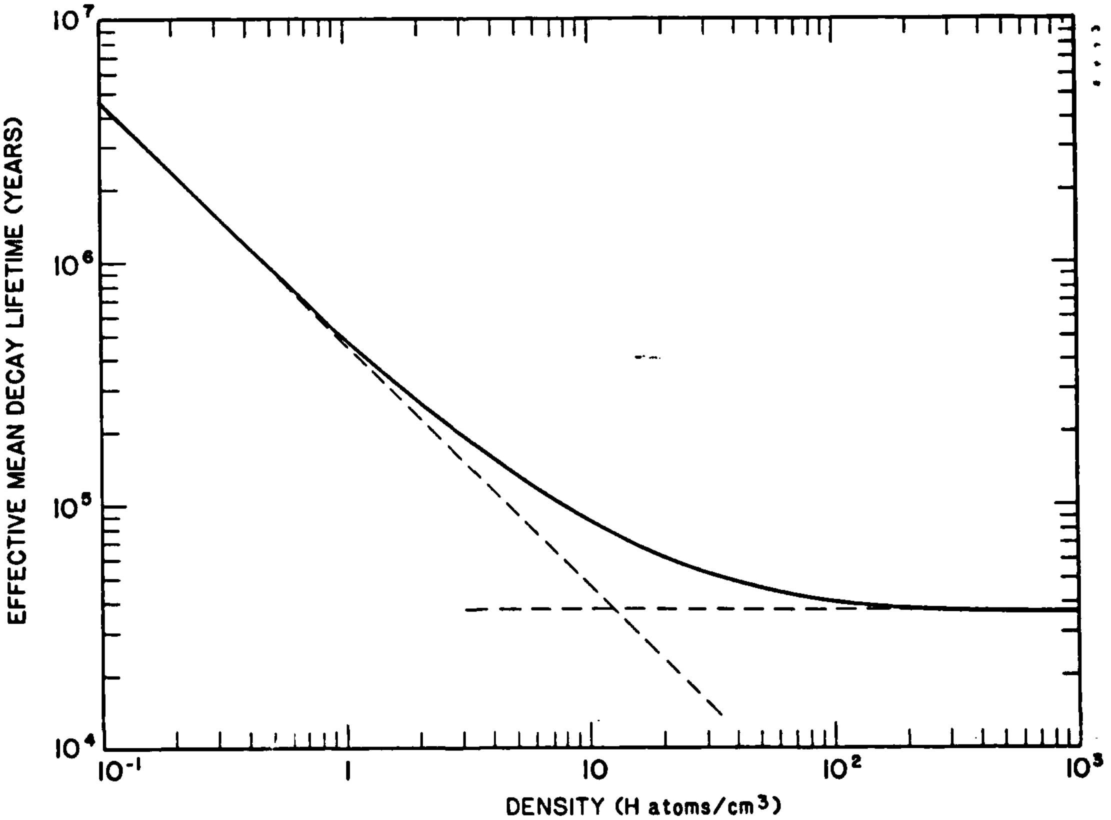

EFFECTIVE MEAN DECAY LIFETIME (YEARS)
10^7
10^6
10^5
10^4
10^{-1}
1
10
10^2
10^3
DENSITY (H atoms/cm^3)

Fig. 7

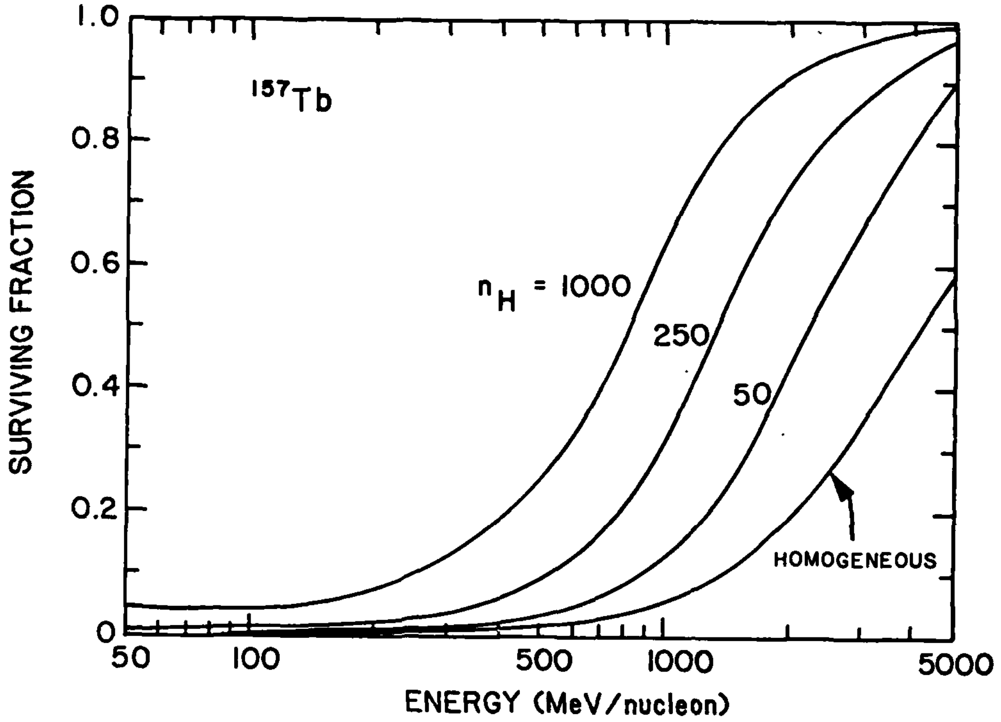

1.0
0.8
0.6
0.4
0.2
0
SURVIVING FRACTION
^{157}Tb
n_H = 1000
250
50
HOMOGENEOUS
50
100
500
1000
5000
ENERGY (MeV/nucleon)

Fig. 10

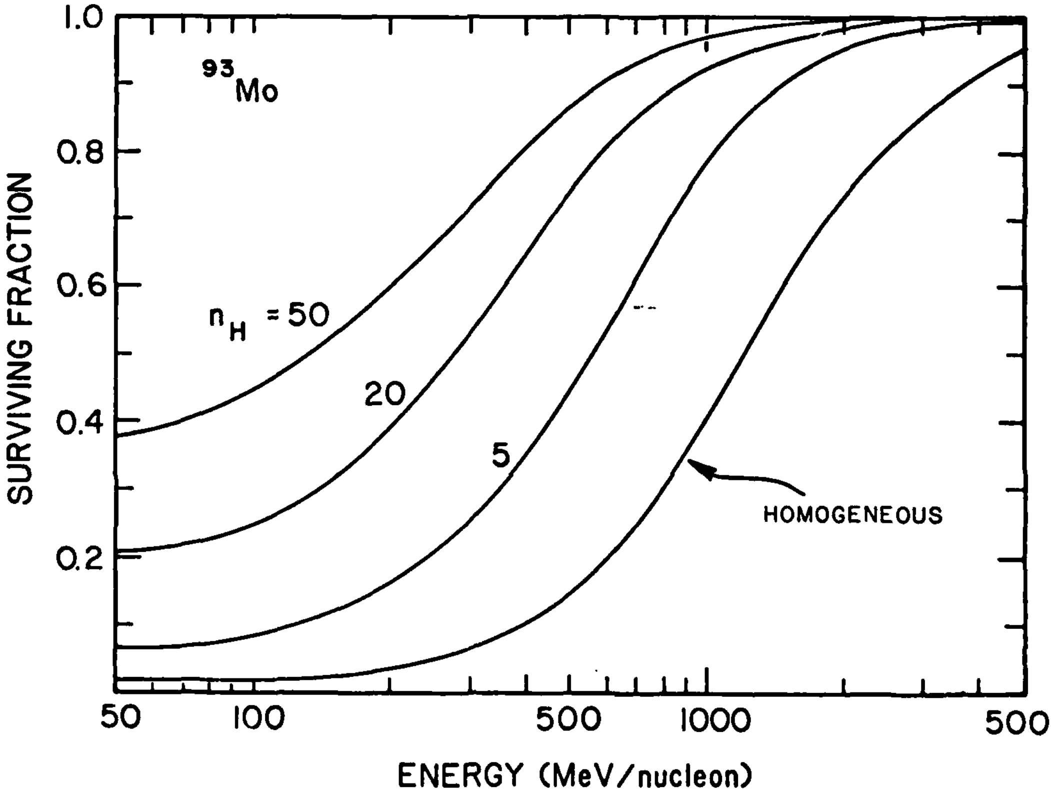

1.0
0.8
0.6
0.4
0.2
SURVIVING FRACTION
^{93}Mo
n_H = 50
20
5
HOMOGENEOUS
50
100
500
1000
5000
ENERGY (MeV/nucleon)

Fig. 9

IEEE Transactions on Nuclear Science, Vol. NS-31, No. 6, December 1984

COSMIC-RAY HEAVY IONS AT AND ABOVE 40,000 FEET

Chen H. Tsao, Rein Silberberg*

and John R. Letaw**

Abstract

The flux and LET-spectra of heavy cosmic ray nuclei and their secondary progeny have been calculated at aircraft flight altitudes. The associated frequency of single event upsets is presented and compared with neutron-induced events.

1. Introduction

Of all particles in space, only the highly-penetrating cosmic ray component is able to propagate deep into the atmosphere. These particles suffer fragmentation and ionization losses from collisions with nitrogen and oxygen nuclei. In this paper we compute the flux of heavy nuclei and their fragments down to 40,000 ft in the atmosphere and associated SEU rates, extending previous calculations.[1] In an accompanying paper, we compute the neutron-induced upsets.[2]

2. Cosmic Ray Heavy Ions

The heavy nuclei are the dominant source of single-event upsets (SEU) down to roughly 60,000 ft.[3] The equation of cosmic-ray propagation is:[3]

$$\frac{dJ_i}{dx} = -\frac{J_i}{\lambda_i} + \sum_{j>i} \frac{J_j}{\lambda_{ij}} + \frac{\partial}{\partial E}\left[J_i\left(\frac{dE}{dX}\right)_i\right] \quad (1)$$

J_i is the differential flux of cosmic rays of species i in units of $(m^2\text{-sec-ster-MeV/nucleon})^{-1}$. λ_i is the mean free path for loss of species i due to fragmentation in air (units of g/cm^2). λ_{ij} is the gain of species i from fragmentation of species j. $(dE/dx)_i$ is the stopping power of species i in air.

We solve Eq. 1 using programs developed at NRL. A hundred and four isotopic species with charges $1 \leq Z \leq 28$ are included in our calculation. Fragmentation parameters are taken from our semiempirical formulas (see Ref. 3). The cosmic ray flux at the top of the atmosphere is propagated to various depths in the atmosphere taking into consideration geomagnetic cutoff (and its variation with zenith and azimuthal angle) and the increased pathlength with increasing zenith angle. The geomagnetic cutoff (see Figure 1) eliminates low energy (i.e., high LET) particles at the top of the atmosphere.

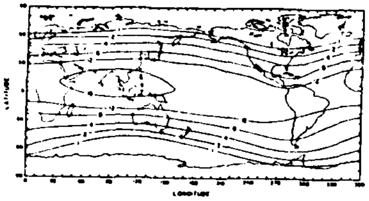

Fig. 1 Geomagnetic cutoff vs. latitude and longitude

Figure 2 shows the variation of cosmic ray fluxes with altitude for a geomagnetic cutoff of 1 GV. We note that heavy ions (such as Fe) decrease rapidly because of high fragmentation and ionization loss rates. Sulfur (Z = 16) is augmented by Fe fragmentation and thus, initially, its flux falls more slowly than oxygen (Z = 8).

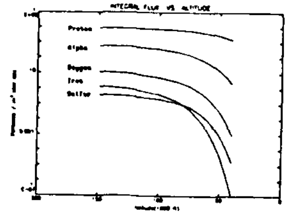

Fig. 2 Integral fluxes as a function of altitudes (R_c = 1 GV) for p, α, O, S and Fe.

For purposes of SEU computations the particle fluxes are summed into LET (linear energy transfer) spectra. The LET characterizes the particles according to their rate of energy deposition in a thin silicon slab. The differential LET flux is given by:

$$J(L) = \sum_i J_i(E) \left[\frac{d}{dE}\left(\frac{dE}{dX}\right)_i\right]^{-1} \quad (2)$$

where $L = (dE/dx)_i$. Integral LET spectra are shown in Figure 3 for a geomagnetic cutoff of 1 GV. Steps in this spectrum arise because all low energy particles are eliminated by the cutoff. High energy particles have roughly constant LET. The highest step is due to protons, the next step to alphas, and so on. The steps are softened as particles slow down (lower altitudes). The cross-over between the spectra at 150,000 and 75,000 ft is due to slowing of high energy Fe. The dotted lines show the effect of 5-gram aluminum shielding. The effect is not very significant.

---

*Naval Research Laboratory
E. O. Hulburt Center for Space Research
Code 4154
Washington, D.C. 20375

**Severn Communications Corporation
Severna Park, Maryland 21146

0018-9499/84/1200-1066$1.00©1984 IEEE

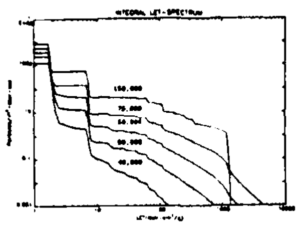

Figure 3: Integral LET-spectra at 150, 75, 60, 50 and 40 thousand feet, (R_c = 1 GV). The dotted lines shows the effect of 5-gram aluminum shielding.

LET spectra can be converted into upset rates once the device dimensions and critical charge are given.[5] The critical charge is the number of free electrons needed to cause a bit-flip. Critical charge is related to energy deposition by:

$$Q(pC) = \frac{\Delta E\ (MeV)}{22.5} \quad (3)$$

The upset rate is:

$$U = A_p \int_0^{\infty} N(L_{min})\ C(p)\ dp \quad (4)$$

where N is the integral LET spectrum, L_{min} is the minimum LET at which the critical charge will be deposited over chord length p, and C(p) is the distribution of chord lengths in the device.

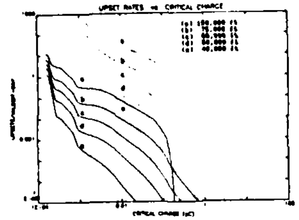

Figure 4: Variation of upset rates at 150, 75, 60, 50, and 40 thousand feet. (R_c = 1 GV). Solid lines are for small devices (5μ x 10μ x 10μ). Dotted lines are for large devices (20μ x 100μ x 100μ).

Upset rates as a function of critical charge are shown for two device sizes in Figure 4. Typically critical charges scale with device size (charge-sensitive volume at the circuitry site) so that the upset rate is roughly independent of size[5]. We note that because of the cross-over in the LET spectrum upset rates can be higher at 75,000 ft than at 100,000 ft. This effect is enhanced in regions of high cutoff. In Figure 5, the upset rate at 75,000 ft for a small device (5μ X 10μ x 10μ) is broken down into charge groups. For a typical device[5] (critical charge between 0.01 and 1.0 pC) cosmic ray protons and alphas do not cause upsets. Sensitive devices are upset by C and O while less sensitive devices will be upset by Mg, Si, and Fe. Secondary protons and alphas, the low energy particles evaporated from excited nuclei after cosmic ray collisions, have LET up to 200 times greater than the corresponding high energy ones shown on the left side of Figure 3. Although there are few of these particles at high altitudes, they are as effective as heavy ions in causing upsets.

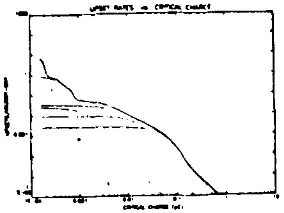

Figure 5: Contribution to Upset Rates at 75,000 ft. from Various Charge Groups.

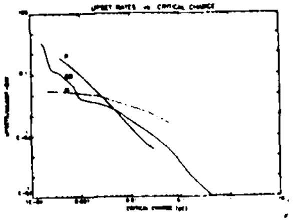

Figure 6: The relative contributions of cosmic rays (CR), neutron interactions (N) and ionization loss of slow secondary protons(P) to single event rate at 55,000 feet (R_c = 1 GV).

3. Neutron Interactions

Below altitudes of 60,000 feet, or atmospheric depths of $x > 60$ g/cm^2, neutron-generated nuclear recoils and nuclear evaporation products become the most important contributors to single event upsets. The event rate is about 5 per cent of that near the top of the atmosphere, (above 130,000 feet). However, these recoils produced in silicon have lower rates of ionization loss than slow iron nuclei. Thus there is a Q_{crit} interval where very heavy cosmic-ray nuclei produce upsets but neutrons do not. For most sensitive future devices, i.e. those having a low Q_c that correspond to less than 10 times the minimum ionization, slow secondary protons become more important contributors to single-event upsets than neutron generated recoils. At 50,000 to 65,000 feet altitude, their contribution to the upset rate is about 20 per cent of that of cosmic rays near the top of the atmosphere.

Acknowledgement

This work is partially supported by DNA/DARPA under the Single Event Radiation Effects Program.

References

1. R. Silberberg, C. H. Tsao, J. H. Adams, and J. R. Letaw, IEEE Trans. Nucl. Sci., NS-30, 4405, (1983).

2. R. Silberberg, C. H. Tsao and J. R. Letaw, "Neutron Generated Single-Event Upsets in the Atmosphere," in these proceedings.

3. J. R. Letaw, R. Silberberg, C. H. Tsao, "Propagation of Heavy Cosmic Ray Nuclei," (to appear in Ap. J. Suppl.).

4. J. H. Adams, R. Silberberg and C. H. Tsao, "Cosmic Ray Effects on Microelectronics, Part I: The Near-Earth Particle Environment," NRL Memo Report, 4506, 1981.

5. E. L. Peterson, P. Shapiro, J. H. Adams, Jr., and E. A. Burke, IEEE Trans. Nucl. Sci., NS-29, 2055, (1982).

1066 - 1068

IEEE Transactions on Nuclear Science, Vol. NS-31, No. 6, December 1984 1183

NEUTRON GENERATED SINGLE-EVENT UPSETS IN THE ATMOSPHERE

Rein Silberberg, Chen H. Tsao[*]

and John R. Letaw[**]

Abstract

Heavy cosmic ray nuclei are mostly attenuated th a shielding of 50 g/cm^2 atmospheric gas. wever, the shielding acts as a generator of utrons, evaporated or knocked out of nuclei. These utrons generate highly ionizing nuclear recoils at produce single-event upsets in microelectronic ponents. To attenuate the secondary neutron flux er 300 g/cm^2 of atmospheric material is required. e numerous slow protons from nuclear interactions shielding will also generate upsets in sensitive ponents, which have a low critical charge. At titudes below 65,000 feet, most single-event upsets e due to these secondary particles. The upset tes due to neutrons and slow secondary protons from mic ray, solar flare particle, and trapped liation particle interactions are presented as a ction of the critical charge.

Introduction

As high-energy heavy cosmic ray nuclei are sorbed by nuclear interactions or by ionization ss, another radiation component--neutrons--that uses single-event upsets in microelectronic puter components builds up in intensity. Neutrons e extraordinarily penetrating due to the absence of ization loss.

Energy deposition in microelectronic chips, in e case of neutrons is due to nuclear collisions , or in the immediate vicinity of the chip. Such lear collisions generate nuclear recoils. Ziegler d Lanford[2] calculated the recoil energies of licon nuclei due to elastic scattering of neutrons. wever, the figures of Ziegler do not take into nsideration the high-energy nuclear recoils nerated in nuclear spallation reactions. For ample, the cross section[3] for 1-MeV recoils nerated by 10^3 MeV neutrons is underestimated about 0 times, and that of higher energy recoils by many ders of magnitude. While Ziegler and Lanford[2] timate that recoil energies up to ~ 3 MeV ntribute significantly, we find that recoil ergies up to 20 MeV are important. Experimental ta on nuclear recoil charge composition and energy ectra have been published by Westfall et al.[3] Our mputations of the single-event upset rate are based n a combination of the elastic scattering data esented by Ziegler and Lanford[2] and our analysis of e data of Westfall et al.[3] on energy spectra of clear recoils.

2. Energy Spectra of Neutrons

The flux of neutrons is nearly constant at atmospheric depths of 30 to 200 g/cm^2, as measured by Hess et al.[4] and Holt et al.[5], and calculated by Armstrong et al.[6] and Light et al.[7]. At solar minimum the flux of neutrons at atmospheric depths of 50 to 150 g/cm^2 (~ 65-50 Kft), at a geomagnetic latitude of $\lambda = 40^\circ$, in the energy interval 1 to 10 MeV is 1 ± 0.2/cm^2 sec, according to Armstrong et al.[5], and Hayakawa,[8] and references therein. Above 10 MeV, the flux is 0.6. At high geomagnetic latitudes, the flux is about 2 times higher, and near the equator, about 5 times lower. At solar maximum, the flux at high geomagnetic latitudes is about 60% of that at solar minimum, and at 40° latitude, about 75%. At geomagnetic latitude of 40°, the flux near sea level is about 200 times less than between 50 and 150 g/cm^2.

Figure 1 shows the neutron energy spectrum at solar minimum, $\lambda \approx 40^\circ$, and 50 to 150 g/cm^2. (At 30 g/cm^2 or 200 g/cm^2, the flux is slightly lower, by 20%.)

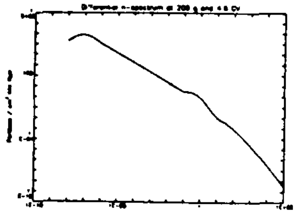

Fig. 1. Neutron energy spectrum at an atmospheric depth of 100 g/cm^2, near solar minimum, at a geomagnetic latitude of 42°.

3. Energy Spectra of Nuclear Recoils

Nuclear spallation reactions transfer a considerable amount of energy to the recoiling residual nucleus. For neutrons with energy > 1 GeV, we adopt the recoil energy spectra measured by Westfall, et al.[3] displayed in Fig. 2 for recoil nuclei $3 < Z < 5$, $6 \leq Z \leq 9$ and $Z \geq 10$, respectively. Fig. 2 displays the differential cross sections measured at 90° in the lab system. The interpolation to lower energy neutrons was carried out using the data of Roche et al.[11], measured near 100 MeV.

---

[*] E. O. Hulburt Center for Space Research
aval Research Laboratory
de 4154
shington, D. C. 20375

[**] Severn Communications Corporation
everna Park, Maryland 21146

0018-9499/84/1200-1183$1.00©1984 IEEE

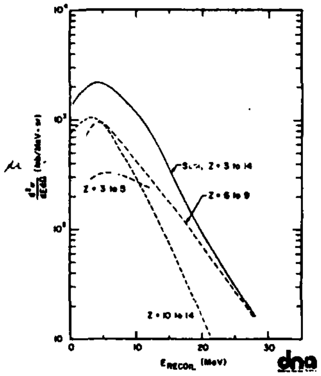

Fig. 2. Energy spectra of spallation products of Si, at 90° in the laboratory, irradiated by nucleons at E ≥ 1 GeV. The energy spectrum of Li, Be, B is discontinued at a range of 10μ, the adopted chip size. The spectra are based on the measurements of Westfall et al.[2], who used an Al target.

4. Burst Generation Rate

We adopt the definition of Ziegler and Lanford[2] for the burst generation rate b or charge deposition by a nuclear recoil in a chip. However, the numerical values of the burst generation rate we use includes the energy spectrum of the residual nuclei induced by spallation, discussed in the previous section. The burst generation rate is approximated by, in units of $cm^2/\mu m^3$,

$$b = 10^{-16} \exp(F_1 + F_2)\left[1 - \exp\left(\frac{E - E_{min}}{20E_b^{1.4}}\right)\right]$$

$$F_1 = 6.0 \exp -\left(\frac{E_b}{7.5}\right) \qquad (1)$$

$$F_2 = 3.2\,(0.4 - E_b^{0.5}) \exp\left[-E_b - \left(\frac{E - 10E_b}{20}\right)^2\right]$$

$$E_{min} = 7.5\,E_b^{1.1} \geq 0.4 \text{ MeV}$$

Figure 3 illustrates the burst generation rate as a function of the neutron energy for various recoil energies E_b.

5. Burst Generation Rate due to Slow Secondary Protons

In very sensitive microelectronic components (i.e., those with a critical charge < 2 × 10^{-3} pC) slow protons can generate single event upsets.

The measurements of low-energy secondary proton energy spectra have been reviewed by Hayakawa[8] and Ziegler and Lanford;[2] the corresponding dose rates have been calculated by Armstrong et al.[9] Armstrong et al.[10] have also calculated the radiation doses due to neutrons and protons generated in solar flare particle interactions.

In our calculations, we combine the energy spectrum of slow protons (E ≤ 30 MeV) of Ziegler and Lanford[2] with the atmospheric depth dependence given by Hayakawa[8]. The flux of slow protons with a rate of ionization loss greater than $(dE/dx)_0$, having an energy less than $E_0 \leq 30$ MeV is approximated by:

$$J[>(dE/dx)_0] = \int_{0.5}^{E_0} K\ E^{\alpha}\ dE\ (cm^2 \sec \text{ Mev})^{-1} \qquad (2)$$

where $\alpha = 1.0$, $K \approx 1.3 \times 10^{-6}$ at atmospheric depths 50 to 100 g/cm^2, 6×10^{-7} at 200 g/cm^2 and 3×10^{-7} at 300 g/cm^2. Although the spectrum of protons below 30 MeV is highly uncertain, the resulting changes in the upset rate are not significant.

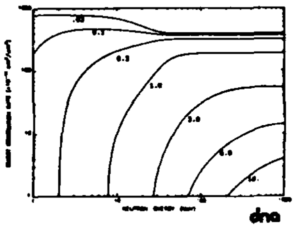

Fig. 3. The burst generation rate as a function of neutron energy for n + Si reactions. The numbers in the figure represent recoil energies E_b.

6. The Upset Rate Due to Neutrons, Secondary Protons and Pions

In the paper "Cosmic Ray Heavy Ions at and Above 40,000 Feet," by Tsao, et al.[12] the contribution of cosmic rays to the single event upset rate, at an altitude of 55,000 feet, is compared to that of cosmic-ray secondaries. The latter were displayed separately for the neutron-generated nuclear recoils, and for ionization loss of slow protons. Below 65,000 feet (or x > 50 g/cm^2), these secondary components are found to dominate.

The pion/proton ratio at 2 GeV is 0.2 near sea level, and less at higher altitudes, and at lower energies[13]. Furthermore, the more highly ionizing slow pions produced in the upper atmosphere will mainly decay into muons in flight. Thus the contribution of pions to upsets is less important.

Figure 4 shows the critical charge spectrum of the upset rate at 100 g/cm^2 of air (55,000 feet) as well as at sea level, due to neutron generated recoils and slow protons. At sea level, also the contribution of ionization losses of slow muons, based on Ziegler and Lanford[2], is shown. The latter is important only for very sensitive devices with a low critical charge.

NUCLEAR CROSS SECTIONS, COSMIC RAY PROPAGATION AND SOURCE COMPOSITION

R. Silberberg and C.H. Tsao
E.O. Hulburt Center
Naval Research Laboratory
Washington, DC 20375

J. R. Letaw
Severn Communications Corporation
Severna Park, MD 21146

ABSTRACT. Most cosmic rays with atomic number $Z \geq 6$ suffer nuclear collisions in the interstellar gas, with transformation of nuclear composition. The isotopic and elemental source composition has to be inferred from the observed composition near the earth. The uncertainty in the inferred source composition is largely due to uncertainties in cross sections--especially for nuclides that have large secondary components. These uncertainties will be explored by comparing the calculated and observed abundances of the secondary components. A precise knowledge of nuclear cross sections is essential for unraveling the parameters of cosmic ray propagation: the mean path length traversed and its energy dependence, the distribution function of path lengths, the confinement time of cosmic rays in the galaxy, and acceleration after fragmentation. Various models of cosmic ray propagation will be critically explored.

1. INTRODUCTION

The majority of cosmic ray nuclei heavier than helium have suffered nuclear collisions in the interstellar medium. These collisions alter the cosmic ray composition and mask the source composition. Determination of the source composition is always difficult and often hopeless because we have limited data on cross sections. On the other hand, the effects of nuclear spallation and the time-dependence of nuclear decay provide valuable information on the propagation and acceleration of cosmic rays, the confinement time in the Galaxy, and the nature of the interstellar medium.

To derive any useful information from data on cosmic ray abundances, it is essential to know (or be able to estimate) the nuclear fragmentation cross sections and reliably estimate their errors. The partial cross sections give the probability of a given incident nuclide to yield a given product nuclide upon collision with some target such as a proton. The total fragmentation cross section yields the overall probability for a change in the mass or charge of the incident nuclide. In this lecture I will discuss the problems of determining cosmic ray source composition and the nature of propagation in the Galaxy. Special emphasis will be placed on the importance of nuclear cross sections in understanding these problems.

Some of the current lectures here are closely related to the present lecture: Dr. Lund has discussed the cosmic ray abundances, both at the source, and near the earth, especially those of the HEAO-3 French-Danish collaboration. Professor Wolfendale has explored the interstellar medium, magnetic fields therein, associated cosmic ray effects, and gamma ray production. Dr. Shapiro will soon discuss the propagation, acceleration and age of cosmic rays, with special emphasis on our recent hypothesis (Silberberg et al. 1983) of distributed acceleration. According to this hypothesis, cosmic rays after their principal acceleration and after appreciable fragmentation undergo some additional acceleration in interstellar space, gaining a factor of four in energy.

2. PRIMARY AND SECONDARY COSMIC RAYS

An inspection of Figure 1 demonstrates the need for cosmic ray propagation calculations that explain and predict the large deviations of cosmic ray abundances from the general stellar or galactic isotopic and elemental abundances. Secondaries, such as Li, Be, and B, are far more abundant in cosmic rays than in the solar system because they are composed substantially of nuclear fragments of heavier elements (C, N, and O). The predominantly primary elements such as C, O, Ne, Mg and Si have small contributions of nuclear fragments but can show appreciably different isotopic compositions.

The figure shows our early (Silberberg et al., 1976) calculated isotopic abundances of the elements. The hatched columns give the abundances at the sources obtained by iterative calculations. The white areas represent the surviving primary components and the black areas the secondary contribution from spallation reactions. Three classes are discernible. The predominantly primary elements(C, O, Ne, Si, Mg, Fe, and marginally S) have a small (< 30%) contribution of fragmentation products; these elements also have nearly the same relative abundances (within a factor of four) as the solar system. The predominantly secondary elements (Li, Be, B, F, P, Cl, K, Sc, Ti, V, and Mn) are composed of more than 80% nuclear fragments. Because of inevitable uncertainties in propagation calculations, their source abundances are indeterminate. The remaining nuclides (N, Na, Al, Ar, and Ca), have secondary contributions between 30% and 80%, hence their source compositions are very difficult to determine. Errors are extremely sensitive to uncertainty in the fragmentation cross sections.

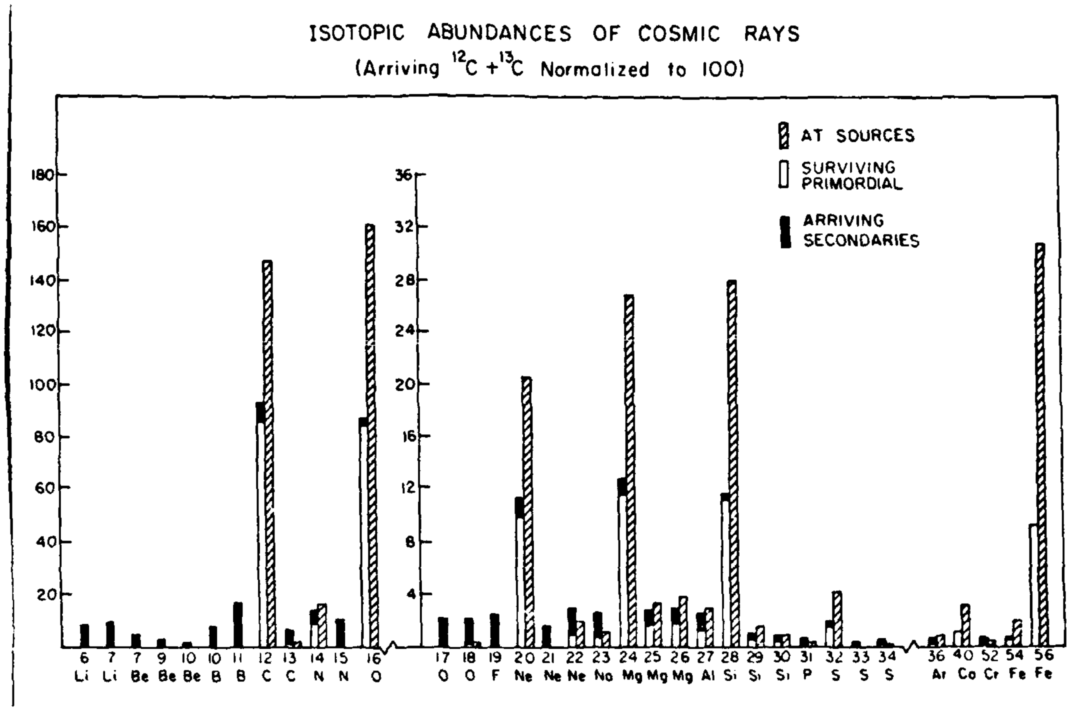

Figure 1 The relative abundances of nuclides at cosmic ray sources and near the earth. The arriving two isotopes of carbon are normalized to 100. In the arriving columns, the secondaries and surviving source components are shown separately.

Subsequent experimental work by many groups, reviewed by Lund, agrees well with the predictions of Figure 1. When we (Tsao et al., 1973) first presented such predictions, we pointed out that the observed isotopic abundances will deviate from these calculations if the isotopic composition at the sources deviates from that of the general abundances and that such comparisons should yield significant astrophysical information. We also pointed out then the possibility of nucleosynthesis in a neutron-rich environment. The latter statement was confirmed in subsequent experiments in which the neutron-rich isotope ^{22}Ne was found to be 4 times overabundant and ^{25}Mg, ^{26}Mg, ^{29}Si and ^{30}Si about 1.6 times over-abundant at cosmic ray sources.

A more up-to-date tabulation of the calculated cosmic ray isotopic abundances is given in our paper Adams et al. (1981), for isotopes from ^{6}Li to ^{64}Ni. Our comparisons of calculated and experimental elemental abundances of cosmic rays with atomic numbers $Z \geq 32$ are given by Letaw et al. (1984a).

3. COSMIC-RAY PROPAGATION EQUATION AND CHANGES IN COMPOSITION

The importance of nuclear transformations in understanding the composition of cosmic rays was demonstrated in the previous section. The procedures of cosmic ray propagation calculations have been described by Ginzburg and Syrovatskii (1964), and the particular methods used in our group by Letaw et al. (1984b).

For the traversal of an amount of matter x (g/cm^2), and without consideration of decay of the long-lived radioactive isotopes, the propagation equation is:

$$\frac{\partial J_i(E,x)}{\partial x} = \frac{-N\sigma_i(E)J_i}{\bar{A}} + \sum_{k>i} \frac{N\sigma_{ik}(E)J_i}{\bar{A}} + \frac{\partial}{\partial E}\left[W_i(E)J_i(0)\right] \qquad (1)$$

where $J_i(x)$ is the flux of species i after propagating through an amount of matter x, $J_i(o)$ is the source term, σ_i is the total inelastic cross section for nuclide of species i, σ_{ik} is the partial cross section for production of species i from k, N is Avogadro's number, $\bar{A}$ is the mean atomic weight of interstellar gas, and $W_i(E)$ is the rate of ionization loss.

At medium and high energies this cosmic ray propagation equation may be simplified to a set of coupled linear equations in one variable of the form:

$$\frac{dJ_i}{dx} = \sum_j M_{ij} J_j \qquad (2)$$

Energy appears in this equation only parametrically, not as an independent variable. Equation 2 is solved by matrix methods, which provides an efficient and powerful means of treating propagation, including various path length distributions. These procedures can be extended to treat ionization loss and solar modulation at energies above a few hundred MeV/nucleon.

The solution to equation (2) is:

$$J_i(x) = \sum_j [\exp Mx]_{ij}\, J_j(0) \qquad (3)$$

where the exponential is defined by its power series expansion. Taking into account the diffusion of particles, one notes that different particles have different path lengths, with a path length distribution, P(x), normalized so that

$$\int_0^\infty P(x)dx = 1 \qquad (4)$$

Then eq. 3 becomes:

$$J_i = \int dx\, P(x)\, [\exp Mx]_{ij}\, J_j(0) \qquad (5)$$

For an exponential path length distribution with mean path length ,

$$P(x) = \frac{1}{\lambda} e^{-x/\lambda} \qquad (6)$$

the integral of eq. 5 can be evaluated analytically, yielding:

$$J_i = [1 - M\lambda]^{-1}_{ij}\, J_j(0) \qquad (7)$$

The solution is then obtained simply from a set of coupled linear equations.

4. NUCLEAR CROSS SECTIONS

Nuclear transformations in cosmic ray collisions with the interstellar gas is an important process in propagation. These transformations involve two sets of physical quantities, the total inelastic cross sections σ_i and the partial cross sections σ_{ij}.

The simplest fit to the total inelastic cross section is $\sigma_i = KA^\beta$, where A is the mass number of the target nucleus. On geometrical basis, $\beta = 2/3$, in a first order approximation. However, a correction for nuclear transparency must be introduced; heavy nuclei are less "transparent" to projectiles than light ones. This consideration effectively raises the value of the exponent β. The experimental high-energy data (assuming that systematic errors in such data are negligible) are fitted to within 2% by the relation:

$$\sigma_i = 45\, A_i^{0.7}\left[1 + 0.016 \sin(5.3 - 2.63\, ln\, A_i)\right] \tag{8}$$

Letaw et al. (1983) found that a factor dependent on A_t provided an improved fit to the data.

At energies below 2 GeV/nucleon the total inelastic cross section varies with energy. (Also at very high energies, E > 100 GeV there is a slight increase in cross sections with energy.) The energy dependence of the total inelastic cross sections has certain systematic similarities over the whole range of mass numbers A. The total inelastic cross section decreases to a minimum (about 15% below the high-energy value) at 200 MeV/nucleon. It then sharply increases to a maximum at about 20 MeV/nucleon (60% above the high energy value). Below this energy, resonance effects become dominant and the cross section fluctuates rapidly with energy. An empirical formula for Li and heavier nuclei at energies greater than 10 MeV/N is given by Letaw, et al. (1983)

$$\sigma_i = 45\, A_i^{0.7}\left[1 + 0.016 \sin(5.3 - 2.63\, ln\, A_i)\right] \times \left[1 - 0.62\, e^{-E/200} \sin(10.9\, E^{-0.28})\right] \text{ mb} \tag{9}$$

where A_i is the mass number of nuclides of type i and E is the energy in units of MeV/N.

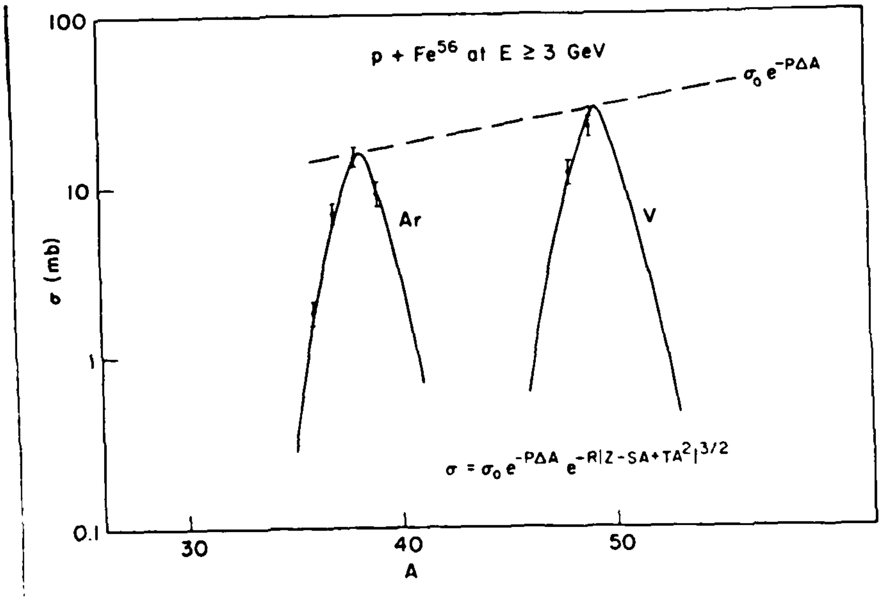

Fig. 2. Illustration of the terms of Rudstam's (1966) spallation equation. The calculated and experimental partial cross sections of Fe into isotopes of Ar and V are compared.

The partial inelastic cross sections σ_{ij} have systematic regularities that permit the design of semi-empirical equations. Rudstam (1966) observed that there are systematic regularities among the relative yields of nuclear reactions that depend on the mass difference of the target and product nuclides and on the neutron-to-proton ratio of the product nuclides. These relationships are illustrated in Figure 2, which shows the spallation cross sections of Fe into various isotopes of argon and vanadium, when iron nuclei are bombarded by protons having energies of 3 GeV. The factor $\exp(-P^{\Delta}A)$ describes the diminution of cross sections as the difference of target and product mass, ΔA, increases. It is closely related to the distribution of excitation energies discussed by Metropolis et al. (1958) in their Monte Carlo study of nuclear spallation reactions. A large excitation energy results in evaporation of many nucleons, i.e., in a large ΔA. The distribution of excitation energies peaks at small values, correspondingly, the partial cross sections are larger for small values of ΔA. The factor $\exp(-R|Z-SA+TA^2|^{\nu})$ in Fig. 2 (with $\nu \simeq 3/2$) describes the distribution of cross sections for the production of various isotopes of an element of atomic number Z. This Gaussian-like distribution is related to the statistical nature of the nuclear evaporation process (Dostrovsky et al. 1958). The width of the distribution of cross sections is represented by the parameter R. The parameter S describes the location of the peaks of these distribution curves for small values of the product mass number A. The parameter T describes the shift of the distribution curves toward greater neutron excess as the atomic number of the product increases. The equation displayed in Fig. 2 and parameters thus are closely related to nuclear systematics of the prompt intra-nuclear cascade and nuclear evaporation processes. This is the reason why these relations provide a surprisingly good fit to the experimental partial cross sections. In addition, the numerical values of the parameters are obtained by fitting to thousands of experimental data points. The parameters Rudstam (1966) assigned to the equation (illustrated in Fig. 2) are applicable to proton interactions with nuclei heavier than calcium, except when the target-product mass difference is small or large, i.e., it is not applicable for $\Delta A < 5$ and $\Delta A > 40$.

The nuclear reaction systematics of spallation reactions are not applicable to fission and fragmentation reactions, nor to the evaporation of light product nuclei. We have developed a semiempirical formula and associated parameters that are applicable for calculating cross sections (in units of mb) of targets having mass numbers in the range $9 \leq A_i \leq 209$ and products with $6 < A_j < 200$ at energies >100 MeV/N:

$$\sigma_{ij} = \sigma_0 f(A_i) f(E) e^{-P\Delta A} \exp(-R|Z - SA_i + TA_i^2|^{\nu})\Omega\eta\xi \qquad (10)$$

(Silberberg and Tsao 1973a, b, 1977a, b; Tsao and Silberberg 1979; Tsao, Silberberg, and Letaw 1983).

The parameters A, Z, P, R, S, T of eq. 10 are defined in the previous paragraph.

In equation (10), σ_o is a normalization factor. The factors f(A) and f(E) apply only to products from heavy targets (with atomic number $Z_t > 30$), when ΔA is large, as in the case of fission, fragmentation, and evaporation of light product nuclei. The parameter Ω is related to the nuclear structure and number of particle-stable levels of a product nuclide. The factor η depends on the pairing of protons and neutrons in the product nucleus; it is larger for even-even nuclei. The parameter ξ is introduced to represent the enhancement of light evaporation products.

Eq. 10 is inapplicable to peripheral reactions, that have small values of $\Delta A = A_j - A_i$. For such reactions, a different equation was constructed. A different equation was devised also for the heaviest target elements, the actinides such as Th and U.

5. CROSS SECTION AND PROPAGATION ERRORS

As I mentioned previously, the uncertainty in cross sections is usually the dominant source of error in cosmic ray propagation calculations. The estimated cross section error at the one standard deviation level is 35% for $Z \leq 28$ and 50 % for higher charges as stated in our 1973 paper. These values have been reduced somewhat by modifications to the original equations and parameters. The implications of cross section errors for the cosmic ray propagation problem have been brought into question by Hinshaw and Wiedenbeck (1983). They showed that depending on the degree of correlation in the cross section errors the source abundances of N, Na, Al, Ar, Ca, and all secondary cosmic rays might be obscured.

To determine the extent of correlations in the semiempirical cross section formulas we have taken an indirect approach through propagation calculations. A bare-bones model of cosmic ray propagation would assume solar system abundances at the source and an exponential pathlength distribution with mean pathlength of about 5 g/cm^2. We have performed this calculation at 4 GeV/nucleon and compared the results with data from HEAO-3 in Figure 3. In this figure error bars were calculated assuming totally correlated and totally uncorrelated cross section errors. The fit is extremely good, in fact, it is so good that a chi-square test shows there is only 1 chance in 5000 that such a good fit would be obtained if the errors were totally correlated. The assumption of 35% errors, uncorrelated, seems adequate to explain deviations of this experiment from calculation.

Further work with the 4 GeV/nucleon HEAO-3 data has led to source abundances and propagation errors in Table 1. Using a rigidity dependence of pathlength $\lambda = R^{0.6}$ we found the best fit value of λ to be about 5.0. In performing this calculation only errors induced by partial cross sections were considered.

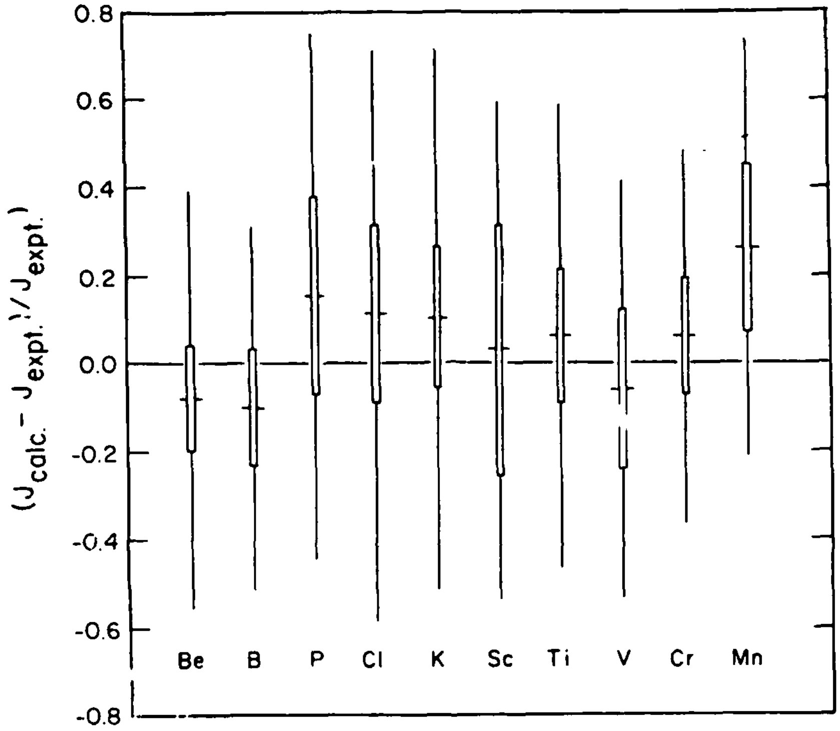

Fig. 3 A comparison of calculated and experimental abundances of cosmic ray elements produced mainly by spallation. The thin and thick error bars are based on assuming totally correlated and totally uncorrelated errors in partial cross sections.

TABLE 1
Calculated Source Abundances of Cosmic Ray Elements at 4 GeV/nucleon

Element	Source Abundance	Arriving Abundance	Arriving Primaries
Be	<0.06	0.28	<0.04
B	<0.20	0.72	<0.10
C	5.22 ± 0.14	3.23	2.84
N	0.65 ± 0.15	0.81	0.34
O	5.25 ± 0.08	2.81	2.62
F	<0.02	0.061	<0.01
Ne	0.91 ± 0.04	0.57	0.42
Na	0.09 ± 0.02	0.10	0.04
Mg	1.29 ± 0.03	0.65	0.56
Al	0.13 ± 0.02	0.10	0.05
Si	1.01 ± 0.02	0.46	0.41
S	0.28 ± 0.02	0.15	0.11
Cl	<0.01	0.020	<0.003
Ar	0.03 ± 0.01	0.039	0.010
K	<0.01	0.020	<0.004
Ca	0.09 ± 0.02	0.070	0.032
Sc	<0.01	0.012	<0.003
Ti	<0.02	0.038	<0.005
V	<0.01	0.016	<0.003
Cr	<0.03	0.041	<0.010
Mn	<0.02	0.033	<0.008
Fe	1.00 ± 0.02	0.34	0.32

Dr. Lund has presented a lecture on the composition of cosmic rays, the source composition and theoretical implications. Hence I shall not dwell on this topic, but discuss instead the importance of cross sections in the analysis of data on ultra-heavy cosmic ray nuclei.

6. EFFECT OF CROSS SECTIONS ON PROPAGATION OF ULTRAHEAVY COSMIC RAYS

Recent observations of cosmic rays in the charge range $36 \leq Z \leq 83$ on HEAO 3 and Ariel 6 permit a comparison of experimental and calculated abundances. The Ariel 6 results are given by Fowler et al. (1981) and HEAO 3 results by Binns et al. (1982) and Waddington et al. (1981), and papers published by the above authors in the late volume of the 1983 Bangalore Cosmic Ray Conference. The experimental abundances of the secondary elements $61 \leq Z \leq 75$ were found to exceed those obtained in propagation calculations.

We explored whether the calculated cross sections of elements Pt to Pb need revision. The recent measurements of Kaufman and Steinberg (1980) for the spallation of ^{197}Au show a substantial increase in the mass range $10 < A < 40$ at 1 GeV, shown in Figure 4. These new data have been incorporated into our semiempirical cross section formulae (Tsao et al., 1983). The high value of the cross sections at 1 GeV suggested that if propagation occurred at 1 GeV per nucleon, and the cosmic rays subsequently underwent an energy gain by a factor of 4, an improved fit to the data would be obtained.

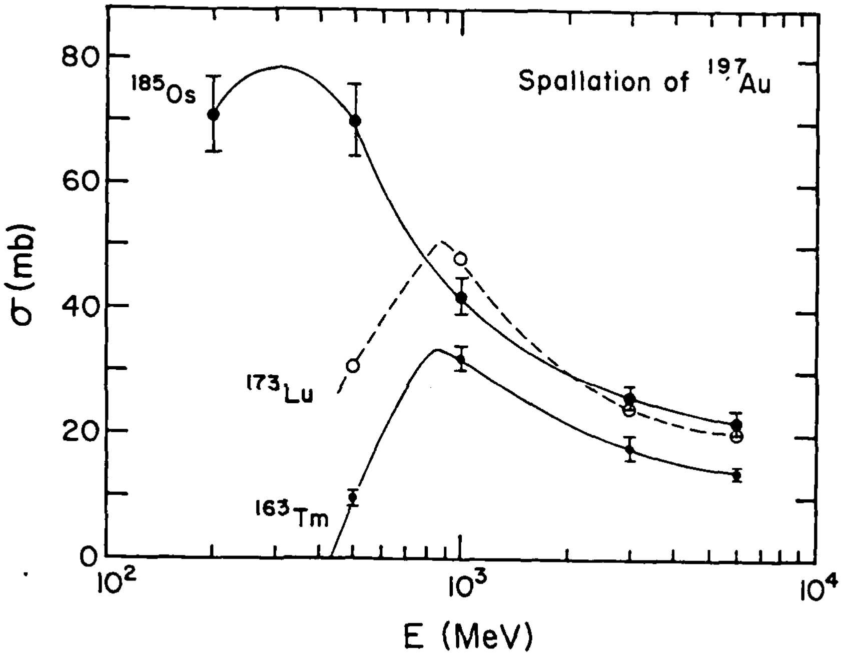

Figure 4. The energy dependence of the spallation of Au into Tm, Lu and Os.

In Figure 5, from Letaw et al. (1984a) we compare the ultra heavy abundances, $Z \geq 33$, with our propagation calculations. These are based on: (1) adopting source abundances similar to solar system abundances modified by a first ionization potential dependent suppression of elements with a high ionization potential, FIP, proportional to exp (-0.27I) for $7 \leq I \leq 13.6$ eV, and (2) an exponential distribution of path lengths with a mean of 6 g/cm^2 of interstellar medium at 5 GeV per nucleon. We note that for $Z < 56$, the fit to the data is good, after the FIP correction is applied, while the calculated abundances for $61 \leq Z \leq 75$ are too low. Fig. 6 shows the resulting calculations, using the cross sections of 1 GeV per nucleon and a path length of 9 g/cm^2, (the use of 6 g/cm^2 at 1 GeV/u gives practically identical results for ultra-heavy nuclei).

The improved fit, shown in Fig. 6,made us explore the associated hypothesis of distributed acceleration of cosmic rays in greater detail (Silberberg et al. 1983). The hypothesis does not imply continuous acceleration. It could occur as a major initial pulse and a minor late pulse. Dr. Shapiro will discuss several more tests of this hypothesis.

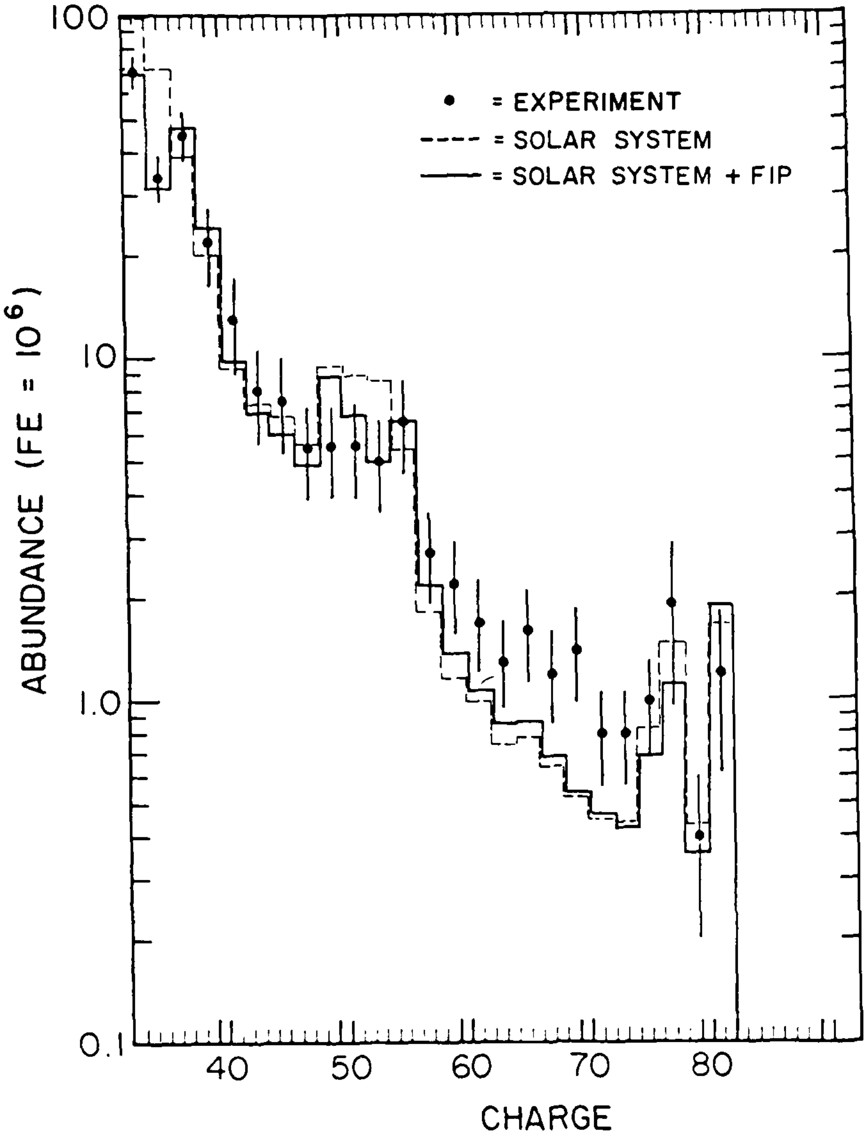

Figure 5 Comparison of experimental data and propagation calculations at 5 GeV/nucleon. The dashed line uses the Cameron (1981) source composition, and the solid line includes a correction dependent on the first ionization potential.

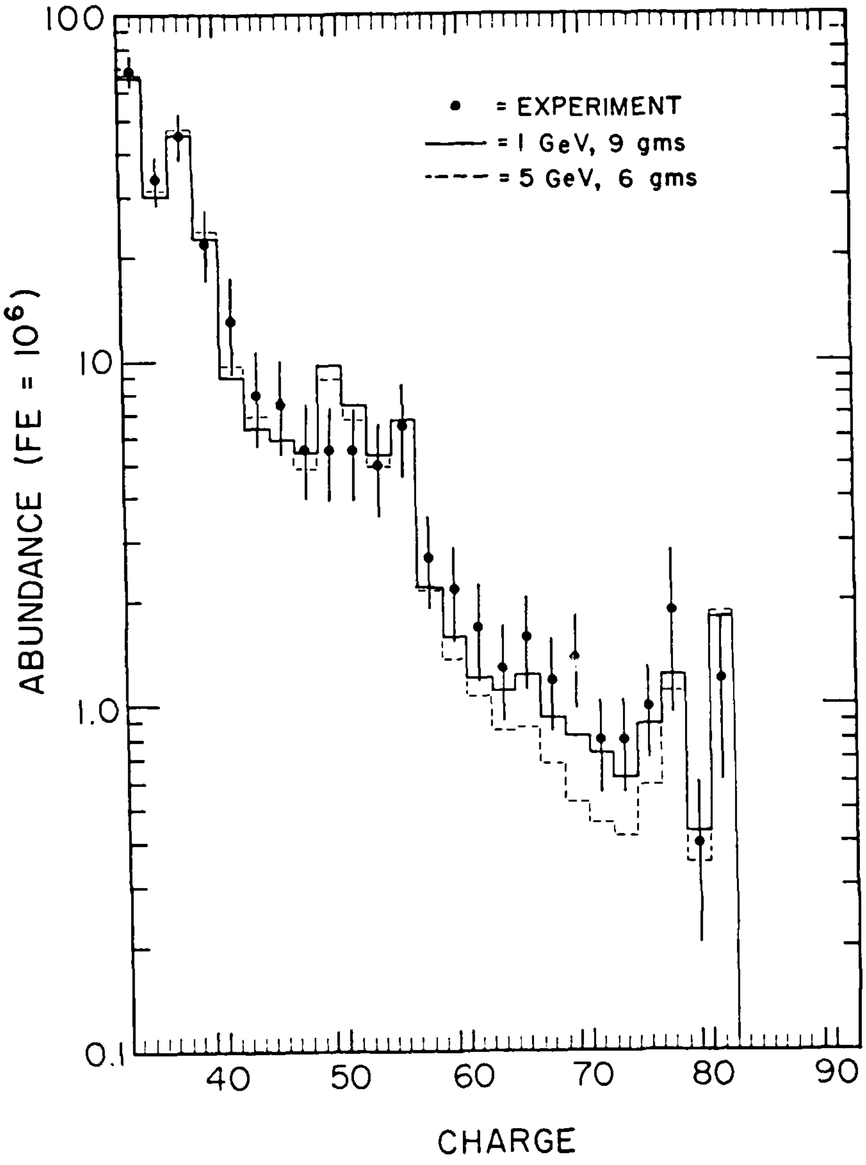

Figure 6 Comparison of experimental data and propagation calculations carried out at 1 GeV per nucleon and 5 GeV per nucleon, respectively.

7. ELECTRON CAPTURE DECAY AND INHOMOGENEITY IN THE INTERSTELLAR MEDIUM

The electron capture decay mode of cosmic rays with $Z < 30$ is strongly inhibited for cosmic rays moving at high energies (> 500 MeV/N) in the tenuous interstellar medium. This nuclear reaction takes place when a K-shell electron (or less likely an L-shell electron) interacts weakly in the nucleus transforming a proton into a neutron with the emission of a neutrino. At high energies, even distant encounters with the ISM efficiently strip electrons from light nuclides. Therefore the fraction of light nuclei with a single K-shell electron is between 10^{-6} and 10^{-3} and the effective decay rate is reduced accordingly. (In addition to the statistical reduction because fewer nuclides have bound electrons, there is a reduction by a factor of 2 because there is only one available K-shell electron).

The decay of ultraheavy nuclides in cosmic rays, unlike that of their lighter counterparts, is much less inhibited. At median cosmic ray energies the decay rate may be reduced by as much as a factor of 10 . On the other hand, actinides are likely to have several attached electrons (an important experimental consideration). The effective charge and electron capture decay rate are very sensitive to charge and energy. I discuss in this section a method for determining the effective electron capture rate in cosmic rays and what we can learn about the ISM by studying electron capture nuclides.

The rate equations describing electron capture reactions in cosmic rays are:

$$\begin{aligned} dN/dt &= -aN + sN^* \\ dN^*/dt &= aN - sN^* - eN^* \end{aligned} \qquad (11)$$

(The electron attachment rate is a, the electron stripping rate is s, and the electron capture decay rate is e.) The stripping and attachment rates have been studied by Crawford (1979) and others. Solving for the ratio (N*/N) we find that it approaches

$$(N^*/N)eq = [\ \{(s-a+e)^2 + 4as\}^{0.5} - (s-a+e)]/2s \qquad (12)$$

at the rate

$$R^* = \{(s-a+e)^2 + 4as\}^{1/2} \qquad (13)$$

R* is always greater than the electron stripping rate which is very fast, i.e., the mean free path never exceeds 0.2 g/cm^2 and is usually much less. The physics of cosmic ray propagation is governed by the fragmentation mean free path (>1 g/cm^2) and the escape mean free path (~8 g/cm^2). Cosmic rays therefore effectively maintain charge state equilibrium so

$$d(N + N^*)/dt = -e(N^*/N)_{eq}[1 + (N^*/N)_{eq}]^{-1}\ (N + N^*) \qquad (14)$$

(other decay modes and fragmentation have been ignored). The equilibrium charge when e = 0 is shown in Figure 7.

Electron capture nuclides are good for measuring energy and density-dependent processes in the ISM. Consider the hypothesis of distributed acceleration: After most fragmentation in the ISM there is additional acceleration of about a factor of 4. This affects our predictions of measured ^{37}Ar, ^{49}V, and ^{51}Cr abundances. If most of their confinement time is spent at 250 MeV/N rather than 1 GeV/N then about half as much will arrive here because decay is less inhibited at 250 MeV/N. This could cause the observed deficiency in these nuclides (Webber 1981) at 600 MeV/N (after adiabatic deceleration in the solar system). These processes affect certain ultraheavy elemental abundances at higher energies (Letaw, Silberberg, and Tsao 1985).

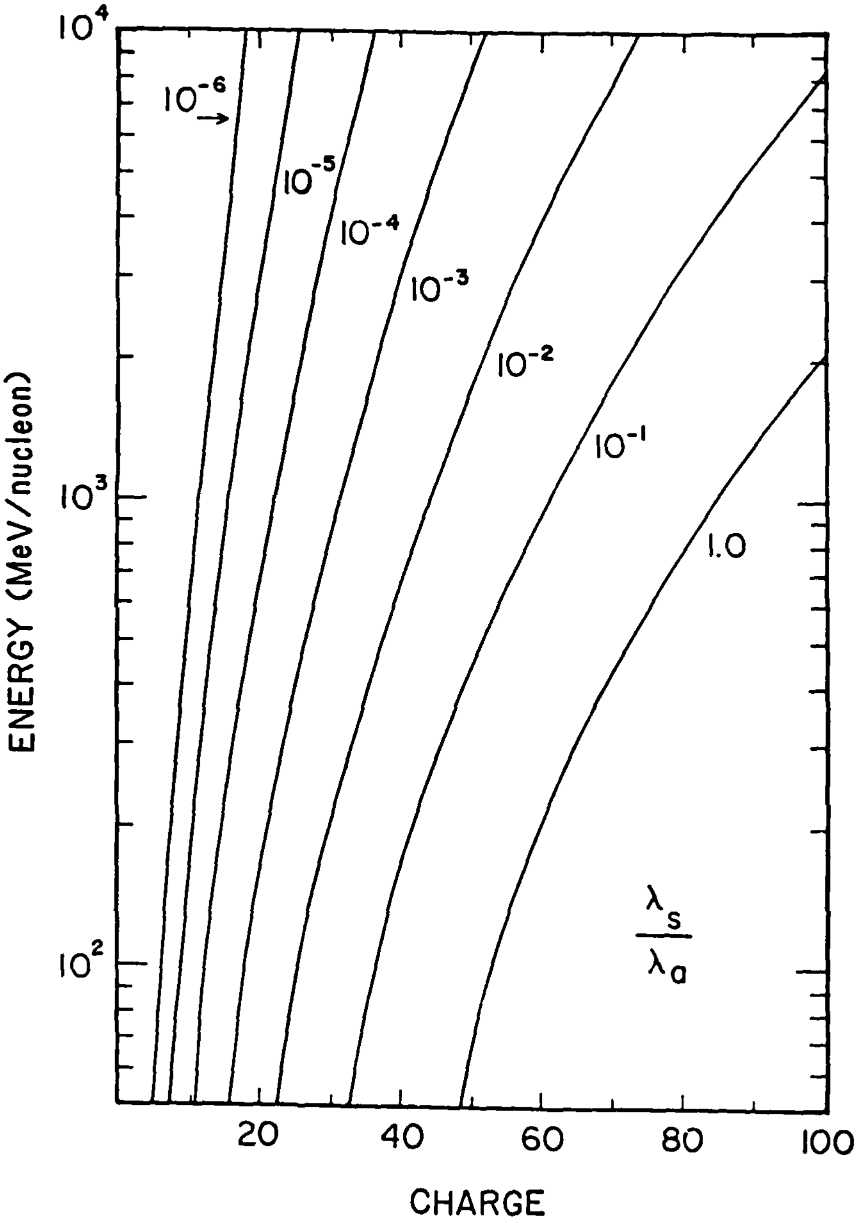

Fig. 7. The equilibrium charge ratio (N*/N) of ions in interstellar medium. When this ratio is greater than 1.0 there is appreciable multiple electron attachment. The ratio (N/N) nearly equals λ_s/λ_a.

The mean density of the ISM in the galactic disk is about 1 atom/cm^3 and the muon density along the cosmic ray path is about 0.3 atom/cm^3. Although most studies of cosmic ray composition have assumed that the medium of propagation is homogeneous, in fact this cannot be so. The ISM is composed of occasional clouds having central densities of about 50 atoms/cm^3 distributed in a very tenous ISM (about 0.003 atoms/cm^3). There are, so far, no observed consequences of this inhomogeneity, but abundances of some electron capture nuclides are affected. In a cloud, a long-lived nuclide such as ^{93}Mo decays slowly because the time between stripping collisions is very short. In the tenuous phase of the ISM decay is again slow because very few attachment (or stripping) reactions take place. Figure 8 shows the surviving fraction of ^{93}Mo as a function of energy for several two-component models of the ISM. The nuclide ^{44}Ti provides another suitable test (Letaw et al., 1985).

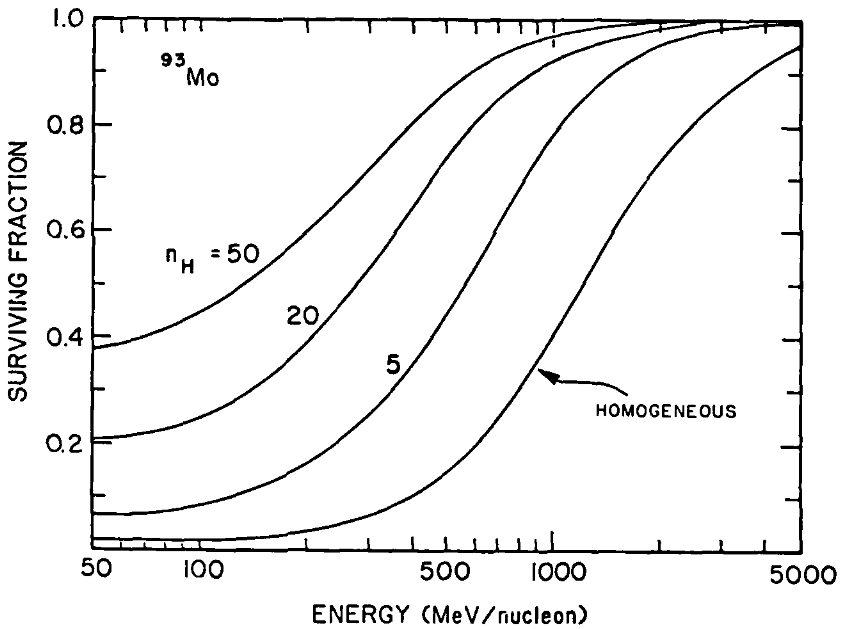

Fig. 8. The fraction of ^{93}Mo that survives as a function energy for two-component models with various matter densities in clouds.

We conclude this section by noting that electron capture nuclides can be a useful diagnostic of the ISM even though little observational evidence is presently available. Abundances of these nuclides depend both on the energy during propagation and the density distribution of the propagation medium. In the future we expect to draw useful conclusions from ultraheavy elemental abundance measurements around Z = 40 using electron capture information.

8. COSMIC RAY PROPAGATION

The simplest model - the leaky box - describes most features of cosmic-ray propagation and permits the associated calculations to reproduce most cosmic-ray abundances. In this model the cosmic rays are considered to be confined to a volume from which they eventually escape by diffusion. (Escape by convection is also possible). The nature of the leaky box is not yet established. It could be the galactic disk with a radio halo of modest dimensions - about 1 Kpc in half thickness. Or there could be a cosmic ray halo of larger dimensions, about 10 Kpc, as Ginzburg has many times proposed (e.g. Ginzburg and Syrovatskii, 1965). On the other hand, the leaky box could be much smaller and more local - a superbubble in which the solar system is imbedded - with a diameter roughly a couple of hundred parsecs. Kafatos (1981) and Streitmatter et al. (1983) have applied the superbubble model to cosmic ray propagation. In the latter model, cosmic rays are reflected at the walls of the superbubble, and some traversal of matter would occur during these encounters.

Data that could help to distinguish between the above models are required. Would the gamma ray flux from cosmic ray interactions in the walls or shells of the superbubble help to distinguish between the superbubble and galactic models? Gamma ray data show that the cosmic ray density in the local galactic neighborhood is not especially high - how large an enhancement is needed for the superbubble model? With nucleosynthesis from numerous supernovae in the superbubble, some ^{244}Pu and ^{247}Cm would be expected to be observed in future experiments when over a 100 actinides get recorded.

In the leaky box model, the energy dependence of the secondary-to-primary ratios is usually interpreted as due to rigidity-dependent diffusion from the confinement region, with the confinement time $T \propto R^{-b}$, where b is 0.4 to 0.7. Higher energy particles accordingly are considered to leak out more readily, and have smaller secondary-to-primary ratios.

There is some evidence that the simple leaky box does not describe all observations. The very small energy dependence of the anisotropy between 10^{10} and 10^{14} eV, after correcting for the Compton-Getting anisotropy is difficult to explain in terms of a rigidity dependent confinement time. (The anisotropy is discussed in my second paper at this School.) The large path length required for the production of $\bar{p}$ and possibly ^{3}He implies that some modification of the simple leaky box picture is required. There are two alternative ways to amend the leaky box: (1) introduce density fluctuations and nested leaky boxes that contain cosmic ray sources within the leaky box or (2) introduce an outer confinement volume. The first modification is associated with the observations of interstellar clouds and supernovae in young OB stellar associations. The second picture considers e.g. superbubbles as the basic leaky box, with the Galaxy (possibly including the halo as the outer confinement box. A more complicated picture, with a 3-fold confinement volume, has been proposed by Stephens (1981a).

The first alternative - the Multiple Cloud Model - was proposed by Silberberg et al. (1983a) which incorporates the nested source leaky box of Cowsik and Wilson (1973, 1975). The model is related to observations of the interstellar medium by adoption of the 3-component interstellar medium of Blandford and Ostriker (1980), and the association of gamma-ray sources and OB stellar associations with clouds, explored by Montmerle (1979).

Since the clouds provide a medium for nuclear interactions, the observational tests rely on information derived from the interaction products. The energy dependence of the secondary to primary ratios $(3 \leq Z \leq 5)/(6 \leq Z \leq 8)$ and $(17 \leq Z \leq 25)/(Z = 26)$ provides such tests. Our paper on High-Energy Cosmic Rays at this school shows the energy dependence of B/C for three models: the closed galaxy of Peters and Westergaard (1977), the Multiple Cloud Model (MCM) and the Leaky Box Model (LBM). The energy dependence of the B/C ratio thus provides a test between the models. A second test has been outlined in section 7 above.

A further experimental test between the MCM and LBM is provided by the surviving fraction of radioactive secondary nuclei ^{10}Be, ^{26}Al and ^{36}Cl. In the MCM the confinement time is 10^7 years, for the LBM model, $T \propto R^{-0.5}$ for $R > 4$ GV/c. The fractions ^{10}Be/Be, ^{26}Al/Al and ^{36}Cl/Cl are shown in Fig. 9 as a function of energy/nucleon. The decrease of ^{26}Al/Al at high energy is due to the decrease of secondary Al relative to primary Al.

The high abundance of antiprotons can be explained in terms of the MCM by postulating source regions where cosmic rays traverse > 30 g/cm^2 materials so that p, $\bar{p}$ and a sizeable fraction of helium nuclei excape, while very few of the heavier nuclei do. Such an origin of the antiprotons has already been proposed by Cowsik and Gaisser (1981) and Cesarsky and Montmerle (1981).

The second alternative picture--cosmic ray confinement in a superbubble--has been explored briefly by Kafatos et al. (1981), and Streitmatter et al. (1983), and Clayton (1984). Stephens (1981b) has pointed out some significant constraints for this model: Acceleration during encounters with the shock wave walls of the bubble must not result in significant acceleration - the ratios of secondary/primary cosmic rays that decrease with energy are not consistent with continued acceleration of particles. However, we consider it plausible that the shock waves of successive supernovae, prior to reaching the bubble walls may accelerate energetic particles emitted by flare stars up to the energies of cosmic ray particles. While the production of anti-protons has not been explored in terms of the superbubble picture, we think that one should explore whether they could be understood from an evolutionary point of view: The superbubble started out with supernova explosions in young OB associations with dense clouds in which extensive traversal of matter by cosmic rays took place prior to the dissipation of these clouds. It is not clear, however, whether the small energy dependence of anisotropy and the large one of the secondary/primary ratios can be reconciled in this model.

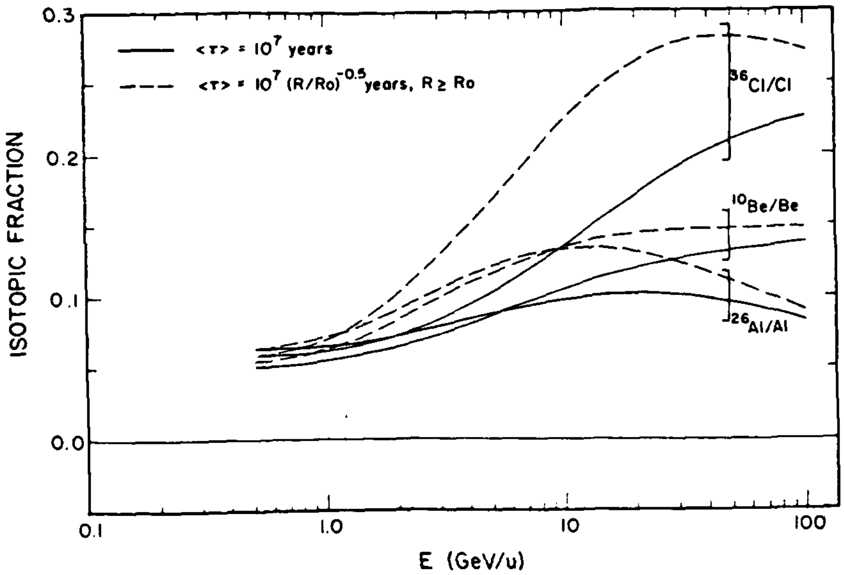

Fig. 9. The ratios ^{10}Be/Be, ^{26}Al/Al and ^{36}Cl/Cl vs. energy for the multiple cloud model (solid curve) and leaky box model (dashed curve).

A more complicated version of the superbubble picture postulates a second confinement volume (Galactic) outside the superbubble. This model is being explored by Lund. With the assumption of very slow leakage from the second or outer confinement volume, i.e. long path lengths, the antiprotons can be attributed to diffusion into the superbubble from the outer regions.

The expected electron flux and energy spectrum in the superbubble needs further exploration to test the viability of the model. The electron flux in the galaxy can be estimated from the Galactic radio spectrum and magnetic field strength. In a superbubble, the cosmic ray flux should differ from that outside. Is the electron flux in the superbubble model different from various directions of the Galaxy? If a long residence time is assumed outside the superbubble, synchrotron losses would steepen the electron spectrum at lower energy. Is the Galactic electron spectrum derived from the radio emission consistent with a longer residence time? These questions demonstrate that much interesting research can be carried out on propagation of cosmic rays in the future.

9. REFERENCES

Adams, J.H., Jr., Shapiro, M.M., Silberberg, R., and Tsao, C.H., 17th Internat. Cosmic Ray Conf., Paris, 2, 256.

Binns, W.R. Fickle, R.K. Garrard, T.L., Israel, M.H., Klarmann, J., Stone, E.C., and Waddington, C.J., 1982, Ap. J. (Letters), 261, L117.

Blanford, R.D. and Ostriker, J.P., 1980, Ap. J., 237, 793.

Cameron, A.G.W. 1981, in Essays in Nuclear Astrophys., ed. C.A. Barnes, D.D. Clayton, and D.N. Schramm (Cambridge: Cambridge University Press).

Cesarsky, C.J. and Montmerle, T.M. 1981, 17th ICRC, Paris, 9, 207.

Cowsik, R. and Wilson, L.W., 1973, 13th ICRC, Denver, 1, 500.

Cowsik, R. and Wilson, L.W., 1975, 14th ICRC, Munich, 2, 659.

Cowsik, R. and Gaisser, T.K., 1981, 17th ICRC, Paris, 2, 218.

Crawford, H.J. 1979, Ph.D. Thesis, University of California, (Berkeley).

Dostrovsky, I., Rabinowitz, P. and Bivins, R. 1958, Phys. Rev. 111, 1659.

Fowler, P.H., Walker, R.N.F., Masheder, M.R.W., Moses, R.T., and Worley, A. 1981, Nature 291, 45.

Ginzburg, V.L. and Syrovatskii, S.I. 1964, The Origin of Cosmic Rays, Pergamon Press, New York.

Hinshaw, G.F. and Wiedenbeck, M.E. 1983, 18th ICRC, Bangalore, 2, 208.

Kafatos, M. Bruhweiler, F. and Sofia, S. 1981, 17th ICRC, Paris, 2, 222.

Kaufman, S.B., and Steinberg, E.P. 1980, Phys. Rev C., 22, 167.

Letaw, J.R. Silberberg, R. and Tsao, C.H. 1983 Ap. J. Suppl. 51, 271.

Letaw, J.R., Silberberg R. and Tsao, C.H. 1984a, Ap. J. 279, 144.

Letaw, J.R., Silberberg, R. and Tsao, C.H. 1984b, Propagation of Heavy Cosmic Ray Nuclei, to be publ. in Ap. J. Suppl.

Letaw, J.R., Silberberg, R., and Tsao, C.H. 1985. Electron Capture Decay of Cosmic Rays, to be publ. in Ap. Space Sci.

Metropolis, N., Bivins, R., Storm, M. Turkevich, A., Miller, J.M. and Friedlander, G. 1958, Phys. Rev. 110, 185.

Montmerle, T. 1979, Ap. J. 231, 95.

Peters, B. and Westergaard, N.J., 1977, Ap. Space Science 48, 21.

Rudstam, G., 1966, Z.F. Naturforschung, 21A, 1027.

Silberberg, R. and Tsao, C.H. 1973a, Ap. J. Suppl., 25, 315.

Silberberg, R. and Tsao, C.H. 1973b, Ap. J. Suppl., 25, 335.

Silberberg, R. and Tsao, C.H. 1977a, Ap. J. Suppl., 35, 129.

Silberberg, R. and Tsao, C.H. 1977b, 15th Internat. Cosmic Ray Conf. (Plovdiv), 2, 84.

Silberberg, R., Tsao, C.H. Shapiro, M.M. and Letaw, J.R. 1983a, 18th ICRC, Bangalore, 2, 179.

Silberberg, R. Tsao, C.H., Letaw, J.R., and Shapiro, M.M. 1983b, Phys. Rev. Letters, 51, 1217.

Stephens, S.A., 1981a, 17th ICRC, Paris 2, 197.

Stephens, S.A. 1981b, 17th ICRC, Paris, Rapporteur Papers 13, 89.

Streitmatter, R.E., Balasubrahmanyan, V.K., Ormes, J.F., and Protheroe, R.J. 1983, 18th ICRC, Bangalore 2, 183.

Tsao, C.H., Shapiro, M.M., and Silberberg, R. 1973, 13th Int. Cosmic Ray Conf., Denver 1, 107.

Tsao, C.H. and Silberberg, R. 1979, 16th Int. Cosmic Ray Conf. (Kyoto), 2, 202.

Tsao, C.H., Silberberg, R., and Letaw, J.R., 1983, 18th Internat. Cosmic Ray Conf. (Bangalore), 2, 194.

Waddington, C.J., Fickle, R.K., Garrard, T.L. Stone, E.C., Binns, W.R. Israel, M.H., and Klarmann, J. 1981, Proc. 17th Int. Cosmic Ray Conf. (Paris), 9, 109.

Webber, W.R., 1981, 17th ICRC, Paris, 2, 80.

RADIATION TRANSPORT OF COSMIC RAY NUCLEI IN LUNAR MATERIAL AND RADIATION DOSES

R. Silberberg, C.H. Tsao, J.H. Adams, Jr.
E.O. Hulburt Center for Space Research
Naval Research Laboratory
Washington, D.C. 20375-5000
and
John R. Letaw
Severn Communications Corporation
Severna Park, Maryland 21146

ABSTRACT

The radiation environment on the lunar surface is inhospitable: there is no radiation-absorbing atmosphere and no overall magnetic field that deflects charged particles. The annual dose equivalent due to cosmic rays at times of solar minimum is about 30 rem. Also, the lunar surface is not protected from solar flare particles; at energies above 30 MeV, the dose equivalent over the 11-year solar cycle is about 1000 rem, most of those particles arrive in one or two gigantic flares, each lasting only about 2 days. These doses greatly exceed the permissible annual dose--0.5 rem for the general public and 5 rem for radiation workers. For permanent lunar residents, it is necessary to construct shelters several meters below the lunar surface. At moderate depths below the lunar surface (<200 g/cm^2) the flux of secondary neutrons exceeds considerably that in the upper atmosphere of the earth. This comes about because cosmic ray interactions with lunar material (that contains many nuclei heavier than atmospheric N and C) generate many more neutrons in the nuclear evaporation process. The annual dose equivalent due to neutrons is about 20 or 25 rem within the upper meter of the lunar surface. Recent experiments show that small doses (an absorbed dose of about 10 rad) of fast heavy nuclei like Ar and Fe have a large probability for generating tumors or fetal abnomalities. We therefore feel it is useful to present the attenuation rate of heavy cosmic ray nuclei in tissue and in shielding material at the lunar surface. The dose equivalent due to gamma rays generated by nuclear interactions near the lunar surface is only of the order of 1% of that due to neutrons. However, gamma ray line emission from excited nuclei and nuclear spallation products generated by cosmic rays near the lunar surface is of considerable interest: these lines permit the determination of lunar composition with electronic counters.

1. INTRODUCTION

The cosmic ray environment on the lunar surface is inhospitable for permanent settlement. This problem can be overcome, however, by adequately shielded conditions. We show in this paper that during the four week lunar day-night cycle, the permanent settlers may work 10 hours per 24 hour interval, for the two week long lunar day on the lunar surface, i.e. about 20% of the total time. The remaining time has to be spent in habitats either under the lunar surface or at the surface under a mound built of lunar material. It should be noted that the lifting of material from the mound requires 1/6 the corresponding energy expenditure on the earth, due to the reduced gravity.

In this paper we explore the results of our radiation transport calculations. The primary cosmic ray nuclei (discussed by Adams and Shapiro (1985) in these proceedings) propagate in the lunar soil and undergo nuclear transformations. Our radiation transport calculations include the stable as well as unstable cosmic ray nuclides from H to Ni, ionization loss and solar modulation. Also the breakup of nuclei of the lunar soil, the production of neutrons and neutron generated nuclear recoils are taken into account. For radiobiological analysis the cosmic ray energy spectra are converted into LET (Linear Energy Transfer or ionization energy deposition) spectra. These are then converted into absorbed doses and dose equivalents as a function of depth of lunar soil, and compared with the permissible dose limit of 5 rem/year for radiation workers.

2. THE PROPAGATION EQUATION

Cosmic ray nuclei fragment in collisions with the atomic nuclei in the lunar soil. The fundamental equation for cosmic ray propagation that includes the effects of nuclear transformations and energy losses based in Ginzburg and Syrovatskii (1964), is

$$\frac{\partial J_i}{\partial x} = \frac{-J_i}{\lambda_i} + \sum_{j>i} \frac{J_i}{\lambda_{ij}} + \frac{\partial}{\partial E}\left[J_i\left(\frac{dE}{dx}\right)_i\right] \qquad (1)$$

Here J_i is the differential flux of cosmic-ray particles of isotopes of type i, x is the path length in units of g/cm^2, dE/dx is the (positive) stopping power, λ_i is the fragmentation mean free path of a nucleus of isotope i, and λ_{ij} is the mean free path of a nucleus of type j yielding one of type i. The cross sections used are those of Silberberg and Tsao (1973), Letaw (1983a), and Letaw et al. (1983b). For a composite material, λ_i and λ_{ij} are weighted over the nuclei of a mixture, with N decomposed so as to represent the individual number of atoms/cm^3 of a given type in the lunar material. For our calculation we adopted the composition given by Reedy (1978), with the relative abundances of nuclei as shown in Table 1.

3. CALCULATION OF DOSE

The output of the propagation program yields the energy spectra dJ_i/dE of all nuclear species at various depths of a given material. For the calculation of the dose, the energy spectra are converted into rate of ionization energy loss (or LET) spectra. Using the abbreviated notation $dJ_i(S)/dS=J_i(S)$, where S is the stopping power or dE/dx, the integral LET spectrum $N_i(S_o)$ is given by

$$N_i(S_o) = \int_{S_o}^{\infty} J_i(S)dS \qquad (2)$$

The absorbed dose rate from nuclides of type i, with stopping power $S > S_o$ is given by

$$\dot{D}_i\,(S_o) = \int_{S_o}^{\infty} J_i(S)SdS \qquad (3)$$

If x is in units of g/cm^2, J in units of particles/cm^2 sec, and E is in units of 100 ergs, then $\dot{D}$ is given in units of rad/sec. For the dose equivalent, the integral of Eq. 3 contains the quantity factor Q(S), defined in terms of LET intervals, and approximated as in Silberberg et al. (1984). The dose equivalent rate is given in units of rem/sec. The doses have been calculated for energy deposition in water, i.e. for biological tissue-like material.

4. DOSE DUE TO COSMIC RAYS

Fig. 1 shows the LET spectra and the integral absorbed dose rates as a function of shielding in lunar material, from 1 to 200 g/cm^2. The total absorbed dose rate in units of rad/year can be read off at the left hand side.

Fig. 2 shows the corresponding LET spectra with the quality factor included in the integration of Equation 3, i.e. the integral dose equivalent rate, from 1 to 200 g/cm^2. The units are rem/year. In both Figs. 1 and 2, the shoulder above approximately 1500 MeV/(g/cm^2) results from the contribution of the highly ionizing iron nuclei. The large reduction of the dose at high values of LET is due to the depletion of cosmic-ray iron with shielding, both because of its large spallation cross section, and high rate of ionization loss as a result of which slower iron nuclei stop in the shielding.

Fig. 3 shows the attenuation of the annual integral absorbed dose and dose equivalent due to cosmic ray nuclei. After about 100 g/cm^2, the dose equivalent due to nuclei is similar to that of the absorbed dose, because of the breakup of heavy nuclei. However, as we show later, when neutron generated nuclear recoils are considered, the difference between the absorbed dose and the dose equivalent persists.

5. DOSE DUE TO NEUTRONS

The dose rate due to neutrons is calculated using (a) the neutron depth profile in lunar material measured by Woolum and Burnett (1974), and the calculations of Lingenfelter et al. (1972), (b) the energy spectra of neutrons in lunar soil, calculated by Reedy and Arnold (1972), and (c) the relationship between the neutron flux and the absorbed dose and dose equivalent, as a function of energy, given by Armstrong et al. (1969). Table 2 gives the annual dose equivalent of the neutron dose in lunar material, as a function of depth.

6. PERMISSIBLE DOSE AND SHIELDING REQUIREMENTS

We note from Table 2, that only for >400 g/cm^2 the annual dose equivalent becomes smaller than 5 rem, the permissible annual dose for radiation workers. At the time of a giant flare, like that of February 1956, the dose over the two-day duration of the flare exceeds the annual dose of Table 2 by an order of magnitude. At the time of such a flare, a shield of 700 g/cm^2 is required to reduce the dose to the level permissible for radiation workers.

For a few astronaut-volunteers over 30 years of age, the Radiobiological Advisory Panel (1970) has permitted higher dosages: an annual dose of 38 rem, and a life-time limit of 200 rem. The latter limit is reached already in about ten years on the lunar surface even in the absence of solar flares.

Fig. 4 shows a comparison of the annual dose equivalent due to cosmic ray nuclei and neutrons, as a function of depth in lunar material, down to 500 g/cm^2. It can be seen that for a shielding >400 g/cm^2, the annual dose is brought down to the level permissible for radiation workers. Even with such shielding, one receives in 40 years a dose of 200 rem, the permissible life-time dose for a few astronaut-volunteers. On rare occasions, a couple of days per 11-year solar cycle, additional shielding is needed at the time of giant solar flares.

7. GAMMA RAY LINES

The biological effects of gamma rays induced by cosmic ray and solar flare particle interactions in the lunar soil are relatively minor. On the other hand, the gamma ray lines are likely to be useful for mineral prospecting on the moon. Concentrations of elements like U, Th, Ti, K can be located as well as the more common elements shown in Table 1. The emission rates of gamma ray lines on the lunar surface have been explored by Reedy (1978).

8. CONCLUSIONS

For permanent residents on the moon, about 20% of time (or 40% of the two-week day-light time) can be spent without significant shielding. Most of the time should be spent in shelters of >400 g/cm^2, or about two meters of densely packed lunar soil, either below the surface, or at the surface beneath a shielding mound. At the time of rare gigantic flares, shelters >700 g/cm^2 are needed - such a protection is particularly important for radiation-sensitive fetuses.

References

Adams, J.H., Jr. and Shapiro, M.M. (1985) Irradiation of the Moon by Galactic Cosmic Rays and Other Energetic Particles, in these Proceedings.

Armstrong, T.W., Alsmiller, R.G., Jr., and Barish, J. (1969) Calculation of the Radiation Hazard at Supersonic Aircraft Altitudes Produced by an Energetic Solar Flare, Nucl. Sci. Eng., 37, pp. 337-342.

Ginzburg, V.L. and Syrovatskii, S.I. (1964) The Origin of Cosmic Rays, publ. by Pergamon/MacMillan, New York.

Letaw, J.R. (1983a) Proton Production Cross Sections in Proton-Nucleus Collisions, Phys. Rev. C, 28, pp. 2178-2179.

Letaw, J.R., Silberberg, R., and Tsao, C.H. (1983b) Proton-Nucleus Total Inelastic Cross Sections: An Empirical Formula for E > 10 MeV, Ap. J. Suppl. 51, pp. 271-274.

Lingenfelter, R.E., Canfield, E.H. and Hampel, V.E. (1972) The Lunar Neutron Flux Revisited, Earth Planetary Sci. Letters, 16, pp. 355-369.

Radiobiological Advisory Panel, Committee on Space Medicine, Space Science Board, NAS/NRC, Washington, D.C. (1970). Radiation Protection Guides for Space-Mission and Vehicle-Design Studies Involving Nuclear Systems, (W.H. Langham, ed.).

Reedy, R.C. (1978) Planetary Gamma Ray Spectroscopy, pp. 98-148 in NASA Tech. Memo. 79619, Gamma Ray Spectroscopy in Astrophysics, ed. by T.L. Cline and R. Ramaty.

Reedy, R.C. and Arnold, J.R. (1972) Interaction of Solar and Galactic Cosmic Ray Particles with the Moon, J. Geophys. Rev. 77, pp. 537-555.

Silberberg, R. and Tsao, C.H. (1973) Partial Cross Sections in High-Energy Nuclear Reactions, and Astrophysical Applications, Ap. J. Suppl. 25, pp. 315-333.

Silberberg, R., Tsao, C.H., Adams, J.H., Jr., and Letaw, J.R. (1984) Radiation Doses and LET Distributions of Cosmic Rays, Rad. Research 98, pp. 209-226.

Woolum, D.S. and Burnett, D.S. (1974) In-Site Measurement of the Rate of 235-U Fission Induced by Lunar Neutrons, Earth Planetary Sci. Letters 21, pp. 153-163.

Table 1. Relative Abundances of the Nuclei of the More Common Elements in Lunar Soil.

Element	Abundance (%)
C	61
Mg	4
Al	9
Si	16
Ca	6
Fe	4

Table 2. The Annual Dose Equivalent Due to Cosmic-Ray Generated Neutrons.

Depth (g/cm^2)	Annual Dose (rem/year)
0	1.5
10	3
20	5
100	13
200	12
300	8
400	5
500	2

Figure Captions

1. The LET-distributions of the integral absorbed dose rates in units of rads/year, as a function of shielding from 1 to 200 g/cm^2.

2. The LET-distributions of the integral dose equivalent rates in units of rems/year, as a function of shielding from 1 to 200 g/cm^2.

3. The attenuation of the annual dose due to cosmic ray nuclei with shielding. The upper and lower curves show the dose equivalent and absorbed dose rates, respectively.

4. A comparison of the annual dose equivalent due to secondary neutrons and cosmic ray nuclei, as a function of shielding. Also the absorbed dose rate due to cosmic ray nuclei is shown.

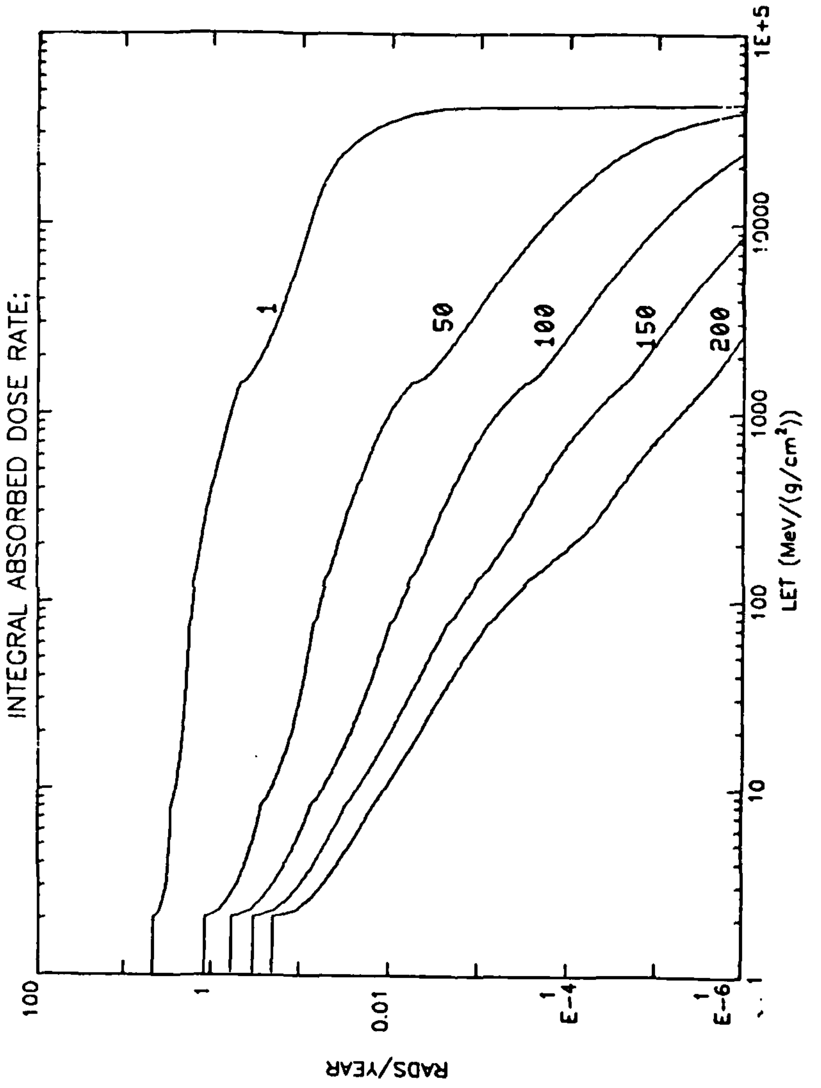

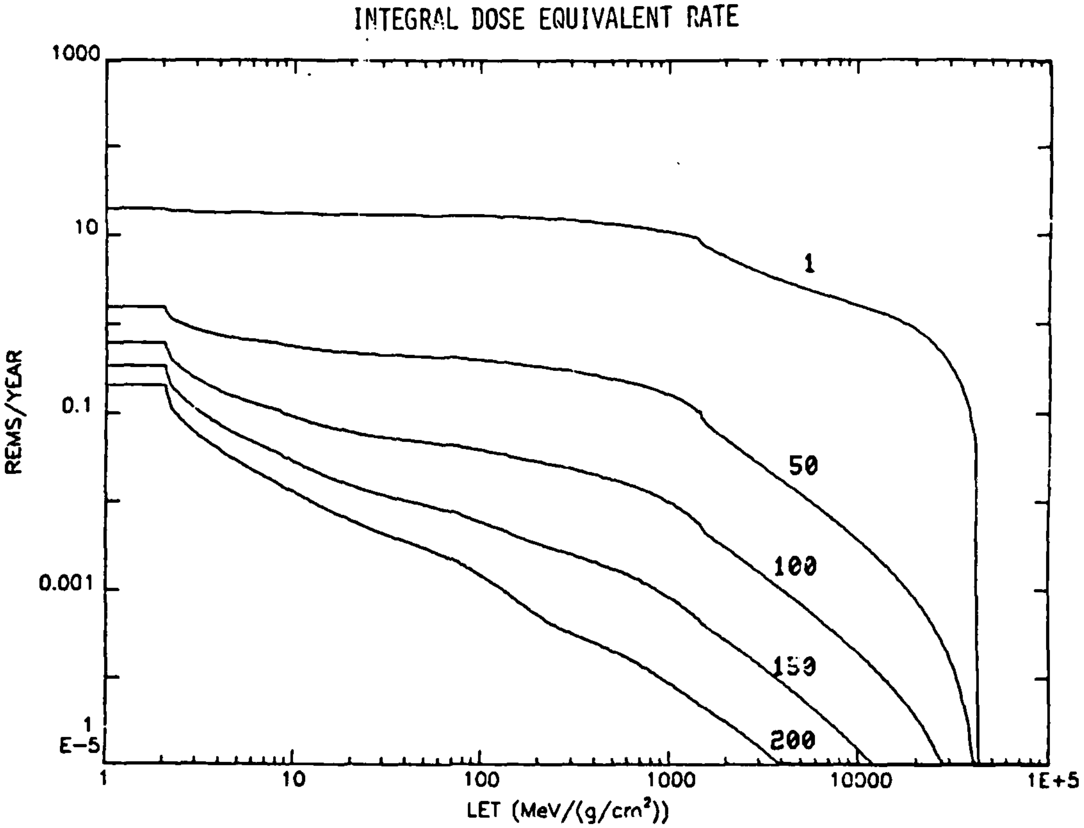
INTEGRAL DOSE EQUIVALENT RATE
1000
10
0.1
0.001
1
E-5
REMS/YEAR
1
10
100
1000
10000
1E+5
LET (MeV/(g/cm²))
1
50
100
150
200

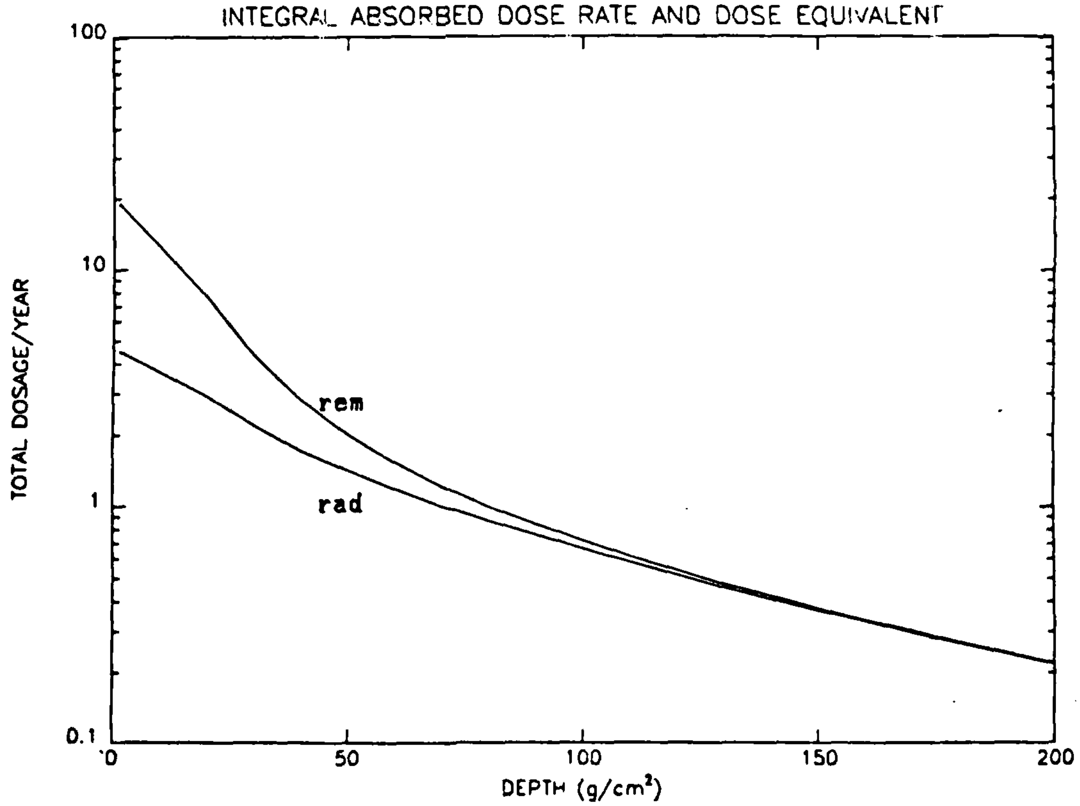
INTEGRAL ABSORBED DOSE RATE AND DOSE EQUIVALENT
100
10
1
0.1
TOTAL DOSAGE/YEAR
0
50
100
150
200
DEPTH (g/cm²)
rem
rad

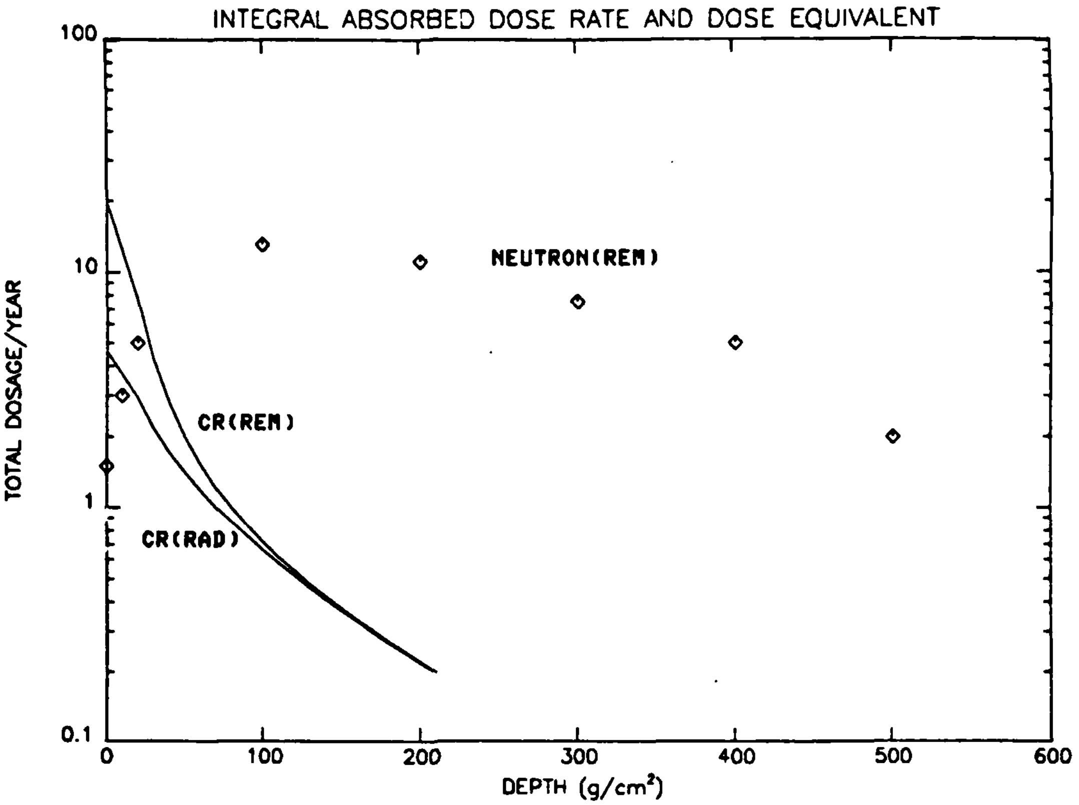
INTEGRAL ABSORBED DOSE RATE AND DOSE EQUIVALENT
TOTAL DOSAGE/YEAR
100
10
1
0.1
NEUTRON(REM)
CR(REM)
CR(RAD)
0
100
200
300
400
500
600
DEPTH (g/cm²)

Non-Geometric Behavior of Nucleus-Nucleus Total Inelastic Cross Sections

John R. Letaw
Severn Communications Corporation
Severna Park, Maryland 21146

and

Rein Silberberg and C.H. Tsao
E.O. Hulbert Center for Space Research
Naval Research Laboratory
Washington, D.C. 20375

Abstract

Geometric models of high energy nucleus-nucleus reactions, in which total inelastic cross sections increase as $A^{2/3}$, are violated under certain conditions. In several elements, for example, Ca, the nuclear skin of lighter isotopes extends farther than for heavier isotopes. Since the mean free path of nucleons in nuclear matter is short, the cross section is correlated more strongly with the total skin extent than with the radius and therefore can be smaller for heavier isotopes.

Introduction

High-energy (> 100 MeV/nucleon) nucleus-nucleus cross sections are of interest in numerous disciplines where the fragmentation of fluxes of heavy ions in passage through matter is important. These disciplines include experimental nuclear physics, radiomedicine, radiation effects, cosmic-ray physics, and high-energy astrophysics. The total inelastic cross section characterizes the total loss of a flux of heavy ions due to fragmentation. In general these cross sections are most accurately represented by semi-empirical formulas[1] which interpolate between the relatively scant experimental data. However, because the experimental data are so patchy, semi-empirical formulas are susceptible to large, systematic errors and tend to wash out detail.

The most primitive model of high-energy total inelastic cross sections is that of two (classical) colliding hard spheres. In this case, the interaction cross section is

$$\pi (R_1 + R_2)^2 \tag{1}$$

where the radii R_1 and R_2 of the nuclei are taken to be proportional to $A^{1/3}$. A better model of the total inelastic cross section was developed by Bradt and Peters[2].

$$\pi (R_1 + R_2 - b)^2 \tag{2}$$

The additional free parameter, b, is the amount of overlap between the hard spheres necessary for an interaction to take place. Both of these models are unsatisfactory because no choice of free parameters accurately predicts all cross sections at all energies.

In an effort to correct the deficiencies of earlier models, Karol[3] introduced the soft-spheres model. Within this model nuclei are treated as spheres with a nuclear density decreasing radially outward from the center. The nuclear density distribution is characterized by the half-way radius, c, and skin thickness, t. For any given impact parameter the overlap of nuclear matter and the total NN cross sections are folded together to yield *the transparency. The total inelastic cross section is found* by integrating over impact parameters.

While conceptually accurate, Karol's model predicts total inelastic cross sections about 10% greater than measured.[4] As first pointed out by Wilson and Townsend[5] some of this disagreement can be traced to Karol's use of the nuclear charge density distribution parameters to represent the matter density distribution. Deconvolution[6] of the charge density distribution using the proton charge density yields a matter density distribution with slightly larger half-way radius and significantly smaller skin thickness. When these new parameters are incorporated into the soft-spheres model we find substantially better agreement with experiment.

In this Letter we show, using the updated soft-spheres model, that among isotopes of a given element the total inelastic cross section on any target may not increase monotonically with mass. This result is *in direct* contrast with *geometric models* (Eqs. (1)-(2)). We trace our result to the strong correlation between the skin extent (radius at 10% central density) and the total inelastic cross section. Although a heavier isotope generally has a larger half-way radius, the skin may actually be thinner because of stronger binding. In some cases (e.g., ^{48}Ca) this results in a skin extent less than that of a lighter counterpart (e.g., ^{42}Ca), hence the total inelastic cross section is smaller.

Cross Section Model

The total reaction cross section within the soft-spheres model[3] is given by

$$\sigma = 2\pi \int_0^\infty [1 - T(r)]\, r\, dr \qquad (3)$$

where T(r), the transparency function, is the probability of projectile passage *through* the *target* at impact parameter r. This semi-classical model is applicable only at high energies where details of nuclear structure, electromagnetic interactions and exclusion principle effects may be ignored. We have not incorporated the phenomenon of photodisintegration[7] which is an important contributor to the cross section when two highly charged nuclei collide.

Within the soft spheres model the transparency function is given by

$$T(r) = \exp\left[-\bar{\sigma} \int_{-\infty}^{\infty} \left(\int_V \rho_T(r,z,\vec{x})\, \rho_P(r,z,\vec{x})\, d^3\vec{x} \right) dz \right] \qquad (4)$$

where ρ_T and ρ_P are the target and projectile matter density distributions, which are taken to be homogeneous. The parameter z is the distance along the beam to a normal plane through the target.

The average nucleon-nucleon collison cross section is

$$\bar{\sigma}(E) = \left[\left(\frac{Z_T}{A_T}\right)\left(\frac{Z_P}{A_P}\right) + \left(\frac{N_T}{A_T}\right)\left(\frac{N_P}{A_P}\right)\right]\sigma_{pp}(E) \; + \\ \left[\left(\frac{Z_T}{A_T}\right)\left(\frac{N_P}{A_P}\right) + \left(\frac{N_T}{A_T}\right)\left(\frac{Z_P}{A_P}\right)\right]\sigma_{pn}(E) \qquad (5)$$

where $Z_{T(P)}$, $N_{T(P)}$, and $A_{T(P)}$ are, respectively, the proton, neutron, and mass numbers of the target (projectile); σ_{pp} is the proton-proton ($\approx$ neutron-neutron) total cross section; and σ_{pn} is the proton-neutron total cross section. All energies are in units of kinetic energy per nucleon. $\bar{\sigma}$ quantifies the average rate at which projectile matter interacts with target matter.

Karol approximates the nuclear matter distribution as Gaussian. For light nuclei ($A < 40$) this is a satisfactory model of the actual distribution. Free parameters are specified by the RMS charge radius a and normalization to the mass. For heavy nuclei the Gaussian is "surface-normalized". Matching the Gaussian distribution to a Fermi distribution at the 50% and 10% of central density radii determines the free parameters in terms of the half-way radius c and skin thickness t. The Gaussian is then a good fit to the surface but overestimates the central density. The approximation is justified because transmission is negligible in the central region regardless of model. The Gaussian approximation allows an analytical solution to Eq. (3).

Our model differs from Karol's in the determination of free parameters in the density distribution. While he uses the parameters of the charge distribution (a or, c and t) as an adequate model of the matter distribution, we deconvolute the charge distribution using the proton charge distribution to determine the matter distribution. The deconvolution is necessary because nucleon-nucleon total cross section measurements implicitly incorporate particle structure. In the case of light nuclei this deconvolution amounts to replacing the RMS charge radius with

$$(a^2 - a_p^2)^{1/2}$$

where a_p is the proton charge radius (0.8 fm). For the heavy nuclei we compute parameters c' and t' such that

$$\rho_q(c,t,\vec{x}) = \int_V \rho_p(\vec{x}-\vec{x}\,')\,\rho_m(c',t',\vec{x}\,')\,d^3\vec{x}\,' \qquad (6)$$

is satisfied at radii c and c ± t/2. ρ_q and ρ_m are the charge and mass densities of the nucleus, both taken to be Fermi distributions. ρ_p is the proton charge distribution. Results of the deconvolution are shown in Table I. We note that c' is slightly greater than c while the skin thickness t' is substantially smaller than t.

Conclusions

The model proposed above predicts total inelastic cross sections roughly 10% smaller than the original soft spheres model. This reduces discrepancies with high energy measurements noted by Webber[4] and Wilson and Townsend[5]. For example, the total reaction cross section for protons on Fe is 703 ± 12 mb at 710 MeV/nucleon and 769 ± 11 mb at 1050 MeV/nucleon, while the original soft spheres model predicts 812 ± 40 mb and 829 ± 40 mb respectively, and the model proposed here predicts 745 ± 35 mb and 759 ± 35 mb respectively.

The isotopes of calcium provide a series of nuclides where the parameters of the charge distribution have been tabulated.[8] The parameters in the matter distribution are derived using Eq. (4). Associated calculations[9] support the conclusion that the matter distribution inferred from these measurements is qualitatively correct despite the neglect of neutrons. The computed total inelastic cross sections of the calcium isotopes are shown in Fig.1 where they are compared with projections based on a geometric model. The difference between the two models is about 10% for ^{48}Ca.

The anomalous behavior of these cross sections may be traced to the importance of the nuclear skin in interactions. Since the mean free path of nuclear matter in nuclear matter is short, the possibility of an interaction depends more on the skin extent

$(c' + t'/2)$ than on the half-way or RMS radii. Charge densities of ^{42}Ca and ^{48}Ca are shown in Fig. 2. Though the half-way radius of ^{48}Ca is greater than that of ^{42}Ca, the skin extent is smaller accounting for the smaller cross section. The smaller skin extent may be traced to the nuclear stability of ^{48}Ca. Similar behavior occurs among Sn isotopes and presumably any element where there are several isotopes with large mass differences.

The predictions made here can be tested with existing facilities. At the Bevalac, isotopic beams of ^{48}Ca passing through any light target should show 10% deviation from geometric models per mean free path. The total inelastic cross sections of all Ca isotopes should lie within ± 5% of one another. In addition to their intrinsic importance these measurements at high energies could also prove to be sensitive probes of the nuclear matter distribution.

References

1) J.R. Letaw, R. Silberberg, and C.H. Tsao, Ap. J. Suppl. 51, 271 (1983).
2) H.L. Bradt and B. Peters, Phys. Rev. 77, 54 (1950).
3) P.J. Karol, Phys. Rev. C 11, 1203 (1975).
4) W.R. Webber and D.A. Brautigam, Ap. J. 260, 894 (1982).
5) J.W. Wilson and L.W. Townsend, Can. J. Phys. 59, 1569 (1981).
6) H. Uberall, Electron Scattering from Complex Nuclei (Academic Press, New York, 1971), Pt. A, p.213.
7) P.B. Price (private communication).
8) H.R. Collard, L.R.B. Elton, and R. Hofstadter, in *Nuclear Radii*, edited by H. Schopper (Springer-Verlag, Berlin, 1967), Landolt-Bornstein, New Series, Vol. 2.
9) H. Uberall, op. cit., p.410.

Table I. Comparison of half-way radius and skin thickness for *charge* (c,t) and *matter* (c',t') densities using a *Fermi* distribution. There is a weak correlation between radius and skin thickness at the level indicated by error bounds.

c (fm)	c' (fm)	t (fm)	t' (fm)
3.00	3.07 ± 0.01	1.50	0.89 ± 0.02
4.00	4.05 ± 0.01	2.00	1.56 ± 0.02
5.00	5.04 ± 0.01	2.50	2.15 ± 0.02
6.00	6.04 ± 0.01	3.00	2.71 ± 0.02
7.00	7.03 ± 0.01	3.50	3.24 ± 0.02
8.00	8.03 ± 0.01	4.00	3.77 ± 0.02

Figure Captions

Figure 1 : The total inelastic cross section for protons on several calcium isotopes at 2 GeV/nucleon as predicted by the soft-spheres model (individual data points) and projected from ^{40}Ca using a geometric model. Errors on data points are due to uncertainties in half-way radius and skin thickness.

Figure 2 : The charge densities of ^{48}Ca and ^{42}Ca. The half-way radius of ^{48}Ca is greater than that of ^{42}Ca, while the skin extent (radius at 10% central density) is smaller. ^{48}Ca in this model has a smaller total inelastic cross section because of its smaller skin extent.

Figure 1

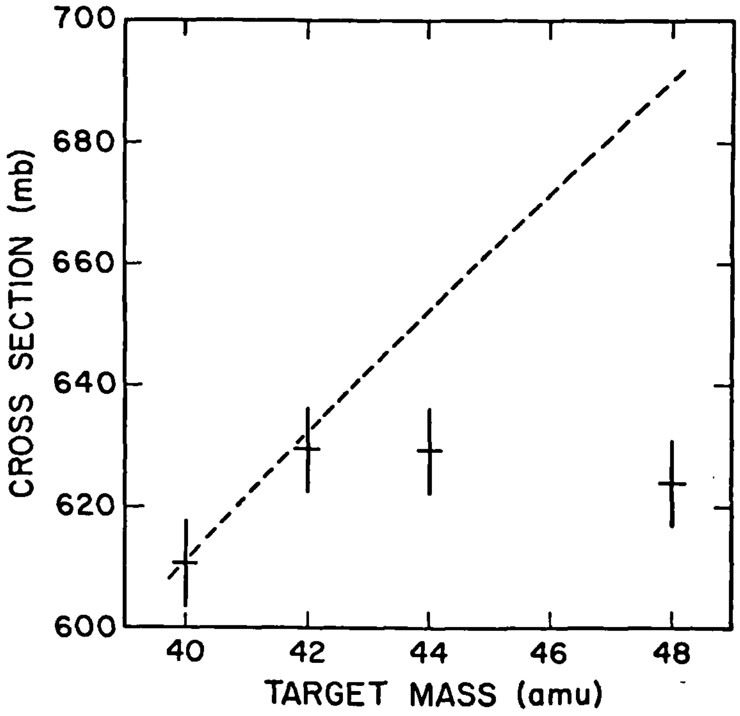

Environmental Models for Single Event Upset Estimation

John R. Letaw
Severn Communications Corporation
P.O. Box 544
Severna Park, MD 21146

1. Introduction

Cosmic ray physics and the associated problem of high energy ion transport have found many important applications in recent years (Fig. 1). These include particle radiation damage to materials, particle beam weapons, radiation dosimetry, radiomedicine, and background in scientific instruments. In space, where particle intensities are great, the natural particle environment is hostile to electronic systems and life.

In this talk we are concerned with the causes of single event upsets (SEUs) in space. These upsets occur in microelectronics when a single ionizing particle passes through sensitive circuitry depositing thousands of electron/hole pairs. Collection of these charges may result in bit flips, latchup, or logical errors. If these errors go uncorrected there is significant potential for spacecraft failure. We have heard some discussion of these failures in this conference.

The procedure we use for estimation of single event upsets is divided into five parts (Fig. 2):

1. Incident particle flux specification
2. Geomagnetic field transmittance
3. One dimensional propagation through thick shielding
4. Geometric integration over angles
5. Energy deposition computations

The natural radiation environment (incident flux) is altered (though not necessarily weakened) by the shielding of Earth's magnetic field and the spacecraft structure. This shielding slows or stops all particles and fragments some particles into lighter, less ionizing, species. There are directional aspects to each of these processes so the calculations are done in many directions then integrated over all angles. The result is the particle fluxes for each charge and energy at the electronics.

The final step in the computation is to determine the rate of energy deposition (and hence the rate of charge deposition) in the chip. For heavy ions such as iron (charge = 26) energy is deposited directly by ionization loss. With protons direct ionization loss is insufficient to cause upsets. They cause upsets indirectly through recoils of silicon nuclei in elastic and inelastic collisions.

Figure 2

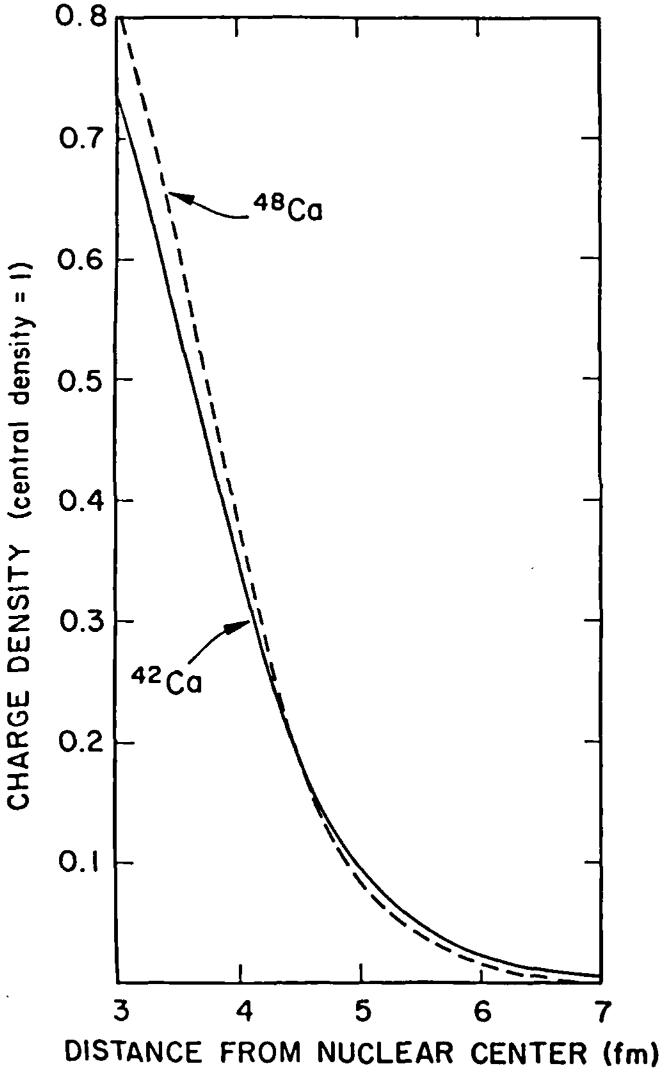

CHARGE DENSITY (central density = 1)
0.8
0.7
0.6
0.5
0.4
0.3
0.2
0.1
^{48}Ca
^{42}Ca
3
4
5
6
7
DISTANCE FROM NUCLEAR CENTER (fm)

2. The Natural Radiation Environment

The natural particle environment is the single greatest source of uncertainty in estimating single event upset rates in spacecraft. A number of factors are responsible for this uncertainty. First, the particle environment has not been fully explored. Uncertainties in the environment, for example, the trapped heavy ion abundances, lead to incomplete environmental modeling. Since trapped heavy ions are very effective at producing upsets they may, even in small numbers, dominate the trapped protons in causing SEUs.

A second factor is the intrinsic unpredictability of some astrophysical processes. Solar energetic particle events are, at best, heralded by light which gives us only a few minutes advanced notice. Intensity and heavy ion enrichment are impossible to forecast. Similarly the dynamics of terrestrial magnetic fields, for example magnetic storms, lead to large uncertainties in radiation belt fluxes.

The natural radiation environment consists of (Fig. 3):

1. Galactic cosmic rays
2. Trapped particles
3. Solar energetic particles

Each of these particle groups has unique characteristics impacting on the question of SEU estimation.

Galactic cosmic rays are composed of all elements from hydrogen to uranium. Protons and alphas are most common. Heavy ions account for about 1% of cosmic rays. Elements heavier than nickel are extremely rare. Composition is roughly the same as in the solar system except that some rare elements are built up by fragmentation of common elements during passage through the interstellar medium (Fig. 4). The mean cosmic ray energy is around 1 GeV/nucleon and the energy spectra are hard (Fig. 5). Because the energy spectrum is so hard, material shielding does little to protect electronics from cosmic rays. Split curves indicate the upper and lower limit of variations with solar cycle.

Heavy ions in cosmic rays are the dominant cause of single event upsets. Iron deposits charge 600 times faster than protons almost making up for its lower abundance. In addition most circuitry is not susceptible to the direct ionization of protons. Recoils from proton interactions are extremely rare, hence the direct ionization of heavy ions dominates.

Solar flares occur at unpredictable intervals. Their intensities vary over a wide range (following a log-normal distribution). The proton flux from one of the most (particle) intense flares ever observed (August, 1972) is shown in Fig. 6. Total fluxes can be many orders of magnitude greater than cosmic ray fluxes, but the energy spectrum is much steeper. Since there are few high energy particles shielding is much more effective against solar flare particles.

In solar flares as well as cosmic rays it is the heavy ions which are responsible for SEUs. Very little statistical information is available about heavy ions in solar flares. Abundances are roughly the same as in cosmic rays; however, some flares are substantially enriched (up to a factor of 10) in heavy ions. Forcasts of heavy ion fluxes in solar flares are not possible. Modeling of heavy ion fluxes is inadequate because effort has not been focused on analyzing available data and gathering new data. We use a variety of worst case models to characterize fluxes.

Trapped protons are extremely abundant in the radiation belts (about 2000 nautical miles at the equator) and tail off near Earth and at geosynchronos orbit (Fig. 7). They are so abundant that even though it takes more than 100,000 trapped protons to do the damage of one cosmic ray heavy ion, in many orbits trapped protons are the dominant cause of SEUs. Even in near Earth orbit trapped particles mirroring at the South Atlantic anomaly may greatly increase instantaneous upset rates. Even minute contributions of heavy ions in the trapped radiation would substantially increase upset rates in the radiation belts.

3. Geomagnetic Shielding

For near Earth orbits the geomagnetic field shields spacecraft from low energy cosmic rays and solar flare particles. Just how effective this shielding is depends on the orbit (Fig. 8). In India the geomagnetic cutoff occurs at rigidity 16 GV. Protons with energies less than about 16 GeV and heavier ions with energies less than about 8 GeV cannot penetrate the field. At the magnetic poles much lower energy particles penetrate.

The cutoff is dependent on orientation (Fig. 9). A factor of 2 difference in cutoff from east to west is not uncommon. Cosmic ray ion intensities are highest coming from the west. Geomagnetic shielding, spacecraft shielding, Earth's shielding and chip orientation all introduce directional dependencies into upset rate estimates. These may offer possibilities for reducing upsets in some space systems.

4. Conclusions

A complete set of particle environment models exist. These are based on cosmic ray and solar flare modeling done at the Naval Research Laboratory and trapped radiation modeling done at NASA. In addition, extensive calculations of geomagnetic shielding have been done at AFGL. At Severn Communications Corporation we have gathered these models together and incorporated them into our propagation and energy deposition codes. These codes are constantly being improved upon to give the most accurate possible estimates of SEU rates in space systems and high altitude aircraft.

Several deficiencies exist in particle environmental models. Among the most pressing issues are the questions of heavy ion abundances trapped in the radiation belts and in solar flares. NRL's TRIS experiment should improve our understanding of the trapped heavy ion population allowing some improvement of the models. A detailed statistical study of solar flare heavy ions would be necessary to accurately characterize worst case models. Data on heavy ions have been collected in several satellite experiments, but we know of no programs to analyze this data.

Among the most pressing issues to come out of this conference was the need for validation of SEU rate estimation procedures. Our current estimation techniques depend on environmental models, propagation models, and device models which have individually been tested. The overall effectiveness of these techniques has not been verified by comparison with observed upset rates. The need for this validation is critical. A desirable outcome of this work would be the standardization of methods for estimating SEU rates allowing for meaningful incorporation into systems reliability specifications.

Figure 1

High Energy Ion Propagation Applications

- Cosmic Ray Physics
- Single Event Upsets
(Space and Atmosphere)
- Radiation Dose in Space
- Particle Beam Weapons
- Gamma Ray Emissions

Figure 2

Program Organization

- Incident Particle Flux
- Geomagnetic Transmittance
- Propagation in Materials
- Geometric Integration
- **Secondary Effects**

Figure 3

Natural Particle Environment

- Galactic Cosmic Rays
- Trapped Particles
- Solar Energetic Particles
- Anomalous Component

Figure 4

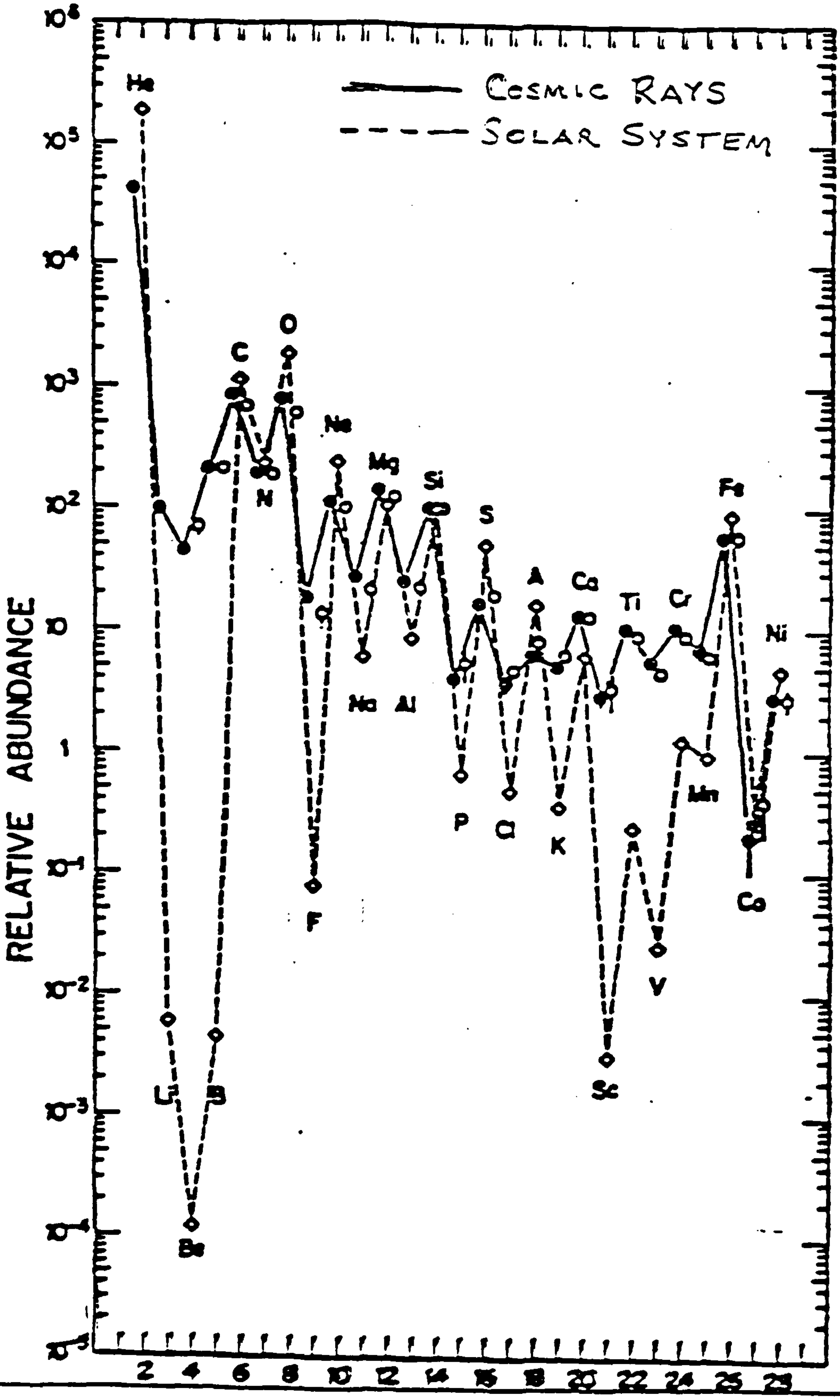
Cosmic Rays
Solar System
RELATIVE ABUNDANCE
10⁶
10⁵
10⁴
10³
10²
10
1
10⁻¹
10⁻²
10⁻³
10⁻⁴
10⁻⁵
2
4
6
8
10
12
14
16
18
20
22
24
26
28
He
Li
Be
B
C
N
O
F
Ne
Na
Mg
Al
Si
P
S
Cl
A
K
Ca
Sc
Ti
V
Cr
Mn
Fe
Co
Ni

Figure 5

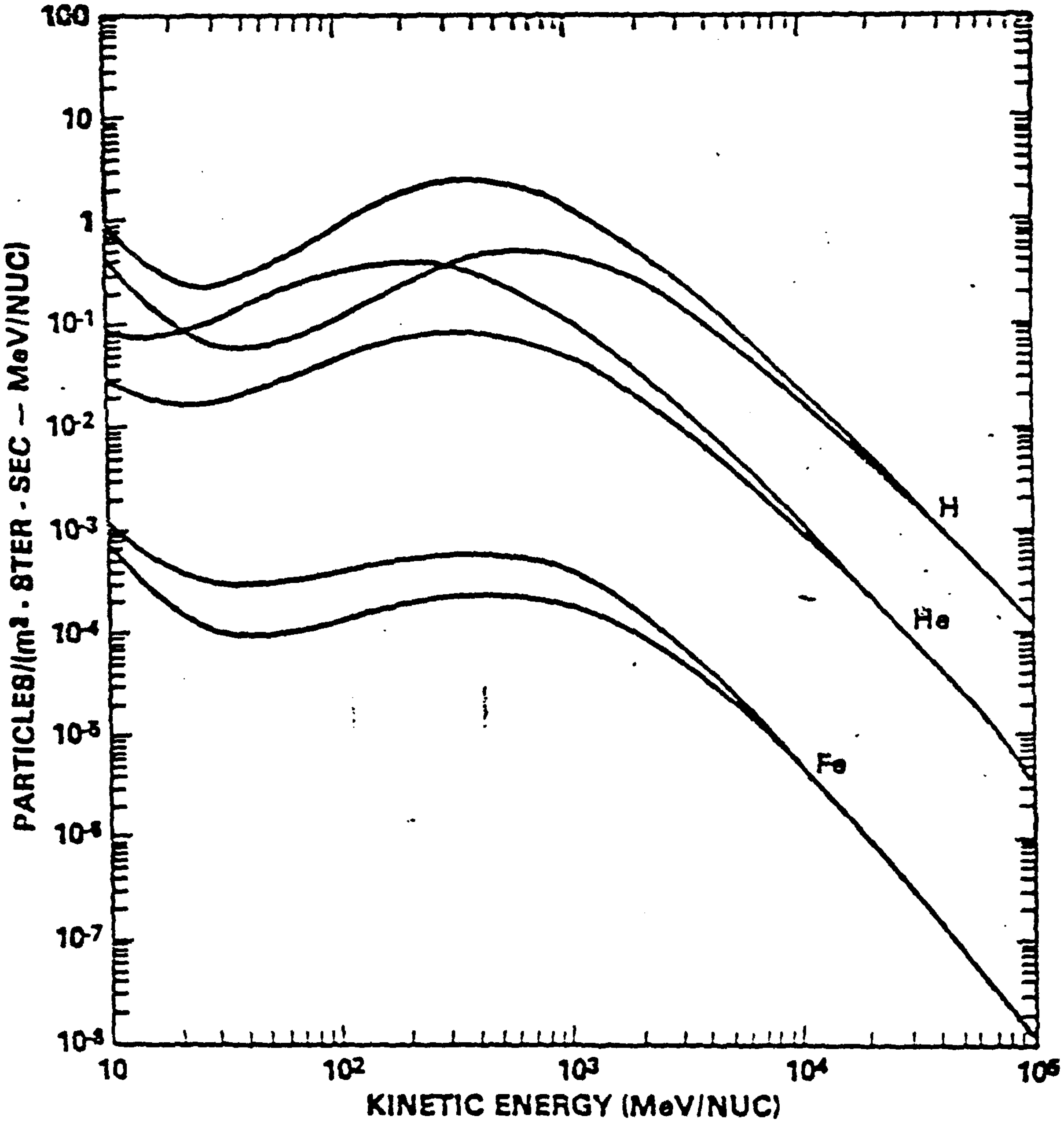

100
10
1
10-1
10-2
10-3
10-4
10-5
10-6
10-7
10-8
PARTICLES/(m² · STER · SEC — MeV/NUC)
10
10²
10³
10⁴
10⁵
KINETIC ENERGY (MeV/NUC)
H
He
Fe

2 3 2

Figure 6

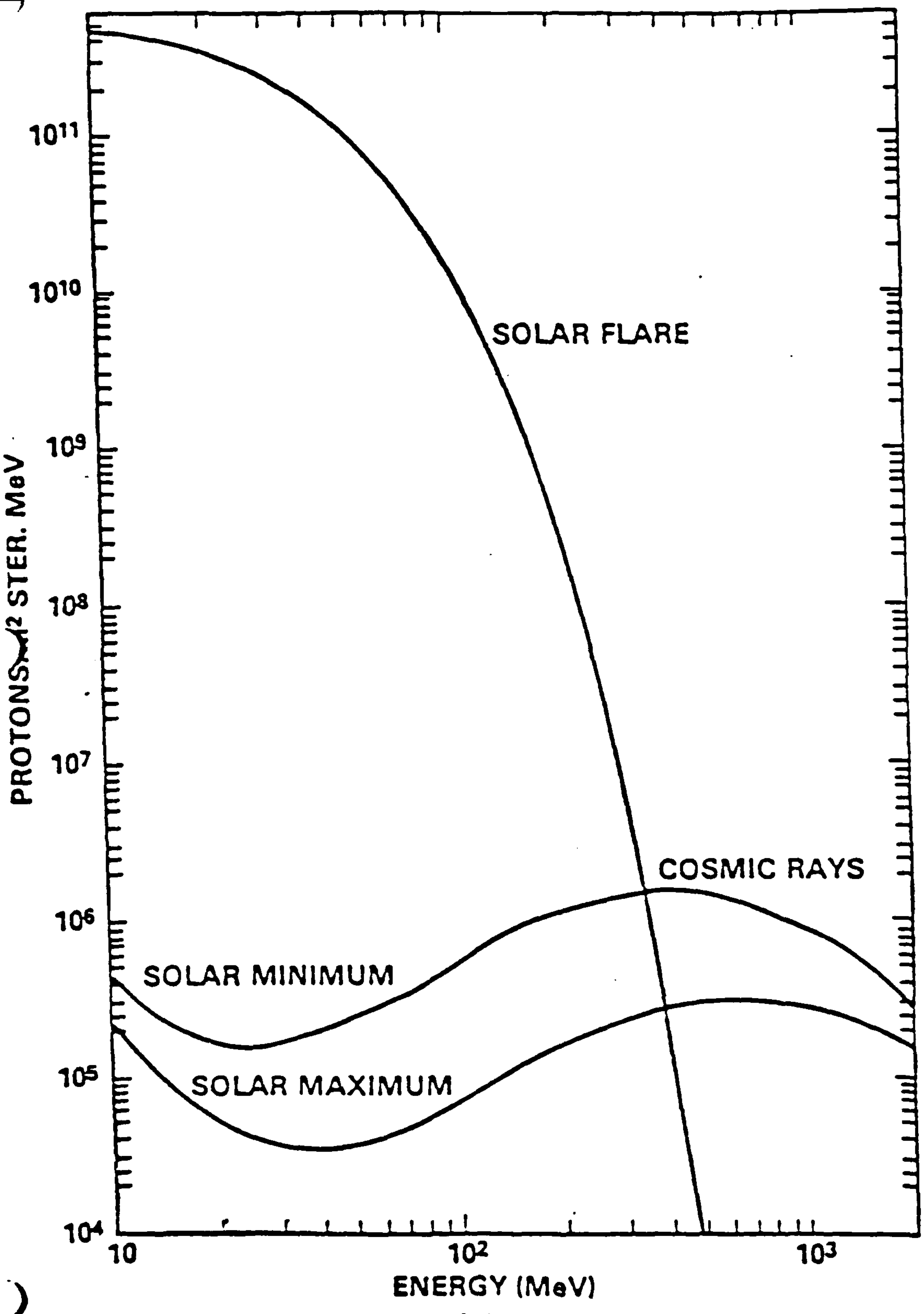
PROTONS/M² STER. MeV
10¹¹
10¹⁰
10⁹
10⁸
10⁷
10⁶
10⁵
10⁴
SOLAR FLARE
COSMIC RAYS
SOLAR MINIMUM
SOLAR MAXIMUM
10
10²
10³
ENERGY (MeV)

2 3 3

Figure 7

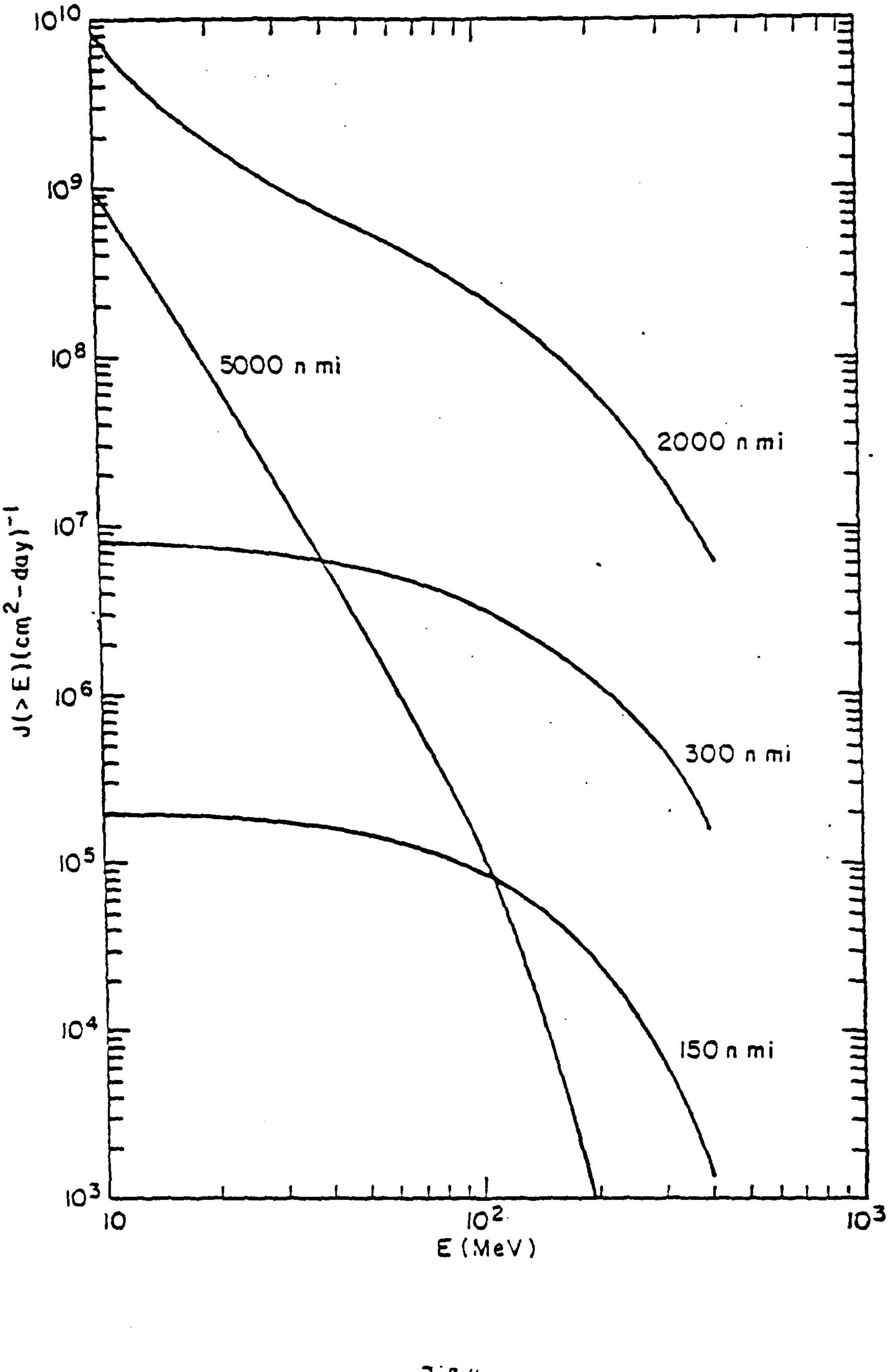
10^10
10^9
10^8
10^7
10^6
10^5
10^4
10^3
J(>E)(cm^2-day)^-1
5000 n mi
2000 n mi
300 n mi
150 n mi
10
10^2
10^3
E (MeV)

2 3 4

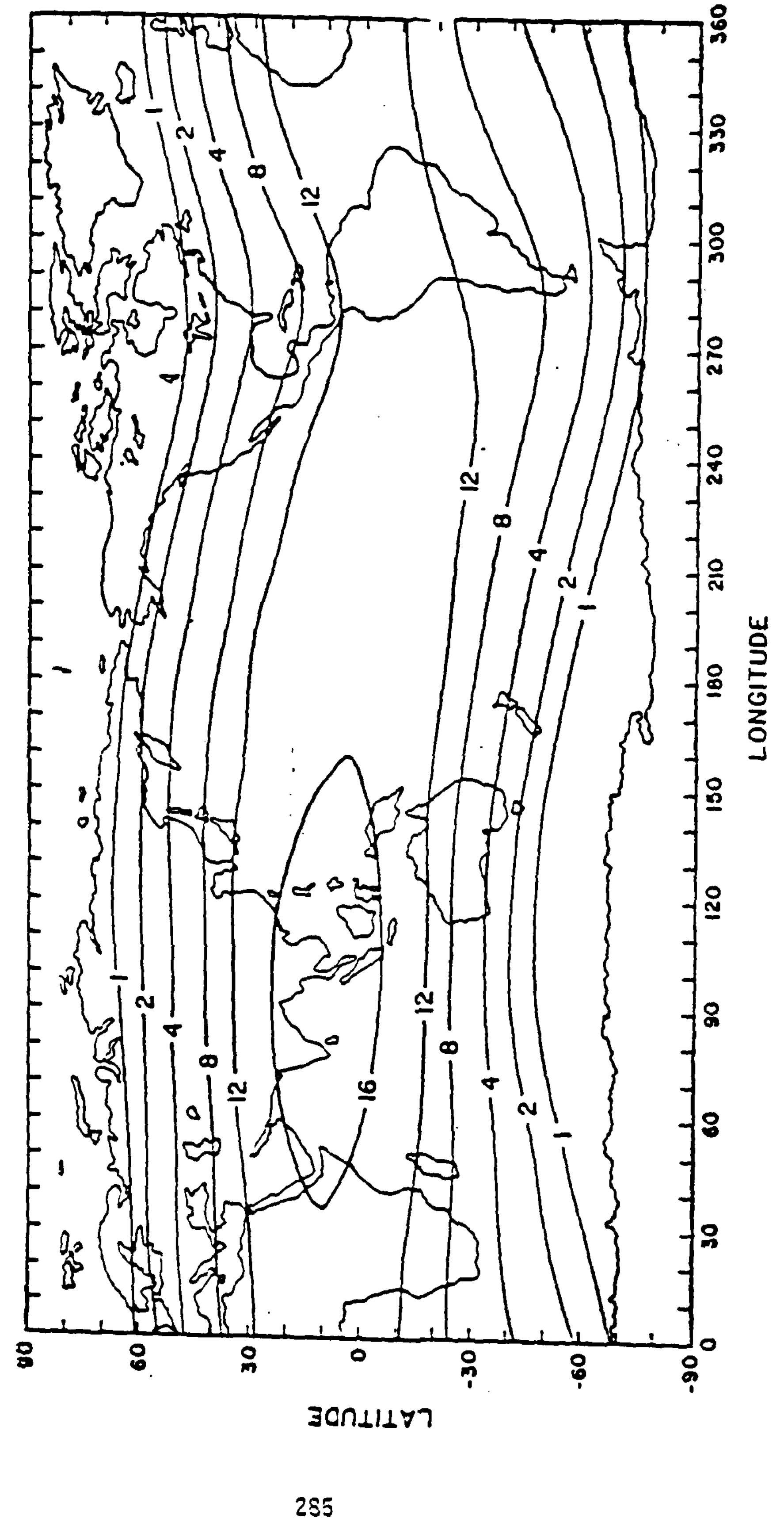
LATITUDE
90
60
30
0
-30
-60
-90
LONGITUDE
0
30
60
90
120
150
180
210
240
270
300
330
360
1
2
4
8
12
16

Figure 9

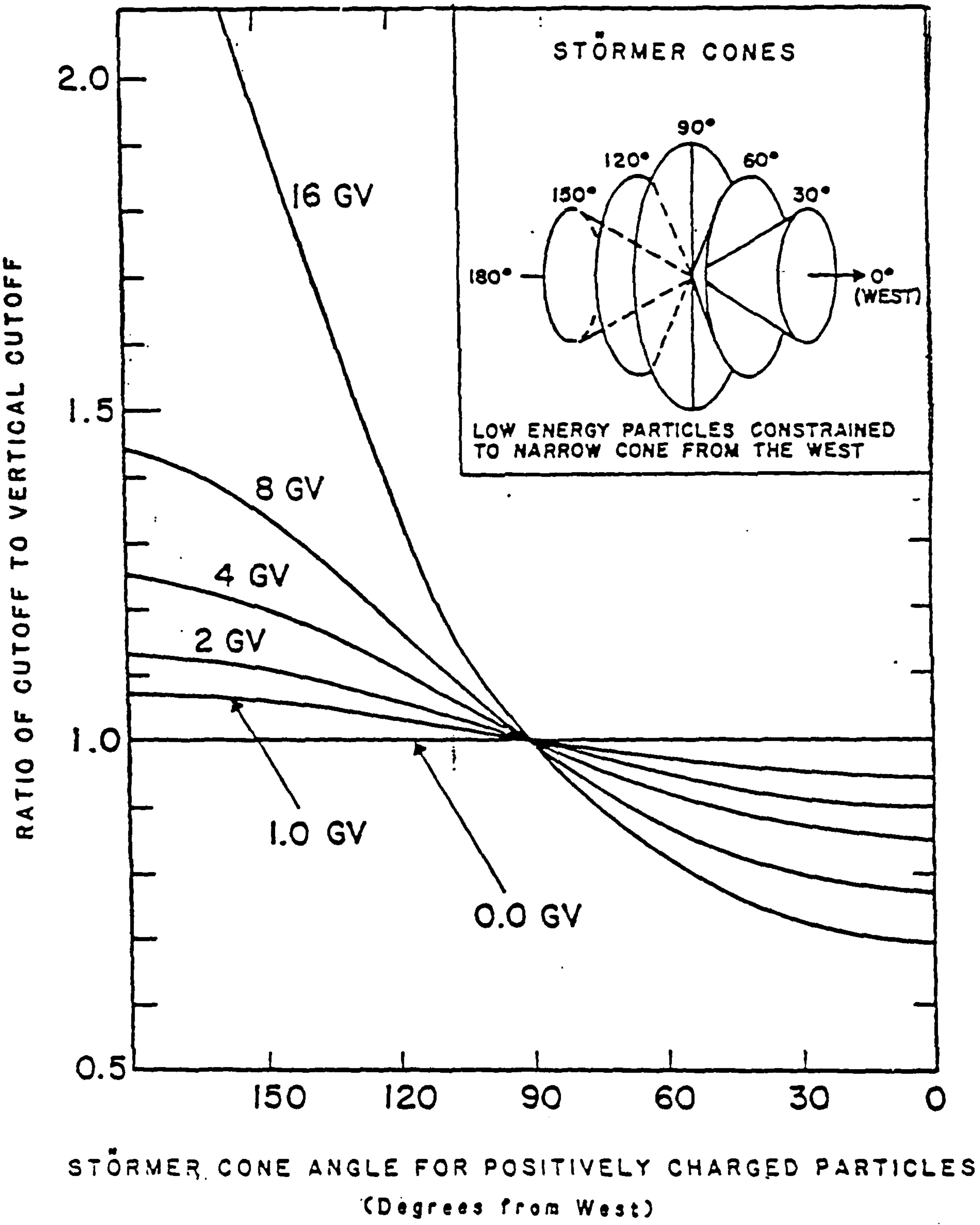
STÖRMER CONES
90°
120°
60°
150°
30°
180°
0° (WEST)
LOW ENERGY PARTICLES CONSTRAINED TO NARROW CONE FROM THE WEST
16 GV
8 GV
4 GV
2 GV
1.0 GV
0.0 GV
2.0
1.5
1.0
0.5
150
120
90
60
30
0
RATIO OF CUTOFF TO VERTICAL CUTOFF
STÖRMER CONE ANGLE FOR POSITIVELY CHARGED PARTICLES
(Degrees from West)

Bulletin of the American Astronomical Society

v. 16, no. 2, p. 448 (1984)

04.11

Uncertainties in Cosmic Ray Source Composition

J. R. Letaw (Severn Communications Corp),
R. Silberberg and C. H. Tsao (NRL, Washington, DC)

The calculation of the composition of cosmic rays at the source regions is affected by uncertainties in partial nuclear cross sections. About half of the light cosmic ray nuclei and up to 90% of the heavier nuclei fragment in interstellar gas between the sources and the earth. Hence many of the elemental abundances are dominated by the contribution of secondary fragments and predictions are sensitive to cross section errors. Henshaw and Wiedenbeck (1983 International Cosmic Ray Conference) calculated the uncertainties in the source composition for the respective cases of correlated and uncorrelated errors in cross section calculations. Based on the differences between the calculated and measured abundances of elements that are predominantly secondary, we find that for elements with $Z < 40$, the errors are mainly uncorrelated.. The implied uncertainties in source abundances are also relatively modest--much less than in the case of correlated errors. For the ultra-heavy secondaries ($61 < Z < 75$), however, *the calculated production* cross sections at 1 GeV/u (prior to adjustments based on data of Kaufman, et al.) were too small by a factor of two. Hence, for the ultra-heavy nuclei, the cross section calculations, especially their energy dependence, had a large correlated component.

Bulletin of the American Physical Society

v. 29, no. 4, p. 735 (1984)

HG 13 Late Stage in Acceleration of Cosmic Rays

R. Silberberg, C.H. Tsao, E.O. Hulburt Center for Space Research, NRL, J.R. Letaw, Severn Communications Corp., and M.M. Shapiro, Univ. of Iowa and Univ. of Bonn

There are several anomalies in the composition of cosmic rays; in particular for low energy N, F, Al, Cr, Mn, the e-capture isotopes ^{37}Ar, ^{49}V, ^{51}Cr, and at higher energies for 61 Z 75. All of these discrepancies are resolved by assuming that cosmic ray spallation reactions occur at an energy about 1/4 of what is observed near the solar system. This observation is interpreted by assuming three stages in the cosmic ray acceleration and propagation process: (1) The principal acceleration of cosmic rays occur near their source regions. (2) This is followed by an extensive period of traversal of interstellar gas with nuclear fragmentation. (3) Thereafter, the particles are further accelerated by weaker and dissipated shock waves in the hot, tenuous regions of the interstellar medium.

Bulletin of the American Physical Society

v. 29, no. 4, p. 735 (1984)

HG 14 Ultraheavy Cosmic Rays and Electron Capture Decay

J.R. Letaw, Severn Communications Corporation,
R. Silberberg and C.H. Tsao, E.O. Hulburt Center for
Space Research, NRL

General results concerning electron stripping and attachment in nuclei, and the treatment of electron capture decay in cosmic ray propagation are presented. We show that all galactic cosmic rays achieve their equilibrium charge state faster than the rate of other interaction processes. Effective decay rates for all cosmic ray species, except possibly actinides, may then be determined assuming each species has at most a single attached electron. These methods are applied to the ultraheavy cosmic rays showing the sensitivity of elemental and isotopic abundances to density and energy.

THE ASTROPHYSICAL JOURNAL SUPPLEMENT SERIES, 56:369-391, 1984 November
© 1984. The American Astronomical Society. All rights reserved. Printed in U.S.A.

PROPAGATION OF HEAVY COSMIC-RAY NUCLEI

JOHN R. LETAW
Severn Communications Corporation
AND
REIN SILBERBERG AND C. H. TSAO
E.O. Hulburt Center for Space Research, Naval Research Laboratory
Received 1984 March 20; accepted 1984 May 29

ABSTRACT

Techniques for modeling the propagation of heavy cosmic-ray nuclei, and the required atomic and nuclear data, are assembled in this paper. Emphasis is on understanding nuclear composition in the charge range $3 < Z < 83$. Details of the application of "matrix methods" above a few hundred MeV per nucleon, a new treatment of electron capture decay, and a new table of cosmic-ray-stable isotopes are presented. Computation of nuclear fragmentation cross sections, stopping power, and electron stripping and attachment are briefly reviewed.

Subject headings: atomic processes — cosmic rays: abundances — cosmic rays: general — particle acceleration

I. INTRODUCTION

Propagation of cosmic rays in the Galaxy has for many years been the subject of much attention (Ginzburg and Syrovatskii 1964; Fichtel and Reames 1968; Gloeckler and Jokipii 1969; Shapiro and Silberberg 1970). Details of cosmic-ray motion within the Galaxy, and certainly sources and acceleration mechanisms, are not well known. However, much about the elemental and isotopic composition of cosmic rays can be understood in terms of intragalactic diffusion models. In these models cosmic rays diffuse through the interstellar medium (ISM) undergoing nuclear fragmentation and decay and suffering energy loss in atomic collisions. Details of the scattering process, including possible acceleration mechanisms, are ignored. Certain characteristics of cosmic-ray composition, such as the anomalously high abundances of Li, Be, and B ($Z = 3$–5) relative to solar system abundances, are well understood within diffusion models. On the other hand, much information about cosmic-ray history, including composition at the sources, the mean diffusion time, and energy losses in the heliosphere, is revealed by observed abundances.

In this paper a discussion of certain propagation techniques and nuclear data required to perform these computations is presented. We emphasize the study of the nuclei Li through Bi ($Z = 3$–83), although much of what is presented applies to other nuclei. We restrict ourselves in this paper to propagation equations of the form:

$$\frac{\partial J_i(E,x)}{\partial x} = -\frac{J_i}{\Lambda_i(E)} + \sum_k \frac{J_k}{\Lambda_{ik}(E)} + \frac{\partial}{\partial E}\left[w_i(E)J_i\right], \tag{1}$$

where Λ_i is the mean free path for losses of species i due to nuclear fragmentation and radioactive decay, Λ_{ik} is the mean free path for gains of species i from species k, and w_i is the (positive) ionization loss rate. Within this model diffusion effects are represented by a path length distribution, $P(x, E)$. Conditions under which such a simplification is possible are discussed by Lezniak (1979).

At medium and high energies this cosmic-ray propagation equation may be simplified to a set of coupled linear equations in one variable of the form:

$$\frac{dJ_i}{dx} = \sum_j M_{ij} J_j. \tag{2}$$

Energy appears in this equation only parametrically, not as an independent variable.

Techniques for solving equation (2) are discussed in § II and are generally termed "matrix methods." The matrix methods provide a powerful and conceptually simple means for treating propagation and, particularly, path length distributions. Further, they may be extended to treat accurately ionization loss and solar modulation at energies above a few hundred MeV per nucleon (henceforth, MeV N^{-1}). In effect, an entire galactic propagation may be reduced to one, or at most a few, computational steps. Stepping through small path lengths can often be avoided in compositional studies by using these methods.

In § II we discuss solutions to equation (1) and the matrix methods with emphasis on general features of the propagation problem, including path length distributions and error analysis. While these methods provide a structure for propagation, nuclear and atomic data are required to carry out actual computations. Later sections treat the physical effects which change the relative elemental and isotopic abundances of cosmic rays. These include nuclear fragmentation and decay, ionization loss, electron attachment and stripping, and solar modulation. In Appendix A a new list of 433 isotopic species which are nearly stable in cosmic-ray propagation is presented. Such a table is required in all propagation problems where nuclear composition is followed, but no complete table has previously been published. Appendix B contains formulae for computing electron stripping and attachment cross sections. A correction term for heavy nuclei, not included in previous cosmic ray treatments, is presented here.

The need for a complete discussion of cosmic-ray propagation data has grown over the last few years for several reasons:

1. Compositional data of unprecedented accuracy and detail are now being reported. Elemental abundances of all cosmic-ray species with $Z \leq 30$, and even-charge elements to $Z = 82$, have been measured by satellite-borne instruments with excellent charge resolution (Engelmann *et al.* 1981; Binns *et al.* 1981; Fowler *et al.* 1981; Binns *et al.* 1982). Isotopic abundances have now been reported for all elements through Ni (Webber 1981; Wiedenbeck and Greiner 1981; Mewaldt *et al.* 1981; Young *et al.* 1981; Garcia-Munoz, Simpson, and Wefel 1981). Correct propagation models applying all known physical effects are necessary to determine the implications of these measurements.

2. While many of the physical data needed in propagation problems are known, *great uncertainty remains in the partial* cross sections. The semiempirical formulation of Silberberg and Tsao (1973*a*, *b*) has errors of up to 50% for heavy elements. The need for more theoretical and experimental work in this area is critical. Because the cross section errors also propagate in propagation studies, techniques for monitoring them should continue to be investigated.

3. Different researchers use different data in their propagation studies. For example, total inelastic cross sections for nuclei on hydrogen are known with a mean error of 5% at 100 MeV N^{-1} (Letaw, Silberberg, and Tsao 1983*a*). At high energies, where the cross sections are energy independent, mean errors are ~1%. However, empirical fits used by different groups vary by as much as 10%. Quantitative evidence of errors resulting from varying data among researchers has been presented by Freier (1981). Such discrepancies can be avoided by careful attention to the data and standardized data bases.

4. Finally, *the importance of many factors in propagation* calculations cannot be overstated. Effects such as ionization loss, electron capture decay modes, energy-dependent cross sections, and solar modulation can cause significant compositional changes. These effects are greater for ultraheavy cosmic rays than for lighter nuclides. Their influence in the analysis of recent ultraheavy data therefore bears investigation (Letaw, Silberberg, and Tsao 1984).

II. PROPAGATION METHODS

Equation (1) is the fundamental equation for propagation of high energy ions in matter in the "straight-ahead" approximation. In this approximation collisions which change the particle species do not change their energy or direction. The energy loss mechanisms are lumped into the stopping power, $w_i(E)$, and are treated as continuous processes which cause no change in particle direction. Thus equation provides an excellent model of heavy nuclei propagating in the ISM when combined with a path length distribution. Collisions of heavy nuclei with the light components of the ISM at high energies very closely conserve the velocity and direction of the projectile fragments (Westfall *et al.* 1978; Greiner *et al.* 1975).

The five quantities appearing in equation (1) are the following:

1) The particle fluxes, J_i;
2) The energy, E;
3) The path length, x;
4) The modification matrix, M_{ij};
5) The stopping power, w_i.

The particle fluxes, J_i, may be expressed in any convenient units, and these units are preserved in propagation because equation (1) is linear. The species index, i, labels all nuclear species in the calculation. If the species are arranged in order of ascending mass, and within that descending charge, computations are considerably simplified because all fragmentation reactions (including charge exchange) proceed to a lower species index. Some nuclear decays, specifically positron and electron capture decay, violate this ordering; hence, *it is generally not possible to order cosmic-ray nuclides such that all compositional changes reduce the species index*. A list of the 433 cosmic-ray nuclides from Li through Bi and associated nuclear data is presented in Appendix A.

The energy, E, is measured in units of MeV N^{-1}. In these *units, the energy of products of fragmentation collisions is* approximately the target energy ("straight-ahead" approximation). Cross sections of protons on target nuclei which are given at E MeV are equal to the cross sections of the same nuclei on a proton target at E/m_p MeV N^{-1} ($m_p = 1.007276$ amu).

The path length, in units of g cm^{-2}, is a measure of the total amount of matter passed through in the ISM. Although H and He are by far the major components of the ISM, all species are included in the definition:

$$x = \rho v t \tag{3}$$

where ρ is the mean density of the ISM, v is the cosmic-ray velocity, and t is universal time. The path length is the mass of a one square centimeter column of ISM with height equal to the distance traveled by the cosmic ray in t seconds. It should be noted that this interpretation applies only in homogeneous media and that the path length is weakly energy dependent. In terms of the number density of H:

$$x = (n_H/N_A)vt\sum_i b_i A_i, \tag{4}$$

where N_A is Avogadro's number and b_i is the abundance of atoms of species i in the ISM relative to H. Using Cameron's (1982) *local galactic abundances for the ISM composition*, the sum is 1.30. The presence of helium substantially changes the path length definition and is not entirely cancelled by corresponding changes in the modification matrix.

The modification matrix, M_{ij}, contains the cosmic ray/ISM interaction terms. The most important of these interactions, from the viewpoint of composition, is nuclear fragmentation. Among the cosmic-ray nuclei heavier than helium, most have suffered nuclear spallation reactions since their acceleration. Many of the elements observed in cosmic rays are overwhelmingly derived from products of nuclear spallation reactions and, hence, provide information on cosmic-ray propagation; some such elements are Li, Be, B, F, $17 \leq Z \leq 19$, $21 \leq Z \leq 25$, and many elements with $Z > 40$. In addition, many elements

have large secondary contributions, and the determination of the residual source component requires highly precise knowledge of cross sections and propagation conditions; some such elements are N, Na, Al, and Ca and Co. Nuclear decay, ionization loss, and *electron stripping and attachment also* contribute to compositional changes. The detailed nature of the modification matrix is discussed in later sections.

The stopping power, w_i, in units of (MeV N^{-1})/(g cm^{-2}) is discussed in § IV. Energy loss due to atomic collisions in the interstellar medium is represented by this term. Energy loss and gain mechanisms due to interactions with ambient electromagnetic fields and shocks are not contained in the stopping power.

An exact, iterative solution to equation (1) is

$$J_j(E_f, x_f) = \Pi(x_f)\frac{w_j(E_i)}{w_j(E_f)}J_j(E_i, x_i = 0) + \Pi(x_f)$$

$$\times \int_0^{x_f}\Pi^{-1}(x)\frac{w_j(E)}{w_j(E_f)}\sum_{k>j}\Lambda_{jk}^{-1}(E)J_k(E, x)\,dx, \tag{5}$$

where energy and path length are related uniquely by

$$x = \int_E^{E_i}\frac{dE'}{w_j(E')},$$

and

$$\Pi(x) = \exp\left[-\int_0^x \Lambda_j^{-1}(E')\,dx'\right].$$

The fluxes of all progenitors of a species must be known to determine its flux in this solution. An equivalent statement of this condition is that the modification matrix must be upper triangular. When this is not possible, as is generally the case, equation (5) may be applied repeatedly to the entire set of nuclides to yield an approximate, rapidly converging solution.

Matrix methods are applicable to cosmic-ray propagation when the transformation equations are of the form of equation (2). We discuss reduction to this form in § IV. The matrix methods were introduced by Davis (1960) and shown by Cowsik and Wilson (1973) to be a natural way in which to treat exponential path length distribution. The solution to equation (2) is

$$J_i(x) = \sum_j [\exp Mx]_{ij}J_j(0). \tag{6}$$

The matrix exponential is defined by its power series expansion. This solution gives the change in a flux of particles upon passage through x g cm^{-2} of ISM. It is generally termed the "slab" model. This model and a measurement (O'Dell, Shapiro, and Stiller 1962) of the L/M ratio were sufficient to give the approximate amount of matter traversed by cosmic rays (Badhwar, Daniel, and Vijayalakshmi 1962).

Early compositional studies (Cowsik *et al.* 1967; Shapiro and Silberberg 1970) showed that, in fact, all cosmic rays do not pass through the same amount of matter. This conforms to the model of propagation by diffusion through the galaxy. Propagation by diffusion is conveniently described using a path length distribution, $P(x)$, normalized so that

$$\int_0^\infty P(x)\,dx = 1. \tag{7}$$

With such a path length distribution, the solution to the propagation problem is

$$J_i = \int_0^\infty dx\,P(x)[\exp Mx]_{ij}J_j(0). \tag{8}$$

If $P(x) = \delta(x - \lambda)$, this is the slab model. If, however, we use an exponential path length distribution with mean path length, λ,

$$P(x) = \frac{1}{\lambda}e^{-x/\lambda}, \tag{9}$$

the integral in equation (8) can be evaluated analytically yielding

$$J_i = [1 - M\lambda]_{ij}^{-1}J_j(0). \tag{10}$$

The propagation is accomplished simply by solving a set of coupled linear equations. The mean path length, like M, can be species and energy dependent.

Other path length distributions may be useful in accounting for various elemental ratios (Shapiro and Silberberg 1970; Protheroe, Ormes, and Comstock 1981). Composition of path lengths is discussed by Simon (1977). Some of the distributions are summarized in Table 1. The integral in equation (8) can often be simplified by diagonalizing the modification matrix (Margolis 1983).

It is often of interest to separate the portions of the cosmic-ray flux which have not undergone interactions—the primaries—from those that have—the secondaries. The modification matrix is structured so that interactions which change the species involve off-diagonal elements. While the total inelastic cross sections contribute a negative amount to a diagonal element, the partial cross sections contribute positive, species-changing amounts off the diagonal. The primaries are therefore found using exclusively diagonal elements of the modification matrix.

In general, cosmic-ray propagation calculations are performed forward in time from sources to the heliosphere. In this case hypotheses concerning the source abundances can be examined for their consequences. While such an approach is desirable from the standpoint of theory, it is often useful in data analysis to proceed in the reverse direction. In this way the source composition suggested by experimental data is found. The matrix formulation is easily adapted to this approach. The source composition implied by flux data which has passed through an x g cm^{-2} slab of ISM (the inverse of eq. [6]) is

$$J_i(0) = \sum_j [\exp(-Mx)]_{ij}J_j(x). \tag{11}$$

TABLE 4

NUCLIDES UNSTABLE TO ELECTRON CAPTURE, AND TO ANOTHER DECAY MODE WITH HALF-LIFE > 1000 YEARS*

Isotope	Nonelectron Capture		Electron Capture	
	Half-Life	Daughter	Half-Life	Daughter
13AL 26	8 78E + 05	12MG 26	4 00E + 06	12MG 26
17CL 36	3 06E + 05	18AR 36	1 58E + 07	16S 36
19K 40	1 43E + 09	20CA 40	1 20E + 10	18AR 40
28NI 59	5 00E + 11	27CO 59	7 50E + 04	27CO 59
41NB 92	5 33E + 10	40ZR 92	3 20E + 07	40ZR 92
47AG 105	1 26E + 04	46PD105	1 13E - 01	46PD105
57LA 138	3 44E + 11	58CE138	1 62E + 11	56BA138
61PM 145	6 32E + 09	59PR141	1 77E + 01	60ND145
64GD 149	5 09E + 03	62SM145	2 55E - 02	63EU149
64GD 151	4 11E + 07	62SM147	3 29E - 01	63EU151
73TA 177	2 23E + 03	72HF177	6 46E - 03	72HF177
78PT 188	9 31E + 04	76OS184	2 79E - 02	76OS188
83BI 206	2 14E + 03	82PB206	1 71E - 02	82PB206
83BI 207	3 17E + 05	82PB207	3 80E + 01	82PB207

*Half-lives in years.

TABLE 5

NUCLIDES UNSTABLE TO ELECTRON CAPTURE, WITH ALLOWED, BUT UNOBSERVED, ALTERNATE DECAY MODE*

Isotope	Half-Life	Daughter
24CR 48	2 46E 03	22TI 48
25MN 54	8 54E - 01	24CR 54
28NI 56	1 67E - 02	26FE 56
36KR 76	1 69E - 03	34SE 76
37RB 83	2 36E - 01	36KR 83
38SR 85	1 77E - 01	37RB 85
40ZR 86	1 88E - 03	38SR 86
41NB 91	1 00E + 04	40ZR 91
44RU 94	9 89E - 05	42MO 94
43TC 95	2 28E - 03	42MO 95
43TC 96	1 18E - 02	42MO 96
44RU 97	7 89E - 03	43TC 97
45RH102	2 90E + 00	44RU102
50SN108	2 00E - 05	48CD108
49IN110	5 59E - 04	48CD110
50SN113	3 15E - 01	49IN113
51SB120	1 58E 02	50SN120
52TE121	4 60E 02	51SB121
54XE122	2 29E - 03	52TE122
53I 123	1 48E - 03	52TE123
56BA131	3 29E - 02	55CS131
58CE132	3 99E - 04	56BA132
60ND138	5 82E - 04	58CE138
61PM143	7 26E - 01	60ND143
61PM144	9 56E - 01	60ND144
63EU150	3 60E + 01	62SM150
65TB156	1 45E - 02	64GD156
66DY157	9 24E - 04	65TB157
67HO159	6 27E - 05	66DY159
70YB164	1 44E - 04	68ER164
72HF170	1 83E - 03	70YB170
71LU172	1 83E - 02	70YB172
72HF173	2 74E - 03	71LU173
74W 174	5 51E - 05	72HF174
73TA178	2.74E - 04	72HF178
74W 179	7 22E - 05	73TA179
76OS180	4 18E - 05	74W 180
75RE181	2 28E - 03	74W 181
75RE182	7 30E - 03	74W 182
75RE184	1 04E - 01	74W 184
76OS185	2 56E - 01	75RE185
77IR187	1 20E - 03	76OS187
80HG190	3 80E - 05	78PT190
77IR190	3 23E - 02	76OS190
79AU191	3 65E - 04	78PT191
80HG193	4 56E - 04	79AU193
79AU193	2 00E - 03	78PT193
80HG195	1 14E - 03	79AU195
82PB196	7 03E - 05	80HG196
82PB198	2 74E - 04	80HG198
83BI199	5 13E - 05	81TL199
81TL199	8 44E - 04	80HG199
81TL202	3 34E - 02	80HG202
83BI204	1 28E - 03	82PB204
83BI208	3.68E + 05	82PB208

*Half-lives in years

Decay of cosmic rays satisfies

$$\left(\frac{dJ_i}{dt}\right)_{\text{decay}} = -\frac{J_i}{\gamma\tau_i} + \sum_j \frac{\rho_{ij}J_j}{\gamma\tau_j}, \tag{25}$$

where τ is the mean lifetime and γ is the time dilation factor. At high energies the lifetime is considerably increased by the γ factor. The branching ratio ρ_{ij} is the fraction of decays of species j which ultimately yield species i. In terms of path length this equation is

$$\left(\frac{dJ_i}{dx}\right)_{\text{decay}} = \frac{N_A \ln 2}{n_H v\gamma\left(\sum_i b_i A_i\right)}\left[-\frac{J_i}{(\tau_i)_{1/2}} + \sum_j \frac{\rho_{ij}J_j}{(\tau_j)_{1/2}}\right]. \tag{26}$$

where $(\tau_i)_{1/2}$ is the half-life of species i.

For many isotopes, a much suppressed positron (or electron) decay competes with the electron capture decay mode (see Table 4). Such isotopes, for example, ^{54}Mn (Casse 1973), are possible cosmic-ray clocks. Those isotopes for which positron decay is possible ($Q \geq 1.022$ MeV) are indicated in Table 5.

Unstable cosmic rays yield information about their origin and propagation which is not available from stable isotopes. The amount of ^{10}Be is strongly dependent on the relation between the material traversed and the time taken to do so; thus, it is a measure of the density. Long-lived primaries, such as U and Th, indicate the age of matter at the sources. Electron capture nuclei carry information about cosmic rays before acceleration and in dense regions, and on adiabatic deceleration in the solar system.

VI. ELECTRON CAPTURE DECAY

Nuclides which decay by capturing a K-shell electron are more stable in cosmic rays than in the laboratory. In addition to the nuclear processes which affect composition, electron stripping and attachment rates are critical in determining the evolution of these nuclides. At low energies, where the attachment rate is comparable to the stripping rate, most nuclei have attached electrons, and electron capture decays are not inhibited. At high energies, at least for lower charge nuclei, stripping occurs much faster than attachment, preventing electron capture decay.

The abundances of primary cosmic rays which decay by electron capture can be used to estimate the time between synthesis and acceleration of cosmic rays. The relative abundances of Fe, Co, and Ni as affected by electron capture nuclides ^{57}Co, ^{56}Ni, and ^{59}Ni (Soutoul, Casse, and Juliusson 1978) and the abundance of ^{44}Ti (Shapiro and Silberberg 1975) are determined by the time spent at low energies where electron attachment is common.

Secondary nuclides such as ^{7}Be, ^{37}Ar, ^{41}Ca, ^{49}V, ^{51}Cr, ^{53}Mn, and ^{55}Fe behave at certain energies as other cosmic-ray clocks (e.g., ^{10}Be). At intermediate energies, where attachment is rare but not negligible, these nuclides can have lifetimes comparable to the cosmic-ray age ($\sim 10^7$ yr). Since the attachment rates are strongly dependent on energy, these nuclides reveal additional information on cosmic-ray deceleration (Raisbeck *et al.* 1973) and acceleration (Silberberg 1983). The possibility of utilizing electron capture nuclides to measure density variations has been explored by Raisbeck *et al.* (1975).

The electron capture nuclides can be incorporated into the cosmic-ray propagation equations in a straightforward way by treating all charge states separately and following the transitions from one state to another with stripping and attachment cross sections. It is not necessary to follow all charge states, though, because the majority of cosmic rays are fully ionized or have one electron attached. The exceptions to this rule are actinides at low energies. We now show that with this provision, *cosmic rays reach their equilibrium charge state in a path length much shorter than the fragmentation mean free path* and so may be considered to maintain that charge state. Thus, the electron capture nuclides may be treated as single isotopes with two decay modes in cosmic-ray propagations.

If N is the number of fully ionized nuclei and N^* is the number of nuclei with one attached electron, the rate equations for transitions are

$$\frac{dN}{dt} = -aN + sN^* - dN, \tag{27}$$

$$\frac{dN^*}{dt} = aN - sN^* - d^*N^*, \tag{28}$$

where a and s are the attachment and stripping rates, respectively, and d and d^* are the decay rates for N and N^*, respectively. These rates are inversely proportional to mean free paths defined in Appendix B. The rate of electron capture is less than one-half the laboratory rate because only a single K-shell electron is available (Wilson 1978). Note that $d^* > d$ because all decay modes allowed for N are allowed for N^*. Creation and destruction by fragmentation are small and ignored here as justified by the consistency of the results

An exact solution to the coupled equations can be obtained. Solving only for the ratio N^*/N we find that it approaches the equilibrium value:

$$(N^*/N)_{eq} = (2s)^{-1}\left\{\left[(s-a+\Delta)^2 + 4as\right]^{1/2} - (s-a+\Delta)\right\} \tag{29}$$

at the rate:

$$R^* = \left[(s-a+\Delta)^2 + 4as\right]^{1/2} \geq s, \tag{30}$$

where $\Delta = d^* - d =$ electron capture rate.

Equation (30) shows that the approach to equilibrium charge state is always faster than the stripping rate in a two-state system. The stripping mean free path in pure hydrogen, λ_s, is shown in Figure 3. (Formulas for computing stripping and attachment cross sections are discussed in Appendix B).

From Figure 3, $\lambda_s \leq 0.2$ g cm^{-2} for all charges and energies, whereas even the highest charged cosmic rays have a fragmentation mean free path $\lambda_f \geq 0.75$ g cm^{-2}. Thus, during propagation cosmic rays may be assumed to exist in their

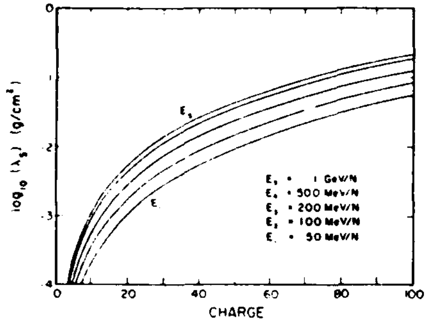

FIG. 3.—Stripping mean free path in H as a function of charge and energy. The stripping mean free path is roughly independent of energy above 1 GeV N^{-1}.

equilibrium charge state. Equations (27) and (28) may be replaced by

$$\frac{d}{dt}(N+N^*) = -\left\{d+\Delta\frac{(N^*/N)_{eq}}{[1+(N^*/N)_{eq}]}\right\}(N+N^*) \qquad (31)$$

Chou and Raisbeck (1970) arrived at two limiting cases of equation (31) through incorrect arguments. If $\Delta \gg s, a$, that is, if the electron capture decay is limited by the attachment rate, then equation (31) becomes

$$\frac{d}{dt}(N+N^*) = -(d+a)(N+N^*). \qquad (32)$$

The effective electron capture half-life, τ_a, corresponding to the attachment rate, a, is shown in Figure 4 as a function of charge and energy. A pure hydrogen medium of density $n_H = 0.3$ atoms cm^{-3} was assumed. This effective half-life is inversely proportional to n_H:

$$\tau_a(\mathrm{My}) = \frac{732.65}{n_H \sigma_a(\mathrm{mb})\beta} \qquad (33)$$

If $\Delta \ll s, a$, that is, if decay is limited by the K-capture rate, then equation (31) becomes

$$\frac{d}{dt}(N+N^*) = -\left[d+\left(\frac{a}{s+a}\right)\Delta\right](N+N^*) \qquad (34)$$

The electron capture decay is reduced by a multiplicative factor $a/(s+a)$. This factor is shown in Figure 5.

Although all the conclusions derived from equation (31) are not necessarily valid for actinides, the conclusion that the equilibrium charge state is approached at the stripping rate is supported by experiment (Fowler 1983). Reduction of the rate equations to the form of equation (31) is therefore possible, but is dependent on knowledge of several stripping and attachment mean free paths. With two K-shell electrons the electron capture rate is roughly doubled; therefore, the multiplicative factor of equation (34) would be increased.

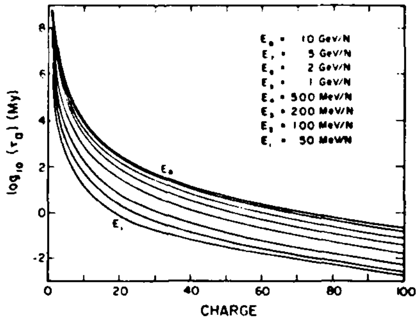

FIG. 4.—The effective electron capture half-life in H as a function of charge and energy. These curves show the rate of decay of nuclides whose electron capture lifetime is short relative to the attachment lifetime.

VII. SOLAR MODULATION

The effect of solar wind on the relative abundances of the isotopes is modeled by an effective potential difference, $\Phi(MV)$, within the heliosphere (Gleeson and Axford 1968). According to the model, the fluxes before and after propagation through the heliosphere are related by

$$J_{\mathrm{after}}(\epsilon) = \frac{\epsilon^2 - M^2}{(\epsilon + Ze\Phi)^2 - M^2} J_{\mathrm{before}}(\epsilon + Ze\Phi), \qquad (35)$$

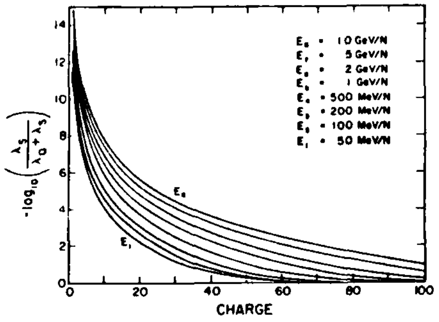

FIG. 5.—Lifetime dilation factor in H as a function of charge and energy. These curves show the increased lifetime of long-lived electron capture nuclei in galactic propagation.

where ϵ is the total energy, and M is the mass and Z is the charge of the propagating nucleus. In terms of the initial kinetic energy per nucleon, this is

$$J_{\mathrm{after}}(E - E_0) = \frac{(E-E_0)^2 + 2m_u(E-E_0)}{E^2 + 2m_u E} J_{\mathrm{before}}(E), \qquad (36)$$

where

$$E_0 = Ze\Phi/A.$$

An expansion around the energy, $E' = E - e\Phi/2$ yields the flux at a rigidity independent energy:

$$J_{\mathrm{after}}(E') = \left[1 - \frac{a(E - E_0 - E')}{E' + T}\right]^{-1} \times \frac{(E-E_0)^2 + 2m_u(E-E_0)}{E^2 + 2m_u E} J_{\mathrm{before}}(E). \qquad (37)$$

For example, we calculate the effect of solar modulation of 400 MV on charged particles with energy of 1 GeV N^{-1}. If the spectral index is 2.7, the flux of charged particles with $Z/A = 0.5$, such as C, N, and O ($Z = 6$–8), is reduced by a factor of 0.744. For uranium, with $Z/A = 0.387$, it is reduced only by a factor of 0.943. Thus, variations of up to 25% in relative abundances are caused by solar modulation.

The authors would like to thank Jim Adams, Nancy Brewster, Hank Crawford, Martin Israel, Steve Margolis, Jake Waddington, and Mark Wiedenbeck for valuable comments and conversations. The work of J.R.L. was supported in part by the Naval Research Laboratory. The work of R.S. and C.H.T. was supported in part by the National Aeronautics and Space Administration (Guest Investigator for *HEAO3*).

APPENDIX A

LIST OF COSMIC-RAY ISOTOPES

In this appendix we present a list (Table 6) of "cosmic-ray-stable" nuclides and associated nuclear data relevant to cosmic-ray propagation. The data are extracted from *Table of Isotopes* (Lederer and Shirley 1978). The 433 cosmic-ray-stable nuclides between Li and Bi are listed in the first column of the table. The nuclides are either (i) absolutely stable; (ii) decay by modes other than electron capture with half-life greater than 1000 yr; or (iii) decay primarily by electron capture with no other known decay mode having a half-life less than 1000 yr.

The isotopes of H and He, and the actinides, are omitted from this list because the study of their abundances demands substantially different treatment from that presented in this paper. To a good approximation, the abundances of the nuclides Li through Bi in the Galaxy neither affect nor are affected by propagation of the omitted nuclides.

Along with each cosmic-ray-stable nuclide are up to six nuclides which decay rapidly (< 1000 yr by modes other than electron capture) into it and the associated branching ratio. These "parents," when produced in fragmentation of a heavier nuclide, in effect, immediately increase the abundance of the stable nuclide. The parents consist of essentially all isotopes known well enough to predict decay-branching ratios. Where necessary, all particle decay chains (including internal transitions) were followed to compute the branching ratios. Unknown isotopes were included when fragmentation cross sections indicated their importance. In the occasional case where there are more than six parents, the remainder have been omitted with a resulting error of less than 1% in the production rate of the stable nuclide. For example, the total production cross section for ^{77}Se from ^{90}Zr in pure hydrogen at 1 GeV N^{-1} is 31 mb. Most of this production comes from immediate decays of ^{77}Br and ^{77}Kr, about two mass units to the neutron-poor side of the mass stability point. We eliminate ^{77}Ga from the list in favor of the less stable ^{77}Sr because the cross section for production of ^{77}Ga is more than three orders of magnitude less than that of ^{77}Sr. In this typical case the overall error in total production of ^{77}Se due to omission of parents is ~ 0.001%.

The final columns contain the half-lives and ultimate "daughters" for the non-electron-capture and electron-capture decay modes. These must be distinguished because of the problems of electron stripping and attachment discussed in the main body of this paper. The half-lives are in years (365^{d}25) and are based on the recommended value in the *Table of Isotopes*. We assume each cosmic-ray-stable nuclide has at most one ultimate daughter of non-electron-capture decays. This is true if branching ratios less than 1% are ignored. The electron capture half-life of ^{91}Nb was not reported; thus, we adopt 10^4 yr as recommended in Muller (1980).

The primary deficiency in nuclear data as it applies to the understanding of cosmic-ray nuclei is the lack of branching ratios between electron capture and positron decay modes. The most important effect of this is that an electron capture isotope, considered stable in our list, might have a rare positron decay mode which effectively makes it unstable. For example, ^{48}Cr generally decays by electron capture, and no positron decay has been observed to the 2% level. Positron decay is allowed with $Q = 0.63$ MeV. Since the electron capture half-life is 2.46×10^{-3} yr, even a positron decay branch of 10^{-5} would convert ^{48}Cr from a cosmic-ray-stable isotope to a parent of ^{48}Ti. In this case, the possibility of ^{48}Cr arriving in cosmic rays depends critically on the minute positron decay branch. There are 55 cosmic-ray-stable isotopes for which allowed beta-decay modes have not been observed. (These isotopes are indicated by a "?" in the non-electron-decay mode lifetime). Of these, ^{54}Mn and ^{102}Rh would be expected to decay by electron, rather than positron, emission.

A further effect of the unknown positron branching ratios is in computing the branching ratios of parents. When positron decay and electron capture compete with electron decay or an internal transition, and the overall lifetime is very short, the electron

TABLE 1

PATH LENGTH DISTRIBUTIONS

Distribution	Normalized Form		Mean Path Length	Model
Delta function	$\delta(x-\lambda)$		λ	slab
Exponential	$\frac{1}{\lambda}e^{-x/\lambda}$		λ	leaky box
Double exponential	$\frac{1}{\lambda_1-\lambda_2}(e^{-x/\lambda_1}-e^{-x/\lambda_2})$		$\lambda_1+\lambda_2$	nested leaky box
Fully truncated exponential	0	$x<\delta$	$\lambda+\delta$	(none)
	$\frac{1}{\lambda}e^{-(x-\delta)/\lambda}$	$x\geq\delta$		
Linearly truncated exponential	$\frac{x/\delta}{(\lambda+\delta/2)}$	$x<\delta$	$\frac{\lambda^2+\lambda\delta+\delta^2/3}{(\lambda+\delta/2)}$	(none)
	$\frac{1}{(\lambda+\delta/2)}e^{-(x-\delta)/\lambda}$	$x\geq\delta$		

The inverses using other path length distributions are found in a like manner

Negative source abundances are often implied by the inverse propagation. These serve to emphasize the importance of error analysis. Such analysis shows, for example, that there is a 50% error in estimating the source abundance of N, primarily due to cross section uncertainties (Guzik 1981). Isotopic uncertainties are even greater. Error analysis in the matrix formulation is straightforward. If the errors are small and random, one can use small error analysis.

The mean square flux error in the exponential path length distribution calculation [eq. (10)] due to uncertainty in the modification matrix is therefore

$$\delta J_i^2 = \lambda^2 \sum_{j,k} \left[(1-M\lambda)_{ij}^{-1}\right]^2 \delta M_{jk}^2 J_k^2; \qquad (12)$$

δM_{jk} is the matrix of root mean square errors in the elements of M_{jk}. Errors in the inverse calculation are dependent on uncertainties in the modification matrix and the arriving fluxes:

$$\delta J_i(0)^2 = \sum_j \left[(1-M\lambda)_{ij}\right]^2 \delta J_j^2 + \lambda^2 \sum_j \delta M_{ij}^2 J_j^2. \qquad (13)$$

The assumption of random errors in the modification matrix is not always justified. Especially when using semiempirical formulae, one must suspect systematic errors which lead to correlations in the elements of δM_{jk} (Hinshaw and Wiedenbeck 1983). These may be estimated by more conservative treatment of the errors; for example, if the errors are totally correlated, equation (13) becomes

$$\delta J_i = \lambda \sum_{j,k} [1-M\lambda]_{ij}^{-1} \delta M_{jk} J_k. \qquad (14)$$

The versatility and elegance of matrix methods in cosmic-ray propagation are evident. Details of the propagation on a small scale may be dealt with independently of large-scale considerations. The method offers a clear treatment of different path length distributions, primary and secondary contributions, and errors. Numerical work requires only matrix routines and can usually be done in closed form. In the remaining sections, small-scale physics of propagation and reduction of the propagation equations to the required form is discussed.

III. NUCLEAR FRAGMENTATION

From the viewpoint of composition, nuclear fragmentation of cosmic rays in collision with atoms of the interstellar medium is the most important physical process in propagation. These transformations involve two sets of physical quantities, the total inelastic cross sections σ_i and the partial cross sections σ_{ij}. For an ISM of pure H, the fragmentation equation is

$$\left(\frac{dJ_i}{dt}\right)_{\text{fragmentation}} = -n_H v \sigma_i J_i + n_H v \sum_j \sigma_{ij} J_j. \qquad (15)$$

The total inelastic cross sections include, in principle, all interactions in which the incoming and outgoing particles differ. In practice, only mass and charge changing reactions are measured and used. An empirical formula for Li and heavier nuclei at energies greater than 10 MeV N^{-1} is given by Letaw, Silberberg, and Tsao (1983*a*):

$$\sigma_i = 45 A_i^{0.7}[1+0.016\sin(5.3-2.63\ln A_i)]$$
$$\times\left[1-0.62 e^{-E/200}\sin(10.9 E^{-0.28})\right] \text{mb}, \qquad (16)$$

where E is the energy in MeV N^{-1} and A_i is the mass of species i. For He an overall multiplicative correction of 0.8 is required. For Be, an energy-dependent multiplicative factor is required at low energies:

$$1+0.75\, e^{-E/75}. \qquad (17)$$

The general nature of the energy dependence in this expression is shown in Figure 1. At low energies, a universal fit is extremely difficult because of resonance effects. Above 100 MeV N^{-1} the mean error is less than 5%.

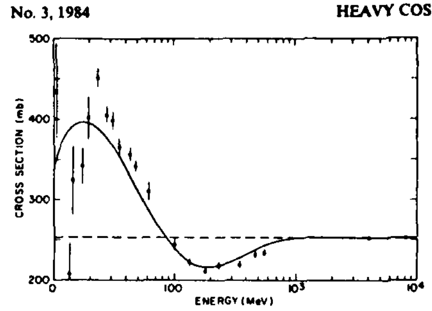

FIG. 1.—Total inelastic cross section of protons on carbon as a function of energy. Experimental data are compared with the empirical formula (eq. [16]).

The most complete source of partial cross sections is the semiempirical formulae (Silberberg and Tsao 1973*a*, *b*, 1977*a*, *b*; Tsao and Silberberg 1979; Tsao, Silberberg, and Letaw 1983) which fill in the numerous gaps in experimental data. The basic equation for calculating the partial cross sections is

$$\sigma_{ij} = \sigma_0 f(A_i) f(E) e^{-P\Delta A} \exp\left(-R|Z - SA_j + TA_j^2|^\nu\right)\Omega\eta\xi. \qquad (18)$$

It is applicable for calculating cross sections (in units of millibarns) of targets having mass numbers in the range $9 \leq A_i \leq 209$ and products with $6 < A_j < 200$, except for peripheral interactions with small values of $\Delta A = A_i - A_j$. For the latter reactions, a different equation was constructed. (A different equation was devised also for target elements as heavy as Th and U.)

In equation (18), σ_0 is a normalization factor. The factors $f(A)$ and $f(E)$ apply only to products from heavy targets (with atomic number $Z_i > 30$), when ΔA is large, as in the case of fission, fragmentation, and evaporation of light product nuclei. The parameter Ω is related to the nuclear structure and number of particle-stable levels of a product nuclide. The factor η depends on the pairing of protons and neutrons in the product nucleus; it is larger for even-even nuclei. The parameter ξ is introduced to represent the enhancement of light evaporation products. The factor $\exp(-P\Delta A)$ describes the diminution of cross sections as the difference of target and product mass, ΔA, increases. It is closely related to the distribution of excitation energies discussed by Metropolis *et al.* (1958*a*, *b*) in their Monte Carlo study of nuclear spallation reactions. A large excitation energy results in evaporation of many nucleons, i.e., in a large ΔA. The distribution of excitation energies peaks at small values; correspondingly, the partial cross sections are larger for small values of ΔA. The remaining exponential factor (with $\nu \approx 1.5$) describes the distribution of cross sections for the production of various isotopes of an element of atomic number Z. This Gaussian-like distribution is related to the statistical nature of the nuclear evaporation process (Dostrovsky, Rabinowitz, and Bivins 1958). The width of the distribution of cross sections is represented by the parameter R. The parameter S describes the location of the peaks of these distribution curves for small values of the product mass number A. The parameter T describes the shift of the distribution curves toward greater neutron excess as the atomic number of the product increases. Equation (18) and its parameters are closely related to nuclear systematics of the prompt intranuclear cascade and nuclear evaporation processes. For this reason these relations provide a surprisingly good fit to the experimental partial cross sections.

These formulae provide cross sections for all isotopes from Li through U fragmenting into nuclei within the same mass range. (A recent extension based on baryon conservation [Letaw 1983] predicts cross sections for light fragment production.) They are applicable at energies above 100 MeV N^{-1}. For the lighter elements ($Z \leq 28$) at energies above 2.3 GeV N^{-1} where the cross sections become energy independent, errors are ~ 35%. For heavier elements, whose cross sections do not become energy independent until ~ 6 GeV N^{-1}, the errors are ~ 50%. At low energies all errors are larger. Errors in the partial cross sections are perhaps the major obstacle to detailed compositional analysis of cosmic rays. Further experimental studies of the fragmentation of abundant cosmic-ray primaries are needed similar to those of Webber and Brautigam (1982). Additional work in semiempirical fits is also required to fill in inevitable gaps in experimental data and to reduce fitting errors.

As a function of path length, equation (15) becomes

$$\left(\frac{dJ_i}{dx}\right)_{\text{fragmentation}} = -\frac{J_i}{\lambda_i} + \sum_j \frac{J_j}{\lambda_{ij}}, \qquad (19)$$

where collisions with other elements in the ISM are incorporated into the mean free paths as follows:

$$\lambda = \frac{10^{27}}{N_A}\left(\sum_j b_j A_j\right)\bigg/\left(\sum_i b_i \sigma^{(i)}\right). \qquad (20)$$

In this expression $\sigma^{(i)}$ is the total or partial cross section in millibarns on a target of species i and b_i is the number density of species i relative to H in the ISM. Some measurements of these nucleus-nucleus cross sections are available (Lindstrom *et al.* 1975; Olson *et al.* 1983); however, only preliminary modeling has been performed (Silberberg, Tsao, and Shapiro 1976; Silberberg and Tsao 1977*c*; Karol 1975).

The mean free path in equation (20) is practically dependent only on the He/H ratio in the ISM. If this ratio is taken to be 0.068 (Cameron 1982), the fragmentation mean free path is ~ 14% greater than in a pure hydrogen medium. Including He in the path length computation (eq. [4]) increases the path length by ~ 27%. Thus, the inferred mean path length in the ISM is ~ 11% greater if He is included.

IV. IONIZATION LOSS

Ionization loss, that is, energy loss in electronic interactions with atoms of the interstellar medium, is a rigidity and

TABLE 6
COSMIC-RAY ISOTOPES

ISOTOPE	PARENTS (BRANCHING RATIO)	NON-E.C. DECAY HALFLIFE	NON-E.C. DECAY DAUGHTER	ELECTRON CAPTURE HALFLIFE	ELECTRON CAPTURE DAUGHTER
3LI 6	2HE 6(1.00)				
3LI 7	3LI 11(0.01) 4BE 11(0.03)				
4BE 7				1.46E-01	3LI 7
4BE 9	3LI 9(0.65)				
4BE 10	3LI 11(0.61)	1.60E+06	5B 10		
5B 10	6C 10(1.00)				
5B 11	3LI 11(0.38) 4BE 11(0.97) 4BE 12(0.09) 6C 11(1.00)				
6C 12	4BE 12(0.91) 5B 12(0.98) 7N 12(0.96) 8O 13(0.12)				
6C 13	5B 13(1.00) 7N 13(1.00) 8O 13(0.88)				
6C 14	5B 14(1.00)	5.73E+03	7N 14		
7N 14	8O 14(1.00)				
7N 15	6C 15(1.00) 6C 16(1.00) 8O 15(1.00)				
8O 16	7N 16(1.00) 7N 17(0.95) 10NE 17(1.00) 11NA 20(0.20)				
8O 17	7N 17(0.05) 9F 17(1.00)				
8O 18	7N 18(1.00) 9F 18(1.00) 10NE 18(1.00)				
9F 19	8O 19(1.00) 10NE 19(1.00)				
10NE 20	8O 20(1.00) 9F 20(1.00) 11NA 20(0.80) 12MG 21(0.32)				
10NE 21	9F 21(1.00) 11NA 21(1.00) 12MG 21(0.68)				
10NE 22	9F 22(1.00) 11NA 22(1.00) 12MG 22(1.00)				
11NA 23	9F 23(1.00) 10NE 23(1.00) 12MG 23(1.00)				
12MG 24	10NE 24(1.00) 11NA 24(1.00) 13AL 24(1.00) 14SI 25(1.00)				
12MG 25	10NE 25(1.00) 11NA 25(1.00) 13AL 25(1.00)				
12MG 26	11NA 26(1.00) 14SI 26(1.00)				
13AL 26		8.78E+05	12MG 26	4.00E+06	12MG 26
13AL 27	11NA 27(1.00) 11NA 28(0.01) 12MG 27(1.00) 14SI 27(1.00)				
14SI 28	11NA 28(0.99) 11NA 29(0.15) 12MG 28(1.00) 13AL 28(1.00) 15P 28(1.00)				
14SI 29	11NA 29(0.85) 11NA 30(0.33) 12MG 29(1.00) 13AL 29(1.00) 15P 29(1.00)				
14SI 30	11NA 30(0.67) 11NA 31(0.30) 12MG 30(1.00) 13AL 30(1.00) 15P 30(1.00) 16S 30(1.00)				
15P 31	11NA 31(0.70) 12MG 31(1.00) 13AL 31(1.00) 14SI 31(1.00) 16S 31(1.00)				
16S 32	12MG 32(1.00) 13AL 32(1.00) 14SI 32(1.00) 15P 32(1.00) 17CL 32(1.00) 18AR 33(0.34)				
16S 33	12MG 33(1.00) 13AL 33(1.00) 14SI 33(1.00) 15P 33(1.00) 17CL 33(1.00) 18AR 33(0.66)				
16S 34	14SI 34(1.00) 15P 34(1.00) 17CL 34(1.00) 18AR 34(1.00)				
16S 36					
17CL 35	15P 35(1.00) 16S 35(1.00) 18AR 35(1.00)				
17CL 36		3.06E+05	18AR 36	1.58E+07	16S 36
17CL 37	16S 37(1.00)				
18AR 36	19K 36(1.00) 20CA 37(0.76)				
18AR 37	19K 37(1.00) 20CA 37(0.24)			9.58E-02	17CL 37
18AR 38	16S 38(1.00) 17CL 38(1.00) 19K 38(1.00) 20CA 38(1.00)				
18AR 40	17CL 40(1.00)				
19K 39	17CL 39(1.00) 18AR 39(1.00) 20CA 39(1.00)				
19K 40		1.43E+09	20CA 40	1.20E+10	18AR 40
19K 41	17CL 41(1.00) 18AR 41(1.00)				
20CA 40	21SC 40(1.00) 22TI 41(0.95) 23V 44(1.00)				
20CA 41	21SC 41(1.00) 22TI 41(0.05)			1.00E+05	19K 41

TABLE 6—*Continued*

ISOTOPE	PARENTS (BRANCHING RATIO)	NON-E.C. DECAY HALFLIFE	NON-E.C. DECAY DAUGHTER	ELECTRON CAPTURE HALFLIFE	ELECTRON CAPTURE DAUGHTER
20CA 42	18AR 42(1.00) 19K 42(1.00) 21SC 42(1.00) 22TI 42(1.00)				
20CA 43	18AR 43(1.00) 19K 43(1.00) 21SC 43(1.00) 22TI 43(1.00)				
20CA 44	18AR 44(1.00) 19K 44(1.00) 21SC 44(1.00)				
20CA 46	19K 46(1.00)				
20CA 48	19K 48(1.00)				
21SC 45	19K 45(1.00) 20CA 45(1.00) 22TI 45(1.00) 23V 45(1.00) 24CR 45(0.75)				
22TI 44	24CR 45(0.25)			4.70E+01	20CA 44
22TI 46	21SC 46(1.00) 23V 46(1.00) 24CR 46(1.00)				
22TI 47	19K 47(1.00) 20CA 47(1.00) 21SC 47(1.00) 23V 47(1.00)				
22TI 48	21SC 48(1.00) 23V 48(1.00)				
22TI 49	19K 49(1.00) 20CA 49(1.00) 21SC 49(1.00)				
22TI 50	19K 50(1.00) 20CA 50(1.00) 21SC 50(1.00)				
23V 49	24CR 49(1.00) 25MN 49(1.00)			9.03E-01	22TI 49
23V 50					
23V 51	21SC 51(1.00) 22TI 51(1.00)				
24CR 48		(?)	22TI 48	2.46E-03	22TI 48
24CR 50	25MN 50(1.00)				
24CR 51	25MN 51(1.00)			7.58E-02	23V 51
24CR 52	22TI 52(1.00) 23V 52(1.00) 25MN 52(1.00) 26FE 52(1.00)				
24CR 53	22TI 53(1.00) 23V 53(1.00)				
24CR 54	23V 54(1.00)				
25MN 53	26FE 53(1.00) 27CO 53(1.00)			3.70E+06	24CR 53
25MN 54		(?)	26FE 54	8.54E-01	24CR 54
25MN 55	24CR 55(1.00)				
26FE 54	27CO 54(1.00)				
26FE 55	27CO 55(1.00)			2.70E+00	25MN 55
26FE 56	24CR 56(1.00) 25MN 56(1.00) 27CO 56(1.00)				
26FE 57	25MN 57(1.00)				
26FE 58	25MN 58(1.00) 27CO 58(1.00)				
26FE 60		3.00E+05	28NI 60		
27CO 57	28NI 57(1.00			7.42E-01	26FE 57
27CO 59	26FE 59(1.00)				
28NI 56		(?)	26FE 56	1.67E-02	26FE 56
28NI 58	29CU 58(1.00)				
28NI 59	29CU 59(1.00)	5.00E+11	27CO 59	7.50E+04	27CO 59
28NI 60	27CO 60(1.00) 29CU 60(1.00) 30ZN 60(1.00)				
28NI 61	26FE 61(1.00) 27CO 61(1.00) 29CU 61(1.00) 30ZN 61(1.00)				
28NI 62	26FE 62(1.00) 27CO 62(1.00) 29CU 62(1.00) 30ZN 62(1.00) 31GA 62(1.00)				
28NI 64	27CO 64(1.00) 29CU 64(0.32)				
29CU 63	27CO 63(1.00) 28NI 63(1.00) 30ZN 63(1.00) 31GA 63(1.00)				
29CU 65	28NI 65(1.00) 30ZN 65(1.00) 31GA 65(1.00) 32GE 65(1.00)				
30ZN 64	29CU 64(0.68) 31GA 64(1.00) 32GE 64(1.00)				
30ZN 66	28NI 66(1.00) 29CU 66(1.00) 31GA 66(1.00) 32GE 66(1.00)				
30ZN 67	28NI 67(1.00) 29CU 67(1.00)				
30ZN 68	29CU 68(1.00) 31GA 68(1.00)				

TABLE 6—*Continued*

ISOTOPE	PARENTS (BRANCHING RATIO)	NON-E.C. DECAY HALFLIFE	NON-E.C. DECAY DAUGHTER	ELECTRON CAPTURE HALFLIFE	ELECTRON CAPTURE DAUGHTER
30ZN 70	29CU 70(1.00)			8.93E-03	30ZN 67
31GA 67	32GE 67(1.00)				
31GA 69	29CU 69(1.00) 30ZN 69(1.00) 32GE 69(1.00) 33AS 69(1.00) 34SE 69(1.00)				
31GA 71	30ZN 71(1.00)			7.89E-01	30ZN 68
32GE 68	33AS 68(1.00) 34SE 68(1.00)				
32GE 70	31GA 70(1.00) 33AS 70(1.00) 34SE 70(1.00)			3.07E-02	31GA 71
32GE 71	33AS 71(1.00) 34SE 71(1.00) 35BR 71(1.00)				
32GE 72	30ZN 72(1.00) 31GA 72(1.00) 33AS 72(1.00)				
32GE 73	30ZN 73(1.00) 31GA 73(1.00)				
32GE 74	30ZN 74(1.00) 31GA 74(1.00) 33AS 74(0.49)				
32GE 76	30ZN 76(1.00) 31GA 76(1.00)			2.20E-01	32GE 73
33AS 73	34SE 73(1.00) 35BR 73(1.00) 36KR 73(0.99)				
33AS 75	30ZN 75(1.00) 31GA 75(1.00) 32GE 75(1.00)			2.30E-02	32GE 72
34SE 72	35BR 72(1.00) 36KR 72(1.00) 36KR 73(0.01)				
34SE 74	33AS 74(0.51) 35BR 74(1.00) 36KR 74(1.00) 37RB 74(1.00)				
34SE 75	35BR 75(1.00) 36KR 75(1.00) 37RB 75(1.00)			3.24E-01	33AS 75
34SE 76	33AS 76(1.00) 35BR 76(1.00)				
34SE 77	32GE 77(1.00) 33AS 77(1.00) 35BR 77(1.00) 36KR 77(1.00) 37RB 77(1.00) 38SR 77(1.00)				
34SE 78	31GA 78(1.00) 32GE 78(1.00) 33AS 78(1.00) 35BR 78(1.00)				
34SE 79	31GA 79(1.00) 32GE 79(1.00) 33AS 79(1.00)	6.50E+04	35BR 79		
34SE 80	32GE 80(1.00) 33AS 80(1.00) 35BR 80(0.03)	1.40E+20	36KR 82		
34SE 82	32GE 82(1.00) 33AS 82(1.00)				
35BR 79	36KR 79(1.00) 37RB 79(1.00) 38SR 79(1.00)				
35BR 81	32GE 81(1.00) 33AS 81(1.00) 34SE 81(1.00)	(?)	34SE 76	1.69E-03	34SE 76
36KR 76	37RB 76(1.00)				
36KR 78	37RB 78(1.00) 38SR 78(1.00)				
36KR 80	35BR 80(0.97) 37RB 80(1.00) 38SR 80(1.00)			2.10E+05	35BR 81
36KR 81	37RB 81(1.00) 38SR 81(1.00) 39Y 81(1.00) 40ZR 81(1.00)				
36KR 82	35BR 82(1.00) 37RB 82(1.00)				
36KR 83	32GE 83(1.00) 33AS 83(1.00) 34SE 83(1.00) 35BR 83(1.00)				
36KR 84	32GE 84(1.00) 33AS 84(1.00) 33AS 85(0.23) 34SE 84(1.00) 35BR 84(1.00) 37RB 84(0.88)				
36KR 86	33AS 86(0.96) 33AS 87(0.02) 34SE 86(1.00) 34SE 87(0.02) 35BR 86(1.00) 35BR 87(0.02)				
37RB 83	38SR 83(1.00) 39Y 83(1.00) 40ZR 83(1.00)	(?)	36KR 83	2.36E-01	36KR 83
37RB 85	33AS 85(0.77) 33AS 86(0.04) 34SE 85(1.00) 35BR 85(1.00) 36KR 85(1.00)				
37RB 87	33AS 87(0.98) 34SE 87(0.98) 34SE 88(0.07) 35BR 87(0.98) 35BR 88(0.06) 36KR 87(1.00)	4.80E+10	38SR 87		
38SR 82	39Y 82(1.00) 40ZR 82(1.00)			6.84E-02	36KR 82
38SR 84	37RB 84(0.12) 39Y 84(1.00) 40ZR 84(1.00)				
38SR 85	39Y 85(1.00) 40ZR 85(1.00)	(?)	37RB 85	1.77E-01	37RB 85
38SR 86	37RB 86(1.00) 39Y 86(1.00)				
38SR 87	39Y 87(1.00) 40ZR 87(1.00) 41NB 87(1.00)				
38SR 88	34SE 88(0.93) 35BR 88(0.94) 35BR 89(0.13) 36KR 88(1.00) 37RB 88(1.00) 39Y 88(1.00)				
39Y 89	35BR 89(0.87) 36KR 89(1.00) 37RB 89(1.00) 38SR 89(1.00) 40ZR 89(1.00) 41NB 89(1.00)	(?)	38SR 86	1.88E-03	38SR 86
40ZR 86	41NB 86(1.00)			2.28E-01	38SR 88
40ZR 88	41NB 88(1.00) 42MO 88(1.00)				
40ZR 90	37RB 90(1.00) 38SR 90(1.00) 39Y 90(1.00) 41NB 90(1.00) 42MO 90(1.00) 43TC 90(1.00)				

TABLE 6—*Continued*

ISOTOPE	PARENTS (BRANCHING RATIO)	NON-E.C. DECAY HALFLIFE	NON-E.C. DECAY DAUGHTER	ELECTRON CAPTURE HALFLIFE	ELECTRON CAPTURE DAUGHTER
40ZR 91	35BR 91(0.91) 35BR 92(0.16) 36KR 91(1.00) 37RB 91(1.00) 38SR 91(1.00) 39Y 91(1.00)				
40ZR 92	35BR 92(0.84) 36KR 92(1.00) 37RB 92(1.00) 37RB 93(0.01) 38SR 92(1.00) 39Y 92(1.00)				
40ZR 93	36KR 93(0.97) 36KR 94(0.15) 37RB 93(0.99) 37RB 94(0.10) 38SR 93(1.00) 39Y 93(1.00)	1.50E+06	41NB 93		
40ZR 94	36KR 94(0.85) 37RB 94(0.90) 37RB 95(0.08) 38SP 94(1.00) 39Y 94(1.00)				
40ZR 96	37RB 96(0.87) 37RB 97(0.27) 38SR 96(1.00) 39Y 96(1.00)				
41NB 91	42MO 91(1.00) 43TC 91(1.00)	(?)	40ZR 91	1.00E+04	40ZR 91
41NB 92		5.33E+10	40ZR 92	3.20E+07	40ZR 92
41NB 93					
41NB 94		2.00E+04	42MO 94		
42MO 92	43TC 92(1.00) 44RU 92(1.00)				
42MO 93	43TC 93(1.00) 44RU 93(1.00)			3.00E+03	41NB 93
42MO 94	43TC 94(1.00)				
42MO 95	37RB 95(0.92) 37RB 96(0.13) 38SR 95(1.00) 39Y 95(1.00) 40ZR 95(1.00) 41NB 95(1.00)				
42MO 96	41NB 96(1.00)				
42MO 97	37RB 97(0.73) 37RB 98(0.13) 38SR 97(1.00) 39Y 97(1.00) 40ZR 97(1.00) 41NB 97(1.00)				
42MO 98	37RB 98(0.87) 38SR 98(1.00) 39Y 98(1.00) 39Y 99(0.01) 40ZR 98(1.00) 41NB 98(1.00)				
42MO100	39Y 100(1.00) 40ZR100(1.00) 41NB100(1.00)				
43TC 95	44RU 95(1.00) 45RH 95(1.00)	(?)	42MO 95	2.28E-03	42MO 95
43TC 96		(?)	42MO 96	1.18E-02	42MO 96
43TC 97				2.60E+06	42MO 97
43TC 98		4.20E+06	44RU 98		
43TC 99	39Y 99(0.99) 40ZR 99(1.00) 41NB 99(1.00) 42MO 99(1.00)	2.14E+05	44RU 99		
44RU 94	45RH 94(1.00)	(?)	42MO 94	9.89E-05	42MO 94
44RU 96	45RH 96(1.00)				
44RU 97	45RH 97(1.00) 46PD 97(1.00)	(?)	43TC 97	7.89E-03	43TC 97
44RU 98	45RH 98(1.00) 46PD 98(1.00)				
44RU 99	45RH 99(1.00) 46PD 99(1.00) 47AG 99(1.00)				
44RU100	43TC100(1.00) 45RH100(1.00)				
44RU101	40ZR101(1.00) 41NB101(1.00) 42MO101(1.00) 43TC101(1.00)				
44RU102	39Y 102(1.00) 40ZR102(1.00) 41NB102(1.00) 42MO102(1.00) 43TC102(1.00)				
44RU104	41NB104(1.00) 42MO104(1.00) 43TC104(1.00)				
45RH101	46PD101(1.00) 47AG101(1.00) 48CD101(1.00)			3.30E+00	44RU101
45RH102		(?)	46PD102	2.90E+00	44RU102
45RH103	41NB103(1.00) 42MO103(1.00) 43TC103(1.00) 44RU103(1.00)				
46PD100	47AG100(1.00) 48CD100(1.00)			9.86E-03	44RU100
46PD102	47AG102(1.00) 48CD102(1.00)				
46PD103	47AG103(1.00) 48CD103(1.00)			4.65E-02	45RH103
46PD104	45RH104(1.00) 47AG104(1.00) 48CD104(1.00) 49IN104(1.00)				
46PD105	41NB105(1.00) 42MO105(1.00) 43TC105(1.00) 44RU105(1.00) 45RH105(1.00)				
46PD106	41NB106(1.00) 42MO106(1.00) 43TC106(1.00) 44RU106(1.00) 45RH106(1.00) 47AG106(1.00)				
46PD107	42MO107(1.00) 43TC107(1.00) 44RU107(1.00) 45RH107(1.00)	6.50E+06	47AG107		
46PD108	42MO108(1.00) 43TC108(1.00) 44RU108(1.00) 45RH108(1.00)				
46PD110	43TC110(1.00) 44RU110(1.00) 45RH110(1.00)				
47AG105	48CD105(1.00) 49IN105(1.00)	1.26E+04	46PD105	1.13E-01	46PD105
47AG107	48CD107(1.00) 49IN107(1.00) 50SN107(1.00) 51SB107(1.00)				

TABLE 6—*Continued*

ISOTOPE	PARENTS (BRANCHING RATIO)	NON-E.C. DECAY		ELECTRON CAPTURE	
		HALFLIFE	DAUGHTER	HALFLIFE	DAUGHTER
47AG109	43TC109(1.00) 44RU109(1.00) 45RH109(1.00) 46PD109(1.00)				
48CD106	49IN106(1.00) 50SN106(1.00)				
48CD108	47AG108(1.00) 49IN108(1.00)				
48CD109	49IN109(1.00) 50SN109(1.00) 51SB109(1.00)			1.24E+00	47AG109
48CD110	47AG110(1.00)				
48CD111	44RU111(1.00) 45RH111(1.00) 46PD111(1.00) 47AG111(1.00)				
48CD112	44RU112(1.00) 45RH112(1.00) 46PD112(1.00) 47AG112(1.00) 49IN112(0.33)				
48CD113	46PD113(1.00) 47AG113(1.00)	9.00E+15	49IN113		
48CD114	45RH114(1.00) 46PD114(1.00) 47AG114(1.00)				
48CD116	46PD116(1.00) 47AG116(1.00)				
49IN110		(?)	48CD110	5.59E-04	48CD110
49IN111	50SN111(1.00) 51SB111(1.00)			7.75E-03	48CD111
49IN113					
49IN115	46PD115(0.95) 47AG115(0.95) 48CD115(0.95)	5.10E+14	50SN115		
50SN108	51SB108(1.00)	(?)	48CD108	2.00E-05	48CD108
50SN110	51SB110(1.00)			4.68E-04	48CD110
50SN112	49IN112(0.67) 51SB112(1.00)				
50SN113	51SB113(1.00) 52TE113(1.00) 53I 113(1.00)	(?)	49IN113	3.15E-01	49IN113
50SN114	49IN114(1.00) 51SB114(1.00) 52TE114(1.00)				
50SN115	47AG115(0.05) 48CD115(0.05) 51SB115(1.00) 52TE115(1.00) 53I 115(1.00) 54XE115(1.00)				
50SN116	49IN116(1.00) 51SB116(1.00) 52TE116(1.00) 53I 116(1.00) 54XE116(1.00) 55CS116(1.00)				
50SN117	48CD117(1.00) 49IN117(1.00) 51SB117(1.00) 52TE117(1.00) 53I 117(1.00) 54XE117(1.00)				
50SN118	46PD118(1.00) 47AG118(1.00) 48CD118(1.00) 49IN118(1.00) 51SB118(1.00)				
50SN119	47AG119(1.00) 48CD119(1.00) 49IN119(1.00)				
50SN120	47AG120(1.00) 48CD120(1.00) 49IN120(1.00)				
50SN122	47AG122(1.00) 48CD122(1.00) 49IN122(1.00)				
50SN124	48CD124(1.00) 49IN124(1.00)				
50SN126	49IN126(1.00)	1.00E+05	52TE126		
51SB119	52TE119(1.00) 53I 119(1.00) 54XE119(1.00) 55CS119(1.00)			4.33E-03	50SN119
51SB120		(?)	50SN120	1.58E-02	50SN120
51SB121	47AG121(1.00) 48CD121(1.00) 49IN121(1.00) 50SN121(1.00)				
51SB123	48CD123(1.00) 49IN123(1.00) 50SN123(1.00)				
52TE118	53I 118(1.00) 54XE118(1.00) 55CS118(1.00) 56BA119(1.00)			1.64E-02	50SN118
52TE120	53I 120(1.00) 54XE120(1.00) 55CS120(1.00) 56BA120(1.00)				
52TE121	53I 121(1.00) 54XE121(1.00) 55CS121(1.00) 56BA121(1.00)	(?)	51SB121	4.60E-02	51SB121
52TE122	51SB122(1.00) 53I 122(1.00)				
52TE123					
52TE124	51SB124(1.00) 53I 124(1.00)				
52TE125	49IN125(1.00) 50SN125(1.00) 51SB125(1.00)				
52TE126	51SB126(1.00) 53I 126(0.02)				
52TE128	50SN128(1.00) 51SB128(1.00)	1.50E+24	54XE128		
52TE130	50SN130(1.00) 51SB130(1.00)	2.00E+21	54XE130		
53I 123	54XE123(1.00) 55CS123(1.00) 56BA123(1.00)	(?)	52TE123	1.48E-03	52TE123
53I 125	54XE125(1.00) 55CS125(1.00) 56BA125(1.00)			1.65E-01	52TE125
53I 127	50SN127(1.00) 51SB127(1.00) 52TE127(1.00)				

TABLE 6—*Continued*

ISOTOPE	PARENTS (BRANCHING RATIO)	NON-E.C. DECAY		ELECTRON CAPTURE	
		HALFLIFE	DAUGHTER	HALFLIFE	DAUGHTER
53I 129	50SN129(1.00) 51SB129(1.00) 52TE129(1.00)	1.60E+07	54XE129		
54XE122	55CS122(1.00) 56BA122(1.00)	(?)	52TE122	2.29E-03	52TE122
54XE124	55CS124(1.00) 56BA124(1.00)				
54XE126	53I 126(0.98) 55CS126(1.00) 56BA126(1.00) 57LA126(1.00)				
54XE127	55CS127(1.00) 56BA127(1.00) 57LA127(1.00)			9.97E-02	53I 127
54XE128	53I 128(1.00) 55CS128(1.00)				
54XE129	55CS129(1.00) 56BA129(1.00) 57LA129(1.00) 58CE129(1.00) 59PR129(1.00)				
54XE130	53I 130(1.00) 55CS130(0.97)				
54XE131	50SN131(1.00) 51SB131(1.00) 52TE131(1.00) 53I 131(1.00)				
54XE132	50SN132(1.00) 51SB132(1.00) 52TE132(1.00) 53I 132(1.00) 55CS132(0.43)				
54XE134	50SN134(0.83) 51SB134(1.00) 51SB135(0.20) 52TE134(1.00) 53I 134(1.00)				
54XE136	51SB136(0.68) 52TE136(0.99) 52TE137(0.08) 53I 136(1.00) 53I 137(0.06)				
55CS131				2.65E-02	54XE131
55CS133	50SN134(0.17) 51SB133(1.00) 52TE133(1.00) 53I 133(1.00) 54XE133(1.00)				
55CS135	51SB135(0.80) 51SB136(0.32) 52TE135(1.00) 52TE136(0.01) 53I 135(1.00) 54XE135(1.00)	3.00E+06	56BA135		
56BA128	57LA128(1.00) 58CE128(1.00)			6.65E-03	54XE128
56BA130	55CS130(0.03) 57LA130(1.00` 58CE130(1.00) 59PR130(1.00) 60ND130(1.00)				
56BA131	57LA131(1.00) 58CE131(1.00	(?)	55CS131	3.29E-02	55CS131
56BA132	55CS132(0.57) 57LA132(1.00)				
56BA133	57LA133(1.00) 58CE133(1.00) 59PR133(1.00) 60ND133(1.00) 61PM133(1.00)			1.07E+01	55CS133
56BA134	55CS134(1.00) 57LA134(1.00)				
56BA135	57LA135(1.00) 58CE135(1.00) 59PR135(1.00) 60ND135(1.00) 61PM135(1.00)				
56BA136	55CS136(1.00) 57LA136(1.00)				
56BA137	52TE137(0.92) 52TE138(0.11) 53I 137(0.94) 53I 138(0.05) 54XE137(1.00) 55CS137(1.00)				
56BA138	52TE138(0.89) 53I 138(0.95) 53I 139(0.10) 54XE138(1.00) 55CS138(1.00)				
57LA137	58CE137(1.00) 59PR137(1.00) 60ND137(1.00) 61PM137(1.00) 62SM137(1.00)			6.00E+04	56BA137
57LA138		3.44E+11	58CE138	1.62E+11	56BA138
57LA139	53I 139(0.90) 53I 140(0.14) 54XE139(1.00) 55CS139(1.00) 56BA139(1.00)				
58CE132	59PR132(1.00) 60ND132(1.00) 61PM132(1.00)	(?)	56BA132	3.99E-04	56BA132
58CE134	59PR134(1.00) 60ND134(1.00) 61PM134(1.00) 62SM134(1.00)			8.67E-03	56BA134
58CE136	59PR136(1.00) 60ND136(1.00) 61PM136(1.00)				
58CE138	59PR138(1.00)				
58CE139	59PR139(1.00) 60ND139(1.00) 61PM139(1.00) 62SM139(1.00) 63EU139(1.00)			3.76E-01	57LA139
58CE140	53I 140(0.86) 54XE140(1.00) 55CS140(1.00) 56BA140(1.00) 57LA140(1.00) 59PR140(1.00)				
58CE142	54XE142(1.00) 55CS142(1.00) 55CS143(0.02) 56BA142(1.00) 57LA142(1.00)				
59PR141	57LA141(1.00) 58CE141(1.00) 60ND141(1.00) 61PM141(1.00) 62SM141(1.00) 63EU141(1.00)				
60ND138	61PM138(1.00) 62SM138(1.00) 63EU138(1.00)	(?)	58CE138	5.82E-04	58CE138
60ND140	61PM140(1.00) 62SM140(1.00) 63EU140(1.00)			9.23E-03	58CE140
60ND142	59PR142(1.00) 61PM142(1.00) 62SM142(1.00) 63EU142(1.00)				
60ND143	55CS143(0.98) 55CS144(0.03) 56BA143(1.00) 57LA143(1.00) 58CE143(1.00) 59PR143(1.00)				
60ND144	55CS144(0.97) 55CS145(0.12) 56BA144(1.00) 57LA144(1.00) 58CE144(1.00) 59PR144(1.00)	2.10E+15	58CE140		
60ND145	55CS145(0.88) 55CS146(0.14) 56BA145(1.00) 57LA145(1.00) 58CE145(1.00) 59PR145(1.00)				
60ND146	55CS146(0.86) 56BA146(1.00) 57LA146(1.00) 58CE146(1.00) 59PR146(1.00)				
60ND148	56BA148(1.00) 57LA148(1.00) 58CE148(1.00) 59PR148(1.00)				
60ND150	58CE150(1.00) 59PR150(1.00)				

TABLE 6—*Continued*

ISOTOPE	PARENTS	NON-E.C. DECAY		ELECTRON CAPTURE	
	(BRANCHING RATIO)	HALFLIFE	DAUGHTER	HALFLIFE	DAUGHTER
61PM143	62SM143(1.00) 63EU143(1.00) 64GD143(1.00)	(?)	60ND143	7.26E-01	60ND143
61PM144		(?)	60ND144	9.56E-01	60ND144
61PM145		6.32E+09	59PR141	1.77E+01	60ND145
62SM144	63EU144(1.00) 64GD144(1.00) 64GD148(1.00) 65TB148(1.00) 66DY148(1.00) 66DY152(1.00)				
62SM145	63EU145(1.00) 64GD145(1.00) 65TB149(0.81) 66DY149(0.81) 68ER153(0.75) 70YB157(0.75)			9.31E-01	61PM145
62SM146	61PM146(1.00) 63EU146(1.00) 64GD146(1.00) 65TB146(1.00) 66DY150(0.90) 68ER154(0.08)	1.03E+08	60ND142		
62SM147	60ND147(1.00) 61PM147(1.00) 63EU147(1.00) 64GD147(1.00) 65TB147(1.00) 66DY151(0.56)	1.06E+11	60ND143		
62SM148	61PM148(1.00) 63EU148(1.00)	8.00E+15	60ND144		
62SM149	58CE149(1.00) 59PR149(1.00) 60ND149(1.00) 61PM149(1.00)				
62SM150	61PM150(1.00)				
62SM152	60ND152(1.00) 61PM152(1.00)				
62SM154	60ND154(1.00) 61PM154(1.00)				
63EU149				2.55E-01	62SM149
63EU150		(?)	62SM150	3.60E+01	62SM150
63EU151	58CE151(1.00) 59PR151(1.00) 60ND151(1.00) 61PM151(1.00) 62SM151(1.00)				
63EU153	61PM153(1.00) 62SM153(1.00)				
64GD149	65TB149(0.19) 66DY149(0.19) 68ER153(0.17) 70YB157(0.17)	5.09E+03	62SM145	2.55E-02	63EU149
64GD150	65TB150(1.00) 66DY150(0.10) 68ER154(0.01)	1.80E+06	62SM146		
64GD151	65TB151(0.99) 66DY151(0.44)	4.11E+07	62SM147	3.29E-01	63EU151
64GD152	63EU152(1.00) 65TB152(1.00)	1.10E+14	62SM148		
64GD153	65TB153(1.00) 66DY153(1.00) 67HO153(1.00) 68ER153(0.08) 70YB157(0.08)			6.61E-01	63EU153
64GD154	63EU154(1.00) 65TB154(1.00)				
64GD155	62SM155(1.00) 63EU155(1.00)				
64GD156	62SM156(1.00) 63EU156(1.00)				
64GD157	62SM157(1.00) 63EU157(1.00)				
64GD158	63EU158(1.00)				
64GD160	63EU160(1.00)				
65TB155	66DY155(1.00) 67HO155(1.00) 68ER155(1.00)			1.45E-02	64GD155
65TB156		(?)	64GD156	1.45E-02	64GD156
65TB157				1.50E+02	64GD157
65TB159	63EU159(1.00) 64GD159(1.00)				
66DY154	67HO154(1.00) 68ER154(0.91)	1.00E+07	64GD150		
66DY156	67HO156(1.00) 68ER156(1.00) 69TM156(1.00)				
66DY157	67HO157(1.00) 68ER157(1.00) 69TM157(1.00)	(?)	65TB157	9.24E-04	65TB157
66DY158	65TB158(1.00) 67HO158(1.00) 68ER158(1.00) 69TM158(1.00) 70YB158(1.00)				
66DY159				3.95E-01	65TB159
66DY160	65TB160(1.00) 67HO160(1.00)				
66DY161	64GD161(1.00) 65TB161(1.00)				
66DY162	64GD162(1.00) 65TB162(1.00) 67HO162(1.00)				
66DY163	65TB163(1.00)				
66DY164	65TB164(1.00)				
67HO159	68ER159(1.00) 69TM159(1.00) 70YB159(1.00)	(?)	66DY159	6.27E-05	66DY159
67HO161	68ER161(1.00) 69TM161(1.00) 70YB161(1.00) 71LU161(1.00)			2.83E-04	66DY161
67HO163	68ER163(1.00) 69TM163(1.00) 70YB163(1.00) 71LU163(1.00) 72HF163(1.00)			3.30E+01	66DY163
67HO165	66DY165(1.00)				

TABLE 6—*Continued*

ISOTOPE	PARENTS	NON-E.C. DECAY		ELECTRON CAPTURE	
	(BRANCHING RATIO)	HALFLIFE	DAUGHTER	HALFLIFE	DAUGHTER
68ER160	69TM160(1.00) 70YB160(1.00)			3.26E-03	66DY160
68ER162	69TM162(1.00) 70YB162(1.00) 71LU162(1.00) 72HF162(1.00)				
68ER164	67HO164(1.00) 69TM164(1.00)				
68ER165	69TM165(1.00) 70YB165(1.00) 71LU165(1.00)			1.19E-03	67HO165
68ER166	66DY166(1.00) 67HO166(1.00) 69TM166(1.00)				
68ER167	66DY167(1.00) 67HO167(1.00)				
68ER168	67HO168(1.00)				
68ER170	67HO170(1.00)				
69TM167	70YB167(1.00) 71LU167(1.00) 72HF167(1.00) 73TA167(1.00)			2.53E-02	68ER167
69TM169	67HO169(1.00) 68ER169(1.00)				
70YB164	71LU164(1.00) 72HF164(1.00)	(?)	68ER164	1.44E-04	68ER164
70YB166	71LU166(1.00) 72HF166(1.00) 73TA166(1.00)			6.47E-03	68ER166
70YB168	69TM168(1.00) 71LU168(1.00) 72HF168(1.00) 73TA168(1.00)				
70YB169	71LU169(1.00) 72HF169(1.00) 73TA169(1.00) 74W 169(1.00)			8.76E-02	69TM169
70YB170	69TM170(1.00) 71LU170(1.00)				
70YB171	68ER171(1.00) 69TM171(1.00) 71LU171(1.00) 72HF171(1.00) 73TA171(1.00) 74W 171(1.00)				
70YB172	68ER172(1.00) 69TM172(1.00)				
70YB173	68ER173(1.00) 69TM173(1.00)				
70YB174	69TM174(1.00) 71LU174(1.00)				
70YB176	69TM176(1.00)				
71LU172		(?)	70YB172	1.83E-02	70YB172
71LU173				1.37E+00	70YB173
71LU175	69TM175(1.00) 70YB175(1.00)				
71LU176		3.60E+10	72HF176		
72HF170	73TA170(1.00) 74W 170(1.00) 75RE170(1.00) 77IR174(1.00) 79AU178(1.00)	(?)	70YB170	1.83E-03	70YB170
72HF172	73TA172(1.00) 74W 172(1.00) 75RE172(1.00) 76OS172(1.00) 77IR176(1.00)			1.87E+00	71LU172
72HF173	73TA173(1.00) 74W 173(1.00) 75RE173(1.00) 76OS173(1.00) 77IR177(1.00)	(?)	71LU173	2.74E-03	71LU173
72HF174	73TA174(1.00)	2.00E+15	70YB170		
72HF175	73TA175(1.00) 74W 175(1.00) 75RE175(1.00) 76OS175(1.00)			1.92E-01	71LU175
72HF176	73TA176(1.00)				
72HF177	70YB177(1.00) 71LU177(1.00)				
72HF178	70YB178(1.00) 71LU178(1.00)				
72HF179	71LU179(1.00)				
72HF180	71LU180(1.00)				
72HF182		9.00E+06	74W 182		
73TA177	74W 177(1.00) 75RE177(1.00) 76OS177(1.00)	2.23E+03	72HF177	6.46E-03	72HF177
73TA178		(?)	72HF178	2.74E-04	72HF178
73TA179				1.70E+00	72HF179
73TA180					
73TA181	72HF181(1.00)				
74W 174	75RE174(1.00) 76OS174(1.00) 78PT178(0.07) 80HG182(0.01)	(?)	72HF174	5.51E-05	72HF174
74W 176	75RE176(1.00) 76OS176(1.00)			2.62E-04	72HF176
74W 178	75RE178(1.00) 76OS178(1.00) 77IR178(1.00)			5.89E-02	72HF178
74W 179	75RE179(1.00) 76OS179(1.00) 77IR179(1.00)	(?)	73TA179	7.22E-05	73TA179
74W 180	75RE180(1.00)				

TABLE 6 – *Continued*

ISOTOPE	PARENTS (BRANCHING RATIO)	NON-E.C. DECAY		ELECTRON CAPTURE	
		HALFLIFE	DAUGHTER	HALFLIFE	DAUGHTER
74W 181				3.31E-01	73TA181
74W 182	73TA182(1.00)				
74W 183	72HF183(1.00) 73TA183(1.00)				
74W 184	72HF184(1.00) 73TA184(1.00)				
74W 186	73TA186(1.00)				
75RE181	76OS181(1.00) 77IR181(1.00) 78PT181(1.00)	(?)	74W 181	2.28E-03	74W 181
75RE182		(?)	74W 182	7.30E-03	74W 182
75RE183	76OS183(1.00) 77IR183(1.00) 78PT183(1.00)			1.94E-01	74W 183
75RE184		(?)	74W 184	1.04E-01	74W 184
75RE185	73TA185(1.00) 74W 185(1.00)				
75RE187	74W 187(1.00)	4.00E+10	76OS187		
76OS180	77IR180(1.00) 78PT180(1.00)	(?)	74W 180	4.18E-05	74W 180
76OS182	77IR182(1.00) 78PT182(1.00) 78PT186(1.00) 79AU182(1.00) 79AU186(1.00) 80HG186(1.00)			2.51E-03	74W 182
76OS184	77IR184(1.00) 78PT184(1.00) 79AU184(1.00)				
76OS185	77IR185(1.00) 78PT185(1.00) 79AU185(1.00)	(?)	75RE185	2.56E-01	75RE185
76OS186	75RE186(1.00) 77IR186(1.00)	2.00E+15	74W 182		
76OS187					
76OS188	74W 188(1.00) 75RE188(1.00) 77IR188(1.00)				
76OS189	74W 189(1.00) 75RE189(1.00)				
76OS190	74W 190(1.00) 75RE190(1.00)				
76OS192	75RE192(1.00)				
77IR187	78PT187(1.00) 79AU187(1.00) 80HG187(1.00)	(?)	76OS187	1.20E-03	76OS187
77IR189	78PT189(1.00) 79AU189(1.00) 80HG189(1.00) 81TL189(1.00) 82PB189(1.00)			3.59E-02	76OS189
77IR190		(?)	76OS190	3.23E-02	76OS190
77IR191	75RE191(1.00) 76OS191(1.00)				
77IR193	76OS193(1.00)				
78PT188	79AU188(1.00) 80HG188(1.00) 81TL188(1.00)	9.31E+04	76OS184	2.79E-02	76OS188
78PT190	79AU190(1.00)	6.00E+11	76OS186		
78PT191				7.94E-03	77IR191
78PT192	77IR192(1.00) 79AU192(1.00)				
78PT193				5.00E+01	77IR193
78PT194	76OS194(1.00) 77IR194(1.00) 79AU194(1.00)				
78PT195	76OS195(1.00) 77IR195(1.00)				
78PT196	76OS196(1.00) 77IR196(1.00)				
78PT198	77IR198(1.00)				
79AU191	80HG191(1.00) 81TL191(1.00) 82PB191(1.00)	(?)	78PT191	3.65E-04	78PT191
79AU193		(?)	78PT193	2.00E-03	78PT193
79AU195				5.01E-01	78PT195
79AU197	77IR197(1.00) 78PT197(1.00)				
80HG190	81TL190(1.00) 82PB190(1.00)	(?)	78PT190	3.80E-05	78PT190
80HG192	81TL192(1.00) 82PB192(1.00)			5.59E-04	78PT192
80HG193	81TL193(1.00) 82PB193(1.00)	(?)	79AU193	4.56E-04	79AU193
80HG194	81TL194(1.00) 82PB194(1.00) 83BI194(1.00)			2.60E+02	78PT194
80HG195	81TL195(1.00) 82PB195(1.00) 83BI195(1.00)	(?)	79AU195	1.14E-03	79AU195
80HG196	79AU196(1.00) 81TL196(1.00)				

TABLE 6 – *Continued*

ISOTOPE	PARENTS (BRANCHING RATIO)	NON-E.C. DECAY		ELECTRON CAPTURE	
		HALFLIFE	DAUGHTER	HALFLIFE	DAUGHTER
80HG197	81TL197(1.00) 82PB197(1.00) 83BI197(1.00)			7.31E-03	79AU197
80HG198	79AU198(1.00) 81TL198(1.00)				
80HG199	78PT199(1.00) 79AU199(1.00)				
80HG200	78PT200(1.00) 79AU200(1.00) 81TL200(1.00)				
80HG201	78PT201(1.00) 79AU201(1.00)				
80HG202	79AU202(1.00)				
80HG204	79AU204(1.00)				
81TL199	82PB199(1.00)	(?)	80HG199	8.44E-04	80HG199
81TL201	82PB201(1.00) 83BI201(1.00)			8.33E-03	80HG201
81TL202		(?)	80HG202	3.34E-02	80HG202
81TL203	79AU203(1.00) 80HG203(1.00)				
81TL205	80HG205(1.00)				
82PB196	83BI196(1.00)	(?)	80HG196	7.03E-05	80HG196
82PB198	83BI198(1.00)	(?)	80HG198	2.74E-04	80HG198
82PB200	83BI200(1.00)			2.45E-03	80HG200
82PB202	83BI202(1.00)			3.00E+05	81TL202
82PB203	83BI203(1.00)			5.93E-03	81TL203
82PB204	81TL204(1.00)				
82PB205	83BI205(1.00)			1.40E+07	81TL205
82PB206	80HG206(1.00) 81TL206(1.00)				
82PB207	81TL207(1.00) 82PB211(1.00) 83BI211(1.00)				
82PB208	81TL208(1.00) 82PB212(0.36) 83BI212(0.36)				
83BI199		(?)	81TL199	5.13E-05	81TL199
83BI204		(?)	82PB204	1.28E-03	82PB204
83BI206		2.14E+03	82PB206	1.71E-02	82PB206
83BI207		3.17E+05	82PB207	3.80E+01	82PB207
83BI208		(?)	82PB208	3.68E+05	82PB208
83BI209	81TL209(1.00) 82PB209(1.00) 83BI213(0.02)				

capture mode may be ignored. However, the relative amounts of positron and other decay modes (such as alpha, electron, and neutron) cannot be computed without knowledge of the electron capture/positron branching ratio. Most of these nuclides can be ignored because their fragmentation contribution to the stable nuclide is less than 1%. The branching ratios for ^{150}Dy, ^{151}Dy, ^{151}Er, and ^{154}Er affect stable nuclides to a much larger extent. We assume for these nuclides that positron decays make up 5% of the $\Delta Z = -1$, $\Delta A = 0$ decay modes. This is supported by recent conclusions (Reus and Westmeier 1983) that electron capture, positron decay, and alpha decay occur with the relative frequency 89.8/4.6/5.6 in ^{151}Dy.

APPENDIX B

ELECTRON STRIPPING AND ATTACHMENT CROSS SECTIONS

The cross sections for attachment and stripping of electrons from cosmic-ray nuclei are essential for determining decay rates of electron capture nuclides. In most cases cosmic rays are either fully stripped or have only one electron attached; thus, we are concerned here with hydrogen-like ions. Theoretical and experimental studies of these processes have been reported by Wilson (1978) and Crawford (1979).

In the process of electron attachment an electron in the target medium becomes bound to the projectile. This process is termed radiative attachment if the electron may be considered free and if a photon is emitted to conserve energy and momentum. It is termed nonradiative if the recoil of a target atom conserves energy and momentum. Radiative attachment dominates at cosmic-ray energies in pure hydrogen, but the importance of nonradiative attachment is sensitive to the amounts of heavier gases in the ISM.

The radiative attachment cross section can be calculated from photoionization cross sections by the method of detailed balance (Raisbeck and Yiou 1971). Wilson (1978) has used this method and the high energy photoionization cross sections presented by Pratt, Ron, and Tseng (1973) to derive the following formula for radiative attachment cross section:

$$\sigma_{ra} = \tfrac{3}{2}\sigma_T Z_p Z_t \beta\gamma(\gamma-1)^{-1} a^{4+2\xi} \exp\left[-2(a/\beta)\cos^{-1}a\right]\left\{M(\beta)\left[1+R(a)\right]+\pi a N(\beta)\right\}, \tag{B1}$$

where σ_T is the Thompson cross section; Z_p, Z_t are the projectile and target charges, respectively; $a = \alpha Z_p$; α is the fine-structure constant, and

$$\xi = (1-a^2)^{1/2} - 1;$$

$$\beta = v/c;$$

$$M(\beta) = \frac{4}{3} + \frac{\gamma(\gamma-2)}{(\gamma+1)}\left[1 - \frac{1}{2\beta\gamma^2}\ln\left(\frac{1+\beta}{1-\beta}\right)\right];$$

$$N(\beta) = \frac{1}{15\beta^3}\left(-4\gamma+34-63\gamma^{-1}+25\gamma^{-2}+8\gamma^{-3}\right) - \frac{(\gamma-2)}{2\beta^2\gamma(\gamma+1)}\ln\left(\frac{1+\beta}{1-\beta}\right).$$

The factor $R(a)$ may be ignored in cosmic rays with charge $Z_p < 29$ with only a small fraction of a percent error. For greater charges an error of up to 10% can result by ignoring $R(a)$. We have fitted the data on $R(a)$ in Pratt, Ron, and Tseng (1973) in the following formula. We suggest its use for $Z_p > 28$:

$$R(a) = -\exp(-8.4a^2 + 14a - 8.28). \tag{B2}$$

The formulae above give the radiative attachment cross section for capture into the K shell. The cross section falls off as n^{-3} for other shells. To correct for capture into other shells, multiply the above cross section by 1.202.

The nonradiative attachment cross section is predicted (Crawford 1979) by

$$\sigma_{nra} = \frac{\pi}{5} 2^{18} a_0^2 Z_p^5 Z_t^5 \gamma^2 S^8 \left[S^2 + (Z_p + Z_t)^2\right]^{-5}\left[S^2 + (Z_p - Z_t)^2\right]^{-5}, \tag{B3}$$

where a_0 is the Bohr radius, and

$$S = \beta\gamma/\alpha.$$

Again the multiplicative factor 1.202 corrects for capture into higher shells. When there is more than one electron in the target K shell the cross section must be multiplied by 2 and the target charge replaced by an effective target charge:

$$\bar{Z}_t = Z_t - 0.3. \tag{B4}$$

Wilson (1978) has derived the following stripping cross section formula from Mott and Massey's (1965) relativistic ionization cross section:

$$\sigma_s = 4\pi a_0^2\left(\frac{\alpha}{Z_p\beta}\right)^2\left(Z_t^2 + Z_t\right)C_1\left(\ln\frac{4\beta^2\gamma^2}{C_2\alpha^2 Z_p^2} - \beta^2\right), \tag{B5}$$

where $C_1 = 0.285$ and $C_2 = 0.048$.

The heavy components of the ISM also contribute to electron stripping and attachment. The mean free path in the ISM characterized by number fractions (relative to H), b_i, of species i with atomic mass, A_i (amu), and cross section σ_i (mb) is

$$\lambda = \frac{10^{27}}{N_A}\left(\sum_i b_i A_i\right)\Big/\left(\sum_i b_i \sigma^{(i)}\right), \tag{B6}$$

where N_A is Avogadro's number. Since the stripping cross section increases as Z_t^2, it is sensitive to elements with $Z_t < 26$ existing in the ISM with solar system abundances.

REFERENCES

Adams, J. H., Bellingham, J., and Graney, P. E. 1984, *NRL Memorandum Rept.*, in press.
Ahlen, S. P. 1978, *Phys. Rev. A*, **17**, 1236.
______ 1982, *Phys. Rev. A*, **25**, 1856.
______ 1980, *Rev. Mod. Phys.*, **52**, 121.
Ahlen, S. P., and Tarle, G. 1983, *Phys. Rev. Letters*, **50**, 1110.
Badhwar, G. D., Daniel, R. R., and Vijayalakshmi, B. 1962, *Progr. Theor. Phys.*, **28**, 607.
Bethe, H. 1932, *Zs. Phys.*, **76**, 193.
Binns, W. R., Fickle, R. K., Garrard, T. L., Israel, M. H., Klarmann, J., Stone, E. C., and Waddington, C. J. 1981, *Ap. J. (Letters)*, **247**, L115.
______ 1982, *Ap. J. (Letters)*, **261**, L117.
Bloch, F. 1933*a*, *Ann. Phys.*, **16**, 285.
______ 1933*b*, *Zs. Phys.*, **81**, 363.
Cameron, A. G. W. 1982, in *Essays in Nuclear Astrophysics*, ed. C. A. Barnes, D. N. Schramm, and D. D. Clayton (Cambridge: Cambridge University Press), p. 23.
Casse, M. 1973, *Ap. J.*, **180**, 623.
Cowsik, R., Yash Pal, Tandon, S. N., and Verma, R. P. 1967, *Phys. Rev.*, **158**, 1238.
Cowsik, R., and Wilson, L. W. 1973, *Proc. 13th Internat. Cosmic Ray Conf.*, **1**, 500.
Crawford, H. J. 1979, Ph.D. thesis, University of California at Berkeley.
Davis, L. 1960, *Proc. 6th Internat. Cosmic Ray Conf.*, **3**, 220.
Dostrovsky, I., Rabinowitz, P., and Bivins, R. 1958, *Phys. Rev.*, **111**, 1659.
Englemann, J. J., *et al.* 1981, *Proc. 17th Internat. Cosmic Ray Conf.*, **9**, 97.
Fano, U. 1963, *Ann. Rev. Nucl. Sci.*, **13**, 1.
Fichtel, C. E., and Reames, D. V. 1968, *Phys. Rev.*, **75**, 1564.
Fowler, P. H. 1983, private communication.
Fowler, P. H., Walker, R. N., Masheder, M. R., Moses, R. T., and Morely, A. 1981, *Nature*, **291**, 45.
Freier, P. S. 1981, *Proc. 17th Internat. Cosmic Ray Conf.*, **2**, 182.
Garcia-Munoz, M., Simpson, J. A., and Wefel, J. P. 1981, *Proc. 17th Internat. Cosmic Ray Conf.*, **2**, 72.
Ginzburg, V. L., and Syrovatskii, S. I. 1964, *The Origin of Cosmic Rays* (New York: Pergamon).
Gleeson, L. J., and Axford, W. I. 1968, *Ap. J.*, **154**, 1011.
Gloeckler, G., and Jokipii, J. R. 1969, *Phys. Rev. Letters*, **22**, 1448.
Greiner, D. E., Lindstrom, P. J., Heckman, H. H., Cork, B., and Bieser, F. S. 1975, *Phys. Rev. Letters*, **35**, 152.
Guzik, T. G. 1981, *Ap. J.*, **244**, 695.
Hinshaw, G. F., and Wiedenbeck, M. E. 1983, *Proc. 18th Internat. Cosmic Ray Conf.*, OG 5.2-7.
Jackson, J. D., and McCarthy, R. L. 1972, *Phys. Rev. B*, **6**, 4131.
Karol, P. J. 1975, *Phys. Rev. C*, **11**, 1203.
Lederer, C. M., and Shirley, V. S. 1978, *Table of Isotopes* (New York: Wiley).
Letaw, J. R. 1983, *Phys. Rev. C*, **28**, 2178.
Letaw, J. R., Silberberg, R., and Tsao, C. H. 1983*a*, *Ap. J. Suppl.*, **51**, 271.
______ 1983*b*, in *Composition and Origin of Cosmic Rays*, ed. M. M. Shapiro (Dordrecht: Reidel), p. 337.
______ 1984, *Ap. J.*, **279**, 144.
Lezniak, J. A. 1979, *Ap. Space Sci.*, **63**, 279.
Lindhard, J. 1976, *Nucl. Instr. Methods*, **132**, 1.
Lindstrom, P. J., Greiner, D. E., Heckman, H. H., Cork, B., and Bieser, F. S. 1975, Lawrence Berkeley Laboratory preprint LBL-3650.
Margolis, S. H. 1983, *Proc. 18th Internat. Cosmic Ray Conf.*, OG 5.2-8.
Metropolis, N., Bivins, R., Storm, M., Miller, J. M., Friedlander, G., and Turkevich, A. 1958*a*, *Phys. Rev.*, **110**, 185.
______ 1958*b*, *Phys. Rev.*, **110**, 204.
Mewaldt, R. A., Spalding, J. D., Stone, E. C., and Vogt, R. E. 1981, *Ap. J. (Letters)*, **251**, L27.
Mott, N. F., and Massey, H. S. W. 1965, *The Theory of Atomic Collisions* (London: Oxford University Press).
Muller, H.-W. 1980, *Nucl. Data Sheets*, **31**, 181.
O'Dell, F. W., Shapiro, M. M., and Stiller, B. 1962, *J. Phys. Soc. Japan*, **17**, Suppl. A-III, 23.
Olson, D. L., Berman, B. L., Greiner, D. E., Heckman, H. H., Lindstrom, P. J., and Crawford, H. J. 1983, *Phys. Rev. C*, **28**, 1602.
Pratt, R. H., Ron, A., and Tseng, H. K. 1973, *Rev. Mod. Phys.*, **45**, 273.
Protheroe, R. J., Ormes, J. F., and Comstock, G. M. 1981, *Ap. J.*, **247**, 362.
Raisbeck, G. M., Comstock, G., Perron, C., and Yiou, F. 1975, *Proc. 14th Internat. Cosmic Ray Conf.*, **2**, 560.
Raisbeck, G. M., Perron, C., Toussaint, J., and Yiou, F. 1973, *Proc. 13th Internat. Cosmic Ray Conf.*, **1**, 534.
Raisbeck, G., and Yiou, F. 1971, *Phys. Rev. A*, **4**, 1858.
Reus, U., and Westmeier, W. 1983, *Atomic Data Nucl. Data Tables*, **29**, 205.
Salamon, M. H. 1980, Lawrence Berkeley Laboratory Rept., LBL-10446.
Shapiro, M. M., and Silberberg, R. 1970, *Ann. Rev. Nucl. Sci.*, **20**, 323.
______ 1975, *Proc. 14th Internat. Cosmic Ray Conf.*, **2**, 538.
Silberberg, R., and Tsao, C. H. 1973*a*, *Ap. J. Suppl.*, **25**, 315.
______ 1973*b*, *Ap. J. Suppl.*, **25**, 335.
______ 1977*a*, *Ap. J. Suppl.*, **35**, 129.
______ 1977*b*, *Proc. 15th Internat. Cosmic Ray Conf.*, **2**, 84.
______ 1977*c*, *Proc. 15th Internat. Cosmic Ray Conf.*, **2**, 84.
Silberberg, R., Tsao, C. H., Letaw, J. R., and Shapiro, M. M. 1983, *Phys. Rev. Letters*, **51**, 1217.
Silberberg, R., Tsao, C. H., and Shapiro, M. M. 1976, in *Spallation Nuclear Reactions and Their Applications*, ed. B. S. P. Shen and M. Merker (Dordrecht: Reidel), 49.
Simon, M. 1977, *Astr. Ap.*, **61**, 833.
Soutoul, A., Casse, M., and Juliusson, E. 1978, *Ap. J.*, **219**, 753.
Sternheimer, R. M., and Peierls, R. F. 1971, *Phys. Rev. B*, **3**, 3681.
Tsao, C. H., and Silberberg, R. 1979, *Proc. 16th Internat. Cosmic Ray Conf.*, **2**, 202.
Tsao, C. H., Silberberg, R., and Letaw, J. R. 1983, *Proc. 18th Internat. Cosmic Ray Conf.*, **2**, 194.
Webber, W. R. 1981, *Proc. 17th Internat. Cosmic Ray Conf.*, **2**, 80.
Webber, W. R., and Brautigam, D. A. 1982, *Ap. J.*, **260**, 894.
Westfall, G. D., Sextro, R. G., Poskanzer, A. M., Zebelman, A. M., Butler, G. W., and Hyde, E. K. 1978, *Phys. Rev. C*, **17**, 1368.
Wiedenbeck, M. E., and Greiner, D. E. 1980, *Ap. J. (Letters)*, **239**, L139.
______ 1981, *Phys. Rev. Letters*, **46**, 682.
Wilson, L. W. 1978, Ph.D. thesis, University of California at Berkeley.
Yiou, F., and Raisbeck, G. M. 1970, *Ap. Letters*, **7**, 129.
Young, J. S., Freier, P. S., Waddington, C. J., Brewster, N. R., and Fickle, R. K. 1981, *Ap. J.*, **246**, 1014.

JOHN R. LETAW: Severn Communications Corporation, Box 544, Severna Park, MD 21146

REIN SILBERBERG and C. H. TSAO: Code 4154, E. O. Hulburt Center for Space Science, Naval Research Laboratory, Washington, DC 20375

The Astrophysical Journal 279 144-150 1984 April 1
[illegible]

ON THE ABUNDANCES OF ULTRAHEAVY COSMIC RAYS

John R. Letaw
Severn Communications Corporation, Severna Park, Maryland

AND

Rein Silberberg and C. H. Tsao
E. O. Hulburt Center for Space Research, Naval Research Laboratory

Received 1983 May 16; accepted 1983 September 15

ABSTRACT

Recent data from the *HEAO 3* and *Ariel 6* satellites on elemental abundances of ultraheavy cosmic rays ($33 \le Z \le 83$) are analyzed using a new propagation code. General agreement with earlier analyses is observed. Evidence for a breakdown of the correlation between ionization potentials and the solar system cosmic-ray source abundance ratio is presented. We find that the best fit to experimental data (~5 GeV per nucleon) occurs when propagation is calculated at lower energies (~1 GeV per nucleon). This is interpreted as evidence for distributed acceleration of cosmic rays. Additional effects, including ionization loss, altered path-length distributions, and *r*-process enhancement, are considered.

Subject headings: cosmic rays: abundances — nucleosynthesis

I. INTRODUCTION

Recent observations by instruments on the *HEAO 3* and *Ariel 6* satellites have provided cosmic-ray abundances in the charge range $26 \le Z \le 83$ at energies of about 5 GeV per nucleon. The first analyses of these data suggest that the cosmic-ray source abundances are similar to solar system abundances (Cameron 1981) modified by a first ionization potential (FIP) effect. In the charge range $26 \le Z \le 40$, Binns *et al.* (1981) conclude that the source composition is inconsistent with *r*-process dominated nucleosynthesis. This conclusion is supported by the rarity of actinides (Binns *et al.* 1982) in local cosmic-ray fluxes.

The data agree roughly with a standard cosmic-ray propagation model consisting of

1. Source abundances identical to solar system abundances modified by an FIP enhancement proportional to $\exp(-kI)$.
2. An exponential distribution of path lengths with mean of 6 g cm^{-2} of interstellar medium (ISM) at 5 GeV per nucleon (Protheroe, Ormes, and Comstock 1981).
3. A mean hydrogen density in the ISM of about 0.3 atoms cm^{-3} (Wiedenbeck and Greiner 1980; Garcia-Munoz, Simpson, and Wefel 1981).

Preliminary examination of the data using this model (Mewaldt 1981) and later, more comprehensive investigations (Brewster, Freier, and Waddington 1983) show striking disagreement with the standard model. Most prominent of these differences are the secondary to primary ratios ($44 \le Z \le 48$)/($50 \le Z \le 56$) and ($60 \le Z \le 74$)/($76 \le Z \le 84$). Predicted values for these ratios differ by a factor of 2 with measured values. Modification of the standard model by increasing the mean path length or introducing a double exponential path-length distribution (Cowsik and Wilson 1973) does not significantly decrease these discrepancies.

In this paper we explore several other effects which could explain the observed ultraheavy abundances. These include altering the FIP effect, truncating the path-length distribution, enhancement of *r*-process nuclei in the source composition, inclusion of ionization loss in the propagation, and propagation at lower energies where some fragmentation cross sections are larger. We find that most of these effects can be adjusted to make up some of the discrepancy in the primary/secondary ratios. We find significant support for two alterations of the standard model.

First, the correlation between FIP and cosmic-ray source composition seems to break down below 7 eV. We find a considerably improved fit to the sensitive elements Sr and Ba if the FIP enhancement is constant below 7 eV. Such a breakdown has been reported earlier by Tarle *et al.* (1979) for Ca and is consistent with observations of Al and Na (Mewaldt 1981, and references therein).

Second, we find that performing the ultraheavy propagation at 1 GeV per nucleon reproduces the observations, which are at energies of 5 GeV per nucleon, to within reported errors. This improvement results from higher partial cross sections at 1 GeV per nucleon for fragmentation of nuclei in the Pt-Pb peak into the secondary region $60 \le Z \le 74$ as reported by Kaufman and Steinberg (1980) and incorporated into the semiempirical cross sections (Tsao, Silberberg, and Letaw 1983). As discussed elsewhere (Silberberg *et al.* 1983), this result supports the idea that the acceleration of cosmic rays is distributed throughout their passage through the Galaxy.

The propagation model used in this work is described elsewhere in more detail (Letaw, Silberberg, and Tsao 1984). It is based on a new list of the 434 cosmic-ray stable isotopes from Li through Bi. These include (i) absolutely stable isotopes, (ii) isotopes which decay with half-lives greater than 10^5 years, and (iii) isotopes which decay almost exclusively by electron capture. Of these isotopes, 138 decay by electron capture and are treated twice in the propagation, once in the fully ionized state and once with one bound electron, considering the electron attachment probability. In addition to these isotopes which are treated in the propagation, about 1000 rapidly decaying isotopes are classed with their ultimate daughter and incorporated into all fragmentation cross section computations.

The propagation is carried out using matrix methods (Cowsik and Wilson 1973; Wilson 1978). The equations are reduced to the form

$$\frac{dJ_i}{dx} = \sum_j M_{ij} J_j \qquad (1)$$

and solved for the appropriate path-length distribution. The modification matrix, M_{ij}, contains all the composition-changing reactions occurring in propagation. Most important of these are fragmentation effects characterized by total (Letaw, Silberberg, and Tsao 1983*a*) and partial (Silberberg and Tsao 1973; Tsao, Silberberg, and Letaw 1983) cross sections for collisions with protons. The decay of each unstable nucleus is included assuming a 0.3 atom cm^{-3} mean hydrogen density in the ISM (Wiedenbeck and Greiner 1980; Garcia-Munoz, Simpson, and Wefel 1981). Electron capture isotopes are assumed to be fully ionized at the source with attachment and stripping cross sections drawn from Wilson (1978). Also incorporated into the model are ionization loss and solar modulation (Letaw, Silberberg, and Tsao 1983*b*). The composition of the ISM is assumed to be identical to Cameron's (1981) solar system abundances.

The ultraheavy abundances have been measured in experiments on the *Ariel 6* and *HEAO 3* satellites. *Ariel 6* results are given in Fowler *et al.* (1981). *HEAO 3* results in the charge range $26 \le Z \le 40$ are presented in Binns *et al.* (1981), and results for actinides in Binns *et al.* (1982). Data in the Sn-Ba peak have been reported, but without reference to overall normalization, by Binns *et al.* (1983). The nuclei heavier than $Z = 50$ have been reported by Waddington *et al.* (1981). As observed abundances, we take the data of Binns *et al.* (1981), for charges 33 to 42. The compilation of Mewaldt (1981) which includes both *Ariel 6* data and raw *HEAO 3* data is drawn on for other charges. These data report a somewhat lower Sn/Te ratio than given by Binns *et al.* (1983). The reported abundances of $Z = 79$-80 and $Z = 83$-84 were corrected for spillover from Pt and Pb due to charge misidentification. Observed ultraheavy abundances are tabulated in Table 1.

II. FIP EFFECT

The correlation of first ionization potential with the ratio of galactic cosmic-ray source abundances to solar system abundances has been well established for elements with $Z \le 28$ (Casse and Goret 1978). The general nature of this correlation extends to elements with $Z \le 40$ (Binns *et al.* 1981) and even higher (Brewster, Freier, and Waddington 1983). Such a correlation might indicate preferential acceleration of cosmic-ray species with low first ionization potentials at the sites of injection.

Straightforward fits to the correlation of the form

$$\exp(-kI), \qquad (2)$$

where I is the ionization potential in eV and k is a constant, may be made. Good fits to noble gases such as Ne and He come at the expense of a poor fit to C, N, and O. In either case, H is poorly fitted. Treating H and He as special cases, a relatively good fit to all other elements is,

$$\begin{aligned} &\exp(-0.27I) \quad (I \le 13.6\ \text{eV}), \\ &\exp[-0.27(13.6)] \quad (I > 13.6\ \text{eV}) \end{aligned} \qquad (3)$$

The flattening above 13.6 eV affects only Kr in ultraheavy propagations.

TABLE 1

OBSERVED ULTRAHEAVY ABUNDANCES[a]

Charge Pair	Abundance (Fe = 10^6)	Est. Error (%)
33-34	69	10
35-36	34	15
37-38	45	15
39-40	22	25
41-42	13	30
43-44	8	30
45-46	7.5	30
47-48	5.5	30
49-50	5.5	30
51-52	5.5	30
53-54	5.0	30
55-56	6.5	30
57-58	2.7	30
59-60	2.2	30
61-62	1.7	30
63-64	1.3	30
65-66	1.6	30
67-68	1.2	30
69-70	1.4	30
71-72	0.8	30
73-74	0.8	30
75-76	1.0	30
77-78	1.9	50
79-80	0.4	50
81-82	1.2	50
83-84	0.05	50

[a] Abundances for $33 \le Z \le 42$ taken from Binns *et al.* 1981, others taken from Mewaldt 1981 and references therein.

We have performed propagations of the ultraheavy cosmic rays at 5 GeV per nucleon using an exponential path-length distribution with a mean of 6 g cm^{-2} ISM. The source abundances are taken from Cameron (1981) modified by the FIP correction equation (3). Three slopes ($k = 0.24$, 0.27, and 0.30) were tried. The abundances of ultraheavy cosmic rays with extremely high (Br, Kr, I, Xe) or extremely low (Rb, Sr, Y, Zr, Cs, Ba) ionization potentials are insensitive to changes in the slope k (see Table 2). Ratios of primaries to secondaries are also insensitive to these changes.

Our results are distinctly higher than the experimental value for Sr and Ba. This disagreement was not discussed in Binns *et al.* (1983) where normalization of Sn, Te, Xe, and Ba relative to Fe was not addressed. Because Ba and Sr are primaries, this disagreement suggests the possibility that the ionization potential correlation breaks down for lower ionization potentials. A similar effect has been observed in lighter elements with low first ionization potentials. The abundance of Ca as measured by Tarle *et al.* (1979) is inconsistent with the standard FIP enhancement. The largely secondary Na and Al, whose source abundances have

TABLE 2

[illegible] FIP CORRECTIONS

[illegible] Ratio	[illegible]	[illegible]	[illegible]	Expt
[illegible] (Rb Kr)	[illegible]	[illegible]	[illegible]	34 ± [illegible]
[illegible] (Rb Sr)	[illegible]	[illegible]	[illegible]	45 ± [illegible]
[illegible] (Y Zr)	[illegible]	[illegible]	26.9	22 ± [illegible]
[illegible]	6.2[illegible]	6.2[illegible]	6.2[illegible]	5.0 ± 1.5
[illegible] Ba	[illegible]	[illegible]	11.4	6.5 ± 2
[illegible]	[illegible]	[illegible]	0.555	1.0 ± 0.1[illegible]
[illegible]	[illegible]	[illegible]	[illegible]	3.1 ± 0.8[illegible]
[illegible]	1.69	1.7[illegible]	1.82	2.1 ± 0.6[illegible]

[illegible]

[illegible] large errors are consistent with either FIP model. [illegible] suggest a flattening (Mewaldt 1981). Ionization models ([illegible] and Goret 1978) of the source composition predict flattening at both high-ionization and low-ionization potentials. To explore the effect of such a breakdown, the FIP enhancement was taken constant below several cutoff ionization potentials. Results are shown in Table 3. The fit to Rb and Sr and their immediate secondaries is improved by 2 and 3 standard deviations, respectively, by a cutoff of 7 eV. In addition, two of the ratios are slightly improved because of a reduction in Ba abundance. Our results suggest that the FIP correction becomes flat below about 7 eV. We modify the standard FIP correction accordingly to

$$\exp[-0.27(7.0)] \quad (I < 7\ \mathrm{eV}),$$
$$\exp(-0.27I) \quad (7 < I < 13.6\ \mathrm{eV}),$$
$$\exp[-0.27(13.6)] \quad (I > 13.6\ \mathrm{eV}) \qquad (4)$$

In Figure 1 the abundances of ultraheavies with $Z > 33$ are plotted. They are compared with our propagations using Cameron's (1981) abundances at the source and these abundances modified by our FIP correction (eq [4]). We note that the distinct secondary valleys remain. The fit for Z [illegible] is excellent.

TABLE 3

[illegible] FIP CORRECTION

[illegible] Ratio	No Cutoff	[illegible]	[illegible]	[illegible]	Expt
[illegible] (Rb Kr)	16.6	[illegible]	[illegible]	[illegible]	34 ± [illegible]
[illegible] (Rb Sr)	[illegible]	[illegible]	[illegible]	[illegible]	45 ± [illegible]
[illegible]	6.2	6.0	[illegible]	4.9	[illegible] ± 1.5
[illegible] Ba	10.5	9.6	[illegible]	[illegible]	6.5 ± 2
[illegible]	[illegible]	[illegible]	[illegible]	[illegible]	1.0 ± 0.1[illegible]
[illegible]	[illegible]	12.4	11.6	10.2	3.1 ± 0.8[illegible]
[illegible]	1.[illegible]	1.[illegible]	1.[illegible]	1.49	2.1 ± 0.6[illegible]

[illegible]

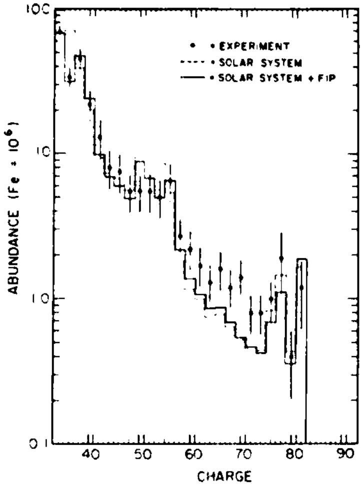

FIG. 1.—Comparison of propagations through 6 g cm⁻² of ISM at 5 GeV per nucleon. Dashed line uses Cameron (1981) as source composition. Solid line has source modified by the FIP correction in this paper (eq [4]). Experimental data are taken from Table 1.

Studies of the elements Sn, Te, Xe, and Ba (Binns *et al.* 1983; Brewster, Freier, and Waddington 1983) using the standard model show agreement with the Sn/Te and Ba/Te ratios and poor agreement with the Xe/Te ratio (see Fig. 2). Using the FIP correction of equation (4), we again find good agreement with the Sn/Te ratio and somewhat better agreement with the Xe/Te ratio but poorer agreement with the Ba/Te ratio. Equation (4) leads to an improvement in the overall normalization of these elements relative to Fe. From Mewaldt (1981), we find the total abundance in the range $49 \leq Z \leq 56$ to be 23 ± 7 relative to Fe $= 10^6$. Our computations using the new FIP correction yield 27 while in the standard model we get 34.

Our results using the standard model differ significantly with Brewster, Freier, and Waddington (1983) in this region. They get roughly 26 for the sum $49 \leq Z \leq 56$ while we get 34. Among the numerous differences in the propagation calculations are their use of rigidity-dependent path lengths, propagation by element instead of isotope, and neglect of ionization loss. Most of the disagreement with this propagation results from their use of different charge-changing total reaction cross sections. The Berkeley charge-changing cross sections (Westfall *et al.* 1979) are roughly 25% larger than the total reaction cross sections (Letaw, Silberberg, and Tsao 1983*a*) minus the partial cross sections for $\Delta Z = 0$ (Silberberg and Tsao 1973). Substantially less destruction of the elements in the Sn-Ba peak therefore occurs in our calculations. This also accounts for the difference in the ratio (60-74)/(76-84) in the two calculations.

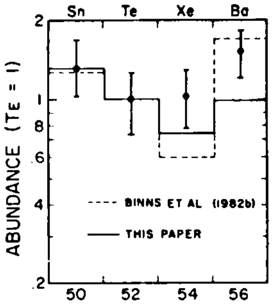

FIG. 2.—Abundances in the Sn-Ba peak relative to Te as predicted using the standard FIP modification (*dashed line*) to the source and the FIP modification in this paper (*solid line*). Our standard model predicts relative abundances similar to the solid line except for Ba which is midway between the values shown in the figure.

The Berkeley charge-changing formula is based on an extrapolation from *p*-Fe collisions, while the total inelastic cross sections (Letaw, Silberberg, and Tsao 1983*a*) are based on reactions of many nuclides. The charge-changing formula disagrees with preliminary measurements on Au (Brewster *et al.* 1983) at 1 GeV per nucleon. The charge-changing formula for Au is ~1700 mb, our total cross section minus $\Delta Z = 0$, and +1 partial cross section yields ~1500 mb, while the experiment gives ~1450 mb.

III. IONIZATION LOSS

So far in this paper, ionization loss has been included in the propagation effects. Ionization loss is potentially important in ultraheavy propagation. As discussed elsewhere (Letaw, Silberberg, and Tsao 1984), a uranium ion loses 140 MeV per nucleon per g cm⁻² of ISM, while Fe loses less than 50 MeV per nucleon. Relative compositional differences of 15% can arise in such nearby elements as Zn and Fe over 6 g cm⁻² ISM.

We have explored the importance of ionization loss by removing the effect in a standard propagation at 5 GeV per nucleon. We found that including ionization loss *reduces* the secondary/primary ratios (44-48)/(50-56) and (60-74)/(76-84) by about 3%. The reduction is apparently due to the greater mean path length of secondaries. We find a negligible reduction in (50-56)/(74-80). At 1 GeV per nucleon, the secondary to primary ratios are reduced by as much as 20%.

IV. TRUNCATION OF THE PATH-LENGTH DISTRIBUTION AND SOURCE ENHANCEMENT

Within the standard model, one assumes the cosmic-ray path lengths are distributed exponentially. Alterations of this distribution which eliminate some or all of the short path lengths are proposed to increase secondary to primary ratios. Brewster, Freier, and Waddington (1983) have explored the use of double exponential path-length distribution on the secondary to primary ratios (44-48)/(50-56) and (60-74)/(76-83). These ratios are calculated to be only slightly closer to experiment than in the standard model.

In this section we discuss results of a propagation using a truncated exponential path-length distribution of the form:

$$P(x) = \begin{cases} 0 & (x < \delta) \\ \exp\left[-\dfrac{(x-\delta)}{\lambda}\right] & (x > \delta) \end{cases} \qquad (5)$$

The mean distribution is $\delta + \lambda$. It is the usual exponential distribution preceded by a slab of thickness δ. Such a distribution may occur under the same astrophysical conditions as the nested leaky box but differs from this model in that no short path lengths occur. Here we take the slab thickness to be 1 g cm⁻². This is inconsistent with the observed abundances of light elements and therefore requires additional assumptions about the cosmic-ray sources. One plausible assumption is that highly evolved stellar systems, rich in ultraheavies, might be associated with dense clouds of interstellar gases. Our results are shown in Figure 3 in comparison with the standard model (now using eq [4] to modify solar system abundances).

A significant improvement is seen in the secondary to primary ratios (see Table 4). The improvement in the sub-Pt/Pt ratio results primarily from a reduction in primaries in the Pt-Pb peak, and hence the valley in the secondary region remains. This is quantified in the ratio (50-56)/(74-80) which remains high. The fit to the Sn-Ba peak is worse in this model. Within this model, a better overall fit is obtained if the abundance of elements in the Pb-Pt peak is doubled

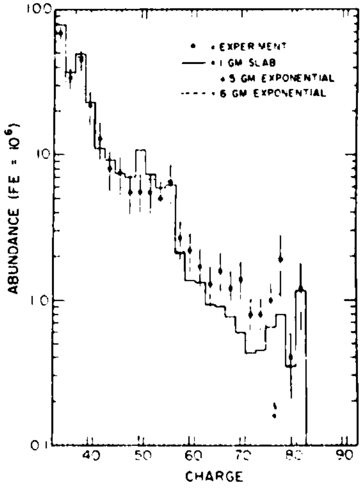

FIG. 3.—Comparison of exponential model with slab exponential model of the same mean path length. The slab exponential model (*solid line*) shows much greater secondary/primary ratios.

TABLE 4

[illegible] RATIOS [illegible] MODELS

				Solar [illegible]	
	R			Pt-Pb	50% r-Process Enhancement
[illegible]	[illegible]		[illegible]	0.78	0.55
[illegible]	[illegible]		[illegible]	[illegible]	1.13
[illegible]	[illegible]		[illegible]	1.7	2.44

[illegible] FIP [illegible]

Such an assumption might be justified by uncertainty in the use of solar system abundances to represent cosmic-ray composition or by galactic evolution since the formation of the solar system (Truran and Cameron 1971). The results of [illegible] a propagation are shown in Figure 4. The ratio [illegible] shows some improvement. The discrepancy in Sn abundance in this model is now well over 3 standard deviations [illegible] significant secondary contribution. [illegible] the Sn abundance reported by Binns [illegible] higher than the value in Table 1.)

The improvement in fit with doubling of the Pt-Pb peak [illegible] be due to an r-process enhancement in solar [illegible]. Such an enhancement was not ruled out

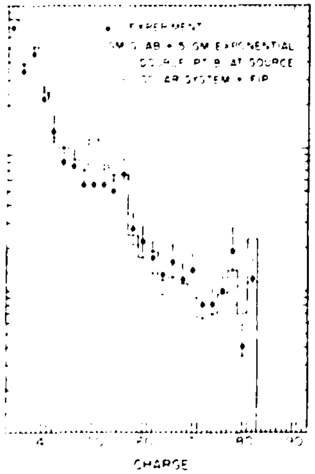

FIG. 4. [illegible] models with mean path [illegible] FIP modification [illegible] Pt-Pb [illegible]

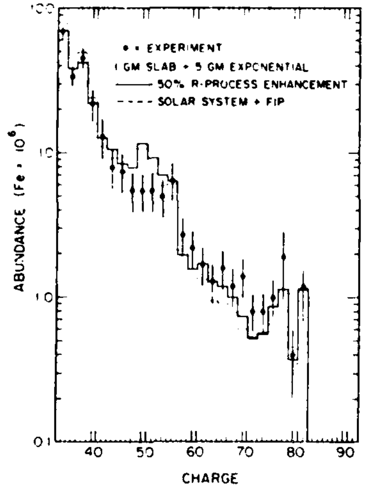

FIG. 5. Comparison of two slab-exponential models with mean path length of 6 g cm⁻². Dashed curve uses our FIP modification to source. Solid curve has a 50% r-process enhanced source.

by Brewster, Freier, and Waddington (1983). It is possible to define such an enhancement by

$$N_{\text{enhanced}} = \left(\frac{f}{f_{0}}\right) N_{\odot} , \tag{6}$$

where $N_{\odot}$ is the solar system abundance and

$$f = \frac{N_r(1 + x) + N_s(1 - x)}{N_r + N_s} \tag{7}$$

Here N_r and N_s are, respectively, the r-process and s-process contributions to Cameron's (1981) abundances and $N_r + N_s = N_{\odot}$. We use the decomposition proposed by Israel *et al.* (1981). The parameter x varies from 1 for pure r-process to −1 for pure s-process. The overall normalization, f_0, is the value of f for Ba which is a cosmic-ray primary consisting of about equal r-process and s-process contributions.

Figure 5 shows a comparison of slab exponential propagations, one with a 50% r-process enhancement at the source and the other with a standard source. Once again good agreement with the secondary to primary ratios is obtained at the expense of a poor fit in the Sn-Ba peak.

V. PROPAGATION AT LOW ENERGIES

Recent measurements of Kaufman and Steinberg (1980) on the spallation of ^{197}Au show a substantial increase in the partial cross sections in the mass range $10 < \Delta A < 40$ at

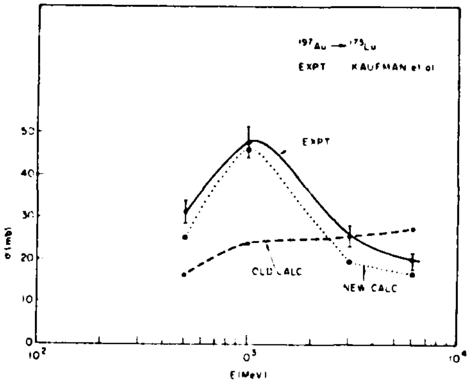

FIG. 6. The energy dependence of spallation cross sections of Au. The dashed and dotted lines show the results of our previous and newly revised semiempirical calculations.

1 GeV (Fig. 6). These new data have been incorporated into the semiempirical cross section formulae (Tsao, Silberberg, and Letaw 1983). The substantial increase in cross sections suggests a possible explanation of the abundance of secondaries in the charge range $60 \leq Z \leq 74$. If the acceleration of cosmic rays is distributed throughout propagation in the Galaxy, or occurs in several pulses, the average energy during propagation would be somewhat lower than the arriving energy. In this case, the cosmic-ray composition would be determined by propagation at an energy lower than the arriving energy.

To explore this hypothesis, a propagation of ultraheavy cosmic rays has been performed at 1 GeV per nucleon using an exponential path-length distribution with a mean value of 9 g cm⁻² (Protheroe, Ormes, and Comstock 1981). This propagation results in an excellent fit to the data which differs by significantly more than 1 standard deviation only for Sn and Yb (see Fig. 7). The secondary "valleys" are still apparent as slight systematic underabundances in the regions $44 < Z \leq 48$ and $60 \leq Z < 74$. Using the path length of 6 g cm⁻² with the new cross sections yields nearly identical results. We note that the improvement in fit could not have resulted from statistical errors in the cross sections. These errors are about 50%, while the systematic increase of 250%, according to the data of Kaufman and Steinberg (1980), is just able to make up the difference.

The 1 GeV per nucleon propagation provides significant evidence for the distributed acceleration of cosmic rays. Additional compositional evidence for such a conclusion is discussed in Silberberg *et al.* (1983). In summary, this hypothesis (1) raises the anomalously low estimate of N at the cosmic-ray source between 50 and 200 MeV per nucleon; (2) reduces high source abundances of F, Na, and Al around 150 MeV per nucleon; (3) reduces arriving abundances of electron capture isotopes (^{37}Ar, ^{49}V, ^{51}Cr) at 600 MeV per nucleon, and (4) reduces source abundances of Mn and Cr at low energies (~250 MeV per nucleon). Conditions

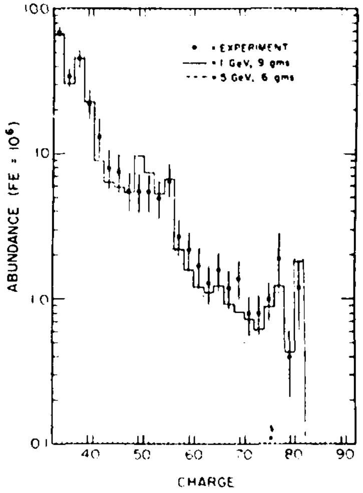

FIG. 7. Comparison of propagations using exponential path length distribution and solar system abundances modified by our FIP correction. Results of a propagation at 1 GeV per nucleon with a mean path length of 9 g cm⁻² are compared with a propagation of 5 GeV per nucleon with a mean path length of 6 g cm⁻².

(1) and (2) result from increased (*p*, *pn*) cross sections at low energies, (3) from increased electron attachment, and (4) from increased Fe spallation into products with a small ΔA at low energies. One consequence of this hypothesis is to reduce the cosmic-ray age by a factor of 2 because the production rate of ^{10}Be is lower at low energies; thus, even for very small measured ^{10}Be abundances, a larger fraction survives.

Independent of conclusions concerning distributed acceleration, we find that ultraheavy propagation in the range 750–1500 MeV per nucleon differs greatly from propagation at higher energies. Data at these lower energies should therefore be analyzed separately from high-energy data. We feel this is of particular importance in analysis of *HEAO 3* ultraheavy data where there is a mixture of particles in these energy ranges.

VI. CONCLUSIONS

Several different effects in the propagation of ultraheavy cosmic rays have been examined. We find the data support a flattening of the FIP correlation below about 7 eV. This flattening is in accord with models presented by Cassé and Goret (1978). Introduction of this FIP correction results in good agreement with the data except for the secondary "valleys" and an overabundance of Sn. In contrast, our propagations using the standard FIP correction fit poorly throughout the Sn-Ba peak.

We have shown that a truncation of the path-length distribution, eliminating all path lengths less than 1 g cm^{-2}, results in significant filling of the valleys. This conclusion holds still more strongly if additional Pt and Pb are introduced at the source or if the ultraheavies with $Z > 60$ are considered to be *r*-process enhanced. A realization of such a distribution would be neutron enrichment in the immediate region of a supernova, followed by propagation through surrounding clouds. However, *r*-process enhancement degrades the fit for $Z < 60$.

Evidence is presented for the distributed acceleration of cosmic rays during propagation. Using improved semiempirical cross sections, a propagation of 1 GeV per nucleon yields a very good fit to the ultraheavy data. This suggests that much of the propagation occurred at energies between 750 MeV per nucleon and 1.5 GeV per nucleon, and that at least two acceleration stages bracket the propagation. The hypothesis of distributed acceleration is reinforced by much additional compositional evidence, both isotopic and elemental, at various energies.

Finally, we show that ionization loss affects abundance ratios at the 3% level at 5 GeV per nucleon and the 20% level at 1 GeV per nucleon.

This work is supported partly by a NASA Guest Investigator grant for *HEAO 3*. The work of J. R. L. was partially supported by the Naval Research Laboratory.

REFERENCES

Binns, W. R., Fickle, R. K., Garrard, T. L., Israel, M. H., Klarmann, J., Krombel, K. E., Stone, E. C., and Waddington, C. J. 1983, *Ap. J. (Letters)*, 267, L93.

Binns, W. R., Fickle, R. K., Garrard, T. L., Israel, M. H., Klarmann, J., Stone, E. C., and Waddington, C. J. 1981, *Ap. J. (Letters)*, 247, L115.

———. 1982, *Ap. J. (Letters)*, 261, L117.

Brewster, N. R., *et al.* 1983, *Bull. Am. Phys. Soc.*, 28, 755.

Brewster, N. R., Freier, P. S., and Waddington, C. J. 1983, *Ap. J.*, 264, 324.

Cameron, A. G. W. 1981, in *Essays in Nuclear Astrophysics*, ed. C. A. Barnes, D. D. Clayton, and D. N. Schramm (Cambridge: Cambridge University Press).

Cassé, M., and Goret, P. 1978, *Ap. J.*, 221, 703.

Cowsik, R., and Wilson, L. 1973, *Proc. 13th Int. Cosmic Ray Conf.* (Denver), 1, 500.

Fowler, P. H., Walker, R. N. F., Masheder, M. R. W., Moses, R. T., and Worley, A. 1981, *Nature*, 291, 45.

Garcia-Munoz, M., Simpson, J. A., and Wefel, J. P. 1981, *Proc. 17th Int. Cosmic Ray Conf.* (Paris), 2, 72.

Israel, M. H., Klarmann, J., Binns, W. R., Fickle, R. K., Waddington, C. J., Garrard, T. L., and Stone, E. C. 1981, *Proc. 17th Int. Cosmic Ray Conf.* (Paris), 2, 56.

Kaufman, S. B., and Steinberg, E. P. 1980, *Phys. Rev. C*, 22, 167.

Letaw, J. R., Silberberg, R., and Tsao, C. H. 1983*a*, *Ap. J. Suppl.*, 51, 271.

———. 1983*b*, in *Composition and Origin of Cosmic Rays*, ed. M. M. Shapiro (Dordrecht: Reidel), p. 337.

———. 1984, *Ap. J. Suppl.*, submitted.

Mewaldt, R. A. 1981, *Proc. 17th Int. Cosmic Ray Conf.* (Paris), 13, 49.

Protheroe, R. J., Ormes, J. F., and Comstock, G. M. 1981, *Ap. J.*, 247, 362.

Silberberg, R., and Tsao, C. H. 1973, *Ap. J. Suppl.*, 25, 335.

Silberberg, R., Tsao, C. H., Letaw, J. R., and Shapiro, M. M. 1983, *Phys. Rev. Letters*, 51, 1217.

Tarle, G., Ahlen, S. P., Cartwright, B. G., and Solarz, M. 1979, *Ap. J. (Letters)*, 232, L161.

Truran, J. W., and Cameron, A. G. W. 1971, *Ap. Space Sci.*, 14, 179.

Tsao, C. H., Silberberg, R., and Letaw, J. R. 1983, *Proc. 18th Int. Cosmic Ray Conf.* (Bangalore), 2, 194.

Waddington, C. J., Fickle, R. K., Garrard, T. L., Stone, E. C., Binns, W. R., Israel, M. H., and Klarmann, J. 1981, *Proc. 17th Int. Cosmic Ray Conf.* (Paris), 9, 109.

Westfall, G. D., Wilson, L. W., Lindstrom, P. J., Crawford, H. J., Greiner, D. E., and Heckman, H. H. 1979, *Phys. Rev. C*, 19, 1309.

Wiedenbeck, M. E., and Greiner, D. E. 1980, *Ap. J. (Letters)*, 239, L139.

Wilson, L. W. 1978, Ph.D. thesis, University of California at Berkeley.

J. R. Letaw: Severn Communications Corporation, Box 544, Severna Park, MD 21146

R. Silberberg and C. H. Tsao: E. O. Hulburt Center for Space Research, Naval Research Laboratory, Washington,

AD-A165 538 SURVEY OF ATMOSPHERIC RADIATION COMPONENTS FOR THE
GAMMA AND COSMIC RAY A.. (U) SEVERN COMMUNICATIONS CORP
SEVERNA PARK MD 31 MAY 85 N00014-84-C-2089

2/2

UNCLASSIFIED F/G 3/1 NL

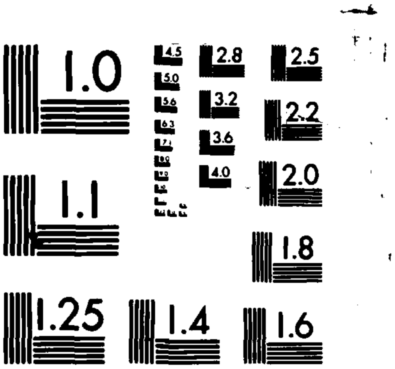
1.0
4.5
5.0
5.6
6.3
2.8
3.2
3.6
4.0
2.5
2.2
2.0
1.1
1.8
1.25
1.4
1.6

MICROCOPY RESOLUTION TEST CHART
DARDS-1963-A

[illegible] Vol.4, No.10, pp.143-151, 1984
Printed in Great Britain. All rights reserved.

0273-1177/84 $0.00 + .50
Copyright © COSPAR

LET-DISTRIBUTIONS AND DOSES OF HZE RADIATION COMPONENTS AT NEAR-EARTH ORBITS

R. Silberberg,[*] C. H. Tsao,[*] J. H. Adams, Jr [*] and
J. R. Letaw [**]

[*] *Naval Research Laboratory, E. O. Hulburt Center for Space Research, Washington, DC 20375, U.S.A.*
[**] *Severn Communications Corporation, Severna Park, MD 21146, U.S.A.*

ABSTRACT

Among cosmic rays, the heavy nuclei ranging from carbon to iron provide the principal contribution to the dose equivalent. The LET-distributions and absorbed dose and dose equivalent have been calculated and are presented as a function of shielding and tissue self-shielding. At solar minimum, outside the magnetosphere, the unshielded dose equivalent of nuclei with atomic number $Z \geq 6$ is about 47 rem/year. The contribution of the target nuclei adds 7 rem/year. With 4 g/cm^2 aluminum shielding, and at a depth of 5 cm in a biological phantom of 30 cm diameter, the respective values are 11 and 10 rem/year. Corresponding dose rates for orbits with various inclinations are presented, as well as the LET distributions of various components of cosmic rays.

INTRODUCTION

Since heavy cosmic ray nuclei contribute a large portion of the dose equivalent during space flights, and since their nuclear interaction mean free path in materials is short, it is essential to carry out radiation propagation calculations with accurate nuclear spallation cross sections.

Our approach is in part based on Curtis /1/, who calculated the LET (Linear Energy Transfer) distribution and dose equivalent due to cosmic rays and solar flare particles for the case of little shielding. However, we include the partial inelastic nuclear cross sections of Silberberg and Tsao /2/ in a radiation transport calculation that includes separately all the isotopes of cosmic rays. This radiation propagation or transport calculation was recently expressed in matrix form by Letaw et al. /3/. It permits the LET distribution and dose to be calculated even in the case of heavy shielding of several nuclear interaction mean free paths. Silberberg et al. /4/ recently applied these procedures to calculating the LET distributions and doses at various depths of a biological water phantom exposed to cosmic rays outside the magnetosphere. The procedure for calculating the LET distribution is similar to that of Heinrich's /5/ calculation in the atmosphere. Here we extend these calculations to various spacecraft orbits. Some of the calculations will be compared with the measured doses onboard the Space Transportation System, STS, obtained by Benton and Henke /6/ and co-workers; however, we have to complete first a radiation transport calculation for trapped protons, and obtain the orbital and shielding parameters of individual STS flights.

PROCEDURES

The procedures for calculating the LET-distribution, the absorbed dose and the dose equivalent (outside the magnetosphere, under shielded conditions) has been published./4/

Hence only a brief summary will be presented here; however, the just-developed procedure of integrating over the spectrum and the orbit (where the geomagnetic cutoff varies) will also be discussed.

We have developed a radiation transport equation in matrix form /3/, using a complete set of stable as well as collision-generated unstable isotopes of cosmic rays, from ^1H to ^{64}Ni, with nuclear interactions, ionization losses and solar modulation included. The calculation starts out with the measured composition and energy spectra of cosmic rays above the atmosphere; these have been reviewed and summarized by Adams et al. /7,8/. The energy spectra of hydrogen, helium and iron nuclei at times of solar minimum and solar maximum are illustrated in fig. 1. The relative abundances of cosmic rays with $3 \leq Z \leq 26$ at energies near 3 GeV/nucleon are shown in fig. 2.

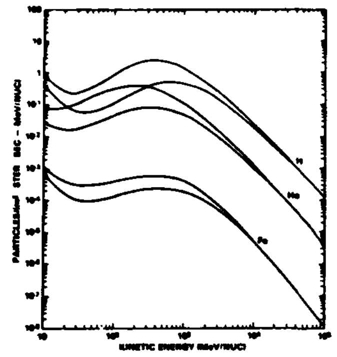

Fig. 1. The differential energy spectra of cosmic-ray hydrogen, helium and iron, near solar minimum and maximum.

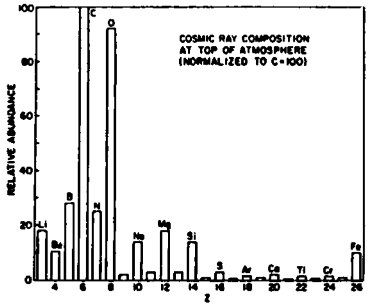

Fig. 2. The relative abundances of cosmic ray nuclei above a rigidity of 4.5 GV. Carbon has been normalized to 100.

The radiation transport calculations require the use of total and partial inelastic nuclear cross sections. About 5500 partial inelastic cross sections are used in the calculations. The partial inelastic cross sections of nuclear reactions with hydrogen are calculated from the semiempirical equations of Silberberg and Tsao /2/. Fig. 3 illustrates the basic form of the spallation equation, for the spallation of Fe into isotopes of Ar and V, with a comparison of experimental and calculated values of the cross sections at energies $E \geq 3$ GeV. These relations yield values of cross sections having one standard deviation uncertainty of 30 per cent, and about 15 per cent when averaged over various product isotopes and the primary cosmic ray nuclides. Fig. 4 compares the ratio of calculated and experimental cross sections in three energy intervals, for the breakup of nuclei with $6 \leq Z \leq 16$. The partial cross sections of nucleus-nucleus reactions are calculated using the procedures of Silberberg and Tsao /9/. The total inelastic cross sections of nuclei with protons, including the energy dependence, are calculated from Letaw et al. /10/, and for nucleus-nucleus reactions, using the equation of Silberberg et al. /4/.

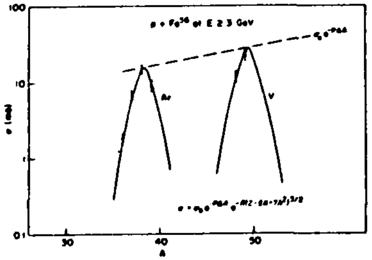

Fig. 3 Illustration of the terms of the spallation equation. The example shows the experimental and calculated cross sections of iron into isotopes of Ar and V, at energies $\geq$ 3 GeV.

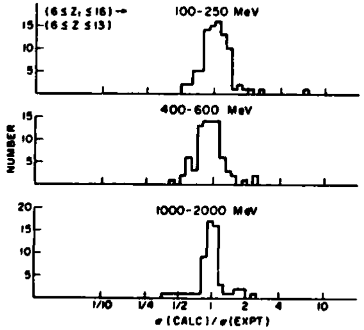

Fig. 4 Comparison of calculated and experimental production cross sections of nuclei with $6 \leq Z \leq 13$ from targets with $6 \leq Z_t \leq 16$, in three energy intervals.

The dose due to the interaction products of cosmic ray protons and secondary neutrons, (from the stationary target nuclei) is adopted from Armstrong et al. /11/.

The output of the propagation program yields differential energy spectra dJ_i/dE of all nuclear species above energies of 1 MeV/nucleon, at various depths of a given material. These spectra are then summed to yield those for each element.

The equations and the procedures for calculating the differential and integral LET spectra of the various nuclides are given in ref. /4/. Also the equations and procedures for calculating the absorbed dose rates and the dose equivalents of the various nuclides are given in ref. /4/.

We shall now consider the effects of geomagnetic cutoff and azimuthal angle dependence on the cosmic ray fluxes and doses, including their integration over the orbit. Vertical geomagnetic cutoffs have been computed at altitudes of 20 km by Shea and Smart /12/, using a precise model of the geomagnetic field. A world map of the vertical cutoff rigidities, expressed in units of GV, is shown in fig. 5.

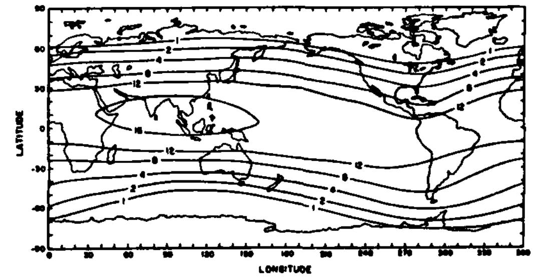

Fig. 5 World map of vertical cutoff rigidities

The cutoff rigidity in directions other than the vertical depends on the angle of arrival relative to magnetic west. At a given location, the lowest energy particles arrive only within a narrow cone surrounding magnetic west, while the cutoff is greatest within the cone due magnetic east. These cones are called Stormer cones.

Fig. 6 shows the ratio of cutoff to vertical cutoff as a function of vertical cutoff and Stormer cone angles.

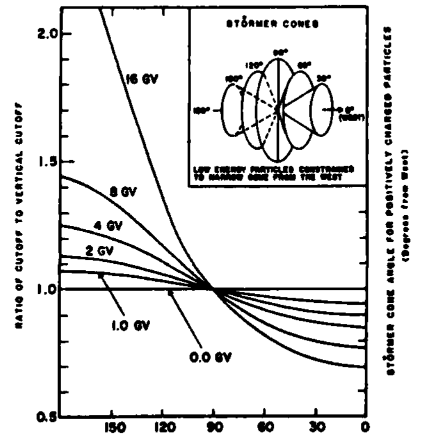

Fig. 6. Geomagnetic cutoffs as a function of the Stormer cone angle.

The Stormer cone angle γ is related to the azimuthal angle ϕ and zenith angle θ by:

$$\cos\gamma = \cos\phi \sin\theta \tag{1}$$

The azimuthal angle ϕ here is measured from the magnetic east. The relation between the Stormer cone angle γ, and cutoff rigidity is approximately:

$$R = 4R_v[1 + (1 - \cos\gamma \cos^3\lambda)^{1/2}]^{-2} \tag{2}$$

where λ is the magnetic latitude and R_v is the vertical cutoff rigidity.

In carrying out the integration over the orbit, the fluxes were summed over about 5000 locations traversed by the spacecraft over a two day period. In this present calculation, only the vertical cutoffs were used; the integration over zenith and azimuthal angles has been reserved for the future.

RESULTS

In this section we present our calculated results of LET distributions, the absorbed dose and the dose equivalent due to cosmic rays. These quantities have been calculated for four cases: (1) outside the magnetosphere, (2) in an orbit of 90° inclination at an altitude of 300 km, (3) in an orbit of 50° inclination at an altitude of 300 km, and (4) in an orbit of 30° inclination, at an altitude of 300 km. Each of these four cases is evaluated for four subcases: (a) at the centers of spheres of water, up to a depth of 30 cm, (b) same as above but with an aluminum shield of 4 g/cm^2 outside the water sphere, (c) at various depths in a water phantom of 30 cm diameter, and (d) with an aluminum shield of 4 g/cm^2 outside the water phantom.

Figs. 7(a) and (b) display the LET distributions and the integral absorbed dose rates at the surface and at the center of the 30 cm diameter water phantom, at solar minimum, outside the earth's magnetosphere. The relative contributions of the elements H, He, Li to B, C to O, F to S and Cl to Fe are shown.

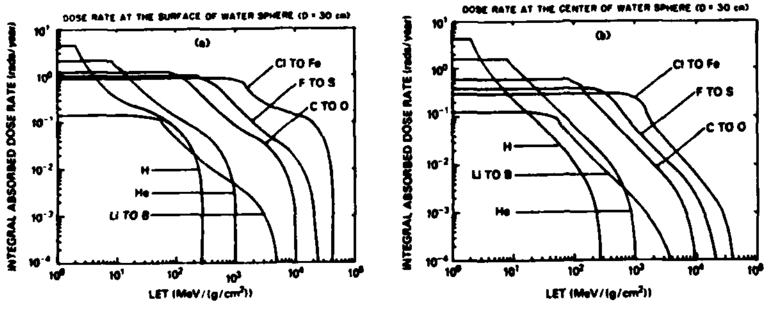

Fig. 7. The relative contributions of sequential cosmic ray elements to the integral LET distributions and annual absorbed doses at (a) the surface and (b) at the center of a sphere of water of 30 cm diameter, at solar minimum, outside the earth's magnetosphere.

Table 1 shows the annual absorbed doses and dose equivalents at various depths 0.1 to 15 g/cm^2, within a spherical water phantom of 30 cm diameter. The values shown are again calculated for solar minimum, outside the earth's magnetosphere. The small degree of attenuation can be noted: the absorbed dose rate changes from 10 rad/year to 7 rad/year between depths of 0.1 and 15 g/cm^2. Particles from breakup of the stationary nuclei contribute another 3 or 4 rad/year. Lines 2 and 3 show the dose equivalent rates with and without a shield of 4 g/cm^2 aluminum, respectively. The relative contributions of different elements in cosmic rays to the dose equivalent rate are shown in Fig. 8, at various depths in the water phantom. The more rapid attenuation of the heavy elements can be seen; yet even at the center of the water phantom, the dose equivalent due to the elements $Z \geq 6$ dominates.

Table 1. The Annual Cosmic Ray Dose at Various Depths within a Sphere of Water of 30 cm Diameter.

Line	(g/cm^2) 0.2	0.5	1	5	10	15
1[A]	9.5	9.1	8.8	7.7	7.3	7.2
2[B]	36	32	29	20	17	16
3[B]	26	25	23	17	15	14

[A] line 1 gives the absorbed dose rate (rads/yr); line 2, the dose equivalent rates (rem/yr); as does line 3 behind an additional shield of 4 g/cm^2 Al.

[B] secondary neutrons and electrons add ~ 5 rem/year to these values. With proton interactions, the total secondary contribution is ~ 9 rem/year.

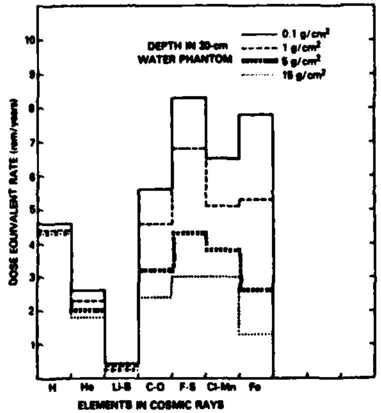

Fig. 8. The annual dose equivalent due to cosmic-ray elements at various depths of a 30-cm water phantom, at solar minimum, outside the magnetosphere.

The attenuation of the LET distribution in water (calculated at the centers of spheres of water of various diameters) is shown in Fig. 9a. The larger attenuation of heavy nuclei that have large values of LET is striking. A comparison of Fig. 9a, 9b, 9c and 9d shows the respective LET distributions and integral absorbed dose rates (a) outside the magnetosphere, (b) at an orbital inclination of 90°, (c) at 50°, and (d) at 30° solar minimum, and at an altitude of 300 km. The contribution of the trapped radiation is not shown--this will be discussed subsequently. The contribution from the breakup of stationary target nuclei due to cosmic ray interactions adds to the absorbed dose ~ 20% at depths ~0 g/cm^2, and ~ 60% at 30 g/cm^2. For cases (b), (c) and (d) a solid angle of 2.7 π steradians is used.

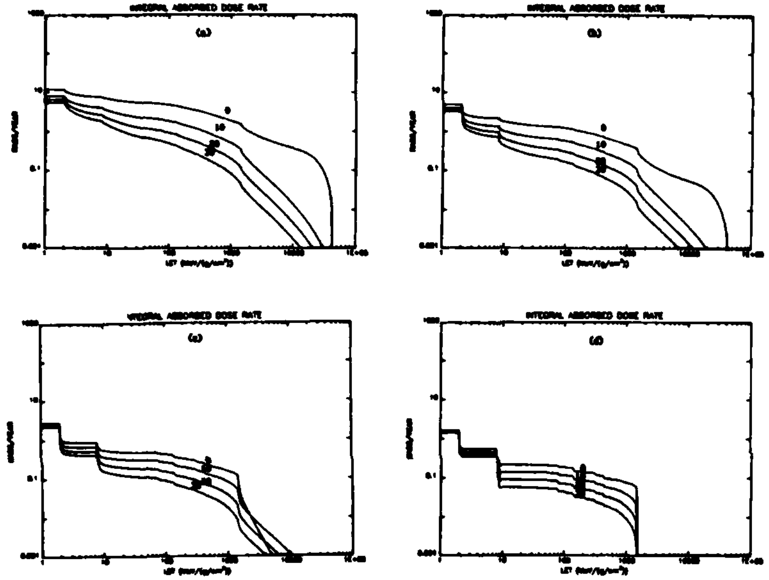

Fig. 9. The integral LET distributions of the annual absorbed dose at centers of spheres of water ~ 0, 10, 20 and 30 cm radii, at solar minimum:
(a) outside the magnetosphere, (b) at a 90° inclination orbit,
(c) at a 50° inclination orbit, (d) at a 30° inclination orbit.

Figures 10a, b, c, and d show the corresponding LET distributions and integral absorbed dose rates for a shield of 4 g/cm^2 Al. The most striking difference when compared to Fig. 9 is the extensive attenuation of low-energy high-LET iron tracks in the shield.

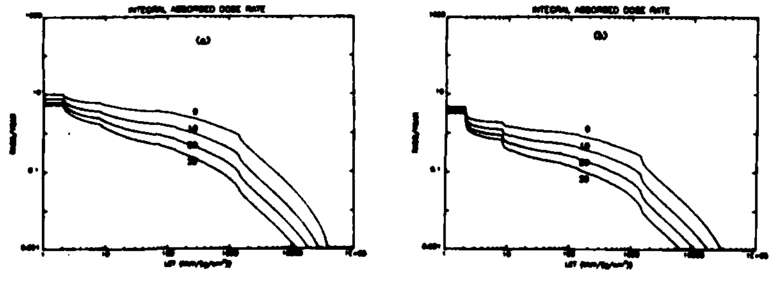

Fig. 10. Same as Fig. 9, but with 4 g/cm^2 aluminum shielding.

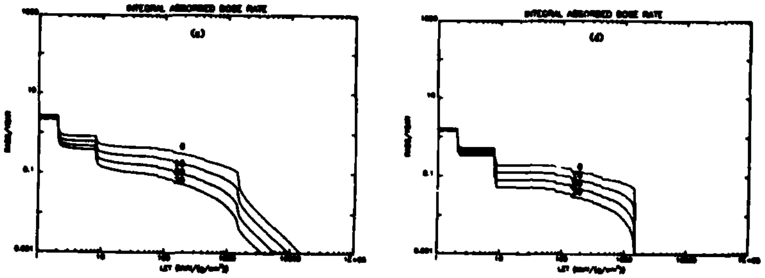

Fig. 10 cont.

Next we explore the LET distributions and doses due to cosmic rays as a function of orbital inclination.

Figs. 11a and b show respectively the LET distributions and the absorbed dose rate with no shielding and behind a shield of 4 g/cm^2 aluminum. Both figures present a comparison for the cases outside the magnetosphere, an orbital inclination of 90°, 50°, and 30°, at an altitude of 300 km, near solar minimum. The unshielded dose equivalent of nuclei with atomic number $Z \geq 6$ is about 47 rem/year. As deduced from Armstrong et al/11/ the additional contribution of target secondaries (neutrons and protons) is about 7 rem/year. Figs. 11c and d are analogous to 11a and b, but with the quality factor included.

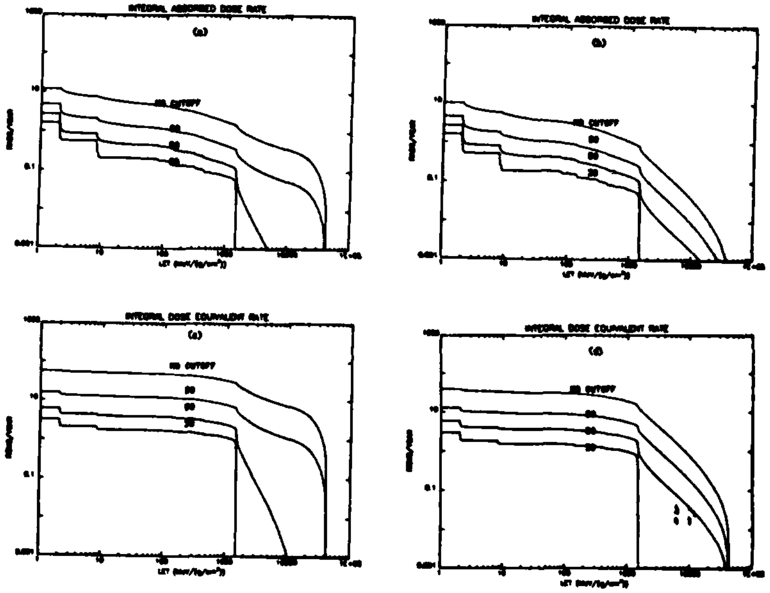

Fig. 11. A comparison of the LET-distributions of the annual absorbed dose outside the magnetosphere at a 90°, 50° and 30° orbit, (a) with no shielding, and (b) shielded by 4 g/cm^2 aluminum. The corresponding dose equivalents are shown in (c) and (d).

Figs. 12a and b present the LET distributions and the dose equivalents due to cosmic rays at solar minimum near the surface of a water phantom of 30 cm diameter, with and without a shield of 4 g/cm^2 Al. The four curves again compare the cases outside the magnetosphere, at an orbital inclination of 90°, 50°, and at 30°. Figs. 12c and d show the corresponding LET distributions and dose equivalents at the center of the water phantom. The contribution of secondary particles from the breakup of stationary target nuclei adds about 20% to the dose equivalent at the surface of the phantom, and about 40% when shielded by 4 g/cm^2 Al. At the center of the water phantom, this secondary contribution adds 50%, and with the Al shielding, about 60%. The contribution by secondaries is estimated on the basis of Armstrong et al. /11/.

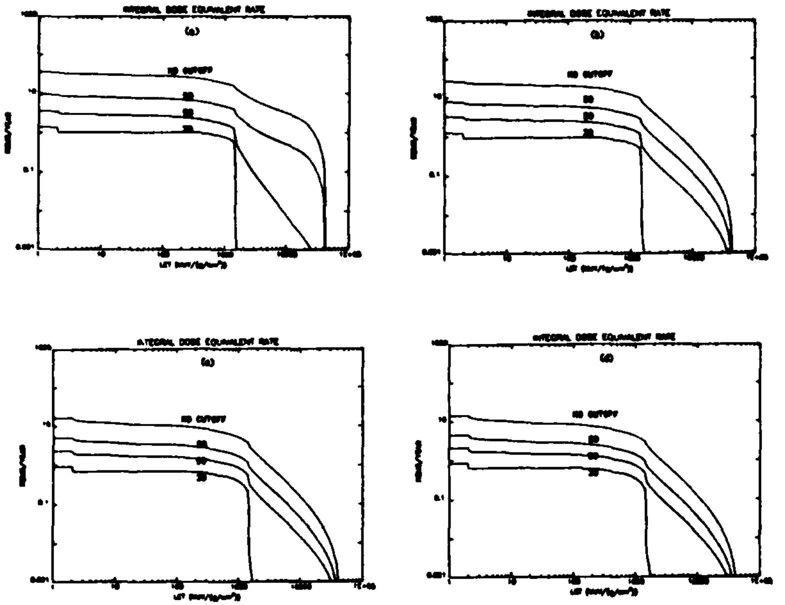

Fig. 12. The LET distributions of the annual dose equivalent outside the magnetosphere, at a 90°, 50° and at a 30° orbit. (a) at the surface of a water phantom of 30 cm diameter, (b) same, but shielded by 4 g/cm^2 aluminum, (c) at the center of the water phantom, and (d) at the center of the phantom, shielded by 4 g/cm^2 of aluminum.

In addition the contribution of the trapped radiation to the total radiation dose must be considered. (The important but sporadic contribution of solar flare particles is not treated in this paper). Benton and Henke /13/ present the dose rates of the trapped radiation at e.g. 5 g/cm^2 aluminum as a function of orbital altitude and orbital inclination, at solar minimum. They estimate that the dose rate at 300 km is 11 rads/year, at an orbit of 30° inclination, and 16 rads/year at 60°. With a few g/cm^2 of shielding, the dose equivalents due to cosmic rays and trapped particles are similar near solar minimum, at 300 km altitude, for orbital inclinations of 30° to 60°.

REFERENCES

1. S. B. Curtis, in: Space Radiation Biology, ed. C. A. Tobias and P. Todd, Academic Press, New York 1974, p. 21.
2. R. Silberberg and C. H. Tsao, Astrophys. J. Suppl. 25, 315 (1973).
3. J. R. Letaw, R. Silberberg and C. H.Tsao, Propagation of heavy cosmic ray nuclei, Astrophys. J. Suppl. in press (1984).
4. R. Silberberg, C. H.Tsao, J. H. Adams, Jr. and J. R. Letaw, Radiation Doses and LET-Distributions of Cosmic Rays, Radiation Research 98, 209 (1984).
5. W. Heinrich, Radiation Effects 34, 143, (1977).
6. E. V. Benton, A. L. Frank, R. P. Henke, G. J. Alwasi, R. M. Cassou, STS-8 Final Dosimetry Report, Tech. Report No. 60, Physics Dept., Univ. of San Francisco, Calif. (1983).
7. J. H. Adams, Jr., M. M. Shapiro, R. Silberberg, and C. H. Tsao, Proc. 17th Internat. Cosmic Ray Conf., Paris, 2, 256 (1981).
8. J. H. Adams, Jr., R. Silberberg and C. H. Tsao, NRL Memo Report 4506 (1981).
9. R. Silberberg and C. H. Tsao, Proc. 15th Internat. Cosmic Ray Conf., Plovdiv, Bulgaria, 2, 89 (1977).
10. J. R. Letaw, R. Silberberg and C. H.Tsao, Astrophys. J. Suppl. 51, 271 (1983).
11. T. W. Armstrong, R. G. Alsmiller, Jr. and K. C. Chandler, Proc. Nat. Symp. on Natural and Manmade Radiation in Space, ed. E. A. Warman, NASA TM X-2440 1972, p. 117.
12. M. A. Shea and D. F. Smart, Report No. AFCRL-TR-75-0185, Hanscom AFB, MA. (1975). and Proc. 18th Internat. Cosmic Ray Conf., Bangalore, 3, 415, (1983).
13. E. V. Benton and R. P. Henke, Adv. Space Res. 3, #8, 171, (1983).

Reprinted from Radiation Research 98, 209–226 (1984)
Copyright © 1984 Academic Press, Inc. Printed in U.S.A.

Radiation Doses and LET Distributions of Cosmic Rays

R. SILBERBERG, C. H. TSAO, AND J. H. ADAMS, JR.

Naval Research Laboratory, Washington, D.C. 20375

AND

J. R. LETAW

Severn Communications Corporation, Box 544, Severna Park, Maryland 21146

SILBERBERG, R., TSAO, C. H., ADAMS, J. H., JR., AND LETAW, J. R. Radiation Doses and LET Distributions of Cosmic Rays. *Radiat. Res.* 98, 209–226 (1984).

Among cosmic rays, the heavy nuclei (HZE particles) like iron provide the dominant contribution to the dose equivalent during exposures in space. The LET distributions and radiation doses of cosmic-ray components have been calculated—with and without the quality factors—for a set of shielding and tissue self-shielding penetration depths. The relative contributions of heavy ions among solar flare particles to the dose equivalent are also explored. The transport calculations of the nuclei in air, shielding materials, and biological tissue-like material were carried out using the partial and total nuclear cross-section equations and nuclear propagation codes of Silberberg and Tsao. Outside the magnetosphere, at solar minimum, the product of the unshielded dose and the quality factors of cosmic-ray protons and heavy nuclei with atomic number $Z > 6$ are about 5 and 47 rem/year, respectively. With 4 g/cm^2 aluminum shielding and at a depth of 5 cm in a biological phantom of 30 cm diameter, the respective values of the dose equivalents are about 4 and 11 rem/year. Due to the hard spectrum of cosmic rays, the attenuation of protons thus is relatively modest, while that of heavy nuclei is larger due to the larger interaction cross section. The dose equivalent of neutrons in the shielded case mentioned above is similar to that of protons. The biological risks are tentatively assessed in terms of the BEIR 1980 report. Uncertainties in risks due to possible large RBE values at low doses of high-LET radiation and due to the microbeam nature of damage by heavy ions are pointed out. Certain experiments and studies by radiobiologists are suggested for reducing the uncertainties in the estimates of the risks.

INTRODUCTION

Radiation exposures in space and the upper atmosphere are due to various sources: galactic cosmic rays, solar flare particles, trapped radiation, and secondary particles. When the Apollo flights were planned, the biological hazards were summarized at the Second Symposium on Protection against Radiations in Space (see Foelsche (*1*)). This was followed by the reports at the National Symposium on Natural and Manmade Radiation in Space (see Armstrong *et al.* (*2*)). A more recent survey of space radiation and biology has been edited by Tobias and Todd (*3*). The chapter by Curtis (*4*) deals with space radiations and the associated doses. The absorbed dose and dose equivalent

0033-7587/84 $3.00
Copyright © 1984 by Academic Press, Inc.
All rights of reproduction in any form reserved.

at aircraft flight altitudes, about 10 to 20 km, have been reviewed (*5*). While our paper deals especially with the heavy nuclei and their radiation transport, there are other important radiation components—secondary protons, neutrons, and pions. The latter can be calculated with the HETC Code of Armstrong and Chandler (*6*) (which can be combined with slow neutron and electromagnetic cascade codes) or the analytic techniques of O'Brien (*7*). More recently, Daniel and Stephens (*8, 9*) have reviewed and calculated the propagation of electrons at atmospheric depths of 2.6 to 100 g/cm^2.

The propagation and nuclear transformations of heavy cosmic-ray nuclei in interstellar hydrogen have been explored by Shapiro and Silberberg (*10*) and more recently by Silberberg *et al.* (*11*) using the partial cross-section equations of Silberberg and Tsao (*12*). The latter equations have been extended to collisions between heavy nuclei, including propagation of heavy nuclei in the atmosphere and in various materials (*13*). Recently we developed a highly precise formalism for calculating the total inelastic proton–nucleus cross sections (*14*).

In this paper the transformations of the nuclear composition and the LET distributions in shielding and in tissue are calculated. The relative contributions of various elements in cosmic rays to the absorbed dose and dose equivalent are estimated. Using the quality factor–LET relation proposed by the RBE Committee (*15*) to the ICRP and ICRU, the dose equivalent due to cosmic rays even behind typical spacecraft shielding is shown to be dominated by the heavy nuclei.

METHODS

To calculate the absorbed dose and dose equivalent due to cosmic rays and solar flare particles in biological tissue behind shielding we used the following procedures: A radiation transport equation in matrix form was developed further by three of the authors of this paper (*16*) so as to include the complete set of isotopes in cosmic rays, from ^{1}H to ^{64}Ni, with ionization losses and solar modulation included.

In this calculation we start from the unshielded composition and energy spectra of cosmic rays and solar flare particles. The composition of cosmic rays adopted here is based on the review of Shapiro and Silberberg (*10*), as updated by Silberberg *et al.* (*11*) and Adams *et al.*[1] (*17*). In the latter publication we provided a modeling procedure to calculate the energy spectra of various cosmic-ray nuclides at different times in the 11-year solar cycle. The integral flux of cosmic-ray protons and helium is adopted from Rygg[2] and the ratio of Fe/(C, O) from Engelmann *et al.* (*18*).

Figure 1 shows the unshielded composition, i.e., the relative abundances of cosmic-ray elements for atomic numbers $3 \leq Z \leq 26$, normalized to 100 for carbon, at a rigidity cutoff of ~4.5 GV, corresponding to a geomagnetic latitude of $\lambda \approx 45°$.

Table I shows the elemental fluxes of cosmic rays at the top of the atmosphere near solar minimum at high geomagnetic latitudes. Also near solar minimum the fluxes and doses vary;[1] values 5% lower and 20% higher than those used here occur in literature. The fluences at rigidity cutoffs of 4.5 and 16.5 GV (corresponding, respectively, to $\lambda = 45°$ and close to the geomagnetic equator) are obtained from Table I by applying respective weighting factors of 0.2 and 0.03 for hydrogen, 0.2 and 0.04 for He, C, O, Ne, Mg, and Si, and 0.3 and 0.06 for Fe. The weighting factors are based on the energy spectra given by Adams *et al.*[1] and references therein.

---

[1] J. H. Adams, Jr., R. Silberberg, and C. H. Tsao, *Cosmic Ray Effects on Microelectronics, Part I; The near-earth particle environment.* NRL Memo Report 4506, 1981.

[2] T. A. Rygg, Cosmic Ray Proton and Helium Measurements over Half a Solar Cycle. M.S. Thesis, University of Maryland, 1970.

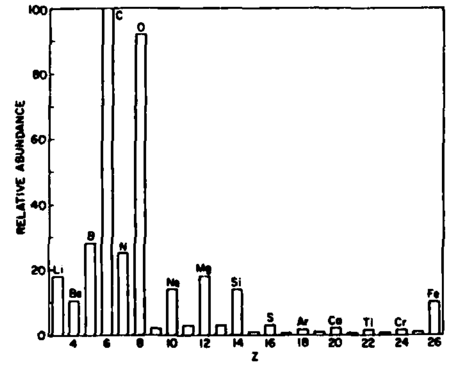

FIG. 1. The relative abundance of elements in cosmic rays, from Li to Fe, normalized to 100 for carbon, at a rigidity cutoff of 4.5 GV.

The composition of solar flare particles varies from flare to flare. We have estimated[1] the average composition for atomic numbers $1 \leq Z \leq 28$, as well as the composition for a degree of heavy ion enhancement such as occurs in 10% of the flares.

The energy spectra of the various cosmic-ray nuclei used in the calculation here are those of our recent review,[1] where the spectra from 10 to 10^5 MeV/nucleon are shown. A comparison of the energy spectrum of a very large solar flare (Aug. 4–6, 1972) with that of cosmic-ray protons is given in Fig. 2.

In addition to the composition and energy spectra of the incident nuclei, the radiation transport calculations require the use of total and partial inelastic cross sections.

Using Rudstam's equation (*19*) as a starting point, we have constructed (*12*) a semiempirical equation applicable for calculating the partial cross sections of target nuclides in the range of mass numbers $9 \leq A_t \leq 209$ and products with $6 \leq A \leq 200$.

$$\sigma = \sigma_0 f(A) f(E) e^{-P\Delta A} \exp(-R|Z - SA + TA^2|^\nu)\Omega\eta\xi. \qquad (1)$$

The factors and parameters of Eq. (1) *are defined in Ref.* (*12*). For targets with $Z_t < 29$, and energies ≥ 1 GeV, calculations with Eq. (1) yield values of cross sections having one standard deviation uncertainty of 30%; when averaged over various product isotopes and target elements, it reduces to about 10 or 15%.

TABLE I

Cosmic-Ray Flux, $E > 160$ MeV/nucl. at Solar Min., in Units of Particles/m^2 ster · sec

H	2500	Ne	0.87	K	0.046
He	240	Na	0.17	Ca	0.11
Li	1.1	Mg	1.1	Sc	0.025
Be	0.58	Al	0.20	Ti	0.072
B	1.6	Si	0.87	V	0.036
C	6.0	P	0.048	Cr	0.072
N	1.4	S	0.17	Mn	0.049
O	5.5	Cl	0.036	Fe	0.48
F	0.095	Ar	0.065		

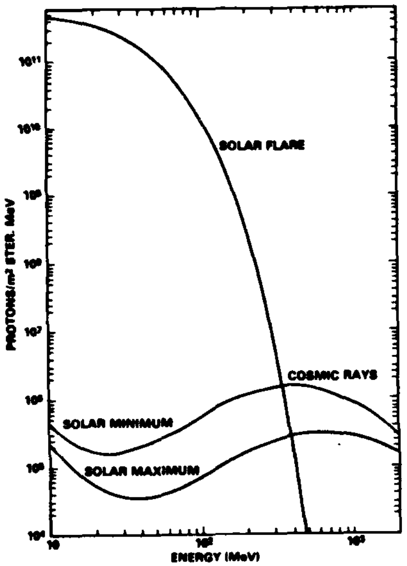

FIG. 2. A comparison of the time-integrated differential energy spectrum of protons for the solar flares of August 4 to 7, 1972, with the spectra of cosmic-ray protons accumulated in 1 week.

The partial cross sections of nucleus–nucleus reactions are roughly proportional to those of proton–nucleus reactions, according to Lindstrom *et al.* (*20*). However, there are modest-size deviations from this scaling relation, and we use here the empirical relationship of Silberberg and Tsao (*13*)

$$\sigma(N_1 + N_2) = \sigma(N_1 + p)S_c\epsilon_L\epsilon_1\epsilon_\Delta \tag{2}$$

for the collision of a cosmic-ray nuclide N_1 (with $Z_1 \geqslant 4$) with a stationary nuclide N_2. Here S_c is the scaling factor, ϵ_L is the enhancement factor for products with $3 \leqslant Z \leqslant 5$, ϵ_1 is the enhancement factor for single nucleon stripping reactions, and ϵ_Δ is the enhancement factor for large values of ΔA. These factors are defined by Silberberg *et al* (*13*) for various sets of target and product nuclei. The energy of the recoil fragment of the stationary nucleus N_2 is a few mega-electron volts; hence its energy deposition is negligible in comparison to the fragment of N_1. However, the contribution of recoils from the numerous cosmic-ray proton interactions and those from the secondary neutrons are important—their contribution is adopted from Armstrong *et al.* (*2*). The total inelastic cross sections of nuclei on protons at high energy, $E > 2$ GeV/nucl., is calculated from Letaw *et al.* (*14*):

$$\sigma_i(\text{H.E.}) = 45A_i^{0.7}[1 + 0.016 \sin(5.3 - 2.63 \ln A_i)]\text{mb}. \tag{3}$$

This relation has one standard deviation uncertainty of ~2%. At lower energies, down to about 10 MeV, the total inelastic cross section is calculated from

$$\sigma_i(E) = \sigma_i(\text{H.E.})[1 - 0.62 \exp(-E/200) \sin(10.9E^{-0.28})], \tag{4}$$

where E is in units of mega-electron volts per nucleon.

The total inelastic cross sections of nucleus–nucleus reactions are calculated from the equation

$$\sigma_t(N_1 + N_2) = 10\pi 1.26^2(A_1^{1/3} + A_2^{1/3} - 0.4)^2\text{mb}. \tag{5}$$

This equation is similar in form to that of Cleghorn *et al.* (*21*), but the numerical parameters are based on our survey of more recent experimental data: Cheshire *et al.* (*22*), Lindstrom *et al.*,[3] and Westfall *et al.* (*23*). The attenuation rate is ~15% higher than with the use of Cleghorn's cross sections.

The production rates of H and He in collisions of cosmic rays having $Z \geqslant 3$ were adopted from the fragmentation parameters of Freier and Waddington (*24*) and Saito (*25*). The production rates of H and ^{3}He in collisions of cosmic-ray helium were adopted from Meyer *et al.* (*26*) and Lingenfelter and Ramaty (*27*).

The nuclear transformations and energy losses of cosmic rays in materials were calculated (using the above cross sections) with the diffusion equation of Ginzburg and Syrovatskii (*28*). This procedure has been described by Shapiro and Silberberg (*10*); with appropriate approximations, the diffusion equations reduce to

$$\frac{\partial J_i}{\partial x} = -J_i\left(\frac{N}{\rho}\right)\sigma_i + \sum_{j>i} J_j\left(\frac{N}{\rho}\right)\sigma_{ij} + \frac{\partial}{\partial E}\left[J_i\left(\frac{dE}{dx}\right)_i\right]. \tag{6}$$

Here J_i is the differential flux of cosmic-ray particles of isotopes of type i, x is the path length in units of g/cm², dE/dx is the (positive) stopping power, N = atoms/cm³, ρ = mass/cm³, σ_i is the total inelastic cross section of a nucleus of isotope i, and σ_{ij} is the partial cross section of a nucleus of type j yielding one of type i. The summation over σ_{ij} also takes care of multiple fragment production. For a composite material, σ_i and σ_{ij} are summed over all the nuclei of a molecule and N represents molecules/cm³; e.g., for water, σ_i in Eq. (6) is replaced by $2\sigma_{i,H} + \sigma_{i,O}$. Equation (6) has been expressed in matrix form by Letaw *et al.* (*16*). The straight-ahead approximation with similar velocities for projectiles and fragments was adopted. The dose due to interactions of cosmic-ray protons and secondary neutrons (the contribution of the stationary target nuclei) is adopted from Armstrong *et al.* (*2*).

The output of the propagation program yields the differential energy spectra dJ_i/dE of all nuclear species above energies of 1 MeV/nucl. at various depths of a given material. These spectra are then summed to yield those for each element. In Eqs. (7) to (9) below, we use the abbreviated notation $dJ_i(E)/dE = J_i(E)$ and $dJ_i(S)/ds = J_i(S)$ as in Eq. (6) above.

The differential LET spectra of the various nuclides i are obtained from

$$J_i(S) = J_i(E)\frac{dE}{dS} \tag{7}$$

where S is the stopping power. The integral LET spectrum is given by

$$J(S > S_0) = \int_{S_0}^{S_{max}} J_i(S)dS. \tag{8}$$

The absorbed dose rate from nuclides of type i, with stopping power $S > S_0$ is given by

$$\dot{D}_i(S > S_0) = \int_{S_0}^{S_{max}} J_i(S)SdS. \tag{9}$$

Here $S = dE/dx$ with S_0 that of singly charged minimum ionization particles; if x is in units of g/cm², J is in units of particles/cm² sec, and E is in units of 100 ergs, then $\dot{D}$ is given in units of rad/sec. For the dose equivalent, the integral of Eq. (9) also contains the quality factor or Q, discussed in the next paragraph. Then $\dot{D}$ (in rem/sec) is given by

$$\dot{D}_i(S > S_0) = \int_{S_0}^{S_{max}} J_i(S)_i Q(S)SdS. \tag{10}$$

---

[3] P. J. Lindstrom, D. E. Greiner, and H. H. Heckman, private communication at American Physics Society Meeting, Washington, D. C., April 1972.

In the case of calculating the doses at various depths of a water phantom of 30 cm diameter, the solid angle is subdivided into intervals, each with its characteristic path length x. The values of dJ_i/dS are then calculated for these values of x. $\dot{D}_i$ is calculated from Eq. (9), and an integration over the solid-angle intervals yields the total absorbed dose rate of each cosmic-ray element i at a given depth in the water phantom. These absorbed dose rates are tabulated in the next section.

The LET distributions of cosmic rays and solar flare particles are multiplied by the LET-dependent quality factors to obtain an estimate for the contribution of various nuclei to the dose equivalent. The quality factors Q defined in terms of LET intervals (*15*) were approximated in our calculations by $Q = 1$ for $\mathrm{LET} < 35$ MeV/(g/cm^{-2} H_2O) and $Q = 0.072\ \mathrm{LET}^{0.74}$ for $35 < \mathrm{LET} < 2000$ and $Q = 20$ for $\mathrm{LET} > 2000$. This approximation may underestimate Q near 1000 to 2000 MeV/(g/cm^{-2}) by about 10%. We also explore the effect of a reduced value of Q for very high values of LET as a result of microbeam structure (*4*) of very highly ionizing particles, when the energy deposition is larger than needed to kill the traversed cell. The corresponding decrease of RBE is illustrated by Todd and Tobias (*29*).

We also explore the effects of a larger quality factor at low doses. The 1980 BEIR report (30) proposes a quality factor of ~25 for neutrons, instead of 10, adopted earlier (*15*). The calculations of Loewe and Mendelsohn (*31*) give a reduced estimate of the neutron dose at Hiroshima and would imply a need to revise the 1980 BEIR report. However, a large RBE (and hence of Q) for low doses of high-LET radiations like neutrons is still supported by the measurements of Bateman *et al.* (*32*) for lens opacification of mice and Shellabarger *et al.* (*33*) for rat mammary carcinogenesis.

RESULTS

In this section we present our calculated results of LET distributions, the absorbed dose, and the dose equivalent due to cosmic rays at various depths of tissue (approximated by water). The propagation (or radiation transport) calculations deal individually with all the nuclides from ^{1}H to ^{56}Fe, though the tables shown here *represent summations over groups of neighboring elements.*

The calculations are made for four sets of cases: (a) at the centers of spheres of water, up to 30 cm in radius; these can readily be converted to attenuation of vertically incident flux in slabs of water of various thicknesses; (b) a set of calculations similar to those in (a), but with an aluminum shield of 4 g/cm^2 outside the spheres of water; (c) an isotropic flux of cosmic rays is considered to be incident on a water phantom of 30 cm diameter; the absorbed dose and dose equivalent is then calculated at various depths (from 0.1 to 15 cm) in the water phantom; (d) a set of calculations similar to those in (c), but with an aluminum shield of 4 g/cm^2 outside the water phantom.

Figures 3a and b (unshielded and with 4 g/cm^2 Al, respectively) show the absorbed doses and the integral LET distributions of the absorbed dose of cosmic rays at centers of spheres of water of ~0, 5, 10, 15, 20, 25, and 30 cm radii for a 1-year exposure. (The integral LET distribution of the absorbed dose represents the absorbed dose above a given value of LET.) The flux is taken to be isotropic, and the energy spectrum like that in the solar system, near the earth orbit, at solar minimum, outside the earth's magnetosphere. The doses and LET distributions would be similar within slabs of water of the above thickness, for a unidirectional fluence similar to the *omnidirectional cosmic-ray fluence integrated over a 4π solid angle, with a similar* energy spectrum and nuclear composition. The unusual features of the curve for ~0 cm of Fig. 3a (especially the shoulder above an LET of 10^3 MeV cm^2/g) are due to the fluxes of particles below 25 MeV/nucl. which are absorbed in less than 1 g/cm^2 of water. As a result, these features are not present in the other curves. Finally, notice the relatively small attenuation (about a factor of 2) in the absorbed dose from 0 to 30 g/cm^2 of water.

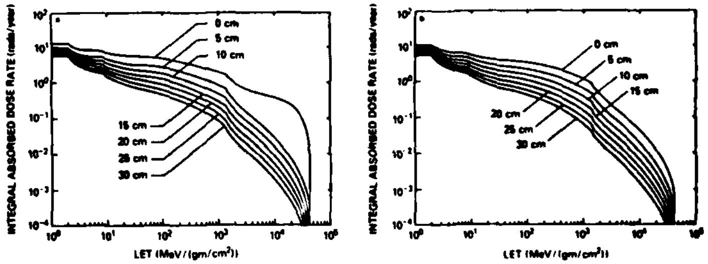

FIG. 3. The integral LET distributions of the annual absorbed dose of cosmic rays at centers of spheres of water of 0, 5, 10, 15, 20, 25, and 30 cm radii, at solar minimum, outside the earth's magnetosphere (a) without shielding, (b) with 4 g/cm^2 aluminum shielding.

Figure 3 does not show clearly the relative contributions of the various nuclides in cosmic rays. These relative contributions are displayed in Fig. 4 for the elements H, He, Li to O, F to S, and Cl to Fe. Figures 4a and b show the annual absorbed doses and the integral LET distributions of galactic cosmic rays for a 30-cm spherical water phantom at the *surface* and at *the center, respectively. The flux is again taken* as isotropic, and the energy spectrum like that at solar minimum near the earth orbit, outside the earth's magnetosphere.

Figures 5a and b show the corresponding annual dose equivalent and the *integral* LET distributions at several depths of a sphere of water 30 cm in diameter.

Table II (lines 1) gives the annual absorbed doses due to various elements in cosmic rays at the centers of spheres of x g/cm^2 of water. Again, the calculations are based on an isotropic flux at solar minimum, near the earth orbit, outside the earth's magnetosphere (close to earth, but outside the atmosphere, and near the magnetic

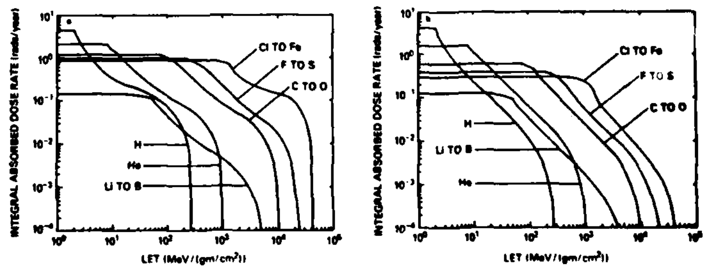

FIG. 4. The relative contributions of cosmic-ray elements H, He, Li to B, C to O, F to S, and Cl to Fe to the integral LET distributions (a) at the surface of a sphere of water of 30 cm diameter, and (b) at the center of a sphere of water of 30 cm diameter, at solar minimum, outside the earth's magnetosphere. The respective annual doses are also shown.

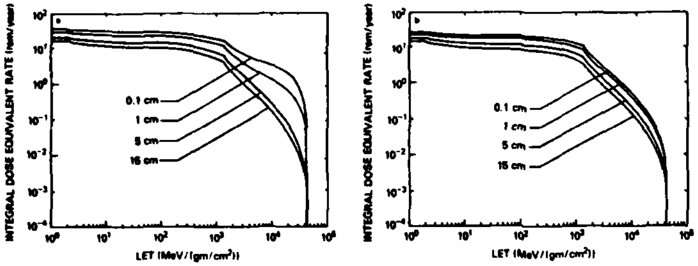

FIG. 5. The integral LET distributions of the dose-equivalent rate (rem/year) of cosmic rays at depths of 0.1, 1, 5, and 15 cm within a 30-cm diameter water sphere. The cosmic ray flux at solar minimum outside earth's magnetosphere is unshielded in (a) and shielded by 4 g/cm² aluminum in (b).

poles, the doses are half of those shown). It should be noted that the total absorbed dose due to the nuclear component is attenuated rather little (from about 11.5 to about 5.4 rad) as the cosmic rays pass through 30 g/cm² of water. However, the dose of HZE particles ($Z \geqslant 3$) is then attenuated by a factor of 6. The odd-Z elements are attenuated less; they have low initial abundances and get built up as secondary products, especially Li and F. For significant amounts of material traversed ($\geqslant 10$ g/cm²) by cosmic rays, secondary particles like neutrons and the nuclear recoils generated by them must also be considered, using, e.g., the HETC Code of Armstrong and Chandler (*6*) or the techniques of O'Brien (*7*) and for electrons, those of Daniel and Stephens (*8, 9*). The last line gives also the contribution of nuclear recoils and secondary protons and alpha particles calculated by Armstrong *et al.* (*2*) due mainly to cosmic-ray protons, and neutrons generated by them.

Table II (lines 2) illustrates the shielding effect of 4 g/cm² aluminum, a value typical of spacecraft shielding. Again, these data present the annual absorbed doses due to various elements in cosmic rays at the centers of spheres of x g/cm² of water. (The relative attenuation is similar for slabs of x g/cm² of water.) We note the modest degree of attenuation by 4 g/cm² aluminum—even for iron nuclei at $x \simeq 0$ g/cm² of water, the dose is attenuated by ~40%. The last line also gives the secondary contribution (*2*).

Table II (lines 3) shows the annual cosmic-ray absorbed dose times the quality factor at the center of a sphere of water of radius x g/cm² at solar minimum, outside the magnetosphere. One notes the appreciable attenuation between $x = 0$ and 30 g/cm² (from 55 rem down to 8 rem); this is due to the attenuation of the heavy nuclei that have large quality factors (up to ~20). Again, the last line also gives the secondary contribution (*2*). The combined values agree within 10% with corresponding calculations by Alsmiller *et al.* (*34*).

Table III (lines 1) gives the annual absorbed doses within a spherical water phantom of 30 cm diameter, at a depth of b g/cm² from the surface of the sphere. Here b ranges from 0.1 to 15 g/cm². The tabulated values again represent those at solar minimum, outside the earth's magnetosphere. One notes here the small degree of attenuation between $b = 0.1$ and 15 g/cm²; the absorbed dose changes from ~10 to ~7 rad/year. The last line also gives the absorbed dose due to secondaries (*2*).

TABLE II

Annual Cosmic-Ray Dose in Water at the Center of a Sphere of Water

		Radius (g/cm²)				
Element	*Line*[a]	*~0*	*5*	*10*	*15*	*30*
H	1	4.7	4.3	4.3	4.2	3.9
	2	4.3	4.3	4.3	4.2	3.8
	3	5.1	4.4	4.3	4.3	3.9
He	1	2.5	2.1	1.8	1.5	1.0
	2	2.4	1.7	1.7	1.4	0.9
	3	3.5	2.1	2.1	1.8	1.1
Li to B	1	0.2	0.2	0.1	0.1	0.1
	2	0.1	0.1	0.1	0.1	0.1
	3	0.5	0.4	0.3	0.3	0.2
C to O	1	1.7	1.1	0.8	0.6	0.3
	2	1.3	1.0	0.7	0.5	0.2
	3	8.5	5.1	3.5	2.4	0.9
F to S	1	1.4	0.8	0.6	0.4	0.1
	2	1.0	0.7	0.5	0.3	0.1
	3	13.2	7.4	4.6	3.0	1.0
Cl to Mn	1	0.7	0.4	0.3	0.2	0.1
	2	0.4	0.3	0.2	0.2	0.1
	3	11.6	5.5	4.1	2.9	1.0
Fe	1	0.7	0.3	0.2	0.1	0.01
	2	0.5	0.2	0.1	0.1	0.01
	3	14	5.4	2.7	1.4	0.2
Total	1	11.5 + 2	9.2 + 3	8.1 + 4	7.2 + 4	5.4 + 3
	2	10.2 + 3	8.6 + 4	7.5 + 4	6.8 + 4	5.2 + 3
	3	55 + 7	31 + 14	22 + 11	16 + 8	8.3 + 6

[a] Lines 1 give the absorbed dose rates (rad/year) in water; lines 2, those shielded by 4 g/cm² of Al; and lines 3, the absorbed dose rate times the quality factor (rem/year). The last three lines also give the secondary dose of Armstrong *et al.* (*2*).

Table III (lines 2) presents the annual cosmic-ray dose equivalent at depths $b = 0.1$ to 15 g/cm² within a spherical water phantom of 30 cm diameter again at solar minimum outside the magnetosphere. As the depth increases from 0.1 to 15 g/cm², the annual dose equivalent is attenuated from ~36 to ~16 rem. At a depth of 0.1 g/cm², HZE nuclei with $Z \geqslant 3$ contribute ~80% of the dose equivalent and at 15 g/cm², ~60%; thus the contribution of the heavy cosmic ray nuclei dominates. In addition to the doses of Table III, there are secondary doses, due mainly to neutron- and proton-generated nuclear recoils and secondary protons (*2*). These are also given in the last line of Table III. More precise values of the latter and of the total doses

TABLE III

Annual Cosmic-Ray Dose Within a Sphere of Water of 30 cm Diameter

Element	*Line*[a]	*Depth (g/cm²)* 0.1	0.5	1	5	10	15
H	1	4.4	4.3	4.3	4.2	4.2	4.2
	2	4.6	4.5	4.4	4.3	4.3	4.3
	3	4.3	4.3	4.3	4.2	4.2	4.2
He	1	2.0	2.0	1.9	1.7	1.6	1.5
	2	2.6	2.4	2.3	2.0	1.8	1.8
	3	2.2	2.1	2.0	1.8	1.7	1.6
Li to B	1	0.1	0.1	0.1	0.1	0.1	0.1
	2	0.4	0.4	0.3	0.3	0.3	0.3
	3	0.3	0.3	0.3	0.3	0.3	0.3
C to O	1	1.2	1.1	1.0	0.8	0.6	0.6
	2	5.6	5.1	4.6	3.2	2.6	2.4
	3	4.3	4.0	3.7	2.6	2.2	2.0
F to S	1	0.9	0.8	0.7	0.5	0.4	0.4
	2	8.3	7.5	6.8	4.3	3.3	3.0
	3	6.3	5.7	5.2	3.4	2.7	2.5
Cl to Mn	1	0.4	0.4	0.3	0.3	0.2	0.2
	2	6.5	5.6	5.1	3.8	3.1	3.0
	3	4.3	4.0	3.7	2.9	2.5	2.4
Fe	1	0.4	0.4	0.3	0.2	0.1	0.1
	2	7.8	6.4	5.3	2.6	1.6	1.3
	3	4.8	4.3	3.8	2.0	1.3	1.1
Total	1	9.5 + 3	9.1 + 3	8.8 + 3	7.7 + 3	7.3 + 4	7.2 + 4
	2	36 + 7	32 + 7	29 + 8	20 + 11	17 + 9	16 + 8
	3	26 + 10	25 + 10	23 + 11	17 + 10	15 + 9	14 + 8

[a] Lines 1 give the absorbed dose rates (rad/year); lines 2, the dose-equivalent rates (rem/year), as do lines 3 behind a shield of 4 g/cm² Al. The last three lines also give the secondary dose of Armstrong *et al.* (*2*).

can thus be obtained by combining the calculations of our nuclear propagation programs with those of the HETC program of Oak Ridge (*6*), and the associated slow neutron and electromagnetic cascade codes.

Table III (lines 3) illustrates the relatively modest effect of a 4 g/cm² aluminum shield on the dose-equivalent rates at various depths within a 30-cm water phantom. The contribution of the heavy nuclei still dominates. This table illustrates the absorbed doses of cosmic-ray nuclei for astronauts in a typical spacecraft outside the magnetosphere. The last line also gives the dose-equivalent ratio due to secondaries from proton interactions (*2*).

The contribution of various elements or groups of elements (H, He, Li–B, C–O, F–S, Cl–Mn, and Fe) to the dose-equivalent rate at various depths of a 30-cm water phantom is illustrated in Fig. 6. This figure displays the relative contribution of the

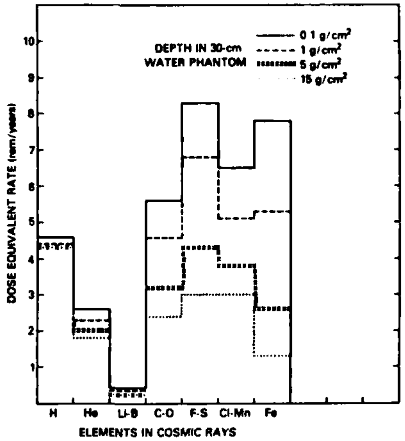

FIG. 6. The annual dose equivalent due to cosmic-ray elements H, He, Li to B, C to O, F to S, Cl to Mn, and Fe at various depths of a 30-cm water phantom, at solar minimum, outside the earth's magnetosphere.

various groups of elements to the dose equivalent, the dominance of the heavy nuclei over protons and helium, and the relatively rapid attenuation of the heavy nuclei with depth within the water phantom.

The errors in the dose-rate estimates are about 20%. The cross sections when averaged over the product isotopes of an element have a standard deviation of 10 to 15%, the relative cosmic-ray abundances about 10%, largely due to the uncertainty in the ratio (C + O)/He, and the uncertainty in the contribution of neutrons and electrons about 10%.

The cosmic-ray dose rates of the figures and graphs are the average values for a couple of years at the time of solar minimum; the peak dose rate is about 10% higher.

Figures 7 and 8 illustrate the attenuation of the heavy nuclei in the atmosphere, for groups of nuclei Li–B, C to F, Ne to Si, Ca to Mn, and Fe to Ni. Figure 7 represents the vertical flux, while Fig. 8 illustrates the total flux from the upper hemisphere of 2π solid angle. Figure 8 is based on our propagation calculations, as is Fig. 7, below 20 g/cm². Between 20 and 60 g/cm², Fig. 7 is based on the calculations done by Allkofer and Heinrich (*35*). The experimental data shown, those of Webber and Ormes (*36*), agree well with the calculations.

At altitudes below 30 km (~12 g/cm²) HZE nuclei become rapidly attenuated, and the high-LET atmospheric radiation component is dominated by neutron-generated interactions. About half of the dose equivalent at airplane flight altitudes is due to neutrons. The absorbed doses and dose equivalents at altitudes 10–20 km have been reviewed by the Advisory Committee for Radiation Biology Aspects of the SST (*5*). Reviews of the experimental data and Monte Carlo calculations of

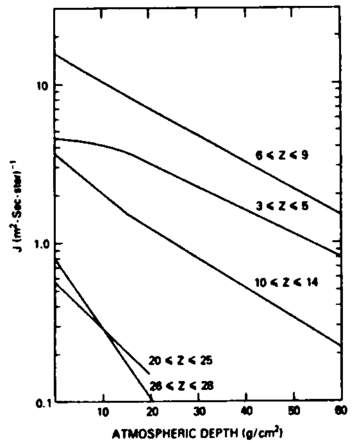

FIG. 7. The attenuation of cosmic-ray nuclei, as a function of atmospheric depth. The fluxes represent the integral vertical intensities at high geomagnetic latitude ($E > 360$ MeV/nucleon) at solar minimum. The experimental data are from Webber and Ormes (*36*).

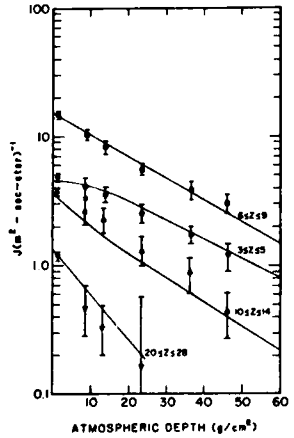

FIG. 8. The attenuation of cosmic-ray nuclei, as a function of atmospheric depth. The total flux from the upper hemisphere of 2π solid angle is shown, calculated with our propagation equations for solar minimum, near the magnetic pole.

neutron fluxes have been made by Merker *et al.* (*37*), Light *et al.* (*38*), and Armstrong *et al.* (*39*). Their data can be converted to dose equivalent using the procedures outlined in ICRU Report 28 (*40*). At an altitude of about 20 to 25 km, the annual dose equivalent at high latitudes near solar minimum is about 14 rem; about half of it is due to neutrons.

Table IV shows the contributions of the cosmic-ray components to the annual dose equivalent at altitudes 15 to 35 km, near solar min, at high geomagnetic latitudes. The data are based on O'Brien (*41*), our calculations of heavy primary nuclei (HZE), and Armstrong *et al.* (*39*) and Daniel and Stephens (*8, 9*). The flux of secondary particles is built up in the atmosphere: the neutron flux peaks between 20 and 25 km, and electrons at slightly over 15 km. In addition, the upper limit of the hourly dose equivalent for the giant flare of the February 23, 1956, flare is given in the last column; these data are from Armstrong *et al.* (*42*). The lower limit of the dose from this flare is about five times less than the upper limit shown in Table IV. For altitudes less than ~25 km, the dose equivalent is dominated by neutrons.

There is a significant difference between cosmic rays and solar flare particles in the relative contribution of heavy nuclei ($Z \geqslant 6$) to the total dose equivalent as a function of shielding: The heavy nuclei in cosmic rays dominate to about 8 g/cm² and contribute significantly to about 15 g/cm² in a material like Al. The relative contribution of the heavy nuclei in solar flare particles is attenuated much more rapidly. Adopting the normal flare particle composition, based on the collected data of Adams *et al.*,[1] the unshielded dose equivalent of heavy nuclei is similar to that of protons, but is attenuated so rapidly that its contribution becomes insignificant (<30% of total dose equivalent with only 1 g/cm² of shielding). For a flattish spectrum below ~0.5 GeV or rigidities < 1 GV like that of the February 1956 flare (*1*), the heavy nuclei become insignificant after 2 g/cm² of shielding. Heavy nuclei are enhanced in some flares. With an enhancement such as occurs in 10% of the flares,[1] the HZE nuclei under unshielded conditions contribute ~75% of the total dose equivalent. If

TABLE IV

Annual Dose Equivalents of Cosmic-Ray Components in the Upper Atmosphere and Comparison with the Hourly Rate of the February 23, 1956, Solar Flare

Altitude (km)	*Depth (g/cm²)*	*Dose equivalent rate (rem/year)*					*Solar flare dose-equivalent rate (rem/hr)*
		e	*n*	*p*	*HPN*	*Total*	
15	110	4[a]	4[a]	2[a]	—	10	4[e]
20	50	3[d]	7[a]	3[a]	—	13	8[e]
25	25	2[d]	6[c]	4[a]	1[b]	13	9[e]
30	12	1[d]	4.5[c]	4.5[a]	4[b]	14	11[e]
35	6	~0.5[d]	2[c]	4.5[a]	8[b]	15	12[e]

[a] O'Brien (*41*).
[b] This work.
[c] Armstrong *et al.* (*39*).
[d] Daniel and Stephens (*8, 9*).
[e] Armstrong *et al.* (*42*), giant flare of Feb. 23, 1956; upper limit.

we also assume a spectrum like that of the February 1956 flare, the HZE nuclei dominate up to about 2 g/cm^2 and contribute significantly up to 4 g/cm^2.

The absorbed dose for solar flare protons with energies > 30 MeV can approach 1000 rad over the duration of the flare (2 or 3 days). As the protons are absorbed by the atmosphere, the dose due to neutrons can build up to rather high levels. For the flare of February 23, 1956, the absorbed dose due to neutron component was between 2 and 10 rad/day at an atmospheric depth of 25 to 40 g/cm^2, i.e., at altitudes of 22 to 25 km.

At altitudes between about 350 and 35,000 km, the dose due to the trapped radiation (mainly protons and electrons) dominates over cosmic rays. At altitudes between 2000 and 5000 km, the absorbed dose rate is ~300 rad/day behind a shield of 1 g/cm^2, which approximately equals that due to the largest solar flares.

DISCUSSION

A procedure has been developed here for calculating the LET distributions of the various cosmic-ray nuclei, their transformations during propagation in materials, and the absorbed doses and dose equivalents due to the nuclei of various elements in cosmic rays. The HZE nuclei give the dominant contribution to the dose equivalent up to a shield thickness of about 10 g/cm^2 around a 30-cm water phantom. For LET > 2500 MeV/(g/cm^2), the RBE and the quality factor probably decrease; however, the fraction of cosmic-ray iron nuclei at low energies that exceed the above LET value is small.

Due to the large fraction of high-energy particles in cosmic rays, the dose is attenuated at a low rate as a function of matter or shielding traversed. Hence the dose is also relatively similar in various organs at various depths in the body. As shown in Table III, the annual absorbed dose from cosmic ray nuclei, at solar min., outside the atmosphere ranges from 10 rad at a depth of 0.1 cm to 7 rad at 15 cm in an unshielded water phantom of 30 cm diameter. The secondary dose due to proton interactions adds ~3 rad (*2*). The corresponding annual dose equivalent (see Table III) ranges from 36 to 16 rem—a modest variation. The secondary dose due to proton interactions adds ~9 rem (*2*). We shall explore below how these values compare with the dose limits developed by panels of radiobiological experts.

The effects of radiation (especially of high-LET radiation) on man are not yet known as well as they should be. Lushbaugh (*43*) has discussed human lethality for total-body irradiation and the effects of dose fractionation (the increase in the lethal dose with fractionation). For an exposure shorter than 1 week, a low-LET dose of 345 rad is lethal to half the human recipients (*43*) and 118 rad to 10%. The 1980 BEIR report (*30*) discusses the probability of generating leukemia and other cancers by radiation; e.g., for the linear-quadratic linear (LQ-L) model, a continuous lifetime exposure to 1 rad per year of low-LET radiation generates about one to three cases of cancer per 100 exposed women and excess cases of leukemia that are ~14% above the normal incidence. A similar absorbed dose of neutrons is estimated (*30*) to increase the excess incidence of leukemia and other cancers by a factor of about 25 relative to that induced by low-LET radiation. The BEIR report also mentions that the threshold of vision-impairing lens opacification is about 200 rad or somewhat greater for low-LET radiation, and that a quality factor of 10 has been proposed for lifetime exposure to high-LET radiation.

Guidelines for radiation protection have been developed by the National Council on Radiation Protection and Measurements (NCRP) and International Commission on Radiological Protection (ICRP). Based on these guidelines, the Advisory Committee for Radiation Biology Aspects of the SST (*5*) has developed recommendations for dose limits at supersonic flight altitudes. An individual limit of 0.5 rem/year was recommended for passengers and the public in general. For radiation workers, the limit is 5 rem/year; the limit for the flight crew could slightly exceed that of the passengers, but should not exceed that of radiation workers. Higher exposure limits have been proposed for space missions (*44*) by the Radiobiological Advisory Panel, Committee on Space Medicine, Space Science Board, NAS/NRC: At a tissue depth of 3 cm, the monthly maximum is 13 rem, yearly maximum is 38 rem, and 10-year or career limit is 200 rem. However, these limits were considered (*44*) to be subject to revision and were applicable only to a few volunteers who are older than 30 years and have established their family size. In the application of exposure limits, the depth distribution of the sensitive organs has to be considered. Some depth distributions are given by Kerr (*45*); e.g., the active bone marrow for Japanese adults is distributed between depths of 0.5 to 7 cm.

Using the relatively high exposure limits of the Radiobiological Advisory Panel (*44*), we shall briefly review and explore the corresponding allowable exposure times for a shield of ~4 g/cm^2 Al. Using the dose rates of Burrell *et al.* (*46*), for the radiation belts, the allowable exposure times for circular orbits with 30° inclination range from about a year at an altitude of 200 n. mi. (370 km), to about a month at 250 n. mi. (460 km), to about 4 hr at 3000 km altitude. These exposure times could be extended by an order of magnitude with a shielding that deflects protons with energies < 200 MeV, e.g., the plasma shielding proposed by Levy and Janes (*47*) and Levy and French (*48*). (The shield needs to be turned on at the South Atlantic Anomaly.) For a space station or space habitat outside the earth's magnetosphere (such as proposed by O'Neill of Princeton University) and a solar flare spectrum like that of February 23, 1956 [Foelsche (*1*) and Armstrong *et al.* (*42*)] the allowable exposure time for a 13-rem dose is only about 2 hr. The total flare dose is reduced below 13 rem by a shield that deflects protons up to 500 MeV, or an inert shield of ~300 g/cm^2 (built of lunar material in the case of the space habitat). (The deflecting shield needs to be activated at a time of a large flare only.) If the RBE (and the quality factor) of high-LET radiation like neutrons is ~25 as in the 1980 BEIR report, the shielding requirements for neutrons become still more severe.

The corresponding allowable time limits for exposure to cosmic rays have uncertainties that require extensive experimental and theoretical investigations by radiobiologists. Consider again a space station or space habitat beyond the earth's magnetosphere. The dose equivalent (including neutrons and secondary protons) at a depth of 5 cm in tissue, surrounded by 4 g/cm^2 Al, is 27 rem/year. While this appears less than the limit (*44*) of 38 rem/year, it is possible on the basis of the 1980 BEIR report (*30*) (where the quality factor for neutrons was taken to be 25 rather than 10) that the quality factor of heavy ions in the range 1000 ≤ LET < 2500 MeV/(g/cm^2 H_2O) should also be increased by a factor of about 3. In this case, the equivalent dose from cosmic rays would exceed the recommended annual limit (*44*) and considerably exceed the 10-year or career limit. All this raises several questions. Do the lower-energy iron nuclei in cosmic rays have such high values of LET that the quality factor and the dose equivalent should be lower as a result of the microbeam effect? Could a cumulative exposure of ≥10 years to cosmic rays generate eye lens cataracts? The dose equivalent exceeds 350 rem, but there may be repair processes during slow cumulative exposures—yet for high-LET radiations the repair process may not be effective. All these problems and questions regarding the high-LET component in cosmic rays imply a need for additional investigations by radiobiologists, some of which are mentioned below.

The generation of tumors and eye lens opacification by heavy ions in rodents (and possibly in other mammals) needs additional investigation. How is the dose of HZE particles related to RBE for various kinds of organic damage? How high are the values of LET where the RBE starts to decrease, and what is the relation between RBE and LET in this region? What is the relative damage in the case of single and fractionated doses as a function of LET—i.e., what is the degree of repair in the case of fractionated doses at various values of LET? How does the degree of repair depend on the dose and dose rate in the case of heavy ions? The answers to these questions are likely to be different for different kinds of organic damage; furthermore, extrapolations from studies with animals are not simply related to effects in men. It would be useful to carry out extended studies of personnel exposed to the space environment or on supersonic aircraft (similar to the studies at Hiroshima and Nagasaki), though it is plausible that no statistically significant conclusions could be drawn until the advent of large space habitats.

There is a significant difference in the nature of radiation in space and the upper atmosphere compared to that at ground level. In the former, under many circumstances, the high-LET radiation dominates in the form of HZE particles for ≤ 10 g/cm^2 of shielding and in the form of neutrons for more extensive shielding.

Investigations outlined in the preceding paragraphs are vital for illuminating the still uncertain risks due to the high-LET radiation. When the results of such radiobiological research are combined with the procedures developed in this paper for calculating the LET distributions, absorbed doses, and dose equivalents of cosmic-ray nuclei (at various depths in tissue), improved safety of long-duration missions should result.

ACKNOWLEDGMENTS

The authors thank Dr. A. Berman for suggesting this research topic, Dr. H. Rossi and Dr. M. M. Shapiro for advice, Dr. G. R. Merriam, Jr. for a private communication, and Mr. A. Gelman and Mr. J. Rogers for some calculations. This investigation was supported in part by ONR and DNA/DARPA.

RECEIVED: March 11, 1983; REVISED: September 1, 1983

REFERENCES

1. T. Foelsche, The ionizing radiations in supersonic transport flights. In *Second Symposium on Protection Against Radiations in Space* (A. Reetz, Jr., Ed.), pp. 287–299. NASA, Washington, DC, 1965.

2. T. W. Armstrong, R. G. Alsmiller, Jr., and K. C. Chandler, Monte Carlo calculations of high-energy nucleon–meson cascades and applications to galactic cosmic-ray transport. In *Proceedings of the National Symposium on Natural and Manmade Radiation in Space* (E. A. Warman, Ed.), pp. 117–122. NASA TM X-2440, 1972.

3. C. A. Tobias and P. Todd (Eds.), *Space Radiation Biology*. Academic Press, New York, 1974.

4. S. B. Curtis, Radiation physics and evaluation of current hazards. In *Space Radiation Biology* (C. A. Tobias and P. Todd, Eds.), pp. 21–99. Academic Press, New York, 1974.

5. Advisory Committee for Radiation Biology Aspects of the SST, Final Report, Cosmic radiation exposure in supersonic and subsonic flight. *Aviat. Space Environ. Med.* **46**, 1170–1185 (1975).

6. T. W. Armstrong and K. C. Chandler, HETC—A high energy transport code. *Nucl. Sci. Eng.* **49**, *110* (1972).

7. K. O'Brien, Cosmic-ray propagation in the atmosphere. *Il Nuovo Cimento Ital. Fis. A* **3**, 521–547 (1971).

8. R. R. Daniel and S. A. Stephens, Propagation of secondary electron–photon component of the cosmic radiation in the atmosphere in the region 1 MeV to GeV. *Proc. 13th Int. Cosmic Ray Conf.* **3**, 2151–2156 (1973).

9. R. R. Daniel and S. A. Stephens, Cosmic-ray produced electrons and gamma rays in the atmosphere. *Rev. Geophys. Space Sci.* **12**, 33–298 (1974).

10. M. M. Shapiro and R. Silberberg, Heavy cosmic ray nuclei. *Annu. Rev. Nucl. Sci.* **20**, 323–392 (1970).

11. R. Silberberg, C. H. Tsao, and M. M. Shapiro, Semiempirical cross sections and applications to nuclear interactions of cosmic rays. In *Spallation Nuclear Reactions and Their Applications* (B. S. P. Shen and M. Merker, Eds.), pp. 46–81. Reidel, Dordrecht/Boston, 1976.

12. R. Silberberg and C. H. Tsao, Partial cross sections in high energy nuclear reactions and astrophysical applications, *Astrophys. J. Suppl.* **25**, 315–368 (1973).

13. R. Silberberg and C. H. Tsao, Calculations of nucleus–nucleus cross sections and attenuation of complex cosmic ray nuclei in the atmosphere. *Proc. 15th Int. Cosmic Ray Conf.* **2**, 89–94 (1977).

14. J. R. Letaw, R. Silberberg, and C. H. Tsao, Proton–nucleus total inelastic cross sections: An empirical formula for E > 10 MeV. *Astrophys. J. (Suppl.)* **51**, 271–276 (1983).

15. Report of the RBE Committee to the International Commissions on Radiological Protection and on Radiological Units and Measurements. *Health Phys.* **9**, 357–386 (1963).

16. J. R. Letaw, C. H. Tsao, and R. Silberberg, Matrix methods in cosmic ray propagation. In *Composition and Origin of Cosmic Rays* (M. M. Shapiro, Ed.), pp. 337–342. Reidel, New York, 1983.

17. J. H. Adams, Jr., M. M. Shapiro, R. Silberberg, and C. H. Tsao, Calculated isotopic source composition and tests for origin and propagation of cosmic rays with mass numbers ≤ 62. *Proc. 17th Int. Cosmic Ray Conf.* **2**, 256–259 (1981).

18. J. J. Engelmann, P. Goret, E. Juliusson, L. Koch-Miramond, P. Masse, N. Perron, U. Rio, A. Soutoul, B. Byrnak, H. Jakobsen, N. Lund, B. Peters, I. L. Rasmussen, M. Rotenberg, and N. Westergaard, Elemental composition of cosmic rays from Be to Zn as measured by the Franch–Danish Instrument on HEAO-3. *Proc. 17th Int. Cosmic Ray Conf.* **9**, 97–100 (1981).

19. G. Rudstam, Systematics of spallation yields. *Z. Naturforsch A* **21**, 1027–1041 (1966).

20. P. J. Lindstrom, D. E. Greiner, H. H. Heckman, B. Cork, and F. S. Bieser, Isotope production cross sections from the fragmentation of ^{16}O and ^{12}C at relativistic energies. Report LBL-3650, Lawrence Berkeley Laboratory, 1975.

21. T. F. Cleghorn, P. S. Freier, and C. J. Waddington, The energy dependence of the fragmentation parameters and mean free paths of cosmic-ray nuclei with $Z \geq 10$. *Can. J. Phys.* **46**, S572–S577 (1968).

22. D. L. Cheshire, R. W. Huggett, D. P. Johnson, W. V. Jones, S. P. Rountree, S. D. Verma, W. K. H. Schmidt, R. J. Kurz, T. Bowen, and E. P. Knider, Fragmentation cross sections of 2.1 GeV/nucleon ^{12}C and ^{16}O ions. *Phys. Rev. D* **10**, 25–31 (1974).

23. G. D. Westfall, L. W. Wilson, P. J. Lindstrom, H. J. Crawford, D. E. Greiner, and H. H. Heckman, Fragmentation of relativistic ^{56}Fe. *Phys. Rev. C* **19**, 1309–1323 (1979).

24. P. S. Freier and C. J. Waddington, The cascading of cosmic-ray nuclei in various media. *Astrophys. Space Sci.* **38**, 419–436 (1975).

25. T. Saito, The interaction mean free paths and the fragmentation probabilities of cosmic heavy nuclei at energies above 10 GeV/nucleon. *J. Phys. Soc. Jpn.* **30**, 1243–1251 (1971).

26. J. P. Meyer, D. E. Hagge, and F. B. McDonald, Measurement and interpretation of isotopic composition of hydrogen and helium cosmic-ray nuclei below 75 MeV/nucleon. *Can. J. Phys.* 46, S503–S508 (1968).

27. R. E. Lingenfelter and R. Ramaty, High energy nuclear reactions in solar flares. In *High Energy Nuclear Reactions in Astrophysics* (B. S. P. Shen, Ed.), Benjamin, New York, 1967.

28. V. L. Ginzburg and S. I. Syrovatskii, *The Origin of Cosmic Rays.* Pergamon/Macmillan, New York, 1964.

29. P. Todd and C. A. Tobias, Cellular radiation biology. In *Space Radiation Biology* (C. A. Tobias and P. Todd, Eds.), pp. 141–195. Academic Press, New York, 1974.

30. National Research Council, Committee on the Biological Effects of Ionizing Radiations, *The Effects on Populations of Exposure to Low Levels of Ionizing Radiation.* Natl. Acad. Sci., Washington, D. C., 1980.

31. W. E. Loewe and E. Mendelsohn, Revised estimates of dose at Hiroshima and possible consequences for radiation-calculated leukemia. Report D-80-14, Lawrence Livermore Laboratory, 1980.

32. J. L. Bateman, H. H. Rossi, A. M. Kellerer, C. V. Robinson, and V. P. Bond, Dose dependence of fast neutron RBE for lens opacification in mice. *Radiat. Res.* 51, 381–390 (1972).

33. C. J. Shellabarger, R. D. Brown, A. R. Rao, J. P. Shonley, V. P. Bond, A. M. Kellerer, H. H. Rossi, L. J. Goodman, and R. E. Mills, Rat mammary carcinogenesis following neutron or X-radiation. In *Biological Effects of Neutron Radiation,* pp. 405–415. International Atomic Energy Agency, Vienna, 1974.

34. *R. G. Alsmiller, Jr., R. I. Santoro, J. Barish, and H. C. Clairborne, Shielding of Manned Space* Vehicles Against Protons and Alpha Particles. Report ORNL-RSIC-35, Oak Ridge National Laboratory, Oak Ridge, Tenn., 1972.

35. O. C. Allkofer and W. Heinrich, Attenuation of heavy nuclei intensities in the atmosphere by fragmentation. *Proc. 13th Int. Cosmic Ray Conf.* 3, 2197–2202 (1973).

36. W. R. Webber and J. F. Ormes, Cerenkov-scintillation counter measurements of nuclei heavier than helium in the primary cosmic radiation. *J. Geophys. Res.* 72, 5957–5976 (1967).

37. M. Merker, E. S. Light, H. J. Verschell, R. B. Mendell, and S. A. Korff, Time dependent worldwide distribution of atmospheric neutrons and of their products, 1. Fast neutron observations. *J. Geophys. Res.* 78, 2727–2740 (1973).

38. E. S. Light, M. Merker, H. J. Verschell, R. B. Mendell, and S. A. Korff, Time dependent worldwide distribution of atmospheric neutrons and their products, 2. Calculation. *J. Geophys. Res.* 78, 2741–2762 (1973).

39. T. W. Armstrong, K. C. Chandler, and J. Barish, Calculations of neutron flux spectra induced in the earth's atmosphere by galactic cosmic rays. *J. Geophys. Res.* 78, 2715–2726 (1973).

40. ICRU, Basic Aspects of High Energy Particle Interactions and Particle Dosimetry. Report 28, International Commission on Radiation Units and Measurements, Washington, D. C., 1978.

41. K. O'Brien, The cosmic ray field at ground level. In *The Natural Radiation Environment II* (J. A. S. Adams, W. M. Lowder, and T. F. Gesell, Eds.), pp. 15–54. USERDA Technical Information Center, Oak Ridge, Tenn., 1972.

42. T. W. Armstrong, R. G. Alsmiller, Jr., and J. Barish, Radiation hazard at supersonic aircraft altitudes. *Nucl. Sci. Eng.* 37, 337–342 (1969).

43. C. C. Lushbaugh, Human radiation tolerance. In *Space Radiation Biology* (C. A. Tobias and P. Todd, Eds.), pp. 475–522. Academic Press, New York, 1974.

44. W. H. Langham, Ed., Radiation Protection Guides and Constraints for Space-Mission and Vehicle-Design Studies Involving Nuclear Systems. Natl. Acad. Sci., Washington, D. C., 1970.

45. G. D. Kerr, Organ dose estimates for the Japanese atomic-bomb survivors. *Health Phys.* 37, 487–508 (1979).

46. M. O. Burrell, J. J. Wright, and J. W. Watts, An Analysis of Energetic Space Radiation and Dose Rates. Report NASA-TN-D-4404, NASA, Washington, D. C., 1968.

47. R. H. Levy and G. S. Janes, Plasma radiation shielding. In *Second Symposium on Protection against Radiation in Space* (A. Reetz, Ed.), pp. 211–215. Report NASA-SP-71, NASA, Washington, D. C., 1965.

48. R. H. Levy and F. W. French, Plasma radiation shield: Concept and applications to space vehicles. *J. Spacecraft* 5, 570–577 (1968).

END
DTIC
4-86